EURISOL User Group

Report on the fourth EURISOL User Group Topical Meeting [1]

# Going to the limits of mass, temperature, spin and isospin with heavy Radioactive Ion Beams

Aula of Polish Academy of Arts and Sciences,
Krakow, Poland, July 1-3, 2013.

The research leading to these results has received funding from the European Union Seventh Framework Programme FP7/2007- 2013 under Grant Agreement n. 262010 - ENSAR.
The EC is not liable for any use that can be made on the information contained herein.

[1] Coordinated by Dieter Ackermann, GSI, Darmstadt, Germany, Ari Jokinen, University of Jyväskylä, Finland, Adam Maj, IFJ PAN Krakow, Bartek Szpak, IFJ PAN Krakow, Angela Bonaccorso, INFN, Sez. di Pisa, Italy.

**Local Organizing Committee**

Piotr Bednarczyk (IFJ PAN Kraków)
Bogdan Fornal (IFJ PAN Kraków)
Maria Kmiecik (IFJ PAN Kraków)
Wojciech Królas (IFJ PAN Kraków)
Adam Maj - chair (IFJ PAN Kraków)
Katarzyna Mazurek (IFJ PAN Kraków)
Paweł Napiorkowski (HIL UW Warsaw)
Małgorzata Niewiara - secretary (IFJ PAN Kraków)
Krzysztof Rusek (HIL UW Warsaw)
Bartlomiej Szpak (IFJ PAN Kraków)

**Advisory Committee**

Dieter Ackermann (GSI, Darmstadt, Germany)
Bertram Blank (CEN, Bordeaux, France)
Yorick Blumenfeld (IPN Orsay, France)
Angela Bonaccorso - chair (INFN, Pisa, Italy)
Piet van Duppen (KU Leuven, Belgium)
Alberto Facco (LNL Legnaro, Italy)
Lidia Ferreira (IST, Lisbon, Portugal)
Hans Fynbo (Uni. Aarhus, Denmark)
Paul Greenless(Uni. Jyvaskyla, Finland)
Ari Jokinen (Uni. Jyvaskyla, Finland)
Marek Lewitowicz (Ganil, Caen, France)
Adam Maj (Inst. Nucl. Phys., Kraków, Poland)
Paddy Regan (Uni. Surrey, Great Britain)

**4th EURISOL TOPICAL MEETING**

**„Going to the limits of mass, temperature, spin and isospin with heavy Radioactive Ion beams“**

## Foreword

This booklet contains the highlights of the fourth EURISOL Topical Meeting which was held in Krakow from July 1st to 3rd 2013. It followed the EURISOL Topical Meetings in Catania on "The formation and structure of r-process nuclei, between N=50 and 82 (including $^{78}$Ni and $^{132}$Sn areas)", in Valencia on "Neutron-deficient nuclei and the physics of the proton-rich side of the nuclear chart" and in Lisbon on "Physics of light nuclei". It was initiated by the User Executive Committee of the EURISOL Users Group and supported by the European Commission via the EURISOL-NETWORK within the ENSAR contract. The local organisation was provided by the Niewodniczanski Institute of Nuclear Physics, Polish Academy of Sciences, under the chair of Prof. Adam Maj (Krakow) and Dr. Angela Bonaccorso (Pisa). The workshop was co-organized by the Heavy Ion Laboratory of the University of Warsaw. The aim of the EURISOL topical meetings was to discuss the various facets of contemporary nuclear physics relevant for the design and planning of the future EURISOL facility.

The Topical Meeting in Krakow had a similar format as the previous workshops. In two and a half days it focused on the following subjects:

- Progress in mean-field and energy density functionals description of heavy nuclei
- Research on Heavy and Superheavy Elements with Radioactive Ion Beams
- Angular momentum dependence of the fission barrier height
- Exotic nuclear shapes and rotational structure at high spin, isospin and temperature
- High-spin isomeric states
- Mass measurements and laser spectroscopy of the heavy elements
- Beta-delayed fission

The programme and the presentations are available at the workshop web site http://eurisol.ifj.edu.pl/.

The subjects listed above were elaborated in the presentation with special emphasis on the peculiarities and boundary conditions in terms of beam species, intensities and production schemes, projected for next generation radioactive ion beam (RIB) facilities like SPIRAL2, FAIR, FRIB, RIKEN and eventually EURISOL. An introduction into the various subjects, ordered under the three topics "high spin", "high atomic mass and charge", and "ground state properties for extreme isospin", is given here. It is followed by summaries of the single contributions to this workshop.

**Structure of medium/high spin and high temperature**

This topic was addressed by F. Camera, G. Casini, M. Ciemała, N. Cieplicka, E. Clement, A. Dobrowolski, J. Dudek, B. Fornal G. Henning, P. Marini, L. Pellegri, C. Rizzo, W. Satuła, J. Simpson and K. Wrzosek-Lipska.

Atomic nuclei belong to those systems whose bulk excited-state collective properties such as rotational ones, are often predetermined by the properties of a few single-nucleonic states with energies close to the Fermi energy. The activity related to the topic of high-spin states, using stable beam facilities, was at his peak in the two last decades of the previous century. Experimental evidence for such rotational phenomena was provided by the structure of rotational bands, back-bending, band-termination, collective rotation above band termination, tri-axiality, shape-coexistence and other phenomena. The discrete in-beam $\gamma$-ray spectroscopy with deep-inelastic reactions turned out to be efficient in elucidating high-spin structures in neutron-rich nuclei. The $\gamma$ decay of the GDR, measured for high spins and high temperatures, was found to be a very useful probe to study the bulk properties of hot nuclei. But the most spectacular outcome of such studies was the discovery of super-deformed high-spin structures throughout the whole chart on nuclei.

On the other hand the search for predicted hyper-deformed structures was not conclusive, despite many attempts. This negative observation was ascribed to that fact that fission competition does not permit to transfer sufficiently high angular momentum to the nuclei of interest. In addition, at the beginning of this century, the advent of facilities with radioactive beams (with relatively low intensities) almost naturally caused a change of experimental interest towards exploitation of exotic nuclei. As an interesting example a new collective phenomenon, the Pygmy Dipole Resonance, was found in exotic nuclei, although its nature is still not fully understood. All of this caused a certain decline of interest in high-spin activities in the last ten years.

EURISOL is expected to deliver beams of nuclei, very rich in neutrons, with intensities comparable to those provided by stable beam facilities, what will allow exploring again the exciting field of high spin physics in unexplored, very exotic regions of the nuclear chart, using fusion reactions. This is related to the fact that the fission limit for very neutron-rich nuclei, produced via fusion-evaporation reaction, is higher by at least 10 units of spin, as a consequence of the significant increase of the fission barrier with the increasing neutron number. Especially interesting is the Cd - Yb mass regions, where extremely large angular momenta (up to 90 $\hbar$) of the residual nuclei can be reached using neutron-rich beams. At the same time theoretical calculations strongly suggest that neutron-rich nuclei in this mass region are good candidates for producing hyper-deformed nuclear states in fusion reactions. This arises because of both favourable shell-effects at low temperatures and the contribution from the liquid drop energy term showing, at spins even higher than 80-90 $\hbar$, a well-defined minimum associated with very large deformations. Also discrete in-beam gamma-ray spectroscopy of deep-inelastic reaction products will greatly benefit from radioactive

beams. Experiments using radioactive beams and modern tracking germanium arrays should extend the investigations of high-spin structures toward the „terra incognita".

With the advent of intense neutron-rich beams also the high-temperature regime will be at the focus of interest. At sufficiently high temperatures the quantum (shell) effects disappear and the nuclei can be described by classical "macroscopic" models such as the Liquid Drop Model. In the high-temperature and high-spin regime new shape change phenomena are predicted to occur, as for example the nuclear Jacobi and Poincare shape transitions. These phenomena can be investigated using, for example, the $\gamma$ decay of the Giant Dipole Resonance (GDR). The amount of isospin mixing, a subject currently of interest in theoretical investigation, can be studied as a function of nuclear temperature using the GDR decay. The use of stable beams permits the isospin mixing systematic study below A=80 nuclei, while the use of radioactive beams, like those provided by the EURISOL facility, will permit the measurements of isospin mixing in heavier nuclei. At very high temperatures the multi-fragmentation process sets in. In this context high intensity neutron-rich beams will give the possibility to study the isospin dependence of the fragment production process.

It was pointed out in several talks that a facility such as EURISOL must possess state of the art instrumentation. The new generation of tracking arrays such as AGATA and GRETA for discrete $\gamma$-spectroscopy, and FAZIA for charged particle and heavy ion measurements, will be ideal.

**High atomic mass and charge (SHE)**

This topic was addressed by D. Ackermann, M. Block, K. Mazurek, Th. Duget, G. Pollarolo, V. Prassa, E. Litvinova, B. Szpak, K. Pormorski, B. Jurado and V. Zagrebaev.

Almost half a century after the postulation of the possible existence of the so called "island of stability" of superheavy elements (SHE) and a very fruitful harvest of experimental data reaching up to Z=118, the quest is still open. Apart from the synthesis and basic properties for $\alpha$-decay and spontaneous fission, the investigation of the nuclear structure of those heavy species has revealed intriguing features like k-isomerism for nuclei as heavy as $^{270}$Ds or the population and observation of spins beyond 20 $\hbar$ for species like $^{256}$Rf.

New methods are being applied, like precise mass measurements for isotopes in penning traps, developed, like laser spectroscopy of stopped species, or envisioned and possibly appearing at the horizon, like the use of neutron-rich radioactive ions as projectiles, possibly provided with higher intensities at EURISOL or its follow ups.

Ground state properties, like the nuclear binding energy are major ingredients towards an understanding of the heavy species themselves as well as for the model predictions. Advanced technologies as high precision mass measurements in Penning traps are complemented by tools like laser spectroscopy to study the atomic properties, reaching into regions beyond $Z \geq 102$.

Following the predictions of the major theoretical approaches, including microscopic-macroscopic models as well as self-consistent theories like Hartree-Fock-Bugoliubov (HFB) or relativistic mean field (RMF) models, the predicted region of spherical shell-stabilized nuclei is out of reach for stable species as projectiles for the traditional fusion–evaporation production scheme. Neutron rich exotic nuclides will be necessary to compose the required proton and neutron numbers. The intensities projected for the next generation RIB facilities, however, are limited and exclude SHE synthesis via the classical approach. Systematic studies of reaction mechanism and nuclear structure features together with alternative approaches, like e.g. deep inelastic reactions and the employment of the compound nucleus spin distribution are promising approaches to the problem. Predictions employing a combination of an adiabatic two-centre shell model, combined with a system of coupled Langevin equations and a statistical model, is used to investigate the possible population of superheavy nuclei (SHN) in the high mass – high Z tail of the nuclide distribution in deep inelastic heavy ion collisions.

The description of heavy nuclei employing the most advanced theoretical approaches is the basis for a successful advancement towards the heaviest species. Deformation, tri-axial behaviour and the prediction of single particle levels, pointing to the formation of the next proton and neutron shell gaps, are at the focus of RMF models, in particular including quasi particle vibrational coupling (QVC), and relativistic energy density functional calculations (REDF). In combination and in continuous exchange with ever advancing experimental nuclear structure results a successful approach towards the region of superheavy spherical shell stabilized species seams promising, in particular, given the perspectives opened by RIB facilities with EURISOL at the horizon.

**Isospin dependent ground and metastable state properties**

This topic was addressed by P. Stevenson, A. Raduta, A. Andreyev, P. Walker, G. Georgiev, A. Jungclaus and J. Pakarinen.

Experimental determination of ground-state properties, like charge radii, atomic masses, nuclear and magnetic moments, spin and parities can be obtained in a variety of experiments. Precision experiments and model independent techniques are often applied at ISOL facilities providing high intensities and cold low-energy beams. In few rare cases also post-accelerated radioactive ion beams can be employed. Isotope shifts measurements have been a rich source of model independent information for charge radii. The data is mainly coming from the present ISOL-facilities which provide intense enough beams of exotic nuclei with ion optical properties matching the requirements of optical spectroscopic setups. In a simple liquid drop type of picture, charge radii have a simple mass dependence $d < r2 > \propto (dA)/(A^{1/3})$. In reality, the nature is more complex and some of the isotopic chains demonstrate large deviations – implying action of the underlying nuclear structure. One of the early examples of such deviations is a kink in the charge radii of lead isotopes. Various theoretical models have been applied to reproduce such behaviour, but a fully consistent approach is still missing. Additional challenges for theories are set by other

discontinuities observed experimentally. With the EURISOL facility, low-energy radioactive ion beams will cover longer isotopic chains while target and ion source development will make new elements available for similar studies.

Isomeric states play a special role in nuclear structure studies. The existence of such states has different origin. Some of the isomeric states are trapped by potential energy variation due to different shapes (shape isomerism). Others are trapped by large spin difference compared to neighbouring states and a third possibility is related to K quantum number traps (so called K-isomers). In all cases, the observation of isomers and the measurement of the decay characteristics (lifetime and excitation energy) provide information on the underlying nuclear structure. Depending on the lifetime of isomers, different techniques have been applied. Some of the modern techniques include storage ring measurements and ion trap techniques. With the EURISOL facility such studies can be extended into regions not available at present ISOL-facilities.

The equation of the state (EOS) of asymmetric nuclear matter has great influence on astrophysics and testing of nuclear models. Experimentally the symmetry energy of the EOS is rather poorly known. Experiments over a wide range of densities and over a large difference in N and Z, i.e. over a wide energy range and using RIB's, respectively, are required. Other facilities, like SPIRAL2 and FAIR will cover energy ranges below 14 MeV/u and beyond 200 MeV/u. The unique opportunity for EURISOL would be to match the intermediate energy range with exotic species.

Nuclear and magnetic moments are rich sources of structure information, like valence particle configurations, nuclear deformation, effective charges and collective properties. A variety of techniques have been applied for low-energy beams from ISOL facilities, for post-accelerated radioactive ion beams and with ions produced in fragmentation reactions. With EURISOL the capabilities of the two first types of experiments can be enhanced, while the use of fragmentation reactions can only be considered if post accelerated beams can reach high enough energies, beyond 150 MeV/u.

Experimental studies of fission reactions have provided a vast amount of mass and charge distribution data. In some cases also total kinetic energies of fission fragments have been measured. These studies have mainly concentrated on two regions; pre-actinides and heavy actinides. With beta-delayed fission, fission studies can be extended to nuclides farer from stability as demonstrated at ISOLDE, where two regions of interest have been explored: neutron deficient nuclei with A=180-200 (N/Z=1.22-1.3) and neutron-rich nuclei with A~230 (N/Z=1.6). The next step of such studies would require identification of fission fragments, measurement of total kinetic energies of fission fragments and further exploration of odd-even staggering. This demands an order of magnitude higher yields as compared to the capability of the present facilities. The EURISOL facility would enable such studies.

## Facilities and instrumentation

This topic was addressed by I. Kelson, Ł. Standyło, L. Trache and J. Srebrny

Technical progress is essential for successful planning, construction and operation of next generation RIB facilities and any further development towards EURISOL. Following the development of instrumentation and accelerator components like separators, detection techniques and ion sources are as essential for the technological progress towards EURISOL as is the experience gained in present facilities, in particular such which apply and further develop the isotope separation online (ISOL) method.

## Conclusion

The next generation RIB facilities with EURISOL in sight are promising interesting opportunities for the physics at the extremes of mass, temperature, spin and isospin. Exploration of the chart of nuclides towards extreme isospin, in particular neutron rich species, highest excitation, mass and Z might receive a boost towards new shores in understanding extremely exotic nuclear species. This workshop has discussed many facets of these exciting perspectives. The following contribution summaries show in detail the visions presented at the 4$^{th}$ EURISOL TOPICAL MEETING, held in Krakow from July 1$^{st}$ to 3$^{rd}$ 2013.

**EURISOL User Group Topical Meeting 2013**
**1-3.07.2013, Kraków, Poland**

# WORKSHOP PROGRAM

## July 1st, Monday

***10:00 – 11:00 Visit to Collegium Maius museum***
***12:00 – 13:30 Registration and buffet***

### Session I, Chairperson: Adam Maj (Kraków)

| | |
|---|---|
| 13:30 - 14:00 | **Yorick Blumenfeld (Orsay)**<br>Latest news about EURISOL |
| 14:00 - 14:30 | **Dieter Ackermann (Darmstadt)**<br>Opportunities for SHE related research at RIB facilities |
| 14:30 - 15:00 | **Michael Block (Darmstadt)**<br>Perspectives for mass measurements (and potentially laser spectroscopy) of the heaviest elements for nuclear structure studies |
| 15:00 - 15:30 | **Valeriy Zagrebaev (Dubna)**<br>Production of heavy and superheavy neutron-rich nuclei |
| 15:30 - 15:50 | **Katarzyna Mazurek (Kraków)**<br>Study of spontaneous fission life-times using nuclear density functional theory |
| 15:50 - 16:10 | **Carmelo Rizzo (Catania)**<br>Fusion dynamics with exotic beams |
| 16:10 - 16:30 | **Paola Marini (Caen)**<br>Constraining the symmetry energy from experimental primary fragment distributions |
| *16:30 - 17:00* | ***Coffee break*** |

### Session II, Chairperson: Lidia Ferreira (Lisbon)

| | |
|---|---|
| 17:00 - 17:30 | **Thomas Duguet (Saclay)**<br>Low-lying spectroscopy of complex nuclei from state-of-the-art multi-reference energy density functional calculations |
| 17:30 - 18:00 | **Vaia Prassa (Jyväskylä)**<br>Structure of heavy and superheavy nuclei with Energy Density Functionals |
| 18:00 - 18:30 | **Elena Litvinova (East Lansing)**<br>Nuclear shell structure and response toward the limits of mass and isospin |
| 18:30 - 19:00 | **Paul Stevenson (Surrrey)**<br>Why is lead so kinky? |
| 19:00 - 19:20 | **Adriana Raduta (Bucarest)**<br>Clusterized nuclear matter in the (proto-)neutron star crust and the symmetry energy |
| 19:20 - 19:40 | **Bartek Szpak (Kraków)**<br>Bayesian Inference and nuclear structure models |
| 19:40 - 20:00 | **Artur Dobrowolski (Lublin)**<br>Estimates of Electric Transitions in $^{156}$Gd Nucleus |
| 20:00 | ***EURISOL User Executive Committee meeting (closed)*** |

## July 2nd, Tuesday

### Session III, Chairperson: Maria Borge (CERN)

| | |
|---|---|
| 9:00 - 9:30 | **Krzysztof Pomorski (Lublin)**<br>Binding energies and fission barrier heights of exotic nuclei |
| 9:30 - 10:00 | **Greg Henning (Darmstadt)**<br>Entry distribution measurements: principles and the example of $^{254}$No |
| 10:00 - 10:30 | **Beatriz Jurado (Bordeaux)**<br>Excitation-energy sorting in fission |
| 10:30 - 11:00 | **Andrei Andreyev (York)**<br>Beta-delayed fission: from neutron-deficient to neutron-rich nuclei |
| *11:00 - 11:30* | ***Coffee Break*** |

### Session IV, Chairperson: Krzysztof Rusek (Warsaw)

| | |
|---|---|
| 11:30 - 11:50 | **Itzhak Kelson (Tel Aviv)**<br>The use of on-line isotope separators for the direct production of generators of medically relevant alpha-emitters |
| 11:50 - 12:10 | **Łukasz Standyło (Warsaw)**<br>Optimization of multiple-frequency heating and gas mixing in ECR charge breeders |
| 12:10 - 12:30 | **Livius Trache (Bucarest)**<br>26mAl isomeric and other RIBs at Texas A&M University |
| 12:30 - 12:50 | **Julian Srebrny (Warsaw)**<br>The central European Array for Gamma Levels Evaluation (EAGLE) |
| *12:50 - 14:00* | ***Buffet*** |

### Session V, Chairperson: Jan Styczeń (Kraków)

| | |
|---|---|
| 14:00 - 14:30 | **Jerzy Dudek (Strasbourg)**<br>Symmetry breaking at high temperatures and spins: nuclear Jacobi and Poincare shape transitions |
| 14:30 - 15:00 | **John Simpson (Daresbury)**<br>Nuclear shapes at the highest spins |
| 15:00 - 15:30 | **Emmanuel Clement (Caen)**<br>Opportunities in shape coexistence studies using in-beam gamma ray spectroscopy |
| 15:30 - 15:50 | **Katarzyna Wrzosek-Lipska (Leuven)**<br>Shape coexistence in the neutron-deficient, even-even $^{182\text{-}188}$Hg isotopes |
| 15:50 - 16:10 | **Natalia Cieplicka (Kraków)**<br>Yrast structure of the $^{205,206,210}$Bi isotopes produced in deep-inelastic reactions |
| *16:10 - 16:40* | ***Coffee Break*** |

### Session VI, Chairperson: Bertram Blank (Bordeaux)

| | |
|---|---|
| 16:40 - 17:10 | **Phil Walker (Surrey)**<br>Isomers, shapes and shells in heavy neutron-rich nuclei |
| 17:10 - 17:40 | **Georgi Georgiev (Orsay)**<br>Nuclear moments with neutron-rich and heavy radioactive beams. What could we aim for? |
| 17:40 - 18:10 | **Andrea Jungclaus (Madrid)**<br>Beta decay and isomer spectroscopy in the $^{132}$Sn region: Present status and future perspectives |
| *19:15* | ***Departure of the buses to Przegorzaly Castle*** |

## July 3rd, Wednesday

### Session VII, Chairperson: Marta Kicińska-Habior (Warsaw)

| | |
|---|---|
| 9:00 - 9:30 | **Janne Pakarinen (Jyväskylä)**<br>Shapes and collectivity in heavy nuclei probed with radioactive beams at REX-ISOLDE |
| 09:30 - 10:00 | **Wojciech Satuła (Warsaw)**<br>Isospin mixing within the multi-reference nuclear DFT and beyond - selected aspects |
| 10:00 - 10:30 | **Franco Camera (Milan)**<br>Isospin mixing at high T from GDR experiments: status and perspectives |
| 10:30 - 10:50 | **Luna Pellegri (Milan)**<br>High lying nuclear states via inelastic scattering of $^{17}$O |
| 10:50 - 11:10 | **Michał Ciemała (Kraków)**<br>Giant Dipole Resonance decay of hot rotating $^{88}$Mo |
| *11:10 - 11:40* | ***Coffee Break*** |

### Session VIII, Chairperson: Angela Bonaccorso (Pisa)

| | |
|---|---|
| 11:40 - 12:10 | **Giovanni Pollarolo (Torino)**<br>Deep inelastic reactions - as tools towards high Z and A |
| 12:10 - 12:40 | **Giovanni Casini (Firenze)**<br>Fragment production and isospin related phenomena in heavy ion collisions |
| 12:40 - 13:10 | **Bogdan Fornal (Kraków)**<br>Yrast spectroscopy of neutron-rich heavy nuclei studied in deep-inelastic collisions |
| 13:10 - 13:40 | **Ari Jokinen (Jyväskylä)**<br>Summary of the meeting |
| 13:40 | **Angela Bonaccorso (Pisa)**<br>***End of the meeting*** |

# LIST OF PARTICIPANTS

Dieter Ackermann
Andrei Andreyev
Piotr Bednarczyk
Bertram Blank
Michael Block
Yorick Blumenfeld
Angela Bonaccorso
Rafał Broda
Franco Camera
Giovanni Casini
Michał Ciemała
Natalia Cieplicka
Emmanuel Clement
Mikail Direkci
Artur Dobrowolski
Jerzy Dudek
Thomas Duguet
Beata Dyląg
Lídia Ferreira
Bogdan Fornal
Maria Jose Garcia Borge
Georgi Georgiev
Greg Henning
Lukasz Iskra
Jerzy Jastrzębski
Marek Jeżabek
Ari Jokinen
Andrea Jungclaus
Beatriz Jurado
Itzhak Kelson
Marta Kicińska-Habior
Maria Kmiecik
Tomasz Kozik
Wojciech Królas
Mateusz Krzysiek
Elena Litvinova
Enrico Maglione
Adam Maj
Tomasz Marchlewski
Paola Marini
Magdalena Matejska-Minda
Katarzyna Mazurek
Witold Męczyński
Paweł Napiorkowski
Małgorzata Niewiara
Janne Pakarinen
Tomasz Pawłat
Luna Pellegri
Giovanni Pollarolo
Krzysztof Pomorski
Vaia Prassa
Adriana Raduta
Carmelo Rizzo
Krzysztof Rusek
Wojciech Satuła
John Simpson
Julian Srebrny
Łukasz Standyło
Paul Stevenson
Jan Styczeń
Bartłomiej Szpak
Livius Trache
Tomasz Twaróg
Phil Walker
Władysław Waluś
Paweł Wasiak
Barbara Wasilewska
Jacek Wrzesiński
Katarzyna Wrzosek-Lipska
Valeriy Zagrebaev
Wiktor Zipper

# Opportunities for SHE related research at RIB facilities

D. Ackermann

*GSI Helmholtzzentrum für Schwerionenforschung GmbH, 64291 Darmstadt, Germany*

**Abstract.** Modern model predictions locate the so called "island of stability" for superheavy elements (SHE) at proton numbers 114, 120 or 126 and neutron number 184. This region is unreachable by fusion reactions with available projectile-target combinations, but n-rich exotic species are required instead. Since recently deep inelastic reactions are considered as alternative approach to populate SHE in the high A and high Z tail of the mass distribution after massive nucleon transfer. Also here n-rich projectiles would be desirable. Next generation rare isotope (RIB) beam facilities like SPIRAL2 at GANIL, RIKEN, FRIB and FAIR are, however, limited in beam intensity. Estimates show for EURISOL an up to a factor of 1000 higher number of RIB projectiles extending the access to more neutron rich species by up to 8 or 9 neutrons.

**Keywords:** Superheavy elements, fusion, fission, nuclear structure, multinucleon transfer, spin distribution
**PACS:** 21.10.Dr, 21.10.Hw, 21.10.Pc, 23.35.+g, 23.60.+e, 24.60.Dr, 24.75.+i, 25.60.-t, 25.60.Je, 25.60.Pj, 25.70.Gh, 25.70.Hi, 25.70.Jj

## INVESTIGATING THE HEAVIEST NUCLEAR SPECIES

The search for SHE has yielded exciting new results throughout the last one to two decades [1, 2, 3, 4]. Decay patterns observed at FLNR/JINR, Dubna for $^{48}$Ca induced reactions on actinide targets [3] have been confirmed for various systems at GSI Darmstadt, Germany and LBNL Berkeley, U.S.A. [5, 6, 7]. Despite these achievements the "island of stability" is still out of reach for projectile-target combinations provided by nature. The production of SHN is governed by the formation probability in the entrance channel as well as by the competition between n-emission and fission during the de-excitation phase of the compound nucleus (CN) in the exit channel. Both phases, are determined by subtle balances of barrier properties like the fusion barrier distribution and fission barrier features. Nuclear structure features of the reaction participants play a decisive role. Reaction mechanism studies and the investigation of specific nuclear structure features provide valuable information for the understanding of the collision details as well as on the stability of the heaviest nuclei. A summary of the up to date studied heaviest species is given in Fig.1. One alternative tool to study the fusion barrier is the CN spin distribution [8]. The competition of fission and $\alpha$-decay for ground and excited states, the deformation and other nuclear structure features like K isomeric states [9, 10] of heavy nuclei contribute to the understanding of the origin of the predicted stabilization of SHE and provide valuable information which are essential to refine the models. As an alternative production scheme for SHN Zagrebaev and Greiner proposed recently multi nucleon transfer reactions. The high A/high Z tail of the distribution of species produced in the collisions of heavy partners should reach into the region of (pos-

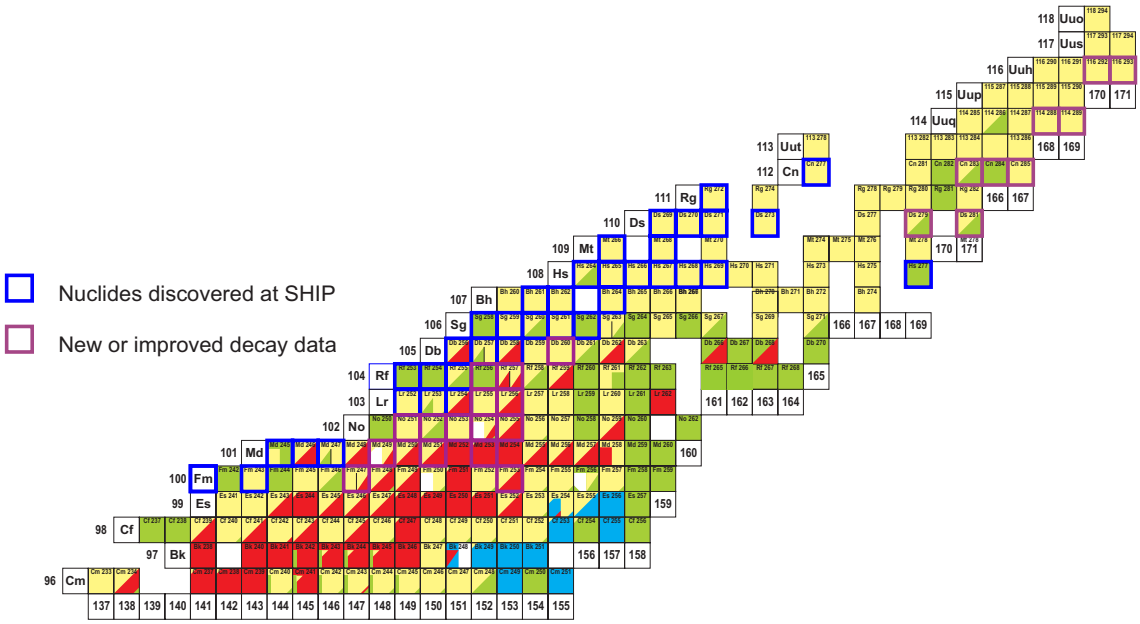


**FIGURE 1.** Upper right part of the chart of nuclides summarizing the isotopes studied up to date. Nuclides studied at the velocity filter SHIP of GSI are indicated by blue and red squares.

sibly new) SHE [11]. The investigations of SHN can be viewed as a staged approach with the final objective to understand in detail the properties of those extreme nuclear species and the fundamental interactions being responsible for them. The first stage is synthesis, typically producing only a few or even only one nucleus, followed by an optimization of the production techniques in order to allow for more detailed studies of their nuclear structure. Here basically two methods are employed, decay spectroscopy after beam separation, revealing already for a low number of events nuclear structure features, and in-beam studies which then allow for access to higher excitation energy and spin. Reaction mechanism studies and continuous method development are essential for progressing to ever higher numbers of protons and neutrons, and towards ever smaller cross sections. With typical beam intensities of $\approx 10^{12-13}$ p/s SHN have been synthesized up to Z = 118 and N = 171[3]. Decay studies have reached $^{270}$Ds discovering $K$-isomers in this nucleus with Z = 110 [10] and in its $\alpha$ decay daughter $^{266}$Hs [12]. Employing in-beam spectroscopy, a rotational band could be populated up to 20 $\hbar$ in $^{256}$Rf, a nucleus with 104 protons [13]. In the early days of SHE studies it was believed that systems with such a large number of protons would not survive the slightest rotation due to the high Coulomb repulsion and disrupt immediately. In table 1 cross sections and production rates are listed for a number of nuclei. With typical rates for present stable beam facilities ($\approx 10^{12}$ p/s) in-beam studies are possible down to cross sections of about 10 nbarn. Basic structure features can still be studied down to cross section values of $\approx$ 10 pbarn in decay spectroscopy after separation from the primary beam, using particle (recoil, $\alpha$ and $e^-$) and photon ($\gamma$ and X-ray) coincidence measurements. SHE synthesis experiments have been performed down to a few 10th of fbarn, however, with irradiation times of years (553 days) [14].

**TABLE 1.** Cross sections and production rates at SHIP for beam currents of $10^{12}$ p/s and $10^{9}$ p/s, respectively.

| reaction | cross section [nbarn] | production rate beam current $10^{12}$p/s | beam current $10^{9}$p/s |
|---|---|---|---|
| $^{208}$Pb($^{48}$Ca,2n)$^{254}$No | 2000 | 15000 /h | 15 /h |
| $^{206Pb}$($^{48}$Ca,2n)$^{252}$No | 430 | 3300 /h | 3.3 /h |
| $^{206Pb}$($^{48}$Ca,3n)$^{251}$No | 25 | 200 /h | 0.2 /h |
| $^{208Pb}$($^{50}$Ti,2n)$^{256}$Rf | 17 | 140 | 0.1 /h |
| $^{209Bi}$($^{40}$Ar,2n)$^{247}$Md | 7 | 80 | 2 /d |
| $^{208Pb}$($^{54}$Cr,1n)$^{261}$Sg | 2 | 15 | 0.4 /d |
| $^{207Pb}$($^{64}$Ni,1n)$^{270}$Ds | 0.013 | 1 /d | 0.4 /y |

## RARE ISOTOPE BEAMS AND SHN RESEARCH

Next generation RIB facilities like SPIRAL2 at GANIL, RIKEN, FRIB and FAIR provide n-rich beams with rather limited intensities. For FAIR projectile rates of $10^{9}$ p/s are estimated for projectiles in the medium mass region with about two more neutrons with respect to the last stable isotope (Fig.2). At EURISOL beam currents are estimated to be a factor of $\approx$ 1000 higher (in-target production) according to reference [15], leading to nuclides with up to eight or nine more neutrons at the same projectile rate. This will allow for more extended isospin dependent systematic reaction mechanism and nuclear structure studies for the various experiment classes as discussed at the end of the previous section. For the production of SHE, to eventually reach the "island of stability", the possibilities also here are still limited. The reaction $^{68}$Ni + $^{238}$U would lead to $^{306}$120, being two neutrons beyond the predicted magic neutron number of N = 184, but still with limited beam intensities, far from the ones necessary for SHE synthesis. Alternative approaches like deep inelastic reactions [11], could also profit from n-rich beams and extend the tail of their mass distribution towards high Z and and high N. In a first test Loveland et al. observed enhanced yields for trans-target reaction products for $^{160}$Gd + $^{184}$W [16]. Systematic studies of this type could clarify the potential of this method in exploring SHN. It has been shown that the CN spin distribution can be used as an alternative method to study the fusion barrier distribution [8]. In this case a complete scan of the fusion barrier in terms of partial wave cross sections can be obtained at one beam energy, rather then measuring a precise fusion excitation function with high statistics and many small energy steps.

In conclusion, RIB facilities will provide opportunities for systematic SHE research, covering reaction mechanism studies and nuclear structure investigations. EURISOL will push the limits even further towards n-rich species. On the basis of cross sections experienced nowadays it seems unlikely that the “island of stability” can be reached. However, the behavior of exotic n-rich species, exhibiting possibly features like neutron skin or similar exotic spatial nucleon distributions, in heavy ion collisions is yet unknown. Properties like deformation or the excitation of specific structures in projectile and/or target, however, have been proven to influence strongly reaction cross sections, in particular close to the interaction barrier [18].

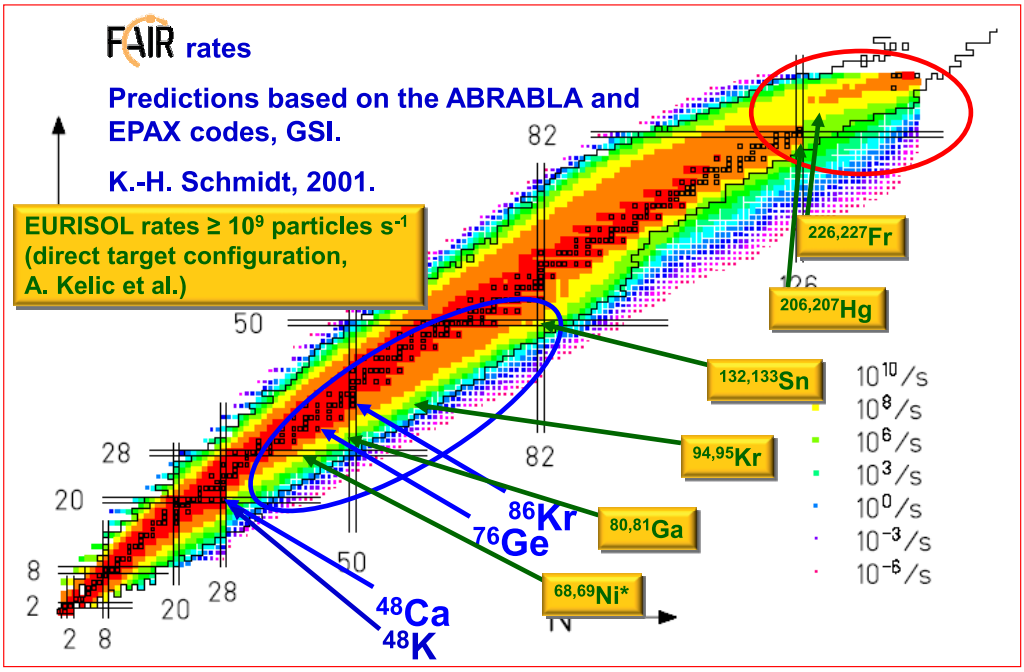


**FIGURE 2.** Yields for rare isotopes for FAIR[17]. Indicated are selected nuclides for which $\approx 10^9$ p/s are estimated to be obtained at FAIR (blue arrows/labels) and at EURISOL (yellow arrows/labels; in-target production) [15].

## REFERENCES


1. Y. T. Oganessian, et al., *Phys. Rev. C* **62**, 041604(R) (2000).
2. S. Hofmann, and G. Münzenberg, *Rev. Mod. Phys.* **72**, 733 (2000).
3. Y. T. Oganessian, *J. Phys. G: Nucl. Part. Phys.* **34**, R165 (2007).
4. K. Morita, et al., *J. Phys. Soc. Jpn.* **73**, 2593 (2004).
5. S. Hofmann, et al., *Eur. Phys. J.* **32**, 251 (2007).
6. C. E. Düllmann, et al., *Phys. Rev. Lett.* **104**, 252701 (2010).
7. L. Stavsetra, et al., *Phys. Rev. Lett.* **103**, 132502 (2009).
8. D. Ackermann, et al., *Eur. Phys. J.* **A20**, 151 (2004).
9. R.-D. Herzberg, and P. Greenlees, *Prog. Part. Nucl. Phys.* **61**, 674 (2008).
10. S. Hofmann, et al., *Eur. Phys. J.* **10**, 5 (2001).
11. V. I. Zagrebaev, and W. Greiner, *Phys. Rev. C* **87**, 034608 (2013).
12. D. Ackermann, et al., *GSI Report 2012-1* p. 208 (2012).
13. P. T. Greenlees, et al., *Phys. Rev Lett.* **109**, 012501 (2012).
14. K. Morita, et al., *J. Phys. Soc. Jpn.* **81**, 103201 (2013).
15. A. Kelic, et al., *EURISOL Design Study Task11, www.eurisol.org* (2009).
16. W. Loveland, et al., *Phys. Rev. C* **83**, 044610 (2011).
17. K.-H. Schmidt, et al., *FAIR Conceptual Design Report, www.fair-center.de* (2001).
18. M. Dasgupta, et al., *Annu. Rev. Nucl. Part. Sci.* **48**, 401 (1998).

# Mass Measurements and Laser Spectroscopy of the Heaviest Elements

Michael Block[a,b]

[a]*GSI Helmholtzzentrum fuer Schwerionenforschung, Planckstrasse 1, 64291 Darmstadt*
[b]*Helmholtzinstitut Mainz, 55099 Mainz*

**Abstract.** High-precision mass measurements have provided accurate binding energies for numerous radionuclides in recent years. This information has been complemented by data from laser spectroscopy on nuclear spins, nuclear moments, and mean square charge radii. In this combination various properties of nuclear ground states and long-lived isomeric states for nuclear structure and nuclear astrophysics studies have been obtained challenging modern nuclear theories. Utilizing reaccelerated radioactive beams for fusion-evaporation and multi-nucleon transfer reactions EURISOL will open the door towards more neutron-rich isotopes of the heaviest elements. This will enable advanced studies of the nuclear structure evolution in this region that is also crucial to the astrophysical r-process.

**Keywords:** Mass measurements, laser spectroscopy, superheavy elements.

**PACS:** 27.90.+b Properties of superheavy elements, 21.10.Dr Binding energies and masses, 82.80.Ms Mass spectrometry, 42.62.Fi Laser spectroscopy

## MASS MEASUREMENTS OF RADIONUCLIDES

High-precision mass measurements of radionuclides provide accurate absolute values of nuclear binding energies and reveal information on the structure of exotic nuclei far away from stability. The evolution of structural features can be tracked and amplified by appropriate filters like two-nucleon separation energies and the so-called shell gap parameter that display shell closures and the onset of deformation. Investigations of radionuclides at the limits of existence with extreme proton-neutron ratios are of particular interest as they often exhibit features not present in nuclei close to stability. Masses thus often provide a first indicator of new structural phenomena in previously unexplored regions of the nuclear chart. Moreover, *Q*-values, i.e. mass differences, determine the energy available for nuclear decays. They allow the identification of exotic decay modes [1] and play an important role in nuclear astrophysics determining the pathway of a given nucleosynthesis process [2]. In general accurate masses of radionuclides provide an excellent benchmark for theoretical nuclear models [3].

The heaviest nuclei owe their very existence entirely to shell effects. The main scientific questions addressed in mass measurements of the heaviest elements are thus the location, the extension, and the strength of shell closures. Experimental data from

decay spectroscopy indicate that shell closures are in some cases rather local effects that fade away quickly, for example around $^{270}$Hs with $Z$ = 108 and $N$ = 162 [4]. Theoretical predictions comparing different parameterizations of energy density functionals demonstrate that instead of distinct magic numbers one may even expect extended regions of enhanced stability in the heaviest nuclei [5].

An accurate measurement of the location and strength of shell effects in the heaviest elements by Penning trap mass spectrometry (PTMS) have not been possible for a long time. The challenges that had to be handled were a very low yield of well below one particle per second and the high energy at which these nuclides are produced. The first direct mass measurements of nobelium and lawrencium isotopes have only been performed recently in pioneering experiments with the Penning trap mass spectrometer SHIPTRAP at GSI [6, 7]. These measurements allowed the mapping the strength of shell effects around neutron number $N$ =152 in nobelium and lawrencium. In addition, the accurate mass values from PTMS yield anchor points to pin down alpha-decay chains originating from superheavy elements, for example the mass of $^{270}$Ds can be fixed with an uncertainty of about 40 keV [7,8]. Several developments like single-ion mass measurement techniques will extend the reach to heavier elements in the near future.

Mass measurements with highest precision are nowadays performed mainly with Penning traps [9]. The mass $m$ of a nuclide is obtained from a measurement of the cyclotron frequency $f_c$ of its ionic state with charge $q$ in a magnetic field of strength $B$ according to the relation

$$f_c = \frac{qB}{2\pi m}. \qquad (1)$$

Originally PTMS has been pioneered at isotope separator on-line (ISOL) facilities that are well suited providing radioactive beams at low energies of a few ten keV. However, the ISOL technique has limitations accessing certain elements, for example refractory elements. Hence, PTMS has been adopted for other production schemes including fast-beam fragmentation and fusion-evaporation reactions. Thus, the access to the elements heavier than uranium by PTMS is now also feasible. Since the nuclides of interest are produced at much higher energies than at ISOL facilities and with rather poor beam quality two developments have been crucial for a successful implementation. The use of buffer gas stopping has paved the way to slow down nuclides of essentially all elements efficiently [10] while radiofrequency quadrupole (RFQ) cooler and buncher devices [11] allow preparing them as bunched low-emittance beams at an energy suitable for PTMS.

The typical layout of a Penning trap mass spectrometer is shown in Fig. 1. The reaction products are separated from the primary beam in a recoil separator. Then they are slowed down in a buffer gas stopping cell, cooled and bunched in a RFQ ion-beam cooler, and finally transferred to a Penning-trap system. Its first stage is a purification trap where unwanted ions including nuclear isobars are removed by a mass-selective cooling and centering procedure. Alternative or additional purification schemes

utilizing a multi-reflection time-of-flight mass spectrometer have recently been introduced [12].

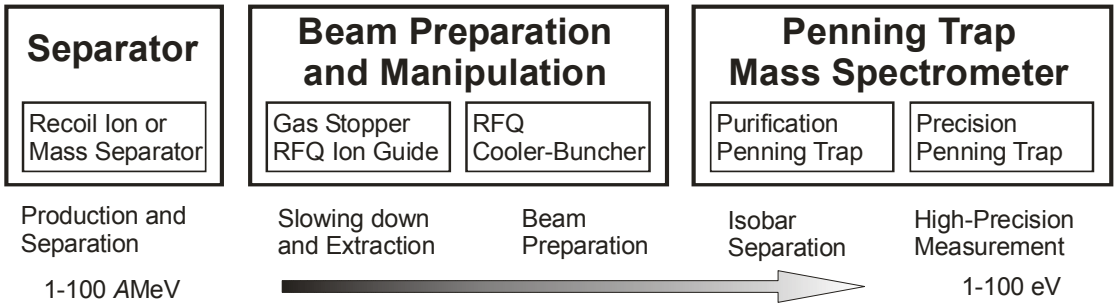


**FIGURE 1.** Schematic layout of a Penning trap mass spectrometer.

In a precision trap the actual mass measurement is performed. In PTMS masses of radionuclides are nowadays measured with relative uncertainties on the order of $10^{-8}$. PTMS is applicable to nuclides with half-lives of about 10 ms and above, while the required yield is presently on the order of particles per minute.

## LASER SPECTROSCOPY OF THE HEAVIEST ELEMENTS

Laser spectroscopic studies of radionuclides by resonance ionization spectroscopy (RIS) or collinear laser spectroscopy provide information of nuclear properties of ground and long-lived excited states in a nuclear-model independent way [13]. In particular, they give access to the nuclear spin, to nuclear moments, and to the mean square charge radius providing information about the evolution of deformation. In the case of the heaviest elements in addition the strong influence of relativistic effects and of quantum electrodynamics on the atomic structure is in the focus. These effects are studied by atomic level energies, ionization potentials, and lifetimes of excited atomic states. The heaviest elements thus combine the interest of atomic and nuclear physics.

Similar to PTMS the low yield and the high energy at which the nuclides are created poses a challenge. In addition, there is a lack of knowledge about atomic levels in the heaviest elements. At present fermium is the heaviest element in which atomic levels have been identified experimentally [14]. RIS in buffer gas cells provides a sensitive tool for laser spectroscopic investigations of radionuclides with yields as low as about 0.1 particles per second and is ideally suited for the search of atomic levels in the heaviest elements. In this method the nuclides of interest are stopped in an inert buffer gas and RIS is performed on the neutral fraction. If the reaction target is installed in the gas cell then the ionization in the gas typically results in a dominant fraction surviving as neutralized atoms. If the gas cell is installed behind a recoil separator a slightly different approach that has been developed in particular for the elements nobelium and lawrencium [15] is pursued. Theoretical atomic structure predictions by relativistic coupled cluster techniques [16] and multi-configuration Dirac-Fock calculations [17] are crucial to guide the atomic level search. Moreover, they are essential to extract mean square charge radii from isotope shift measurements.

Due to the Doppler broadening the resolution of laser spectroscopy inside a gas cell is limited. Thus, once atomic levels have been identified techniques like collinear laser spectroscopy in conjunction with cooled and bunched beams will be utilized to achieve higher resolution. Recently in-gas jet laser spectroscopy has been shown to offer an attractive alternative [18]. This will pave the way for measurements studying the evolution of deformation in long isotopic chains covering for example the neutron shell closures at $N = 152$ for different elements around nobelium.

## CONCLUSIONS

Mass spectrometry and laser spectroscopy have experienced a renaissance in recent years fueled by the development of many novel methods and sensitive techniques that extended their reach to more exotic nuclides. A versatile toolbox for studies of various nuclear properties of ground and long-lived isomeric states is at hand providing accurate data for nuclear structure and astrophysics studies. In addition, the combination of laser spectroscopy and PTMS opens up possibilities for novel experiments. For example, the high selectivity of laser spectroscopy in combination with mass spectrometric separation allows preparing beams of highest purity for laser/trap-assisted decay spectroscopy experiments. In certain cases even state-selected beams can be prepared. Moreover, the use of laser ion sources has gained ever more importance at ISOL facilities to deliver high-purity beams to experiments.

An additional motivation for the application of these methods at EURISOL is the potential to access more neutron-rich, supposedly longer-lived, isotopes of the heaviest elements that can be produced in fusion-evaporation and in multi-nucleon transfer reactions with intense reaccelerated radioactive beams.

## REFERENCES


1. M. Pfuetzner et al., *Nucl. Instrum. Methods* B **266,** 4153 (2008).
2. F. -K. Thielemann, A. Arcones, A.; R. Kaeppeli, R. et al., *Prog. Nucl. Part. Phys.***66**, 346 (2011).
3. D. Lunney, J. Pearson, C. Thibault, *Rev. Mod. Phys.***75**, 1021 (2003).
4. J. Dvorak et al., *Phys. Rev. Lett.* **97**, 242501 (2007).
5. M. Bender et al., *Phys. Lett. B* **515**, 42 (2001).
6. M. Block et al., *Nature* **463**, 785 (2010).
7. E. Minaya Ramirez et al., *Science* **337**, 1207 (2012).
8. D. Ackermann et al., *GSI scientific report 2011-1*, 200 (2011).
9. K. Blaum, *Phys. Rep.*, **205**, 1 (2006).
10. G. Savard, *J. of Phys. Conf. Series* **312**, 052004 (2011).
11. F. Herfurth et al., *Nucl. Instrum. Meth.A* **469**, 254 (2001).
12. F. Wienholtz et al., *Nature* **498**, 346 (2013).
13. B. Cheal and K.T. Flangan, *J. Phys. G* **37**, 113101 (2010).
14. M. Sewtz et al., *Phys.Rev. Lett.* **90**, 163002 (2003).
15. H. Backe et al., *Eur. Phys. J. D* **45**, 99 (2007).
16. A. Borschevsky et al., *Eur. Phys.J. D* **45**, 99 (2007).
17. S. Fritzsche, *Eur. Phys.J. D* **33**, 15 (2005).
18. Yu. Kudryavtsev et al., *J. Instrum. Meth. B* **297**, 7-22 (2013).

# Production of Heavy and Superheavy Neutron Rich Nuclei

V.I. Zagrebaev* and Walter Greiner†

*Flerov Laboratory of Nuclear Reactions, JINR, Dubna, Moscow Region, Russia
†Frankfurt Institute for Advanced Studies, J.W. Goethe-Universität, Frankfurt, Germany

**Keywords:** neutron-rich nuclei, superheavy elements, multinucleon transfers
**PACS:** 25.70.Jj, 25.70.Lm, 28.20.Fc, 28.70.+y

## Motivation

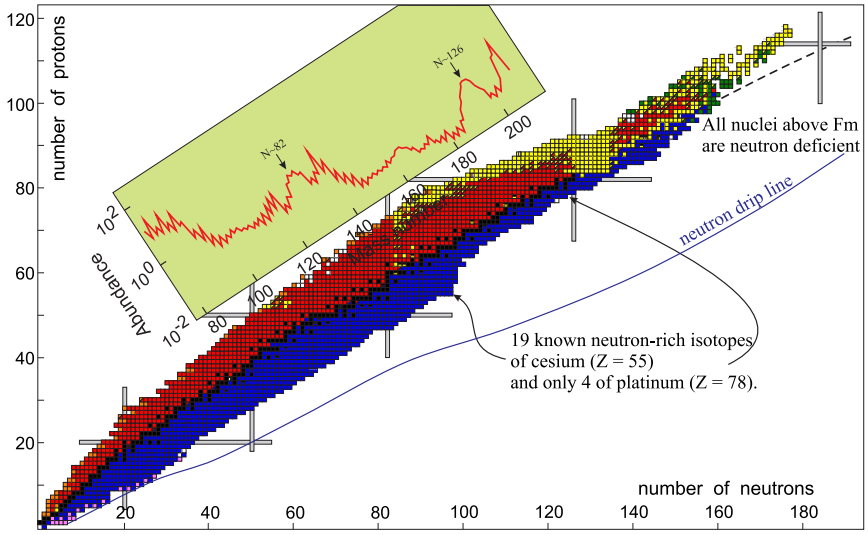


**FIGURE 1.** Nuclear map as it looks today. On the inset relative abundance of the elements in the universe is shown with clear visible maxima in the regions of the "waiting points" along the neutron closed shells $N = 82$ and $N = 126$.

The upper part of the present-day nuclear map consists mainly of proton rich nuclei, while the unexplored area of heavy neutron enriched nuclides (also those located along the neutron closed shell $N = 126$ to the right-hand side of the stability line) is extremely important for nuclear astrophysics investigations and, in particular, for the understanding of the r process of astrophysical nucleogenesis, see Fig. 1. For elements with $Z > 100$ only neutron deficient isotopes (located to the left of the stability line) have been synthesized so far. Due to the bending of the stability line toward the neutron axis, in fusion reactions only proton-rich isotopes of heavy elements can be produced. That is the main reason for the impossibility of reaching the center of the island of stability ($Z \sim 110 \div 120$ and $N \sim 184$) in the superheavy (SH) mass region by fusion reactions with stable projectiles. Moreover, the whole "northeast" area of the nuclear map is still terra incognita. Production and studying properties of nuclei located in this region will open a new field of research in nuclear physics. There are only three methods for the

production of heavy elements, namely, fusion reactions, a sequence of neutron capture and $\beta^-$ decay processes and multi-nucleon transfer reactions.

## Fusion reactions and neutron capture process

Fusion reactions of stable projectiles (even with actinide targets) lead to formation of neutron deficient isotopes of heavy elements located to the left of the stability line. Recently, many speculations appeared on the use of radioactive ion beams for the synthesis and study of new heavy elements and isotopes. The use of accelerated neutron enriched fission fragments for the production of SH nuclei in rather symmetric fusion reactions does not look very encouraging and needs beam intensities at the hardly reachable level of $10^{13}$ pps or higher [1]. The lighter radioactive ions could be more useful here. In fusion reactions of $^{18-20}$N, $^{20-22}$O or $^{22-24}$F with actinide targets new (though not so much neutron enriched) isotopes of elements with $Z > 100$ might be synthesized at rather low beam intensities of $10^8$ pps owing to much larger cross sections [1]. A hypothetical pathway to the middle of the island of stability was proposed recently owing to possible $\beta^+$ decay of SH nuclei located from the up–left side of this island [2]. Such nuclei could be formed in the ordinary fusion reactions $^{48}$Ca+$^{250}$Cm and/or $^{48}$Ca+$^{249}$Bk. In these reactions relatively neutron enriched isotopes of SH elements 114 and 115 are formed as $\alpha$ decay products of the corresponding evaporation residues. These isotopes should have rather long half-lives and, thus, they could be located already in the "red" area of the nuclear map, i.e., they may be $\beta^+$-decaying nuclei. If it is really true, the narrow pathway to the middle of the island of stability is surprisingly opened by production of these isotopes in subsequent $\alpha$-decays of elements 116 and/or 117 produced in the $^{48}$Ca+$^{250}$Cm and $^{48}$Ca+$^{249}$Bk fusion reactions. For the moment, this is the only method which is proposed for the production of SH nuclei located just in the middle of the island of stability.

The neutron capture process is an alternative (oldest and natural) method for the production of new heavy elements. The synthesis of heavier nuclei in the multiple neutron capture reactions with subsequent $\beta^-$ decay is a well studied process. The key quantity here is the time of neutron capture, $\tau_n = (n_0\sigma_{n\gamma}^{Z,A})^{-1}$, where $n_0$ is the neutron flux (number of neutrons per square centimeter per second) and $\sigma_{n\gamma}^{Z,A}$ is the neutron capture cross section. If $\tau_n$ is shorter than the half-life of a given nucleus $T_{1/2}(Z,A)$ then the next nucleus $(Z,A+1)$ is formed by neutron capture. Otherwise the nucleus $(Z,A)$ decays before it captures next neutron. In nuclear reactors typical value of $\tau_n \sim 1$ year, and the nucleosynthesis takes place along the stability line by a sequence of neutron capture and $\beta^-$ decay processes breaking at the short-living fissile fermium isotopes $^{258-260}$Fm (so called "fermium gap"). Recently it was shown that the multiple rather "soft" nuclear explosions could be really used for the production of a noticeable (macroscopic) amount of neutron rich long-living SH nuclei [3]. We found a sharp increase of the probability for formation of heavy elements with $Z \geq 110$ in the multiple neutron irradiations: enhancement by several tens of orders of magnitude! The same process of multiple neutron exposures might be also realized in pulsed nuclear reactors of the next generation. An increase of the neutron fluence by about three orders of magnitude as compared with existing pulsed reactors could be quite sufficient to

bypass the two gaps of fission instability [3].

## Multinucleon transfer reactions

Renewed interest in the multinucleon transfer reactions with heavy ions is caused by the limitations of other reaction mechanisms for the production of new heavy and SH nuclei (see above). Multinucleon transfer processes in near barrier collisions of heavy ions seem to be the most promising reaction mechanism allowing us to produce and explore neutron-rich heavy nuclei including those located at the SH island of stability. These are the shell effects which may significantly enhance the yield of SH nuclei for appropriate projectile–target combinations. Contrary to the conventional quasi-fission phenomena, in low-energy collisions of $^{238}$U with $^{248}$Cm target nucleons may predominantly move from the lighter partner to heavy one, i.e., U transforms to a Pb-like nucleus and Cm to complementary SH nucleus. In this case, appearance of the lead shoulder in the mass and charge distributions of the reaction fragments automatically leads to a pronounced shoulder in the region of SH nuclei. We named it "inverse" (anti-symmetrizing) quasi-fission process [4]. This process may really lead to enhanced yields of trans–target nuclides, see Fig. 2.

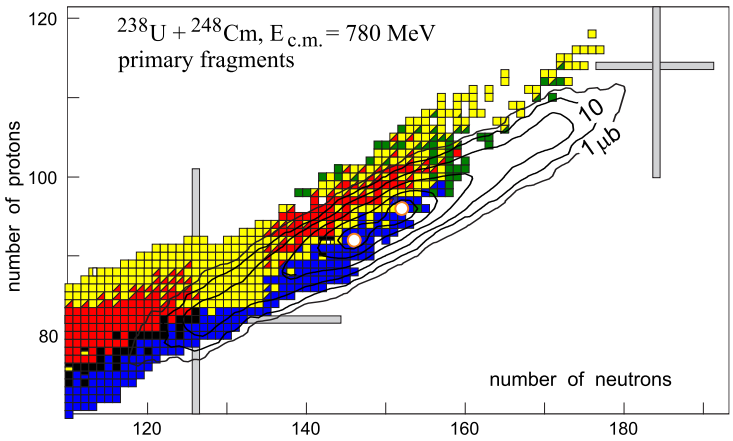


**FIGURE 2.** Landscape of the calculated cross sections for the production of primary reaction fragments in collisions of $^{238}$U with $^{248}$Cm target at $E_{\text{c.m.}}$=780 MeV.

Actinide beams (as well as actinide targets) might be successfully used also for the production of new neutron rich nuclei around the closed neutron shell $N = 126$, the region having largest impact on astrophysical r process. Near barrier collisions of $^{136}$Xe and $^{192}$Os with $^{208}$Pb target were predicted to be quite promising for the production of new nuclei with $N \sim 126$ [5, 6]. The corresponding cross sections were found to be about 1 $\mu$b and less. The use of heavy radioactive ion beams (such as $^{132}$Sn [6] or $^{154}$Xe [7]) gives a noticeable gain in the nucleon transfer cross sections. Low-energy collisions of stable neutron enriched isotopes of elements located below lead (such as $^{192}$Os or $^{198}$Pt) with available actinide nuclei look even more favorable for the production and study of new neutron rich nuclei located around neutron closed shell $N = 126$ [8]. Estimated cross sections for the production of the final (survived) isotopes of the elements with $Z = 71 \div 78$ in low energy collisions of $^{198}$Pt with $^{238}$U are shown in Fig. 3. On average, the cross sections for the production of new neutron rich heavy nuclei

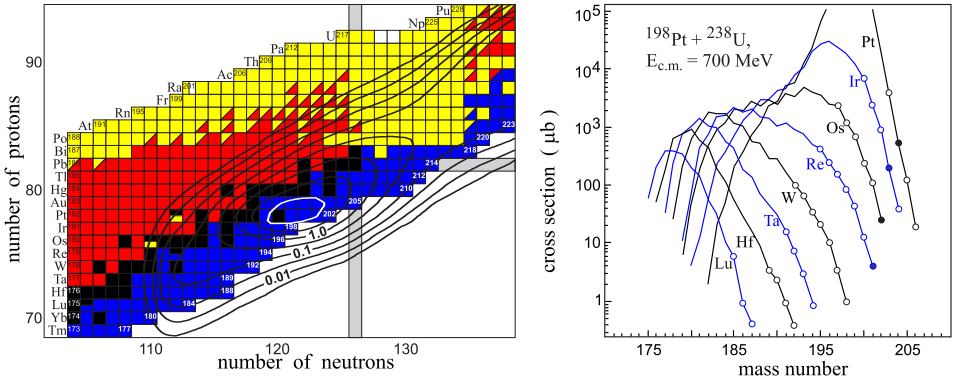


**FIGURE 3.** (Left panel) Contour plot of the cross sections (in logarithmic scale) for the formation of primary reaction fragments in collisions of $^{198}$Pt with $^{238}$U at $E_{\rm c.m.}$=700 MeV. Contour lines are drawn over half an order of magnitude and the units of measurement are shown in millibarns. (Right panel) Isotopic yields of elements below lead (from Lu to Pt) in collisions of $^{198}$Pt with $^{238}$U. Circles denote not-yet-known isotopes (with solid circles showing isotopes with the closed neutron shell $N = 126$).

(including those located along the closed neutron shell $N = 126$) in this reaction are higher than in collisions of $^{136}$Xe or $^{192}$Os with $^{208}$Pb target (though a contamination by uranium fission fragments probably may reduce this gain in the cross sections).

### Project GaLS

In contrast with fusion reactions it is more difficult to separate a given nucleus from all the transfer reaction products. The neutron rich heavy nuclei with $Z > 70$ formed in the multinucleon transfer reactions cannot be separated and studied at available setups created quite recently just for studying the products of deep inelastic scattering (such as VAMOS, PRISMA and others). These fragment separators (as well as other setups) cannot distinguish heavy nuclei with $Z > 70$ by their atomic numbers. However during the last several years a combined method of separation is intensively studied based on stopping nuclei in gas and subsequent resonance laser ionization of them (see, for example, [9]. One of such setups (named GaLS: in gas cell laser ionization and separation) is currently created at Flerov Laboratory (JINR, Dubna). Experiments at this setup aimed on the production and studying properties of new neutron rich heavy nuclei are planned to start in 2015.

## REFERENCES


1. V.I. Zagrebaev and W. Greiner, Phys. Rev. C **78**, 034610 (2008).
2. V.I. Zagrebaev, A.V. Karpov and W. Greiner, Phys. Rev. C **85**, 014608 (2012).
3. V.I. Zagrebaev, A.V. Karpov, I.N. Mishustin and W. Greiner, Phys. Rev. C **84**, 044617 (2011).
4. V.I. Zagrebaev et al., Phys. Rev. C **73**, 031602 (2006).
5. V. Zagrebaev and W. Greiner, Phys. Rev. Lett. **101**, 122701 (2008).
6. V.I. Zagrebaev and W. Greiner, Phys. Rev. C **83**, 044618 (2011).
7. C.H. Dasso, G. Pollarolo, A. Winther, Phys. Rev. Lett. **73** (1994) 1907.
8. V.I. Zagrebaev and W. Greiner, Phys. Rev. C **87**, 034608 (2013).
9. Yu. Kudryavtsev et al., Nucl. Instr. and Meth. Phys. Res. **B267** (2009) 2908.

# Study of spontaneous fission life-times using nuclear density functional theory

K. Mazurek[*,†] and J. Sadhukhan[†,**]

[*]*The Niewodniczanski Institute of Nuclear Physics - PAN, ul. Radzikowskiego 152, PL-31-342 Krakow, Poland*
[†]*Department of Physics and Astronomy, University of Tennessee, Knoxville, Tennessee 37996, USA*
*Physics Division, Oak Ridge National Laboratory, P. O. Box 2008, Oak Ridge, Tennessee 37831, USA*
[**]*On leave of absence from VECC, Kolkata, India.*

**Abstract.** The microscopic potential energy surface (PES) and the mass tensors obtained in a two-dimensional collective space of quadrupole moments ($Q_{20}$,$Q_{22}$) representing elongation and triaxiality, are main elements used to calculate the spontaneous fission life-times. These are obtained by solving the self- consistent Hartree-Fock-Bogoliubov (HFB) equations with the Skyrme energy density functional and mixed paring interaction. The perturbative Adiabatic Time-Dependent HFB approach according to Ref. [1] allows to compute the mass tensors. The numerical techniques Ritz Method (RM) and the Dynamical Programing Method (DPM) [2, 3] have been tested by minimizing the collective action to obtain the collective trajectories corresponding to different outer turning points. The values of spontaneous fission life-times, obtained in this way, are compared with the static path results.

**Keywords:** spontaneous fission, life-time, nuclear density functional theory
**PACS:** 24.75.+i, 25.85.Ca, 21.60.Jz, 21.60.Ev, 27.90.+b

## METHOD

The induced nuclear fission is the dynamical process, where hot nucleus deexcites by separating in two parts with emitting light particles like neutrons, protons, $\alpha$. It can be described quite successfully within classical physics for example by solving the set of Langevin equations. On the other hand, the spontaneous fission occurs due to quantum tunneling where the nearly cold nucleus passes through by the potential barrier.

The spontaneous fission half-life $T_{1/2}$ is given by [2, 3]

$$T_{1/2} = \frac{ln2}{nP}, \quad P = \left(1 + \exp\left[2S(L)\right]\right)^{-1}, \tag{1}$$

where $n$ is the number of assaults of the nucleus on the fission barrier per unit time. It is often considered to be $10^{20.38} s^{-1}$ [3]. The penetration probability $P$ is estimated from the semi-classical WKB approximation as [2, 3], where $S(L)$ is the action-integral calculated along the fission path $L(s)$ in the multidimensional deformation space,

$$S(L) = \int_{s_1}^{s_2} \left[\frac{2}{\hbar}\mathscr{M}_{eff}(s)\left(V_{eff}(s) - E_0\right)\right] ds. \tag{2}$$

where: $V_{eff}(s)$ is the potential energy and $\mathscr{M}_{eff}(s)$ is effective mass along the fission path $L(s)$. The limits of the fission path: $s_1$ and $s_2$ are classical turning points on $L(s)$ and $ds$ is the element of path length along $L(s)$. In Eq. (2), $E_0$ is the Zero-Point Energy (ZPE) calculated at the ground state configuration. We have calculated the minimum action path by following two different numerical techniques, called the dynamic-programming method (DPM) described in ref. [2] and the Ritz method (RM) [3]. In case of RM, trial paths are expressed as Fourier series of collective coordinates and, then, the coefficients of different Fourier components are extracted by minimizing the action integral given by Eq. (2).

The collective potential and the collective mass tensor are suitably well estimated using the self-consistent density functional theory, which in case of present project is represented by Approximated Time-Dependent Hartree-Fock-Bogolyubov (ATDHFB) method [1] with Skyrme functionals. The ATDHFB approach treats the problem of large-amplitude collective motion. The motion of the system can be described in terms of collective coordinates $\{q_i\}$ and canonically conjugated collective momenta $p_i = i\delta/\delta q_i$. Also there is an adiabatic assumption that the collective motions is slow- the collective velocity of the system $\{q_i\}$ is below the average-particle velocity of the nucleons.

The potential energy surface is obtained in the collective coordinate space of quadrupole moments ($Q_{20}$, $Q_{22}$) by subtracting the zero-point energy (ZPE) from total energy $E_{tot}$. In the present work, ZPE is estimated by using the Gaussian overlap approximation [4].

The components of collective inertia tensor in two-dimension are calculated within the cranking approximation of ATDHFB formula, written as [1]

$$\mathscr{M}^{C}_{ij} = \frac{1}{2\dot{q}_i\dot{q}_j}\sum_{\alpha\beta}\frac{\left(F^{i*}_{\alpha\beta}F^{j}_{\alpha\beta} + F^{i}_{\alpha\beta}F^{j*}_{\alpha\beta}\right)}{E_\alpha + E_\beta}, \tag{3}$$

where $\dot{q}_i$ and $\dot{q}_j$ represent time derivatives of the collective coordinates $Q_{20}$ and $Q_{22}$. The sum is evaluated over all quasiparticle states and $E_\alpha$ denotes the quasiparticle energy. The matrices $F^i$s are obtained from the relation [1]

$$-F^{i*} = \left(B^T\frac{\partial\rho}{\partial q_i}A + B^T\frac{\partial\kappa}{\partial q_i}B - A^T\frac{\partial\kappa^*}{\partial q_i}A - A^T\frac{\partial\rho^*}{\partial q_i}B\right)\dot{q}_i, \tag{4}$$

where $A$ and $B$ are HFB wave functions computed during the calculation of $E_{tot}$. The particle $\rho$ and pairing $\kappa$ densities are determinate uniquely from $A$ and $B$. The derivatives of densities with respect to the deformation coordinates are achieved by applying the Lagrange three-point formula [5, 6]. Explicit calculation of the time derivatives in Eq. (4) is complicated and time consuming. Therefore, these derivatives are often estimated perturbatively in terms of quadrupole operators $\hat{Q}_i$s and the corresponding mass formula is expressed as [1, 4]

$$\mathscr{M}^{Cp} = [M^{(1)}]^{-1}[M^{(3)}][M^{(1)}]^{-1}, \quad \text{where} \quad M^{(k)}_{ij} = \sum_{\alpha\beta}\frac{\langle 0|\hat{Q}_i|\alpha\beta\rangle\langle\alpha\beta|\hat{Q}^\dagger_j|0\rangle}{\left(E_\alpha + E_\beta\right)^k} \tag{5}$$

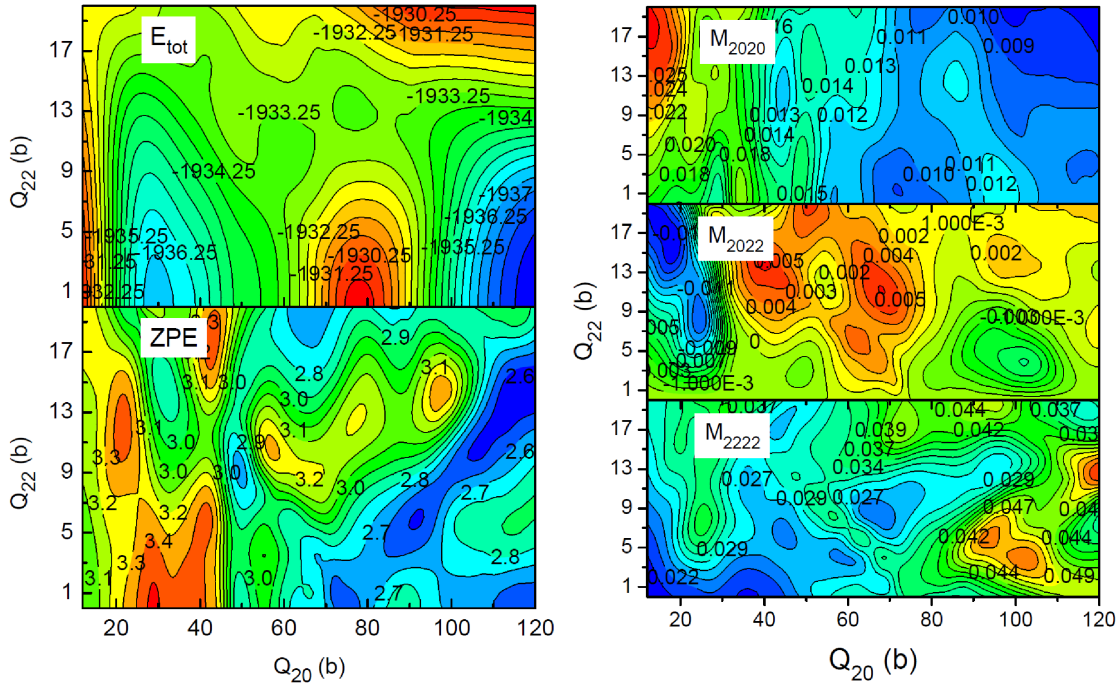


**FIGURE 1.** Left panel: total energy and ZPE, right panel - mass tensors in the quadrupole surface for $^{264}$Fm. An illustration taken from [8]

The energy-weighted moment tensors written in the quasiparticle basis and $|\alpha\beta\rangle$ represents a two-quasiparticle wave function. The effective mass [2, 3] is obtained from:

$$\mathscr{M}_{eff}(s) = \sum_{ij} \mathscr{M}_{ij} \frac{dQ_{20}}{ds} \frac{dQ_{22}}{ds} \tag{6}$$

along two different quadrupole axes. In Eq. (6), $s$ defines the path length on the two-dimensional potential profile.

The one dimensional calculations done with method describe above are presented in [7] for several Fermium isotopes allow to compare our results for axial quadrupole moments, only.

## PRELIMINARY RESULTS

The preliminary results presented in this report, has been partially published in [8], and few plots are replot only to show the scheme of obtaining spontaneous life-times. The Skyrme energy density functional is used with SkM* parametrization [9], which is optimized for fission barrier height of $^{240}$Pu.

The first step is the calculation of the total energy and mass tensors in two-dimensional collective coordinate surface. The surfaces of $E_{tot}$ and ZPE for $^{264}$Fm is illustrated in Fig. 1 (left panel). The $^{264}$Fm has been chosen as the ideal example where the spontaneous fission should provide two identical daughter nuclei $^{132}Sn$, which should be

**TABLE 1.** Comparison of the life-times obtained with static path, assuming the path along $Q_{22} = 0$ line and with dynamical action minimization for spontaneous fission of $^{264}$Fm.

| ZPE=0 | S(s) | $T_{1/2}$ [log10 ($T_{1/2}$ /yr )] | | S(s) | $T_{1/2}$ [log10 ($T_{1/2}$ /yr )] |
|---|---|---|---|---|---|
| static | 24.36 | -6.9 | $Q_{22} = 0$ | 23.12 | -7.96 |
| PDM | 19.25 | -11.3 | RM | 19.25 | -11.3 |

double magic and stable. In this case the octupole coordinate, responsible for the mass asymmetry in the fission process is negligible. In Fig. 1 (left panel) only the quadrupole moments are taken into account, by so, the nuclear shapes as prolate-triaxial-oblate are studied. The total energy has minimum for quadrupole axially symmetric shape but the static saddle point has huge nonaxially symmetric component.

The components of the perturbative cranking mass $\mathscr{M}^{Cp}$ are also shown in Fig. 1, (right panel). The large fluctuations in mass parameters are manifestations of crossings of single-particle levels near the Fermi energy [10].

The life-times calculated with Eq. 1 are tabulated in Table 1. In this results the ZPE is assumed 0 MeV while in the [8] there are presented calculation with more realistic ZPE.

## SUMMARY

The fission life time is decreased by 3 orders of magnitude when the nonaxiality is taken into account. The dynamic path gives shorter life times by at least 4 orders of magnitude. The static barrier is lower then dynamic one but the mass parameters are recompensate this and the action integral is higher. The 3D calculations involving quadrupole axiality, nonaxiality and octupole momenta are in progress.

**Acknowledgement**
This project is done in collaboration with A. Baran, J. Dobaczewski, W. Nazarewicz and J. A. Sheikh.

## REFERENCES

1. A. Baran, J. A. Sheikh, J. Dobaczewski, W. Nazarewicz, and A. Staszczak, *Phys. Rev. C* **84**, 054321 (2011).
2. A. Baran, K. Pomorski, A. Lukasiak, and A. Sobiczewski, *Nucl. Phys. A* **361**, 83 – 101 (1981).
3. A. Baran, *Phys. Lett. B* **76**, 8 – 10 (1978).
4. A. Staszczak, S. Pilat, and K. Pomorski, *Nucl. Phys. A* **504**, 589 – 604 (1989).
5. M. J. Giannoni, and P. Quentin, *Phys. Rev. C* **21**, 2076–2093 (1980).
6. E. Yuldashbaeva, J. Libert, P. Quentin, and M. Girod, *Phys. Lett. B* **461**, 1 – 8 (1999).
7. A. Staszczak, A. Baran, and W. Nazarewicz, *Phys. Rev. C* **87**, 024320 (2013).
8. J. Sadhukhan, K. Mazurek, and W. Nazarewicz, *Eur. Phys. J. A, Web of Conferences* (2013), proceedings of FISSION 2013, Caen, France.
9. J. Bartel, P. Quentin, M. Brack, C. Guet, and H.-B. Hakansson, *Nucl. Phys. A* **386**, 79 – 100 (1982).
10. W. Nazarewicz, *Nucl. Phys. A* **557**, 489 – 514 (1993).

# Symmetry Energy Effects On Low Energy Reaction Mechanisms

Carmelo Rizzo[a], Maria Colonna[a] ,Massimo Di Toro[a] and Virgil Baran[b]

[a] *Laboratori Nazionali del Sud INFN, I-95123 Catania, Italy.*
[b] *Physics Faculty, Univ. of Bucharest and NIPE-HH, Romania.*

**Abstract.** We focus on the interplay between reaction mechanisms, fusion vs. break-up (fast-fission, deep-inelastic) in Heavy Ion Collisions with exotic nuclear beams at low energies. Fusion probabilities for reactions induced by 132Sn on 64,58Ni targets at 10AMeV are evaluated looking at the evolution of the phase-space quadrupole collective modes. The break-up events appear sensitive to the stiffness of the symmetry energy, because the neutron-rich neck connecting the two partners can survive a longer time producing in the case of break-up very deformed final fragments, eventually leading to ternary/quaternary fragmentation events. 197Au + 197Au collisions at 15 and 23 AMeV are simulated to investigate the main modes of re-separation of a heavy nuclear system.

**Keywords:** Symmetry Energy Effects, Fusion-Break Up Competition, Fragment Deformations, Ternary Break-Up.
**PACS:** 25.60.Pj; 25.70Jj; 21.65.Ef; 21.30.Fe

## INTRODUCTION

We focus the attention on the fusion vs. deep-inelastic mechanism interplay for dissipative Heavy Ion Collisions (HIC) with exotic nuclear beams at low energies, just above the Coulomb Barrier (between 5 and 20 AMeV). Unstable ion beams with large asymmetry and with good intensities in this energy range will be soon available in Radioactive Ion Beam facilities. The goal of this analysis is to pin down specific observables which are sensitive to the symmetry energy to learn about its poorly known density behaviour.

The reaction path followed by HIC with neutron-rich (or exotic) nuclear beams at low energies is investigated within a transport theory based on a Stochastic Mean-Field (SMF) approach, extension of the microscopic Boltzmann-Nordheim-Vlasov transport equation [1,2], where two parameterizations for the density dependence of symmetry energy (Asysoft and Asy-stiff) are implemented [1].

We performed the $^{132}$Sn + $^{64,58}$Ni reactions at 10 AMeV for semi-peripheral impact parameters (from b =4.5 fm to b = 8.0 fm, with $\Delta$b= 0.5 fm) to study isospin and symmetry energy effects on the competition between fusion and break-up (deep-inelastic).

We show that the reaction dynamics undergoes a fusion/break-up path bifurcation at very early times due to Coulomb and angular momentum effects. In such critical transition stage the final outcome is essentially ruled by dynamical fluctuations and it will be rather sensitive to differences in the neutron-repulsive symmetry term.

# FUSION DYNAMICS FOR $^{132}$SN INDUCED REACTIONS

The method described here can indicate when the reaction mechanism is changing [3]. To extract the fusion cross section at relatively early times, fusion probabilities for reactions induced by $^{132}$Sn beam at 10AMeV are evaluated by the evolution of the phase-space quadrupole collective modes: $Q(t) =< 2z^2(t) - x^2(t) - y^2(t) >$ the quadrupole moment in coordinate space averaged over the space distribution in the composite system and $QK(t) =< 2p^2_z(t) - p^2_x(t) - p^2_y(t) >$, the quadrupole moment in momentum space evaluated in a spatial region around the center of mass (z-axis coincides with the symmetry axis, the x-axis is on the reaction plane). The information on the final reaction path is deduced investigating the quadrupole fluctuations of the system at early times (200-300 fm/c), when the formation of composite elongated configurations is observed [3].

The Q(t) behaviour is different for more peripheral impact parameters (increasing trend, i.e. break-up) and that obtained for b=5-6 fm, where we have still a little oscillation in the time interval between 100 and 300 fm/c, indication of a fusion contribution. These observations can be interpreted assuming that starting from about b = 5 fm, we have a transition from fusion to a break-up mechanism, like deep-inelastic. The Q(t)-slope values should be associated with a quadrupole deformation velocity of the dinuclear system that is going to a break-up (Q(t)-slope > 0) or to a fusion (Q(t)-slope < 0) exit channel.

When order increasing impact parameter the quadrupole deformation in momentum space QK(t), in a sphere of radius 3 fm around the center of mass, becomes more negative in the time interval between 100 and 300 fm/c. Since the angular momentum is large, the components perpendicular to the symmetry axis, that is rotating in reaction plane, are increasing leading to a separation of the deformed dinuclear system. The break-up probability increases when the quadrupole moment in p-space is more negative [3].

The Figure 1 show the Q slope-QK correlation plots for the systems $^{132}$Sn + $^{64}$Ni and the two asy-EOS. We can evaluate the normal curves of the displayed quantities and the relative areas for each impact parameter in order to select the events: break-up events will be located in the regions with both positive slope of Q and negative QK. In this way, we can evaluate the fusion events for each impact parameter by the difference between the total number of events and the number of break-up cases [3]. In Figure 2 we present the fusion distribution plots. For the $^{132}$Sn + $^{64}$Ni system (left panel), we note a difference between the σ-fusion corresponding to the two different asy-EOS in the centrality transition region, with larger values for Asysoft, a 4-5% effect in the neutron rich system: 1128 mb (Asysoft) vs. 1078 mb (Asystiff), and even smaller, 1020 mb vs. 1009 mb, for the $^{58}$Ni target (Figure 2, right panel). However, through a selection in angular momentum, $130 \leq l \leq 180$ ($\hbar$ ), we find that the Asysoft cross section curve is significantly above the Asystiff one, 10-15% in the case of the more neutron-rich system. We like to note that for the neutron-rich case, $^{132}$Sn+$^{64}$Ni, our absolute value of the total fusion cross section presents a good agreement with recent data, at lower energy (around 5 AMeV), taken at the ORNL [4].

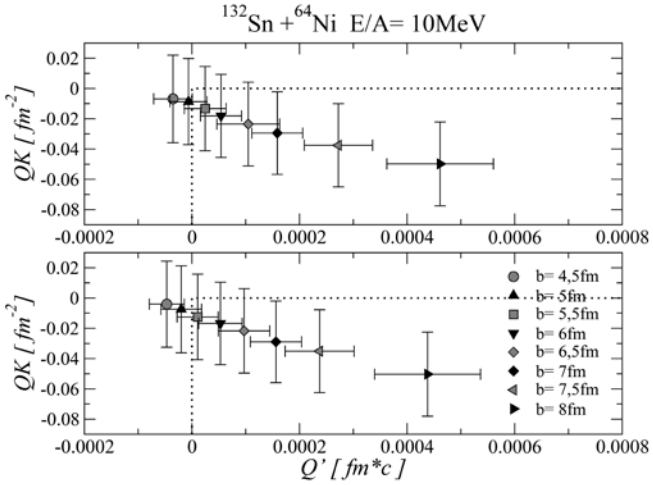


**FIGURE 1**. Mean value and variance of QK vs Q'(slope), averaged over the100-300 fm/c time interval, at various centralities in the transition region for the $^{132}$Sn + $^{64}$Ni system. The box limited by dotted lines represents the break-up region. Upper panel: Asystiff. Bottom Panel: Asysoft.

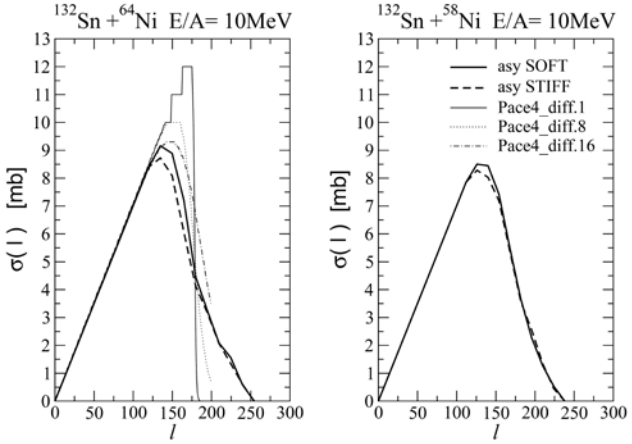


**FIGURE 2** Angular momentum distributions of the fusion cross sections (mb) for the two reactions and the two choices of the symmetry term. For the $^{132}$Sn + $^{64}$Ni system (left panel), the results of PACE4 [5,6] calculations are also reported, for different l-diffuseness.

The larger fusion probability obtained with the Asysoft choice seems to indicate that the reaction mechanism is regulated by the symmetry term at suprasaturation density, where the Asysoft choice is less repulsive for the neutrons [1, 7].

A first transport approach analysis of symmetry energy effects on break-up events in peripheral collisions of $^{132}$Sn +$^{64}$ Ni at 10 AMeV has been reported in ref.[8]. The neck dynamics on the way to separation is found influenced by the symmetry energy below saturation. This can be observed in the deformation pattern of the Projectile-Like (PLF) and Target-Like Fragments (TLF): larger deformations are seen in the Asystiff case for peripheral impact parameters, corresponding to a smaller symmetry repulsion at the low densities probed in the separation region[9, 10].

## ANALYSIS OF TERNARY EVENTS ON $^{197}$AU + $^{197}$AU REACTION

A study of the $^{197}$Au + $^{197}$Au reaction at an energy of 15*A* MeV was carried out [9,10] by the CHIMERA Collaboration at Laboratori Nazionali del Sud. For this system at relatively small impact parameters, corresponding to strongly damped collisions [11], a rather fast break-up into three or four massive fragments of comparable mass has been experimentally revealed. An interesting aspect is an alignment of the observed fragments along the axis of the system reseparation into PLF and TLF. In the ternary partitioning case, $^{197}$Au + $^{197}$Au → TLF + PLF → TLF + F1 + F2, the PLF break-up is collinear with PLF-TLF separation axis; this excludes a purely statistical fission in ternary events. Moreover the mass spectra of F1 and F2 fragments differ significantly [10].

In Figure 3, left panel, we present a theoretical simulation of the $^{197}$Au + $^{197}$Au system at 15 AMeV for b=4fm and b=6fm impact parameters. It is investigated in a transport theory based on a SMF model, where Asy-stiff parameterizations for the density dependence of symmetry energy is implemented. Through a qualitative study of the time evolution of the space density distributions projected on the reaction plane, Figure 3, the reaction mechanism seems to be heavily dominated by the quadrupole and octupole modes. The neutron-rich neck connecting the two partners survives a longer time producing very deformed primary PLF/TLF especially for more central impact parameters , that lead to three or four massive fragments of comparable size.

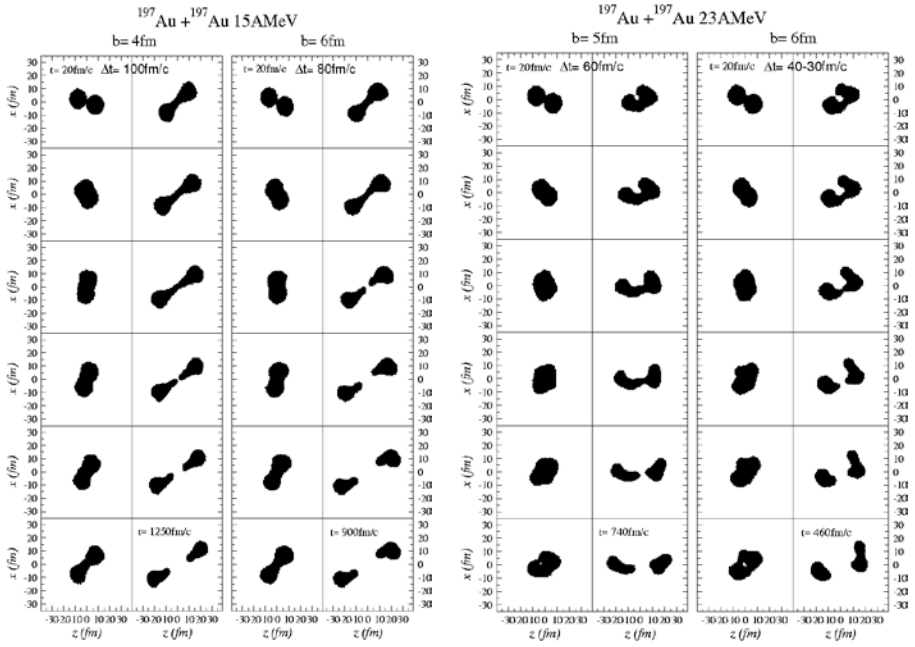


**FIGURE 3** Time evolution of the space density distributions for the 197Au +197Au semicentral collisions. Left Panel: reaction at 15 AMeV beam energy, b=4 and b=6fm impact parameter. Right Panel: 23 AMeV beam energy, b=5 and b=6fm.

Assuming that the ternary events have a larger probability than quaternary, we try in a simple way to evaluate the breaking fragment masses from the PLF or TLF residues

with large deformation: first we evaluate the center of the larger agglomerate inside the deformate PLF or TLF then we obtain the nucleon number $N1_{part}$ integrating from the left extreme to the center (with fragment orientation as shown in left panel of the figure 4).

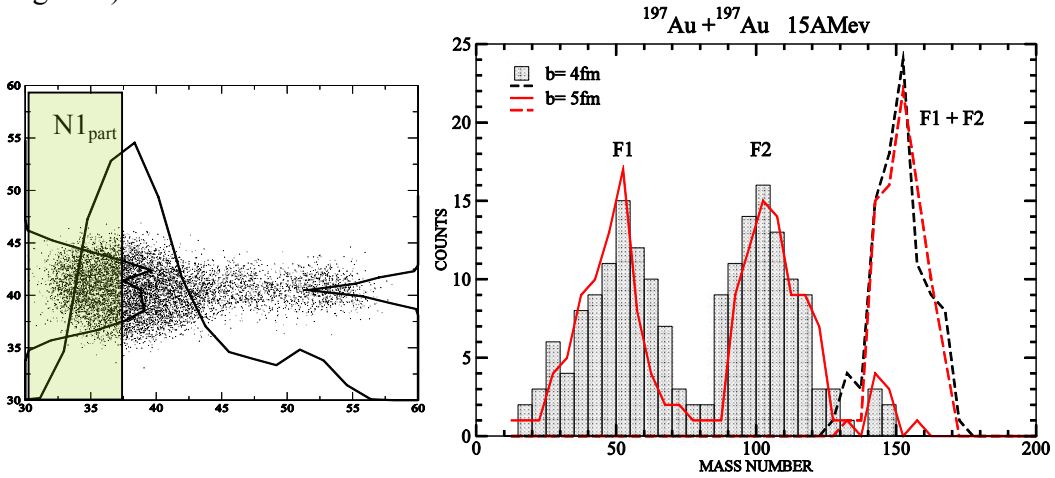


**FIGURE 4** Left panel: scheme to evaluate the breaking fragment masses from the PLF or TLF (see text). Right panel: the mass spectrum of mass numbers of fragments F1 and F2, for b=4fm and b=5fm impact parameter, reconstructed by the method describe up

Assuming that the ternary events have a larger probability than quaternary, we try in a simple way to evaluate the breaking fragment masses from the PLF or TLF residues with large deformation: first we evaluate the center of the larger agglomerate inside the deformate PLF or TLF then we obtain the nucleon number $N1_{part}$ integrating from the left extreme to the center (with fragment orientation as shown in left panel of the figure 4). We can evaluate the F1 and F2 mass for each event by $F2= 2N1_{part}$ and $F1= N_{tot} – F2$. The Figure 4 (right panel) shows the reconstructed mass spectrum of F1 and F2 fragments obtained by this method, for two relatively small impact parameters where we observe almost all break up events. The mass distribution presents a good agreement with recent data at 15AMeV (shown in ref.[10], fig.4), taken at the LNS. In particular we can reproduce the distance between the F1 and F2 centroids and the ratio between the centroid and the variance of the distribution. This seems to be a nice evidence that the ternary partitioning in comparable masses comes from semi peripheral impact parameters. We underestimate the fragments mass, by about 20 units, with respect to the experimental data [10]. It is probably due the overestimation in the code, of the number of evaporated particles because the break up time is very large at low energy especially for b=4fm and b=5fm.

In this work we report first results of the partitioning study of the same $^{197}$Au + $^{197}$Au system at the higher bombarding energy of 23AMeV. In addition to the partitions observed at low energies, a intense emission of Intermediate mass fragments is observed in experimental data at 23AMeV, [12]. In Figure 3 (right panel) a increasing instability in the neck region is observed. The plots shows that a process of neck fragmentation during reseparation of the colliding system plays an important role. It could explain that the F1 and F2 fragments data are also concentrated around a kind of ‘Coulomb ring’.

# REFERENCES


1. V. Baran, M. Colonna, V. Greco, M. Di Toro M, *Phys. Rep*. 410 335 (2005).
2. J. Rizzo, P. Chomaz, M. Colonna, *Nucl. Phys.A* 806 40 (2008)
3. C. Rizzo, V. Baran, M. Colonna, A. Corsi, M.Di Toro, *Phys. Rev. C83*, 014606 (2011).
4. J. F. Liang et al., *Phys. Rev*.C75, 054607 (2007).
5. A. Gavron, *Phys. Rev*. 21 230 (1979).
6. O. B. Tarasov, D. Bazin, *Nucl. Inst. Methods* B 204 174 (2003).
7. M. Colonna et al., *Phys. Rev*.C57, 1410 (1998).
8. M. Di Toro et al., *Nucl. Phys*.A 787 585c (2007).
9. I. Skwira-Chalot et al., *Phys. Rev. Lett*. 101 262701 (2008).
10. J. Wilczynski et al., *Phys. Rev*.C81, 024605 (2010).
11. J. Wilczynski et al., *Phys. Rev*.C 81, 067604 (2010).
12. T. Cap et al., *Phys. Scr.* T154 014007 (2013).

# The investigation of the nuclear equation of state

P. Marini and A. Chbihi

*GANIL, Bd. H. Bequerel, Caen, FRANCE*

**Abstract.** Dynamical and statistical properties of excited nuclei are strongly influenced by a fundamental property of nuclear matter: the nuclear equation of state (EOS). Despite its importance, strong uncertainties and a significant model-dependence still affect the available parametrizations of the EOS. In particular, experimental constraints are highly needed on the term of the EOS dependent of the difference between the number of neutrons and protons of the system. Beams on a wide range of energy and neutron-proton asymmetry are crucial to enhance the sensitivity of experimental measurements of this key term. In this respect the EURISOL facility, complementary to the future european FAIR and SPIRAL2, is highly needed from the reaction community.

**Keywords:** Symmetry energy, nuclear equation of state, rare ion beams
**PACS:** 25.70.Lm, 25.70.Mn, 26.60.Kp

The nuclear equation of state (EOS) describes the basic properties of nuclei and nuclear matter in the whole phase diagram and influences both their dynamical and statistical properties. At zero temperature the EOS is often expressed as a term related to symmetric nuclear matter and a term which accounts for the possible asymmetry and depends quadratically on the difference between the number (or density, in nuclear matter) of neutrons and protons:

$$E(\rho,(N-Z)) = E(\rho,(N-Z=0)) + E_{sym}(\rho)\frac{(N-Z)^2}{A} \quad (1)$$

The investigations of this term, often referred to as symmetry energy, and of its dependence on the density, are a challenging task, because of the small multiplicative term ($\frac{(N-Z)^2}{A}$) which reduces the effects on $E_{sym}$ on the experimental observables when dealing with stable beams ($\frac{(N-Z)^2}{A} = 0.46$ for $^{78}$Kr, for instance). Several experimental and theoretical studies [1, 2, 3, 4, 5, 6, 7] are devoted to the investigations of the density dependence of $E_{sym}$, but this term is still poorly constrained. However this dependence impacts many fields: nuclear reactions, where it influences the occurring reaction mechanism and the isotopic composition of the reaction products; nuclear structure of exotic nuclei [8, 9] (20% of $^{92}$Kr mass comes from the symmetry term, to be compared to 2% for $^{78}$Kr, for instance), as well as astrophysical objects [10, 11], such as neutron stars, due to the strong asymmetry between neutron and proton densities of the environment. Different densities are explored in the different systems: from low ($\rho \simeq \frac{1}{6} - \frac{1}{3}\rho_0$) to high densities ($2-3\rho_0$) in nuclear reactions, from $2/3\rho_0$ to $\rho_0$ in ground state of nuclei and from very low ( $\rho \simeq \frac{1}{6}$) to rather high densities (up to $10\rho_0$) in astrophysical environments. Experimental constraints on $E_{sym}$ are therefore necessary in all the density regions and a theoretical effort should be done to provide a coherent description of all the observables, both from heavy ion collisions and nuclear masses and astrophysical

observations.

In the past ten years an international effort has been carried out to place stringent constraints on the density dependence of $E_{sym}$ in laboratories all over the world.

Investigations on the high density region $(2-3\rho_0)$ were recently carried out at GSI, by the ASY-EOS Collaboration [12, 13]. This region is the one which presents the biggest uncertainties, and the highest impact on the astrophysical processes. Stable beams at relativistic energies (400 MeV/nucleon) were impinged on stable target to measure the neutron-proton elliptic flow. Important constraints are expected from the results of this experiment, which is part of an experimental program for the investigation of the symmetry energy at high densities to be carried out at FAIR with radioactive beams.

Among the others, experimental works carried out at MSU and Texas A&M, with stable beams with energies between 25 and 100 MeV/nucleon, allowed to place some constraints in the low density region of the phase diagram ($\simeq \frac{1}{6} - \frac{1}{3}\rho_0$) and around saturation density [14, 15, 16, 4]. The most common observables used in these works are fragment yields [3, 4, 5, 6], used to build different quantities (isoscaling [17], isobaric yield ratios [18, 19], imbalance ratio) and neutron-to-proton ratio [20]. Fragment yields were typically measured with ($4\pi$, in the best case) charged particle detectors, whose mass resolution goes up to $Z < 12$, coupled to neutron detectors (for instance the Neutron Ball [21] at Texas A&M) providing multiplicities information. These measurements suffer from the limited mass resolution of the experimental setup, as well as from the known influence of the secondary deexcitation on the observables, which distorts the signatures of the symmetry energy. To overcome mass resolution issues, some measurements were carried out by using spectrometers [5], however the information on the associated emitted particles was not available.

The availability of a high mass resolution for the forward emitted fragments and the full information on the associated emitted particles represents an important advance in this kind of measurements, since it promises to provide the necessary information to experimentally account for the secondary de-excitation. Recently, the INDRA-VAMOS Collaboration performed an experimental campaign coupling a $4\pi$ charged particle array (INDRA [22], with a mass resolution up to $Z = 4$) to a magnetic spectrometer. The stable beams at 35 MeV/nucleon delivered by the GANIL cyclotron and impinged on stable targets allow to place stringent constraints in the region around normal density, experimentally accounting, for the first time, for the effects of the secondary decay. Indeed, primary fragments and their excitation energies are experimentally reconstructed exploiting the combined information from the spectrometer and the INDRA detector [23, 24]. Only very recently a similar setup was used in an experiment carried out at RIKEN with both stable and rare ion beams - RIB (although with rather low intensities) from the MSU group.

The use of RIBs is crucial in the investigation of the symmetry energy, because the strong neutron-proton asymmetry characterizing these beams amplifies the effects of the symmetry energy term of the EOS. Indeed, for instance, the multiplicative term in eq. 1, $(\frac{(N-Z)^2}{A})$, increases of one order of magnitude moving from the stable $^{78}$Kr to the radioactive $^{92}$Kr, which is expected to be available in the Phase2 of the SPIRAL2 project. It is therefore important to have facilities able to provide high intensity beams on a wide range of asymmetries. An other key feature for these investigations is the

availability of a wide range of beam energies. Indeed different density regions can be explored by varying the beam energy. Focusing of the future european RIB facilities, SPIRAL2, with its energies up to 14 and 10 MeV/nucleon for stable light ($Z \leq 20$) and rare heavy ($Z > 20$) beams, respectively, will allow the investigation of densities around saturation density. The relativistic energies, above 200 MeV/nucleon expected at FAIR, will give us access to the high density ($2-5\rho_0$) region of the EOS. In this context the energies between 20 and 150 Mev/nucleon of the EURISOL facility, allowing the exploration of the low density region, are complementary to those available in the short future and highly needed.

Crucial for the development of programs devoted to the investigation of the role of the asymmetry between the number of neutron and proton both in the dynamical and statistical features of nuclei is the capability of detecting and identifying both in charge and mass, with the lowest possible threshold, all the emitted reaction products on the whole solid angle. The FAZIA project [25] aims at providing those information, taking advantage of pulse shape analysis techniques to achieve low identification thresholds while preserving a good energy resolution with the use of silicon detectors.

An other important issue to fully exploit the potentiality of high intensity RIBs for extracting meaningful information on the symmetry energy is a better understanding and control of the effects of the secondary decay on the observables commonly used to extract the symmetry energy [26]. Techniques to account for those effects in a model independent way need to be identified and explored. The preliminary results from the INDRA-VAMOS experiment seem very promising in this respect [23, 24]. The characteristics of fragments before their deexcitation (primary fragments) were reconstructed and compared to those of fragments after the deexcitation. The symmetry energy for both primary and secondary fragments was extracted and compared [27]. Also, there are indications that very exotic nuclei, beyond the drip lines, were produced in the analysed reactions in the region around and below the Z of the beam. This opens up the possibility of studying their decay, via charged particle spectroscopy, to point out possible new decay modes due to Coulomb instabilities (close to the proton drip line) and to the strong neutron-proton asymmetry (close to the neutron drip line).

One could envisage, at the EURISOL facility, experiments with Sn beam/target combinations in the $20-100$ MeV/nucleon range. For instance reactions such as 106Sn+112Sn and 132Sn+124Sn would allow to span a $\frac{(N-Z)^2}{A}$ from 0.3 to 7.8 ($N/Z = 112-164$) and produce nuclei beyond the drip lines in the region between $Z \simeq 28$ and $Z \simeq 50$, which is of high interest also for the nuclear structure and astrophysics communities. These reactions would allow a detailed investigation of the influence of the N-Z asymmetry on the phase diagram and on the properties of nuclei. As experimental setup, we could think of FAZIA, coupled to a spectrometer, to have a complete charge and mass identification. A angular resolution better than $0.5^\circ$ for charged particles would allow detailed decay studies, allowing the use of correlation techniques. Finally, crucial will be the capability of having an experimental information on (at least) the multiplicity of emitted neutrons on an event-by-event basis.

## Conclusion

Despite the strong influence of the density dependence of the symmetry energy and several theoretical and experimental efforts, strong uncertainties and a significant model-dependence still affect the available parametrizations. Experimental constraints are highly needed in all the density regions. Beams on a wide range of energy and neutron-proton asymmetry, as the ones expected from EURISOL, SPIRAL2 and FAIR, are crucial to enhance the sensitivity of experimental measurements of this key term. In this respect the EURISOL facility is complementary to the future european FAIR and SPIRAL2. The use of detectors capable of identifying in Z and A the reaction products with very low identification thresholds, together with a better understanding of the secondary deexcitation process will be mandatory for future investigations.

## REFERENCES


1. B.-A. Li. *Phys. Rev. Lett.*, 88:192701, 2002.
2. L. W. Chen *et al. Phys. Rev. Lett.*, 90:162701, 2003.
3. M. B. Tsang *et al. Phys. Rev. Lett.*, 86:5023, 2001.
4. M. B. Tsang *et al. Phys. Rev. Lett,*, 92:062701, 2004. and refs therein.
5. G. A. Souliotis *et al. Phys. Rev. C*, 68:024605, 2003.
6. D. V. Shetty *et al. Phys. Rev.C*, 76:024606, 2007.
7. A. Ono *et al. Phys. Rev. C*, 70:041604(R), 2004.
8. C. Horowitz *et al. Phys. Rev. C*, 85:032501(R), 2012.
9. J.T.H. Krivine *et al. Nucl. Phys. A*, 336:155, 1980.
10. A. W. Steiner *et al. Phys. Rev. C*, 85:055804, 2012.
11. F. J. Fattoyev *et al. Phys. Rev. C*, 86:015802, 2012.
12. R. C. Lemmon and P. Russotto for the ASY-EOS Collaboration. Constraining the symmetry energy at supra-saturation densities with measurements of neutron and proton elliptic flows. *Experiment proposal at GSI*.
13. P. Russotto *et al. J. Phys.: Conf. Ser.*, 420:012092, 2012.
14. M. Colonna *et al. Phys. Rev. C*, 82:054613, 2010.
15. S. Hudan *et al. Phys. Rev. C*, 86:021603, 2012.
16. Z. Kohley *et al. Phys. Rev. C*, 86:044605, 2012.
17. M. B. Tsang *et al. Phys. Rev. C*, 64:054615, 2001.
18. M. Huang *et al. Phys. Rev. C*, 81:044620, 2010.
19. P. Marini, A. Bonasera, A. McIntosh, R. Tripathi, S. Galanopoulos, K. Hagel, L. Heilborn, Z. Kohley, L. W. May, M. Mehlman, S. N. Soisson, G. A. Souliotis, D. V. Shetty, W. B. Smith, B. C. Stein, S. Wuenschel, and S. J. Yennello. *Phys. Rev. C*, 85:034617, 2012.
20. M. A. Famiano, T. Liu, W. G. Lynch, M. Mocko, A. M. Rogers, M. B. Tsang, M. S. Wallace, R. J. Charity, S. Komarov, D. G. Sarantites, et al. *Phys. Rev. Lett.*, 97:052701, 2006.
21. S. Wuenschel *et al. AIP Conf. Proc.*, 1099:816, 2009.
22. J. Pouthas *et al. Nucl. Instr. and Meth. in Phys. Res. A*, 357:418, 1995.
23. P. Marini *et al. J. Phys.: Conf. Ser.*, 420:012096, 2012.
24. P. Marini *et al. Acta Physica Polonica B*, 44:581, 2013.
25. `http://fazia2.in2p3.fr/spip/`.
26. P. Marini *et al. Phys. Rev. C*, 87:024603, 2013. and ref. therein.
27. P. Marini and A. Chbihi. paper in preparation.

# Multi-reference nuclear energy density functional calculations

T. Duguet

*CEA-Saclay DSM/Irfu/SPhN, F-91191 Gif sur Yvette Cedex, France*
*NSCL and Department of Physics and Astronomy, Michigan State University, East Lansing, MI 48824, USA*

**Abstract.** We briefly review the status of state-of-the-art energy density functional calculations.

**Keywords:** nuclear energy density functional, multi-reference calculations, neutron-rich nuclei

## GENERALITIES

Low-energy nuclear physics is currently going through an unprecedented revival due to several combining factors. First, the explicit link between quantum chromo dynamics, the fundamental theory of the strong force, and A-nucleon (AN) interactions is being realized thanks to effective field theory (EFT) based on chiral perturbation theory. Second, successive generations of radioactive ion beam (RIB) facilities on the way to EURISOL are accessing an increasingly larger fraction of (briefly) existing atomic nuclei, among which exotic nuclei with a large neutron excess display unusual properties compared to those located near the valley of $\beta$ stability. Third, rapidly increasing computational capabilities are authorizing the development and application of ambitious theoretical quantum many-body methods. Fourth, several astrophysical problems, e.g. the understanding of the explosive nucleosynthesis of heavy elements in the universe or the physics of neutron stars, and tests of the Standard Model, e.g. the unitarity of the Cabibbo-Kobayashi-Maskawa (CKM) matrix, require reliable and systematic nuclear inputs and thus act as a driving force to advance our experimental and theoretical knowledge of nuclear systems.

In such a context, the challenge of contemporary low-energy nuclear theory is to describe, in a controlled and unified manner, the entire range of nuclei along with the equation of state of extended nuclear matter, from a fraction to few times nuclear saturation density and over a wide range of temperatures. To do so, nuclear theorists are developing a portfolio of methods that, roughly speaking, separate into three categories; i.e. (i) (essentially) exact ab-initio methods [Faddeev or Yakubowski [1], Green's function monte-carlo (GFMC) [2], no-core shell model (NCSM) [3], lattice effective field theory (LEFT) [4]] that solve the quantum many-body problem in terms of elementary 2N and 3N interactions and can address nuclei with $A \leq 16$, (ii) ab-initio many-body methods based on controlled expansions [Coupled-cluster (CC) [5, 6], self-consistent Green's function (SCGF) [7, 8], in-medium similarity renormalization group (IMSRG) [9, 10]]

and addressing doubly closed-shell nuclei[1] ($\pm 1$ and $\pm 2$ nucleons) with $A \leq 60$ and (iii) effective methods [configuration interaction (CI) [15], energy density functional (EDF) [16, 17]] expressed in terms of phenomenological in-medium interactions and tackling medium/heavy nuclei.

As of today, the EDF method in its most advanced *multi-reference* implementation (see below) is capable to provide within one consistent framework[2], (i) the detailed and complete picture of a specific nucleus of interest [18, 19], (ii) systematic trends over a large set of nuclei [20, 21, 22] and (iii) extrapolations in the region of the nuclear chart where experimental data are and will remain unavailable [23]. A fundamental aspect of the method is that it relies heavily on the concept of spontaneous breaking and restoration of symmetries. As such, the nuclear EDF method is intrinsically a two-step approach

1. The first step is constituted by the so-called single-reference[3] (SR) implementation where symmetries dictated by the underlying Hamiltonian are authorized to break spontaneously in order to account for static collective correlations.
2. The second step is carried out through the multi-reference[4] (MR) extension where collective fluctuations, including the restoration of symmetries, are incorporated to grasp dynamical correlations.

Within such a frame, ground-state properties as well as individual, vibrational and rotational excitations are accessed, along with electromagnetic and electroweak transition probabilities between them. The key ingredient to the method is the *transition* energy kernel $E[\rho^{g'g}, \kappa^{g'g}, \kappa^{gg'*}]$, which is taken to be a functional of transition (i.e. off-diagonal) density matrices

$$\rho_{ij}^{g'g} \equiv \frac{\langle \Phi^{(g')} | a_j^\dagger a_i | \Phi^{(g)} \rangle}{\langle \Phi^{(g')} | \Phi^{(g)} \rangle} \ , \ \kappa_{ij}^{g'g} \equiv \frac{\langle \Phi^{(g')} | a_j a_i | \Phi^{(g)} \rangle}{\langle \Phi^{(g')} | \Phi^{(g)} \rangle} \ , \ \kappa_{ij}^{gg'*} \equiv \frac{\langle \Phi^{(g')} | a_i^\dagger a_j^\dagger | \Phi^{(g)} \rangle}{\langle \Phi^{(g')} | \Phi^{(g)} \rangle} \ . \quad (1)$$

computed from two Bogoliubov states $\langle \Phi^{(g')}|$ and $|\Phi^{(g)}\rangle$ that differ by the value of a collective label $g \equiv |g| e^{i\alpha}$. The norm $|g|$ tracks the extent to which the symmetry (e.g. translational, rotational, particle number) is broken by $|\Phi^{(g)}\rangle$, i.e. its "deformation", whereas the phase $\alpha$ characterizes the orientation of the deformed body with respect to the chosen reference frame. While the SR implementation only invoke the *diagonal* part of the EDF kernel obtained for $g' = g$, the MR implementation makes full use of it.

An efficient parametrization of $E[\rho^{g'g}, \kappa^{g'g}, \kappa^{gg'*}]$ is the key to an effective summation of the bulk of many-body correlations. Modern parametrizations, i.e. Skyrme, Gogny, or relativistic energy functionals, provide a good description of ground-state properties and, to a lesser extent, of spectroscopic features of known nuclei. Still, as of today, EDF parametrizations are phenomenological as they rely on empirically-postulated

---

[1] SCGF [11, 12], IMRSG [13] and CC [14] are currently being extended to open-shell nuclei.

[2] The idealized infinite nuclear matter system relevant to the description of compact astrophysical objects such as neutron stars is accessible to EDF calculations as well.

[3] The SR implementation is traditionally referred to as the "mean-field" level.

[4] The MR implementation is traditionally referred to as the "beyond mean-field" level.

functional forms whose free coupling constants are adjusted on a selected set of experimental data. This raises questions regarding (i) the connection between currently used EDF parametrizations and elementary AN forces, which is neither explicit nor qualitatively transparent, and regarding (ii) the predictive power of extrapolated EDF results into the experimentally unknown territory. Their lack of microscopic foundation often leads to parametrization-dependent predictions away from known data, i.e. to significant systematic errors, and makes difficult to design systematic improvements.

## RECENT DEVELOPMENTS OF THE METHOD

State-of-the-art MR-EDF calculations are currently limited to even-even nuclei. In their most advanced form, they rely on the restoration of neutron number, proton number and angular momentum from triaxially deformed Bogoliubov states and on the further mixing of quadrupole shapes. Such calculations are available for non-relativistic Skyrme [24] and Gogny [25] functionals as well as for relativistic Lagrangians [26]. Still, those cutting-edge calculations are limited to light nuclei such that approximations are needed at this point (e.g. limiting oneself to axially deformed shapes) to tackle heavy systems. Another powerful implementation consists of restoring both good angular momentum and isospin from triaxially deformed Slater determinants [27]. The goal is to evaluate isospin mixing and isospin-breaking corrections to super-allowed $\beta$-decay in view of testing the unitarity of the CKM matrix [28]. The versatility of the MR method permits to address other delicate questions such as the quest for neutrino-less double $\beta$-decay to pin down the Dirac or Majorana character of neutrinos [29].

The current forefront corresponds to extending MR-EDF schemes in several (complementary) directions. First and foremost, it is crucial to perform MR-EDF calculations of odd-even and odd-odd nuclei. This poses a great technical challenge [30] but will extend the reach of the method tremendously and will greatly enhance the synergy with upcoming experimental studies. Along the same line, MR-EDF schemes must be extended such as to include *diabatic* effects [31], i.e. configurations generated through $2n$ quasi-particle excitations. This is expected to improve significantly the description of, e.g., the first $2^+$ excited state in near-spherical nuclei and to allow a clean description of K isomers. Of importance will also be to combine quadrupole and octupole degrees of freedom [32] as well as the pairing one [33, 34]. The latter impacts moment of inertia significantly and allows the description of pairing fluctuations/vibrations near closed shell, as well as the computation of pair transfer overlap functions.

Several approximations to or variants of the full-fledged MR-EDF approach are also being pursued with great success. First is the quasi-particle random phase approximation that provides vibrational excitations (i.e. low-lying states and giant resonances) of various multipolarities and associated ground-state correlations. The method was systematically developed for deformed nuclei in recent years [35, 36, 37, 38, 39] on the basis of complete EDF parametrizations and efficient algorithms [40, 41, 42]. This will permit to address many upcoming challenges including the quest of potentially new exotic vibrational modes [43]. Second are five-dimensional collective (e.g. Bohr) Hamiltonians developed on the basis of non-relativistic Skyrme [44, 45] and Gogny [46, 47] functionals as well as of relativistic Lagrangians [48]. Work is currently being pursued

to improve on the Inglis-Belyaev moments of inertia and cranking mass parameters by means of Thouless Valentin [49, 50]. Within such a scheme, low-lying collective spectra of heavy nuclei can be computed while including the full quadrupole dynamics. Last but not least, it is worth mentioning the recent revival of the interacting boson model within a microscopic setting, i.e. based on the mapping of triaxial SR energy landscapes generated from a Gogny functional [51] or a relativistic Lagrangian [52]. Such a method allows the efficient description of low-lying collective spectra of complex heavy nuclei. As for full-fledge MR-EDF calculations, modern accounts of the three above methods are only available for even-even nuclei such that extensions to odd-even and odd-odd nuclei must be envisioned in the future.

## STATUS AND PERSPECTIVES

Very significant advances have been made in the last 15 years within the frame of the nuclear energy density functional method. In doing so, the focus of the field has shifted in several respects, with the consequences that

1. routine applications have moved from SR to MR calculations,
2. one can address, e.g. neutron-rich, nuclei that do not fit the mean-field paradigm,
3. applications are now equally dedicated to ground and excited states,
4. one can provide *at the MR level* both
   (a) the detailed quantitative picture of a given nucleus of interest,
   (b) trends through large-scale systematic calculations,
5. advances in the field are bound to making consistent progress regarding
   (a) the foundations of the approach and its formal consistency [53, 54, 55, 56, 57],
   (b) the rooting of EDFs into ab-initio methods and basic interactions [58, 59, 60],
   (c) the building of EDF parametrizations from enlarged data set [61],
   (d) the further development of powerful numerical tools,
   while points (a), (b) and (c) were essentially discarded 15 years ago,
6. applications more strongly impact astrophysics and particle physics.

The field can be expected to move forwards in these directions in the next 10 years. Most probably, this will be the era of a strong overlapping with emerging ab-initio methods for mid-mass nuclei and of the materialization of powerful numerical tools dedicated to the description of odd-even and odd-odd nuclei. This is needed to make the MR method fully mature when EURISOL comes online. This is particularly relevant given that exotic nuclei with a large neutron excess are likely to require more systematically the inclusion of MR correlations from the outset, i.e. to be less-good "mean-field" nuclei than many of those located near the valley of $\beta$ stability. In addition to these already on-going trends, one can expect unexpected concerns to emerge that will guide the development of EDF methods in new directions.

# REFERENCES


1. A. Nogga, H. Kamada, and W. Glöckle, *Phys. Rev. Lett.* **85**, 944 (2000).
2. S. Pastore, S. C. Pieper, R. Schiavilla, and R. Wiringa (2013), 1302.5091.
3. P. Navratil, S. Quaglioni, I. Stetcu, and B. R. Barrett, *J. Phys.* **G36**, 083101 (2009).
4. E. Epelbaum, H. Krebs, T. A. Lahde, D. Lee, and U.-G. Meissner, *Phys.Rev.Lett.* **109**, 252501 (2012).
5. G. Hagen, T. Papenbrock, D. J. Dean, and M. Hjorth-Jensen, *Phys. Rev.* **C82**, 034330 (2010).
6. S. Binder, J. Langhammer, A. Calci, P. Navratil, and R. Roth (2012), 1211.4748.
7. W. H. Dickhoff, and C. Barbieri, *Prog. Part. Nucl. Phys.* **52**, 377 (2004).
8. A. Cipollone, C. Barbieri, and P. NavrÃątil (2013), 1303.4900.
9. K. Tsukiyama, S. Bogner, and A. Schwenk, *Phys. Rev. Lett.* **106**, 222502 (2011).
10. H. Hergert, S. Bogner, S. Binder, A. Calci, J. Langhammer, et al., *Phys.Rev.* **C87**, 034307 (2013).
11. V. Soma, T. Duguet, and C. Barbieri, *Phys.Rev.* **C84**, 064317 (2011).
12. V. Soma, C. Barbieri, and T. Duguet, *Phys.Rev.* **C87**, 011303 (2013).
13. H. Hergert, S. Binder, A. Calci, J. Langhammer, and R. Roth, *Phys. Rev. Lett. 110,* **242501** (2013).
14. A. Signoracci, T. Duguet, and G. Hagen (2013), unpublished.
15. E. Caurier, G. Martínez-Pinedo, F. Nowacki, A. Poves, and A. P. Zuker, *Rev. Mod. Phys.* **77**, 427 (2005).
16. M. Bender, P.-H. Heenen, and P.-G. Reinhard, *Rev. Mod. Phys.* **75**, 121 (2003).
17. T. Niksic, D. Vretenar, and P. Ring, *Prog.Part.Nucl.Phys.* **66**, 519 (2011).
18. J.-M. Yao, S. Baroni, M. Bender, and P.-H. Heenen, *Phys.Rev.* **C86**, 014310 (2012).
19. J. Yao, H. Mei, and Z. Li, *Phys.Lett.* **B723**, 459 (2013).
20. M. Bender, G. F. Bertsch, and P. H. Heenen, *Phys. Rev.* **C73**, 034322 (2006).
21. M. Bender, G. Bertsch, and P.-H. Heenen, *Phys.Rev.* **C78**, 054312 (2008).
22. L. Robledo, and G. Bertsch, *Phys.Rev.* **C84**, 054302 (2011).
23. S. Goriely, S. Hilaire, M. Girod, and S. Peru, *Phys. Rev. Lett.* **102**, 242501 (2009).
24. M. Bender, and P.-H. Heenen, *Phys.Rev.* **C78**, 024309 (2008).
25. T. R. Rodriguez, and J. L. Egido, *Phys. Rev.* **C81**, 064323 (2010).
26. J. Yao, J. Meng, P. Ring, and D. Vretenar, *Phys.Rev.* **C81**, 044311 (2010).
27. W. Satula, J. Dobaczewski, W. Nazarewicz, and M. Rafalski, *Phys.Rev.* **C81**, 054310 (2010).
28. W. Satula, J. Dobaczewski, W. Nazarewicz, and T. Werner, *Phys.Rev.* **C86**, 054316 (2012).
29. T. R. Rodriguez, and G. Martinez-Pinedo, *Phys.Rev.* **C85**, 044310 (2012).
30. B. Bally, B. Avez, M. Bender, and P.-H. Heenen, *Int. J. Mod. Phys.* **E21**, 1250026 (2012).
31. T. Duguet, *Problème à N corps nucléaire et force effective dans les méthodes de champ moyen auto-cohérent*, Ph.D. thesis, Commissariat à l'Energie Atomique, Saclay, 91191 Gif sur Yvette Cedex, France (2002), http://tel.archives-ouvertes.fr/docs/00/04/49/86/PDF/tel-00001784.pdf.
32. J. Meyer, P. Bonche, M. S. Weiss, J. Dobaczewski, H. Flocard, and P.-H. Heenen, *Nucl. Phys.* **A588**, 597 (1995).
33. M. Bender, and T. Duguet, *Int. J. Mod. Phys.* **E16**, 222 (2007).
34. N. L. Vaquero, T. R. Rodriguez, and J. L. Egido, *Phys.Lett.* **B704**, 520 (2011).
35. S. Peru, and H. Goutte, *Phys.Rev.* **C77**, 044313 (2008).
36. K. Yoshida, *Eur.Phys.J.* **A42**, 583 (2009).
37. D. Pena Arteaga, and P. Ring (2009), 0912.0908.
38. C. Losa, A. Pastore, T. Dossing, E. Vigezzi, and R. Broglia, *Phys.Rev.* **C81**, 064307 (2010).
39. J. Terasaki, and J. Engel, *Phys.Rev.* **C82**, 034326 (2010).
40. T. Nakatsukasa, T. Inakura, and K. Yabana, *Phys.Rev.* **C76**, 024318 (2007).
41. J. Toivanen, B. Carlsson, J. Dobaczewski, K. Mizuyama, R. Rodriguez-Guzman, et al., *Phys.Rev.* **C81**, 034312 (2010).
42. P. Avogadro, and T. Nakatsukasa, *Phys.Rev.* **C84**, 014314 (2011).
43. N. Paar, *J.Phys.* **G37**, 064014 (2010).
44. L. Prochniak, P. Quentin, D. Samsoen, and J. Libert, *Nucl. Phys.* **A730**, 59 (2004).
45. L. Prochniak, and S. Rohozinski, *J.Phys.* **G36**, 123101 (2009).
46. J. Libert, M. Girod, and J.-P. Delaroche, *Phys.Rev.* **C60**, 054301 (1999).
47. J. Delaroche, M. Girod, J. Libert, H. Goutte, S. Hilaire, et al., *Phys.Rev.* **C81**, 014303 (2010).
48. T. Niksic, Z. Li, D. Vretenar, L. Prochniak, J. Meng, et al., *Phys.Rev.* **C79**, 034303 (2009).
49. Z. Li, T. Niksic, P. Ring, D. Vretenar, J. Yao, et al., *Phys.Rev.* **C86**, 034334 (2012).

50. N. Hinohara, Z. Li, T. Nakatsukasa, T. Niksic, and D. Vretenar, *Phys.Rev.* **C85**, 024323 (2012).
51. K. Nomura, T. Otsuka, R. Rodriguez-Guzman, L. Robledo, and P. Sarriguren, *Phys.Rev.* **C83**, 014309 (2011).
52. K. Nomura, T. Niksic, T. Otsuka, N. Shimizu, and D. Vretenar, *Phys.Rev.* **C84**, 014302 (2011).
53. D. Lacroix, T. Duguet, and M. Bender, *Phys. Rev.* **C79**, 044318 (2009).
54. M. Bender, T. Duguet, and D. Lacroix, *Phys. Rev.* **C79**, 044319 (2009).
55. T. Duguet, and J. Sadoudi, *J. Phys. G: Nucl. Part. Phys.* **37**, 064009 (2010).
56. J. Messud, M. Bender, and E. Suraud, *Phys. Rev.* **C80**, 054314 (2009).
57. T. Lesinski (2013), `1301.0807`.
58. T. Duguet, *Phys. Rev.* **C69**, 054317 (2004).
59. B. Gebremariam, S. Bogner, and T. Duguet, *Nucl. Phys.* **A851**, 17 (2011).
60. N. Kaiser, *Eur. Phys. J.* **A48**, 36 (2012).
61. M. Kortelainen, J. McDonnell, W. Nazarewicz, P. Reinhard, J. Sarich, N. Schunck, M. V. Stoitsov, and S. M. Wild, *Phys.Rev.* **C85**, 024304 (2012).

,

# Structure of heavy and superheavy nuclei with Energy Density Functionals

V. Prassa*, T. Nikšić† and D. Vretenar†

*Physics Department, University of Jyväskylä, P.O. Box 35 (YFL) FI-40014, Finland
†Physics Department, Faculty of Science, University of Zagreb, 10000 Zagreb, Croatia

**Abstract.** A fully microscopic theoretical framework based on nuclear relativistic energy density functionals (REDFs) is applied to studies of nuclear properties of heavy and superheavy nuclei. On the self-consistent mean-field level the microscopic approach is used in the calculation of $\alpha$-decay energies and ground-state shapes of heavy and superheavy nuclei.

An especially interesting feature in the region of heavy and superheavy elements is the possible occurrence of shape-phase transitions and critical-point phenomena. A collective Hamiltonian model, based on microscopic REDFs is employed in studies of shape coexistence phenomena, complex excitation patterns and electromagnetic transition rates.

**Keywords:** Nuclear Density Functional Theory, Superheavy Nuclei, $\alpha$-decay
**PACS:** 21.60.Jz,21.10.Dr, 21.10.Re, 24.75.+i, 27.90.+b

The framework of relativistic energy density functionals (REDF) is applied to an illustrative study of shell effects, shape transitions and shape coexistence in superheavy nuclei (SHN) with $Z = 110 - 120$.

There are several advantages in using functionals with manifest covariance and, in the context of this study, the most important is the natural inclusion of the nucleon spin degree of freedom, and the resulting nuclear spin-orbit potential which emerges automatically with the empirical strength. Our aim is to test the recently introduced functional DD-PC1 [1] in self-consistent relativistic Hartree-Bogoliubov (RHB) calculations of energy surfaces (axial, triaxial, octupole), shape transitions and $\alpha$-decay energies of heavy and superheavy nuclei, in comparison to available data and previous theoretical studies.

The model is first tested in calculations of ground state energies, quadrupole deformations, fission barriers, fission isomers, and $\alpha$-decay energies of even-even actinide nuclei. We then apply the RHB framework based on the functional DD-PC1 and a separable pairing interaction in a description of triaxially deformed shapes and shape transitions of even-even heavy and superheavy nuclei. The microscopic, REDF-based, quadrupole collective Hamiltonian model is used to study observables related to the effect of explicit treatment of collective correlations in the $Q_\alpha$-energies in superheavy nuclei.

The “double-humped" fission barriers of actinide nuclei provide an important test for nuclear energy density functionals. The fission barriers calculated in the present work are shown in Fig. 1, where we plot the potential energy curves of $^{236,238}$U, $^{240}$Pu, and $^{242}$Cm, as functions of the axial quadrupole deformation parameter $\beta_{20}$. To be able to analyze the outer barrier heights considering also reflection-asymmetric (octupole) shapes, the results displayed in this figure have been obtained in a self-consistent RMF plus BCS calculation that includes either triaxial shapes, or axially symmetric but reflection-

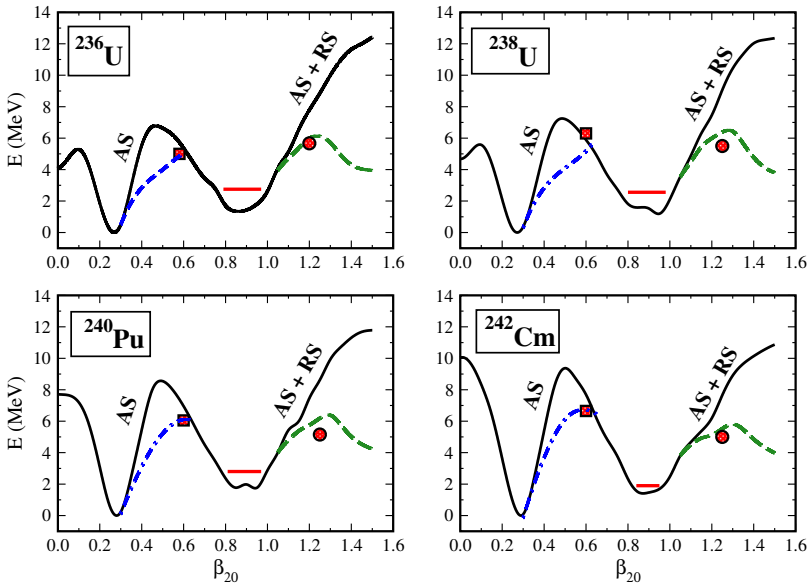


**FIGURE 1.** Constrained energy curves of $^{236,238}$U, $^{240}$Pu, and $^{242}$Cm, as functions of the axial quadrupole deformation parameter. Results of self-consistent axially and reflection-symmetric, triaxial, and axially reflection-asymmetric RMF+BCS calculations are denoted by solid (black), dot-dashed (blue), and dashed (green) curves, respectively. The red squares, lines, and circles denote the experimental values for the inner barrier height, the excitation energy of the fission isomer, and the height of the outer barrier, respectively. The data are from Ref. [2].

asymmetric shapes. The solid (black) curves correspond to binding energies calculated with the constraint on the axial quadrupole moment, assuming axial and reflection symmetry.

The dot-dashed (blue) curves denote paths of minimal energy in calculations that break axial symmetry with constraints on quadrupole axial $Q_{20}$ and triaxial $Q_{22}$ moments. Finally, the dashed (green) curves are paths of minimal energy obtained in axially symmetric calculations that break reflection symmetry (constraints on the quadrupole moment $Q_{20}$ and the octupole moment $Q_{30}$). The red squares, lines, and circles denote the experimental values for the inner barrier height, the excitation energy of the fission isomer, and the height of the outer barrier, respectively. The data are from Ref. [2]. The excitation energies of fission isomers are fairly well reproduced by the axially sym- metric and reflection symmetric calculation, but the paths constrained by these symmetries overestimate the height of the inner and outer barriers. The inclusion of triaxial shapes lowers the inner barrier by $\approx 2$ MeV, that is, the axially symmetric barriers in the region $\beta_{20} \approx 0.5$ are bypassed through the triaxial region, bringing the height of the barriers much closer to the empirical values. As shown in the figure, the inclusion of octupole shapes (axial, reflection-asymmetric calculations) is essential to reproduce the height of the outer barrier in actinide nuclei. A very good agreement with data is obtained by following paths through shapes with non-vanishing octupole moments.

In very heavy deformed nuclei the density of single-nucleon states close to the Fermi level is rather large, and even small variations in the shell structure predicted by different effective interactions can lead to markedly distinct equilibrium deformations. To

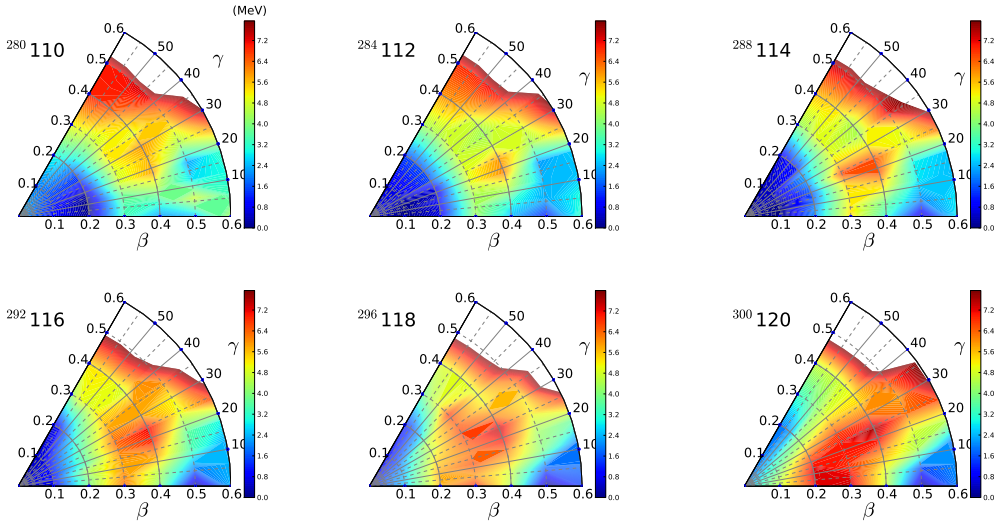


**FIGURE 2.** Self-consistent RHB triaxial energy maps of the even-even isotopes in the $\alpha$-decay chain of $^{300}120$ in the $\beta-\gamma$ plane ($0 \leq \gamma \leq 60^{\circ}$). Energies are normalized with respect to the binding energy of the absolute minimum.

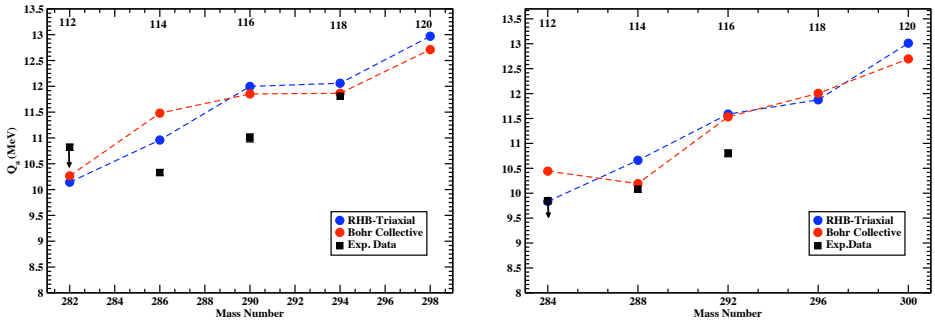


**FIGURE 3.** (Color online) $Q_{\alpha}$ values for the $\alpha$-decay chains of $^{300}120$. The theoretical values are calculated as the difference between the mean-field minima of the parent and daughter nuclei (blue diamonds), and as the difference between the energies of the $0^{+}$ ground states of the quadrupole collective Hamiltonian (red circles). The data (squares) are from Ref. [4].

illustrate the rapid change of equilibrium shapes for the heaviest nuclear systems, Fig. 2, displays the results of self-consistent triaxial RHB calculations of the energy surfaces in the $\beta-\gamma$ plane ($0 < \gamma < 60^{0}$) for isotopes in the $\alpha$-decay chain of $^{300}120$ [3]. The heaviest systems display soft oblate axial shapes with minima that extend from the spherical configuration to $\beta_{20} \approx 0.4$ ($Z = 120$) and $\beta_{20} \approx 0.3$ ($Z = 118$). The intermediate nuclei with $Z = 116$ are essentially spherical but soft both in $\beta$ and $\gamma$, whereas prolate deformed mean-field minima develop in the lighter systems with $Z = 114$, $Z = 112$ and $Z = 110$.

The two main decay modes in this region are $\alpha$-emission and spontaneous fission. The theoretical values denoted by (blue) diamonds in Fig. 3 correspond to transitions between the self-consistent mean-field minima on the triaxial RHB energy surfaces. Such a calculation does not explicitly take into account collective correlations related to

symmetry restoration and to fluctuations in the collective coordinates $\beta$ and $\gamma$. Physical transitions occur, of course, not between mean-field minima but between states with definite angular momentum. For this reason we have also used a recent implementation of the collective Hamiltonian based on relativistic energy density functionals [5], to calculate $\alpha$-transition energies between ground states of even-even nuclei ($0^+ \rightarrow 0^+$ transitions). The (red) circles in Figs. 3 denote the $Q_\alpha$ values, computed for transitions $0^+_{\text{g.s.}} \rightarrow 0^+_{\text{g.s.}}$ between eigenstates of the collective Hamiltonian. The differences with respect to mean-field values are not large, especially for the heaviest, weakly oblate deformed or spherical systems. For the lighter prolate and more deformed nuclei, the differences can be as large as the deviations from experimental values. The trend of the data is obviously reproduced by the calculations, and the largest difference between theoretical and experimental values is less than 1 MeV.

This analysis demonstrates the potential of the new class of semi-empirical REDFs for studies of shape coexistence and triaxiality in the heaviest nuclear system, including the explicit treatment of collective correlations using a microscopic collective Hamiltonian. This opens the possibility for a more detailed analysis of this region of SHN, including all presently known nuclides with $Z = 110 - 118$, as well as spectroscopic studies of nuclei with $Z > 100$.

## ACKNOWLEDGMENTS

This work was supported by the Finland Distinguished Professor Programme (FiDiPro) and the MZOS - project 1191005-1010, the Croatian Science Foundation.

## REFERENCES

1. T. Nikšić, D. Vretenar, and P. Ring, Phys. Rev. C 78, 034318 (2008).
2. R. Capote, M. Herman, P. Obložinský, P. G. Young, S. Goriely, T. Belgya, A. V. Ignatyuk, A. J. Koning, S. Hilaire, V. A. Plujko, M. Avrigeanu, O. Bersillon, M. B. Chadwick, T. Fukahori, Zhigang Ge, Yinlu Han, S. Kailas, J. Kopecky, V. M. Maslov, G. Reffo, M. Sin, E. Sh. Soukhovitskii, and P. Talou, Nucl. Data Sheets 110, 3107 (2009); Reference Input Parameter Library (RIPL-3) [http://www-nds.iaea.org/RIPL-3/].
3. V. Prassa, T. Nikšić, G.A. Lalazissis, D. Vretenar, Phys. Rev. C 86, 024317 (2012).
4. Yu. Ts. Oganessian, J. Phys. G: Nucl. Part. Phys. 34, R165 (2007).
5. T. Nikšić, Z. P. Li, D. Vretenar, L. Próchniak, J. Meng, and P. Ring, Phys. Rev. C 79, 034303 (2009).

# Nuclear shell structure and response toward the limits of mass, temperature and isospin

E. Litvinova[*], B.A. Brown[†], D.-L. Fang[*,**], T. Marketin[‡], P. Ring[§], V.I. Tselyaev[¶] and R.G.T. Zegers[†,**]

[*]*National Superconducting Cyclotron Laboratory, Michigan State University, East Lansing, MI 48824-1321, USA*
[†]*Department of Physics and Astronomy and National Superconducting Cyclotron Laboratory, Michigan State University, East Lansing, MI 48824-1321, USA*
[**]*Joint Institute for Nuclear Astrophysics, Michigan State University, East Lansing, MI 48824-1321, USA*
[‡]*Physics Department, Faculty of Science, University of Zagreb, 10000 Zagreb, Croatia*
[§]*Physik-Department der Technischen Universität München, D-85748 Garching, Germany*
[¶]*Nuclear Physics Department, St. Petersburg State University, 198504 St. Petersburg, Russia*

**Abstract.** We present a short overview of our recent theoretical developments aiming at the description of exotic nuclear phenomena to be reached and studied at the next-generation radioactive beam facilities. Applications to nuclear shell structure and response of nuclei at the limits of their existence, with a special focus on the physics cases of astrophysical importance, are discussed.

**Keywords:** nuclear shell structure, nuclear spin-isospin response, extended covariant density functional theory, particle-vibration coupling, coupling to single-particle continuum
**PACS:** 21.10.Pc, 21.60.Jz, 25.40.Lw, 27.60.+j, 21.30.Fe, 21.60.Cs, 24.30.Cz, 25.40.Kv, 24.10Jv

Last decades, low-energy nuclear physics has expanded considerably its domain due to the opportunities opened by rare isotope beam facilities of the new generation. In particular, the techniques of the isotope separation online and in-flight production have been implemented at the major low-energy nuclear physics facilities with great success: numerous experiments on synthesis of exotic nuclei and on studies of their dynamical properties have been performed. This has produced a strong catalyzing effect on theoretical developments toward finding a high-precision and highly universal solution of the nuclear many-body problem. In this contribution, we give a brief overview of our recent developments and applications to nuclear systems toward the limits of mass, isospin and temperature.

## QUASIPARTICLE-VIBRATION COUPLING IN RELATIVISTIC FRAMEWORK: SHELL STRUCTURE OF SUPERHEAVY Z=120 ISOTOPES

We show how the shell structure of open-shell nuclei can be described in a fully self-consistent extension of the covariant energy density functional theory. The approach implies quasiparticle-vibration coupling (QVC) in the relativistic framework being an extension of the Ref. [1] for superfluid systems [2]. Medium-mass and heavy nuclei

represent Fermi-systems where single-particle and vibrational degrees of freedom are strongly coupled. Collective vibrations lead to shape oscillations of the mean nuclear potential and, therefore, modify the single-particle motion. As a result, single mean-field states split into levels occupied with fractional probabilities which correspond to spectroscopic factors of these fragments. The Dyson equation is formulated in the doubled quasiparticle space of Dirac spinors and solved numerically for nucleonic propagators in tin isotopes which represent the reference case: the obtained energies of the single-quasiparticle levels and their spectroscopic amplitudes are in excellent agreement with data, see Fig. 1(a). Because of high universality of the approach it can be

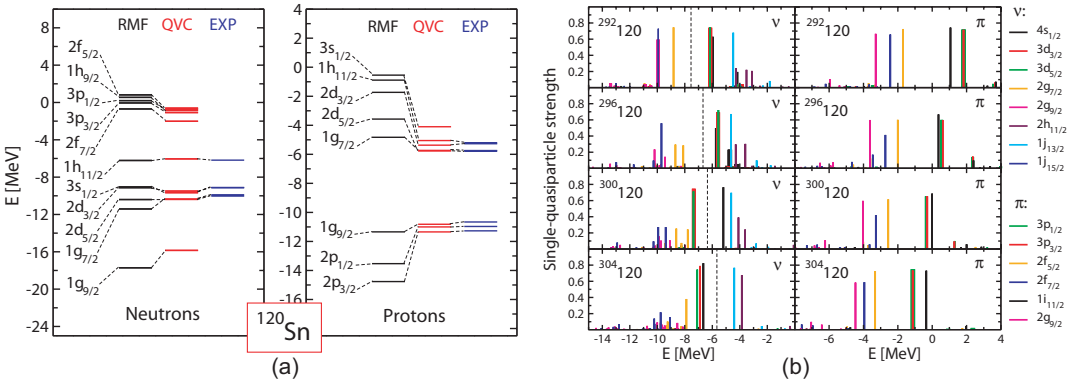


**FIGURE 1.** (a) Single-quasiparticle spectrum of $^{120}$Sn: Relativistic mean field (RMF, left column), QVC (center) and experimental data (right). In the 'QVC' and 'EXP' cases only the dominant levels are shown. (b) Single-quasiparticle strength distribution for the orbits around the Fermi surfaces in the neutron (left panels) and proton (right panels) subsystems of the Z=120 isotopes calculated in the relativistic quasiparticle-vibration coupling model. The dashed lines indicate the neutron chemical potentials.

applied to nuclei at the limits of their existence with respect to their proton and neutron numbers, for instance, to superheavy nuclei. Selected results on the single-quasiparticle strength distributions in the neutron and the proton subsystems of the Z = 120 isotopic chain are displayed in Fig. 1(b). One can see the evolution of these distributions with an increase of the neutron number from N = 172 to N = 184. The shell gap in the proton subsystems of the considered nuclei diminishes only little when the neutron number increases, so that the proton number Z = 120 remains a rather stable shell closure while the detailed structure of the proton levels shows some rearrangements induced by the neutron addition. In the neutron subsystems both pairing and QVC mechanisms are active and show a very delicate interplay: pairing correlations tend to increase the shell gap while the QVC alone tends to decrease it and at the same time causes the fragmentation of the states in the middle of the shell. As a result, in the presence of both mechanisms the gap in the neutron subsystem remains almost steady while the newly occupied levels jump down across the gap when the neutrons are added. Thus, in contrast to the pure mean field studies [3], no sharp neutron numbers appear as the candidates for the spherical shell closures in this region: the shell closures are delocalized.

# SPIN-ISOSPIN RESPONSE OF NEUTRON-RICH NUCLEI

Although last decade the three major concepts in low-energy nuclear theory (i) ab-initio approaches, (ii) configuration interaction models (known also as shell-models) and (iii) density functional theory (DFT) have advanced considerably, they still have to be further developed to meet the requirements demanded by contemporary nuclear experiment and astrophysics. Furthermore, each of these concepts has principal limitations of their applicability in the nuclear physics domain. Fig. 2(a) shows an image of the nuclear chart taken from Ref. [4]. The areas of the nuclear landscape which can be described by each of the three theoretical concepts are outlined (here we focus on the spin-isospin nuclear properties, e.g., Gamow-Teller response).

The sectors of the nuclear landscape where the applicability areas of the different models overlap are of particular interest because within these sectors the models can constrain each other. Ab-initio models can replace the phenomenological input which is traditionally used in the shell-model with the microscopic effective interaction computed from the first principles. In turn, the shell model with its very advanced configuration interaction concept can guide the DFT-based developments beyond its standard random phase approximation. Thus, in contrast to considering different models as independently developing alternatives, we rather admit their complementarity which can be used for their further advancements.

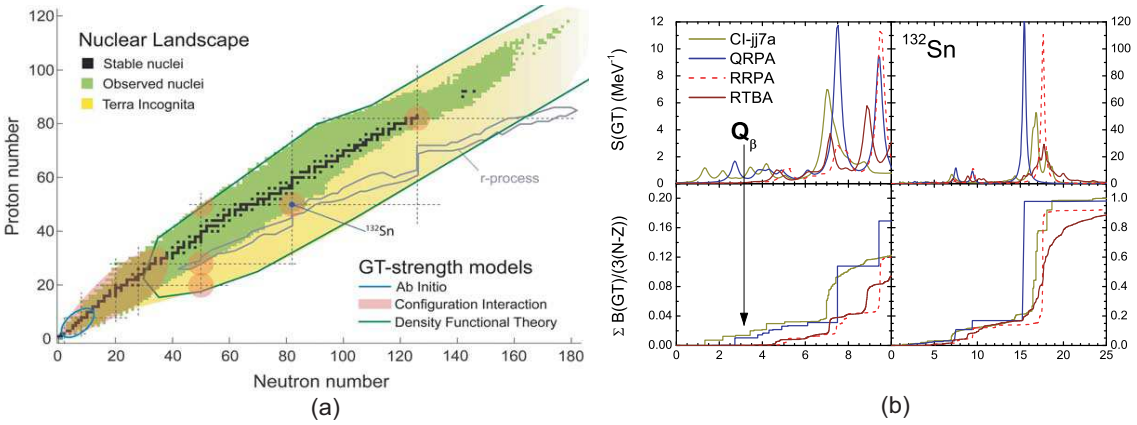


**FIGURE 2.** (a) Chart of the nuclei [4] representing stable nuclei and nuclei found in nature (black), those produced and investigated in the laboratory (green) and theoretical limits of bound nuclei (yellow). The domain of ab-initio models is the lightest nuclei (blue outline), the configuration interaction approach is applicable in the pink areas and density functional theory covers the region outlined in green. (b) The Gamow-Teller strength distribution in neutron-rich $^{132}$Sn calculated within the various theories (see text for details): low-energy and total strength distributions (upper panels) and their cumulative sums (lower panels), respectively.

In Fig. 2(b) we present studies of the Gamow-Teller resonance (GTR) in $^{132}$Sn within the three theoretical concepts: (i) non-relativistic quasiparticle random phase approximation (QRPA) with realistic G-matrix interaction [5], (ii) covariant DFT-based relativistic random phase approximation (RRPA) and its extension to particle-hole$\otimes$phonon configurations called relativistic time blocking approximation (RTBA) [6], and (iii) shell-model (SM) with the configuration interaction CI-jj7a truncated by the Tamm-Dancoff

proton-neutron phonon coupled to particle-hole core vibrations [7]. The gross and fine features of the GTR obtained within these models are compared, the advantages and drawbacks of the considered models are discussed. Based on such comparative studies, future directions are outlined for each of the above mentioned microscopic models [8]. Constraints on the many-body coupling schemes and underlying interactions from measurements at the future rare isotope facilities are anticipated.

## FINITE-TEMPERATURE EFFECTS ON LOW-ENERGY NUCLEAR RESPONSE

Excitation energy is another characteristic of excited nuclei which imposes limitations of their existence and plays a very important role in astrophysical modeling. We consider the finite-temperature effect on the low-energy nuclear response known as upbend phenomenon, which was first reported in Ref. [9], later observed systematically in the $\gamma$-ray strength functions below neutron threshold of various light and medium-mass nuclei and probed by different experimental techniques [10]. Studies of Ref. [11] have revealed that this phenomenon, occurring in various astrophysical sites, can have a significant impact on their elemental abundances.

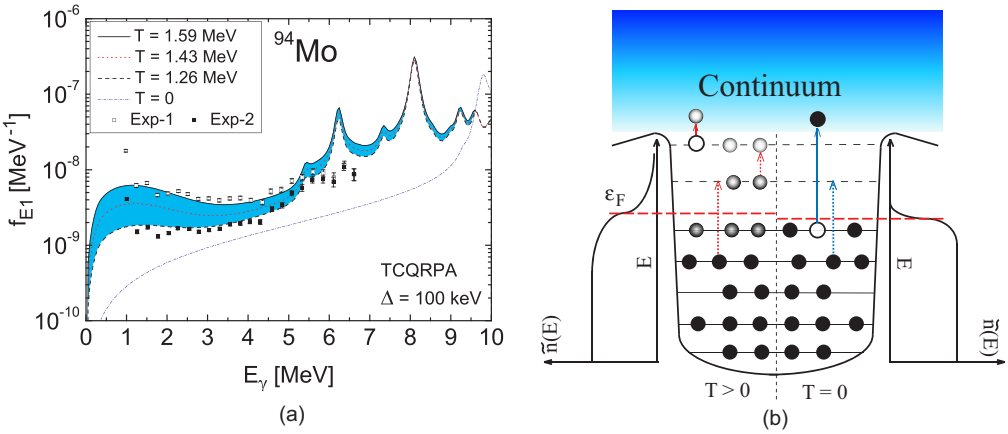


**FIGURE 3.** (a) The E1 $\gamma$-strength for the thermally excited state of $^{94}$Mo near the neutron separation energy (blue band), compared to the strength for the ground state (dash-dotted) and to Oslo data. (b) Schematic picture of the lowest-energy single-quasiparticle transitions from the thermally unblocked states with effective occupation probabilities $\tilde{n}(E)$ to the continuum.

We propose a microscopic approach for the radiative strength function which is based on the statistical description of an excited compound nucleus. The thermal mean field describes the nuclear excited states of the compound type very reasonably and, at the same time, it is simple enough to allow a straightforward generalization of very complicated microscopic approaches to nuclear response in terms of finite temperature corresponding to the nuclear excitation energy. To describe transitions from a thermally excited state, in the first approximation we employ the finite-temperature continuum QRPA developed in [12]. The two-quasiparticle propagator in nuclear medium is calculated in terms of the Matsubara temperature Green functions in the coordinate space. The continuum part of

this propagator is responsible for transitions from the thermally unblocked discrete spectrum states to the continuum. The radiative dipole strength function $f_{E1}$ is determined from the propagator in the standard way. Fig. 3(a) displays the $\gamma$-strength in $^{94}$Mo at the excitation energy around its neutron separation energy, that represents the case of radiative thermal neutron capture, compared to $\gamma$-strength in the ground state. The origin of the $\gamma$-strength upbend due to the transitions to the continuum is illustrated schematically in Fig. 3(b). The upbend appears as a typical feature of the $\gamma$-strength in medium mass nuclei while in heavy nuclei the strength is flat at $E_\gamma \to 0$ [13]. The obtained results have an important consequence for astrophysics, namely for the approaches to r-process nucleosynthesis: as shown in Ref. [11], the low-energy upbend in the $\gamma$-strength can give rise to a considerable enhancement of the neutron capture rates in neutron-rich nuclei and, consequently, influences the global abundance distribution.

Based on the obtained results, we expect further advancements of the theoretical approaches discussed in this contribution. The proposed developments on many-body coupling schemes and underlying interactions will need constraints from data on nuclei away from the valley of stability. Such data will be obtained in experiments performed at existing, and vastly enhanced capabilities presented by future rare isotope facilities.

## REFERENCES


1. E. Litvinova and P. Ring, Phys. Rev. C **73**, 044328 (2006).
2. E. Litvinova, Phys. Rev. C 85, 021303(R) (2012).
3. W. Zhang et al., Nucl. Phys. A **753**, 106 (2005).
4. G.F. Bertsch, J. Phys.: Conf. Ser. **78**, 012005 (2007).
5. J. Suhonen, T. Taigel and A. Faessler, Nucl. Phys. **A486**, 91 (1988).
6. T. Marketin, E. Litvinova, D. Vretenar, and P. Ring, Phys. Lett. B **706**, 477 (2012).
7. M. Horoi and B. A. Brown, Phys. Rev. Lett. **110**, 222502 (2013).
8. D.-L. Fang, T. Marketin, B.A. Brown, E. Litvinova, and R.G.T. Zegers, in preparation.
9. A. Voinov *et al.*, Phys. Rev. Lett. 93, 142504.
10. M. Wiedeking *et al.*, Phys. Rev. Lett. 108, 162503.
11. A.C. Larsen and S. Gorieli, Phys. Rev. C 82, 014318 (2010).
12. E.V. Litvinova, S.P. Kamerdzhiev, and V.I. Tselyaev, Phys. Atomic Nuclei 66, 558 (2003).
13. E. Litvinova and N. Belov, arXiv:1302.4478.

# Mean-field inferences from isotope shifts in lead

P. D. Stevenson, P. M. Goddard and A. Rios

*Department of Physics, University of Surrey, Guildford, Surrey, GU2 7XH, United Kingdom*

**Abstract.** Charge radius isotope shifts show pronounced kinks at many places acrodss the nuclear chart. These occur at many shell closures, caused by a change in single particle occupation, and away from closures, indicating underlying causes such as shape changes. In this contribution, we highlight some recent results from mean-field theory, concentrating on the case of the N=126 shell gap, and nearby.

**Keywords:** Nuclear Forces, Nuclear Matter
**PACS:** 21.65.-f, 21.60.Jz, 21.65.Cd, 21.65.Ef

## INTRODUCTION

Kinks in the nuclear charge radius along an isotopic chain are widespread across the nuclear chart [1, 2, 3]. They occur in particular across shell closures, indicating the effect of the change in the single-particle occupation. Since the effect occurs on the charge radius through the addition of neutrons, one can infer details of the proton-neutron interaction through the effect.

The kink across the N=126 shell closure has been dubbed the *anomalous kink effect* [4], though perhaps more for the failure of many models to reproduce the kink, more than its uniqueness. The experimental data across the N=126 shell gap in lead isotopes is shown in figure 1. The fit is given by a piecewise linear function. The gradient for the section below N=126 is 0.005457(63) fm, and above N=126 it is 0.010884(92) fm. The linear approximation to each line is therefore a good one, with a $\simeq 1\%$ error in the regression. The kink is pronounced with a doubling of the gradient across the gap.

## MEAN-FIELD DESCRIPTIONS AT N=126

Though mean-field approaches, such as the selfconsistent Skyrme approach [7, 8], are well able to reproduce the magic numbers, they are not always able to reproduce the kinks. In particular, Skyrme forces in general were not able to reproduce the $N = 126$ kink, whereas relativistic mean fields were [4]. A solution came by comparing the spin-orbit ponentials in the two approaches [9, 10]. By changing the Skyrme spin-orbit force to have the freedom to resemble the realtivistic mean field, the kink was easily reproduced in the Skyrme case.

It is important to note, however, that if one makes a fit to the kink, then its reproduction is possible, even with the original Skyrme mean field - as is the case with the SkI5 parameterisation [9]. The key factor is the ordering and hence occupation of the single particle levels. In the case of the increased slope of the isotope shift after N=126 it is

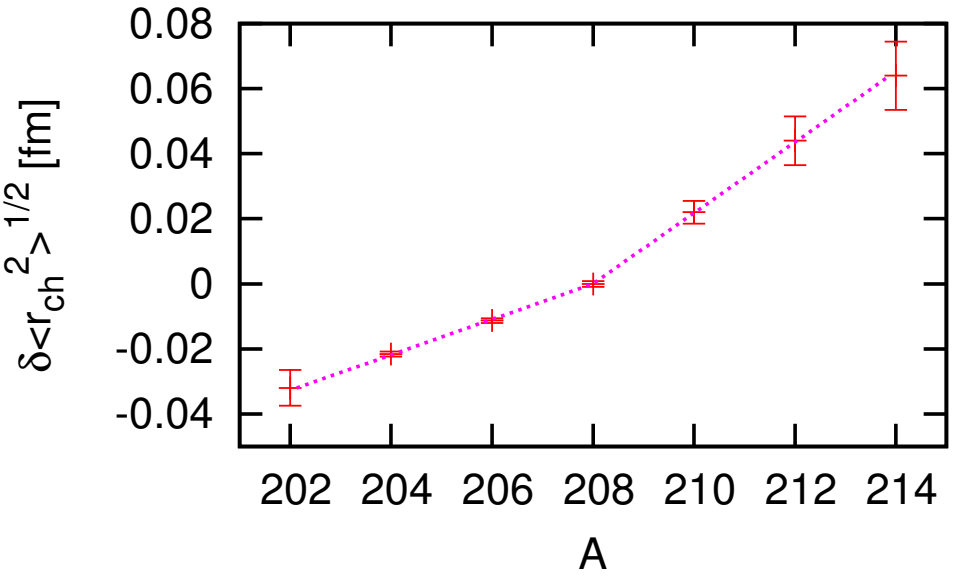


**FIGURE 1.** Experimental charge radius isotope shift in lead isotopes. Data from [1], normalised relative to $^{208}$Pb. Line of fit as explained in text.

crucial that the $i_{11/2}$ neutron orbital is occupied. Though it has a smaller radius than the $g_{9/2}$ neutron orbital, its nodal structure gives it a larger spatial overlap with the deeply-bound proton states, pulling them to a larger radius [11]. It is necessary, therefore, whether by the nature of the spin-orbit force, or another means (e.g. a low effective mass [12]) that the relative ordering of the $g_{9/2}$ and $i_{11/2}$ is such that $i_{11/2}$ orbital is at least partially occupied through pairing correlations above N=126.

## HEADING EAST

The way in which the ordering of single-particle levels can affect observables such as the isotope shift is quite general and exists across the periodic table. As well the effect described above, shape changes can lead to sudden gradient changes in isotope shifts, such as in the well-known case of the zirconium nuclei [1, 13]. We present, in figure 2, the isotope shift in the proton radius, for two sample Skyrme interactions; SLy4 [14] and NRAPRii [15, 11]. SLy4 shows a steady increase in proton radius as N increases. NRAPRii shows a steady increase up to N=134, after which the ground state is predicted to be slightly deformed so that the proton radius shows a kink. Unlike the case of the kink across the N=126 magic number, the deformation-based kink is highly dependent on the nature of the nature of the potential energy surface, as a function of deformation.

In the case of the N=126 kink, the nuclei are safely mean-field nuclei, well represented by a single Slater determinant with a well-defined (zero) deformation. Away from N=126, as the potential energy surface gets softer, the mean-field approximation becomes less good. The true ground state, as one would find from a beyond-mean-field calcualation, would involve mixing of many deformations and would certainly have a

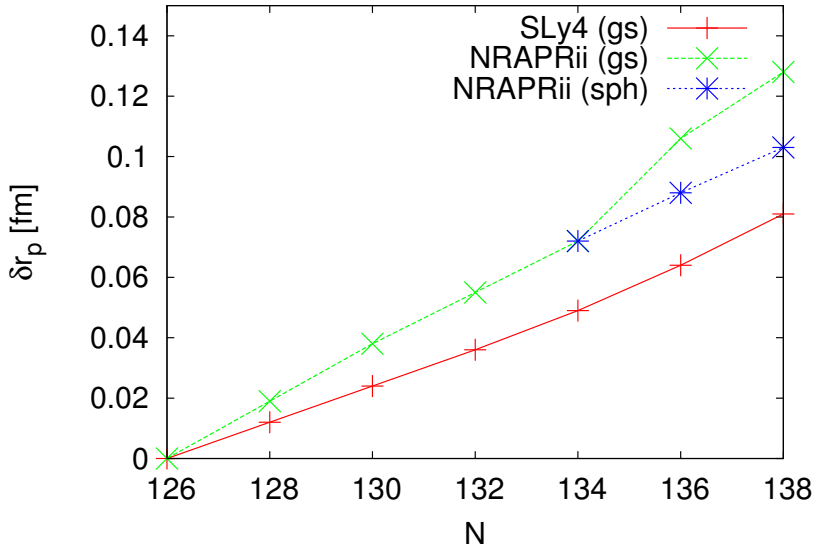


**FIGURE 2.** Proton radius isotope shifts in lead isotopes for N≥126 for SLy4, in which all ground states are spherical, and NRAPRii, in which deformation sets in for N≥136

radius greater than a rigidly spherical state. The difference between SLy4 and NRAPRii would therefore remain in a more sophisticated calculation. Such effects are then a possible experimental probe of differences between effective interactions.

## CONCLUSIONS

Isotope shifts in charge radii give an indication of underlying shell structure. Different mean-field interactions give different predictions for the isotope shifts and thus experimental data no this observable may discriminate between models. We have demostrated the effect of this in stable lead nuclei, and also as one moves to the more neutron-rich region at the limits of current experimental reach.

## ACKNOWLEDGMENTS

This work was funded by the UK STFC under grant numbers ST/J00051/1, ST/J500768/1 and ST/I005528.1.

## REFERENCES

1. I. Angeli, K. P. Marinova, *At. Data Nucl. Dara Tables* **99**, 69 (2013).
2. T. E. Cocolios *et al.*, *Phys. Rev. Lett.* **106**, 052503 (2011).
3. B. A. Brown, C. R. Bronk and P. E. Hodgson, *J. Phys. G* **10**, 1683 (1984).
4. R. Niembro, S. Marcos, M. Lopez-Quelle and L. N. Savushkin, *Phys. At. Nucl.* **75**, 269 (2012).
5. E. de Guerra, O. Moreno and P. Sarriguren, *J. Phys.: Conf. Ser.* **312**, 092045 (2012).

6. P. D. Stevenson, P. M. Goddard, J. R. Stone and M. Dutra, *AIP Conf. Proc.* **1529**, 262 (2013).
7. J. R. Stone and P.-G. Reinhard, *Prog. Part. Nucl. Phys.* **58**, 587 (2007).
8. M. Bender, P.-H. Heenen and P.-G. Reinhard *Rev. Mod. Phys.* **75**, 121 (2003).
9. P.-G. Reinhard and H. Flocard, *Nucl. Phys.* **A584**, 467 (1995)
10. M. M. Sharma, G. Lalazissis, J. König and P. Ring, *Phys. Rev. Lett.* **74**, 3744 (1995)
11. P. M. Goddard, P. D. Stevenson and A. Rios, *Phys. Rev. Lett.* **110**, 032503 (2013)
12. P. M. Goddard, P. D. Stevenson and A. Rios, *arXiv: 1306,4492* (2013)
13. D. H. Forest, J. Billowes, P. Campbell, P. Dendooven, K. T. Flanagan, J. A. R. Griffith, J. Huikari, A. Jokinen, R. Moore, A. Nieminen, H. L. Thayer, G. Tungate, S. Zemlyanoi and J. Äystö, *J. Phys. G* **28**, L63 (2002)
14. E. Chabanat, P. Bonche, P. Haensel, J. Meyer and R. Schaeffer, *Nucl. Phys.* **A 635**, 231 (1998)
15. A. W. Steiner, M. Prakash, J. M. Lattimer and P. J. Ellis, *Phys. Rep.* **411**, 325 (2005)

# On the meaning of symmetry energy in the case of dis-homogeneous nuclear matter: a (proto-)neutron star crust study

Ad. R. Raduta*, F. Aymard† and F. Gulminelli†

*IFIN-HH, Bucharest-Magurele, POB-MG6, Romania
†ENSICAEN, LPC, CNRS, UMR6534, F-14050 Caen cédex, France

**Abstract.** The symmetry energy plays a significant role in the evolution of core-collapsing supernovae and the structure of nascent neutron stars. Despite this, little is known in what concerns its value away from normal nuclear density and, even more important, the meaning of this quantity in the case of dis-homogeneous matter, as the one thought to constitute the neutron star crust. In this contribution we investigate the meaning of the symmetry energy in the case of clusterized systems and its sensitivity to the isovector properties of the effective interaction. To this aim, a recently developed nuclear statistical equilibrium model in which clusters and unbound interacting nucleons are consistently described by the same energy functional is employed.

**Keywords:** nuclear equation of state, symmetry energy, clusterized matter, neutron stars
**PACS:** 21.65.Mn,26.60.Gj,21.10.Dr

In thermodynamics, an equation of state (EOS) is any mathematical relation among state variables. In nuclear physics it most often refers to the dependence of energy per particle, $e(\rho,\delta)$, on isoscalar ($\rho=\rho_n+\rho_p$) and isovector ($\delta=(\rho_n-\rho_p)/(\rho_n+\rho_p)$) densities.

By performing series-expansion of $e(\rho,\delta)$ in terms of $\delta$ around $\delta=0$,

$$e(\rho,\delta)=e_0(\rho,\delta=0)+e_{sym}(\rho,\delta=0)\delta^2+\mathscr{O}(\delta^2) \tag{1}$$

and $\rho$ around $\rho_0$, the normal nuclear matter density,

$$e_0(\rho)=e_0(\rho_0)+L_0\chi+\frac{K_0}{2!}\chi^2+\mathscr{O}(\chi^3), \tag{2}$$

$$e_{sym}(\rho)=\frac{1}{2!}\frac{\partial^2 e(\rho,\delta)}{\partial\delta^2}|_{\delta=0}=e_{sym}(\rho_0,\delta=0)+L\chi+\frac{K_{sym}}{2!}\chi^2+\mathscr{O}(\chi^3), \tag{3}$$

it comes out that, for any $(\rho,\delta)$, the energy per particle may be expressed as a function of 5 parameters: $e_0(\rho_0)$ (saturation energy), $K_0$ (compression modulus), $e_{sym}(\rho_0)$ (symmetry energy at saturation), $L$ (slope of the symmetry energy at $\rho_0$) and $K_{sym}$ (curvature of the symmetry energy at $\rho_0$) [1]. Extensive nuclear matter studies confirm that this is true and accurate for uncharged homogeneous matter.

---

[1] the absence of odd-terms in eq. (1) stems from the exchange symmetry between protons and neutrons in lack of Coulomb interaction and assuming charge symmetry of nuclear forces; because of the definition of saturation, $L_0\equiv 0$.

Experimental data obtained in terrestrial laboratories constrain well all the isoscalar properties such as the commonly accepted values for $\rho_0$, $e_0$, $K_0$ and $e_{sym}$ span relatively narrow domains. The opposite holds in what regards the isovector properties. The reason is obviously due to the fact that all data roughly correspond to isospin symmetric systems. As such, it is equally clear that no significant progress could be achieved before exotic beam facilities become available.

The astrophysical consequences of the poorly known isovector properties of EOS are a subject of hot scientific debate as in the evolution of core-collapsing supernova (CCSN) and in the neutron-star (NS) crust the baryonic matter is highly neutron rich. The situation is nevertheless very delicate as it is not clear whether the formalism developed for nuclear matter (NM) and in base on which the EOS-parameters are defined stands valid in the case of stellar matter. Indeed, NM is defined as electrically uncharged and homogeneous while baryonic matter in compact objects is charged and dishomogeneous. The dishomogeneities stem from the contrasting effects of Coulomb and nuclear interactions and make the nuclear matter consist of two components: one dense with a density close to the normal nuclear density, most often modelized as a gas of clusters, and one dilute, usually regarded as an interacting gas of nucleons. The two phases are in thermal and chemical equilibrium.

The aim of our present study is twofold. First, we want to see to what extent the two existing definitions of the symmetry energy as the curvature of the energy per baryon in the isospin direction,

$$e_{sym}^{(1)} = \frac{1}{2}\frac{\partial^2 e}{\partial \delta^2}, \tag{4}$$

and, alternatively, the cost of converting symmetric matter in neutron matter

$$e_{sym}^{(2)} = e(\rho, \delta = 1) - e(\rho, \delta = 0) \tag{5}$$

apply and agree. Then, we want to see to what extent the stellar matter symmetry energy is sensitive to the isovector properties of the EOS.

To this aim we adopt the nuclear statistical equilibrium (NSE) model recently proposed in Ref. [1]. NSE models [2] are known to constitute valuable tools for addressing thermal and chemical properties of baryonic matter over the huge relevant ranges of temperature ($10^9 < T < 2 \cdot 10^{11}$ K), density ($10^5 < \rho < 10^{14}$ g/cm$^3$) and proton fraction ($0 \leq Y_p \leq 1$) populated in the course of CCSN with moderate computational effort. At variance with previous versions, the version of Ref. [1] treats clusters and unbound nucleons consistently by using the same energy functional [3].

The left panel of Fig. 1 spots the evolution of the total energy per baryon as a function of the isospin asymmetry for the arbitrary thermodynamical case characterized by $T$=0.5 MeV and $\rho = 10^{-8}$ fm$^{-3}$. For the sake of the argument, also the behavior of the clusterized component is represented. As one may notice, because of dishomogeneities, the parabolic approximation breaks and, because of Coulomb, the isospin-symmetry is violated. This means that any symmetry energy extracted from the curvature of the energy per baryon in the isospin direction will depend on the interval on which the fit was done and eqs. (4) and (5) will lead to different results.

A more complete image on the density and temperature dependence of the dilute star matter symmetry energy calculated according to eq. (4) is offered by the middle panel

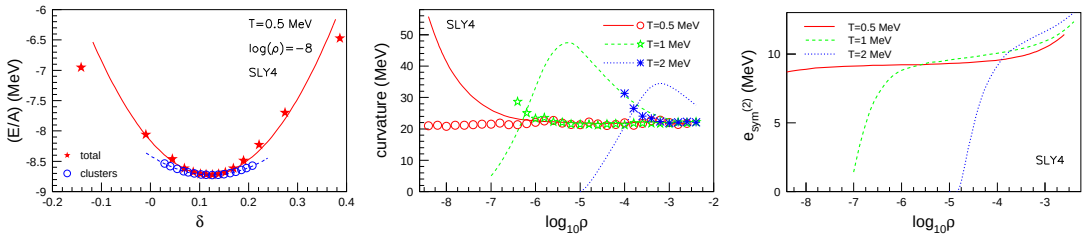


**FIGURE 1.** Left: Test of the quadratic approximation of the energy per baryon versus asymmetry for T=0.5 MeV and $\rho = 10^{-8}$ fm$^{-3}$. The total energy per baryon (stars) is plotted together with the clusterized component value (open circles) as a function of the respective $\delta = 1 - 2Y_p$ values. The full and dashed lines correspond to a second order polynomial fit of $e(\delta)$ and $e_{cl}(\delta_{cl})$, respectively. Middle: $e^{(1)}_{sym}$ for the whole system (lines) and, respectively, the clusterized component (symbols) as a function of total baryonic density at various temperatures: T=0.5, 1 and 2 MeV. Right: The evolution with total baryonic density of $e^{(2)}_{sym}$ for T=0.5, 1 and 2 MeV. In all cases, the considered effective interaction is SLY4. Figures adapted from Ref. [1].

of Fig. 1 in comparison with the corresponding values of the clusterized component. Several features are to be noted: (i) $e_{sym} \rightarrow (e_{sym})_{cl}$ only at very low temperatures (in this case $T \leq 1$ MeV) and densities exceeding a certain value, that is when matter chiefly consists out of nuclear clusters; (ii) at very low densities, where dilute matter dominates, it either steepens the dependence of $e(\delta)$ with respect to $(e(\delta))_{cl}$, leading to a $e^{(1)}_{sym}$-value highly superior to the one of bulk symmetric matter, or - if the temperature is too high to allow clusters to appear, makes $e^{(1)}_{sym}$ vanish; (iii) for $T \geq 1$ MeV, even $(e_{sym})_{cl}$ deviates from the bulk symmetric matter value because of the translational kinetic energy contribution.

The right panel of Fig. 1 illustrates the evolution with total baryonic density of the symmetry energy calculated according to eq. (5) at T=0.5, 1 and 2 MeV. The most important message is the one learnt by comparison with the middle panel: eqs. (4) and (5) are not equivalent, as we have anticipated.

Taking into account that (1) baryonic star matter partially consists out of a dense component (whose relative abundance obviously depends on the thermodynamical conditions) and (2) nuclear EOS is well constrained around the normal nuclear matter density, one can expect dilute star matter present a reduced sensitivity to the isovector properties with respect to pure nuclear matter. To check to what extent this holds we employ four Skyrme-like effective interaction potentials having as much as possible similar isoscalar behaviors but different isovector characteristics: SLY4 [4], SGI [5], SkI3 [6] and LNS [7]. Their bulk properties are listed in Table 1 together with the corresponding liquid drop model (LDM) parameters as provided in Ref. [3].

Fig. 2-right panel illustrates the evolution with the total baryonic density of the symmetry energy defined by eq. (4) for each considered potential at T=0.5 MeV. The general trends obtained for SLY4 are confirmed by the other potentials. Because of the clusters and contrary to what happens for pure nuclear matter (left panel), the system keeps the EOS-memory even at very low densities. Again, because of the clusters and contrary to what happens for pure nuclear matter, a constant dispersion of moderate

**TABLE 1.** Bulk nuclear properties for different Skyrme interactions as given in Ref. [3]

| NN-potential | $\rho_0^0$ (fm$^{-3}$) | $K_0$ (MeV) | $L$ (MeV) | $K_{sym}$ (MeV) | $a_v$ (MeV) | $a_s$ (MeV) | $a_v^a$ (MeV) | $a_s^a$ (MeV) | $a_c$ (MeV) |
|---|---|---|---|---|---|---|---|---|---|
| SLY4 | 0.1595 | 230.0 | 46.0 | -119.8 | 15.97 | 18.24 | 32.00 | 16.60 | 0.69 |
| SGI | 0.1544 | 261.8 | 63.9 | -52.0 | 15.89 | 17.48 | 28.33 | 12.76 | 0.69 |
| SkI3 | 0.1577 | 258.2 | 100.5 | 73.0 | 15.98 | 17.77 | 34.83 | 12.77 | 0.69 |
| LNS | 0.1746 | 210.8 | 61.5 | -127.4 | 15.31 | 15.77 | 33.43 | 14.10 | 0.69 |

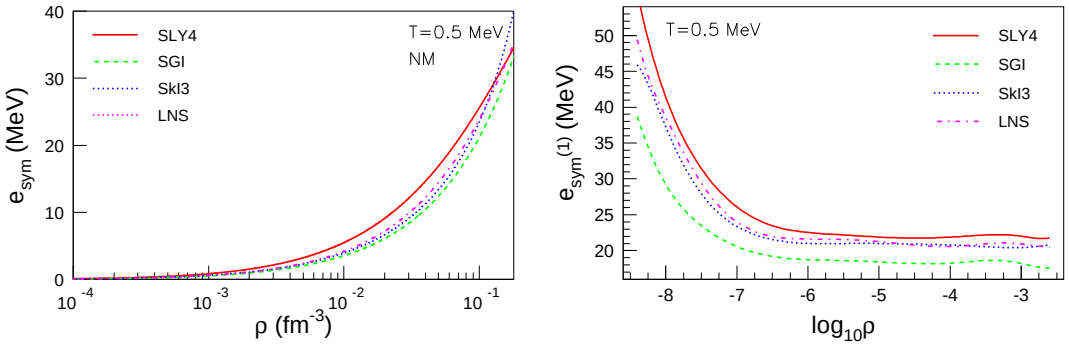


**FIGURE 2.** Sensitivity of the symmetry energy to the effective interaction as a function of baryonic density. Left: pure nuclear matter, right: $e_{sym}^{(1)}$ in case of dilute clusterized matter. In both cases, T=0.5 MeV. Figure adapted from Ref. [1].

magnitude is obtained over the whole considered density range. Not surprising, this dispersion of about 3 MeV corresponds precisely to the one the different EOS present at saturation density.

In conclusion, the Coulomb-induced dishomogeneties strongly influence the star matter global energetics in both isoscalar and isovector directions. Not only that the baryonic energy is non-zero in the $\rho \to 0$ limit, but the parabolic approximation on which the symmetry energy is defined fails. Moreover, the isospin symmetry breaking makes the curvature energy in the isospin direction be different than the energy difference between neutron and symmetric matter. Finally, the effective density explored in stellar matter is different from the average density because of density fluctuations. As a consequence, the uncertainties present in the isovector part of the EOS are partially washed out though better constraints are definitely needed for a fully quantitative prediction for astrophysical applications.

## REFERENCES


1. Ad. R. Raduta, F. Aymard and F. Gulminelli, arXiv:1307.4202.
2. A. C. Phillips, The Physics of Stars (John Wiley & Sons, Chichester, 1994).
3. P. Danielewicz and J. Lee, Nucl. Phys. A 818 (2009) 36.
4. E. Chabanat *et al.*, Nucl. Phys. A 635 (1998) 231.
5. N. van Giai and H. Sagawa, Phys. Lett. B 106 (1981) 379.
6. P.-G. Reinhard and H. Flocard, Nucl. Phys. A 584 (1995) 467.
7. L. G. Cao, U. Lombardo, C. W. Shen and N. V. Giai, Phys. Rev. C 73 (2006) 014313.

# Bayesian Inference and Nuclear Structure Models

B. Szpak*, J. Dudek† and B. Fornal*

*The Niewodniczanski Institute of Nuclear Physics - PAN, ul. Radzikowskiego 152, PL-31-342 Krakow, Poland

†IPHC/DRS and Université de Strasbourg, 23 rue du Loess, B.P. 28, F-67037 Strasbourg, France

**Abstract.** We apply bayesian formulation of probability theorem to estimate the parameters of a spherical Skyrme-Hartree-Fock model. We show that the bayesian methods allows to consistently include the *a priori* expectations about the model parameters which helps to regularize the parameter estimation problem. The advantages of the method are advocated throughout the text.

**Keywords:** nuclear structure, bayesian inference, least-squares methods, nuclear density functional theory
**PACS:** 21.60.Jz, 21.10.-k, 21.30.Fe, 21.65.Mn

## INTRODUCTION

To estimate the parameters of empirical nuclear structure models one usually performs a least-square fit to experimental data and then (ralely) follows with the covariance analysis [1, 2]. The deficit of experimental data and the character of a model can cause that the problem is ill-posed [3]. This results in a situation when a model has very poor predictive power as its estimated parameters are higly sensible to a random noise of experimental data. Below we show that the application of Bayesian Inference methods can help to regularize the problem and obtain solutions with enhaced predictive power.

## METHOD

Let us introduce a set of experimental data represented by a vector $\mathbf{d}$ of length $m$, a vector of model parameters $\mathbf{m}$ of length $n$ and a physical model described by a $m \times n$ matrix $\mathbf{G}$ such that:

$$\mathbf{d} = \mathbf{G}\mathbf{m}\,. \tag{1}$$

In realistic case the model and/or experimental measurment is not exact. Very often this information is represented by assuming that:

$$\mathbf{d} = \mathbf{d}^{th} + \mathbf{e}\,, \tag{2}$$

where $\mathbf{d}_i^{th} = (\mathbf{G}\boldsymbol{\mu})_i$ and by $\boldsymbol{\mu}$ we denote an optimal solution of (1), where the criterium of *optimality* will be specified below. In (2) $\mathbf{e}$ is a multivariate random variable representing both a noisy character of experimental measurement and approximate character of physical model. The common assumption is that $\mathbf{e}$ has a multivariate normal distribution $\mathscr{N}(0, \sigma^2\mathbf{P}^{-1})$ with zero mean and variance $\sigma^2\mathbf{P}^{-1}$. The matrix $\mathbf{P}$ is often reffered as a weighting matrix and $\sigma$ represents a single number called variance factor. In the following discussion we will consider the problem in which the $\mathbf{P}$ is known and that $\sigma$ is to be estimated. The estimated value of $\sigma$ will be denoted as $\hat{\sigma}$.

In Bayesian approach [4, 5] one is interested in calculating the probability of having a specified values of parameters given the set of experimental data that is $p(\mathbf{m}, \sigma^2|\mathbf{d})$, rather then probability of obtaining the data given the parameters. The conditional probability $p(\mathbf{m}, \sigma^2|\mathbf{d})$ is obtained by using a Bayes theorem:

$$p(\mathbf{m}, \sigma^2|\mathbf{d}) = \frac{p(\mathbf{d}|\mathbf{m}, \sigma^2)p(\mathbf{m})}{c}, \tag{3}$$

where $p(\mathbf{m})$ denotes the *prior* distribution of model parameters which can be determined from the *a priori* knowledge about the distribution for model parameters and $c$ is a normalization constant of no importance until one starts to compare different models. The major difference between the Bayesian and classical approaches in the context of current work is that the Bayes approach allows to incorporate prior information about the solution that comes from previous experiments or experience. When no *a priori* information about the model parameters is available (a so called non-informative prior) the frequentionist and bayesian approaches would lead to the same solution.

To obtain analitically tractable form of a posterior distribution one need to use *conjugate prior*. In the considered case (Gaussian noise with unknown variance) we assume that the prior information can be characterized by normal-gamma distribution. We characterize our beliefs about model parameters by its mean value $\boldsymbol{\mu}_p$ with covariance matrix $\mathrm{cov}(\boldsymbol{\mu}_p) = \sigma_p^2\mathbf{S}$. We assume that the expected value of variance factor is $\sigma_p^2$ and its variance is $V_{\sigma^2}$. It then can be shown that the posterior distribution for $\mathbf{m}$ and $\tau$ is also normal-gamma distribution:

$$\mathbf{m}, \tau|\mathbf{d} \sim \mathscr{NG}(\boldsymbol{\mu}_0, \mathbf{V}_0, b_0, p_0) \tag{4}$$

with the parameters:

$$\begin{aligned}
\boldsymbol{\mu}_0 &= (\mathbf{G}^T\mathbf{P}\mathbf{G} + \mathbf{S}^{-1})^{-1}(\mathbf{G}^T\mathbf{P}\mathbf{d} + \mathbf{S}^{-1}\boldsymbol{\mu}_p), && (5)\\
\mathbf{V}_0 &= (\mathbf{G}^T\mathbf{P}\mathbf{G} + \mathbf{S}^{-1})^{-1}, && (6)\\
2b_0 &= 2\big((\sigma_p^2)^2/V_{\sigma^2} + 1\big)\sigma_p^2 + (\boldsymbol{\mu}_p - \boldsymbol{\mu}_0)^T\mathbf{S}^{-1}(\boldsymbol{\mu}_p - \boldsymbol{\mu}_0)\\
&+ (\mathbf{d} - \mathbf{G}\boldsymbol{\mu}_0)^T\mathbf{P}(\mathbf{d} - \mathbf{G}\boldsymbol{\mu}_0), && (7)\\
2p_0 &= m + 2(\sigma_p^2)^2/V_{\sigma^2} + 4. && (8)
\end{aligned}$$

The posterior marginal distribution for $\boldsymbol{\mu}$ is multivariate $t$-distribution:

$$\boldsymbol{\mu}|\mathbf{d} \sim t(\boldsymbol{\mu}_0, b_0\mathbf{V}_0/p_0, 2p_0)\,. \tag{9}$$

with the expected value:

$$\hat{\sigma}^2 = \frac{b_0}{p_0 - 1} \tag{10}$$

The covariance matrix of $\boldsymbol{\mu}$ is given by:

$$\mathrm{cov}(\boldsymbol{\mu}) = \hat{\sigma}^2(\mathbf{G}^T\mathbf{P}\mathbf{G} + \mathbf{S}^{-1})^{-1}\,. \tag{11}$$

Presented formulas can be generalized to the case of a nonlinear model.

## RESULTS

To illustrate the method we use a spherical Skyrme-Hartree-Fock model [2] with parameters fitted to binding energies, radii and single particle energies of seven doubly magic nuclides: $^{16}$O, $^{40,48}$Ca, $^{56}$Ni, $^{90}$Zr, $^{132}$Sn, $^{208}$Pb. To analyze the method we compare the results obtained with the Bayesian Inference method to the results of the least-squares fit (denoted as L-S). We also fit to the whole data set (Bayes All fit) or exclude the single particle energies (Bayes BR fit). As prior values for the model parameters we choose: $\rho_c = 0.160 \pm 0.05$, $E^{\mathrm{NM}}/A = 16.0 \pm 0.2$, $K^{\mathrm{NM}} = 230 \pm 30$, $a_{\mathrm{sym}}^{\mathrm{NM}} = 32.5 \pm 2.5$, $L_{\mathrm{sym}}^{\mathrm{NM}} = 58 \pm 18$, $M_s^{*-1} = 1.18 \pm 0.07$, $M_v^{*-1} = 1.36 \pm 0.29$, $C_0^{\Delta\rho} = -63 \pm 14$, $C_1^{\Delta\rho} = -27 \pm 52$, $C_0^{\nabla J} = -92 \pm 10$, $C_1^{\nabla J} = -16 \pm 33$. Our choice for the prior values of nuclear matter parameters are based on [6]. As prior mean values and variance for the last four parameters we choose a mean and variance of almost 200 different Skyrme force parameterization.

The posterior estimates for model parameters are presented in Table 1. To obtained physically meaningful results with the least-square method three of the model parameters has to remain fixed at prior values. These are: $K^{\mathrm{NM}}$, $M_s^{*-1}$, $M_v^{*-1}$, however other choices are also possible. This is not needed in the case of Bayesian Inference method. As seen from the Table 1 the Bayesian Inference method allow to reduce the error estimate of model parameters by almost an order of magnitude. The obtained correlation matrix for model parameters is presented in Figure 1.

The influence of the fitting method to the predictive power of a model can be visualized by performing predictions of properties of nuclei that were not included in the fit. For this aim we choose $^{100}$Sn (interpolation) and $Z = 114, N = 162$ superheavy nucleus (extrapolation). The obtained estimates are presented in Tables 2 and 3, respectively. Analysis of presented results clearly indicates that the inclusion of *a priori* information has an important impact on uncertainty of model predictions and helps to obtain more robust estimates.

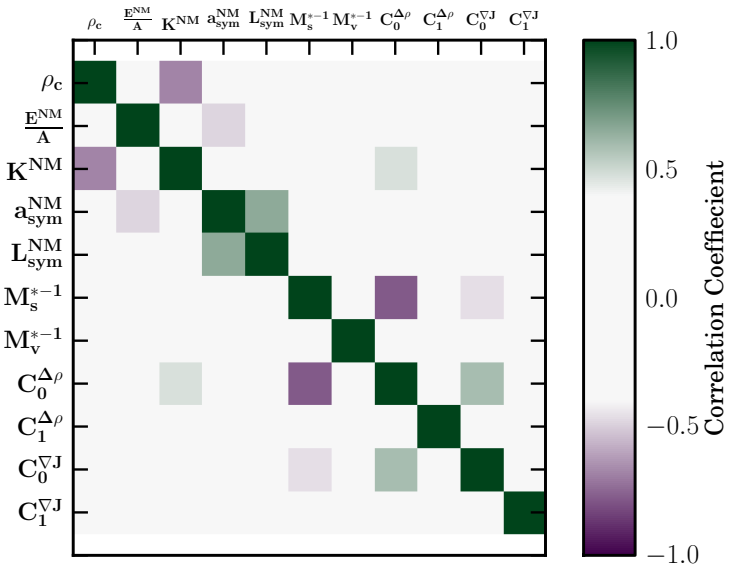


**FIGURE 1.** The correlation matrix of model parameters for the Bayes All model as obtained with the Bayesian Inference method.

We believe the methods of Bayesian Inference should be explored in details in further works.

## REFERENCES


1. J. Toivanen, J. Dobaczewski, M. Kortelainen and K. Mizuyama, *Phys. Rev.* **C 78** 034306 (2008)
2. M. Kortelainen *et. al. Phys. Rev.* **C 82** 024313 (2010)
3. J. Dudek *et. al.* J. Phys. G: Nucl. Part. Phys. **37**, 064031 (2010)
4. D. Calvetti, E. Somersalo, Introduction to Bayesian Scientific Computing, Springer 2010
5. K-R. Koch, Introduction to Bayesian Statistics, Springer 2007
6. M. Dutra *et. al. Phys. Rev.* **C 85** 035201 (2012)

**TABLE 1.** The obtained values of model parameters for different parameterizations used in the current work. The error given in bold font indicates that the parameter has been kept constant in the minimization procedure.

| | Parameterization | | | | | |
|---|---|---|---|---|---|---|
| Parameter | L-S (error) | | Bayes All (error) | | Bayes BR (error) | |
| $\rho_c$ | 0.157 | (0.024) | 0.158 | (0.002) | 0.159 | (0.002) |
| $E^{NM}/A$ | -15.900 | (0.294) | -16.005 | (0.065) | -16.032 | (0.045) |
| $K^{NM}$ | 230. | (**0.0**) | 264. | (18.) | 253. | 12. |
| $a_{sym}^{NM}$ | 31.35 | (7.64) | 31.47 | (1.36) | 31.86 | (0.90) |
| $L_{sym}^{NM}$ | 55. | (83.) | 57. | (14.) | 57. | (9.) |
| $M_s^{*-1}$ | 1.18 | (**0.0**) | 1.08 | (0.05) | 1.19 | 0.03 |
| $M_v^{*-1}$ | 1.36 | (**0.0**) | 1.47 | (0.23) | 1.35 | 0.16 |
| $C_0^{\Delta\rho}$ | -65.2 | (5.95) | -57.1 | (3.0) | -63.0 | (2.1) |
| $C_1^{\Delta\rho}$ | -52. | (165.) | -463. | (45.) | -44. | (29.) |
| $C_0^{\nabla J}$ | -89.7 | (8.5) | -83.0 | (3.6) | -81.1 | (2.6) |
| $C_1^{\nabla J}$ | 8. | 99. | -6. | (26.) | -10. | (17.) |

**TABLE 2.** The predictions of the properties of $^{100}$Sn nuclide as obtained with different parameterizations.

| | Parameterization | | | | | |
|---|---|---|---|---|---|---|
| Property | L-S (error) | | Bayes All (error) | | Bayes BR (error) | |
| Proton radius | 4.436 | (0.075) | 4.400 | (0.011) | 4.395 | (0.009) |
| Neutron radius | 4.364 | (0.073) | 4.330 | (0.010) | 4.324 | (0.008) |
| Binding energy | -828.88 | (2.37) | -828.98 | (1.42) | -828.83 | (1.34) |
| $\pi 1g_{9/2}$ | -2.983 | (0.193) | -2.872 | (0.100) | -2.970 | (0.092) |
| $\pi 2d_{5/2}$ | 2.328 | (0.284) | 2.461 | (0.132) | 2.600 | (0.139) |
| $\pi 1g_{9/2}$ | -16.645 | (0.239) | -16.674 | (0.106) | -16.795 | (0.103) |
| $\pi 2d_{5/2}$ | -11.291 | (0.133) | -11.331 | (0.124) | -11.159 | (0.137) |

**TABLE 3.** The predictions of the properties of $Z = 114$ and $N = 162$ nuclide as obtained with different parameterizations.

| | Parameterization | | | | | |
|---|---|---|---|---|---|---|
| Property | L-S (error) | | Bayes All (error) | | Bayes BR (error) | |
| Proton radius | 6.130 | (0.103) | 6.075 | (0.015) | 6.068 | (0.012) |
| Neutron radius | 6.224 | (0.118) | 6.168 | (0.019) | 6.161 | (0.016) |
| Binding energy | -1971.90 | (6.04) | -1975.71 | (2.97) | -1973.12 | (2.68) |
| $\pi 1g_{9/2}$ | -2.560 | (0.388) | -2.497 | (0.179) | -2.581 | (0.172) |
| $\pi 2d_{5/2}$ | -0.780 | (0.348) | -0.766 | (0.175) | -0.820 | (0.164) |
| $\pi 1g_{9/2}$ | -9.043 | (0.461) | -9.104 | (0.164) | -9.151 | (0.149) |
| $\pi 2d_{5/2}$ | -7.443 | (0.214) | -7.268 | (0.143) | -7.307 | (0.140) |

# Estimates of Electric Transition Probabilities in $^{156}$Gd Nucleus

A. Dobrowolski and A. Góźdź, A. Szulerecka

*Institute of Physics, M. Curie–Skłodowska University,*
*Radziszewskiego 10, 20-031 Lublin, Poland*

**Abstract.** A collective approach combining the zero– and one–phonon excitations in the quadrupole and octupole modes together with the rotational motion is used to verify the possibility of reproducing the experimental electric $B(E\lambda)$ probabilities in $^{156}$Gd nucleus in presence of the high–rank tetrahedral/octahedral symmetry of collective quadrupole, octupole and rotational states.

**Keywords:** Tetrahedral/Octahedral symmetry, Irreducible representation, Electric transition probability
**PACS:** 21.10.Ma, 25.70.Gh, 25.85.-w

## INTRODUCTION

The systematic knowledge of electromagnetic reduced transition probabilities $B(E\lambda)$ is essential to discover a possible high–rank symmetries as, e.g. tetrahedral, octahedral in nuclear systems. A symmetry, among other physical effects, is a key factor determining the structure of the wave functions, thus strongly affecting the reduced transition probabilities $B(E\lambda)$. In this work we apply a harmonic-like model, discussed in details in [1, 2], to reproduce the experimental $B(E1)$ and $B(E2)$ probabilities in $^{156}$Gd, a nucleus supposed to possess low-lying tetrahedral, negative-parity band and for which some data of interest are available from the recent experiments [3, 4]. We thus analyze the behavior of the electric transition probabilities within and between the ground-state and the negative-parity bands in order to find out to which irreducible representation of the tetrahedral group $T_d$ (or the octahedral group $O$) the state of interest could belong. The proposed collective model contains twelve collective variables $(\alpha_{20}, \alpha_{22}, \{\alpha_{3\nu}\}, \{\Omega\},\ \nu = 0, \pm1, \pm2, \pm3)$, describing respectively the axial and non-axial quadrupole vibrational modes, all the seven octupole vibrational modes and the three rotational modes described by the Euler angles. Nuclear surface in the intrinsic coordinate system is described in terms of those nine shape variables $(\alpha_{20}, \alpha_{22}, \{\alpha_{3\nu}\})$ using the multipole expansion given, e.g. in [5]. In this work, for simplicity of calculations we apply the idea of the adiabatic separation of vibrational and rotational motions. As a consequence, we may introduce a factorized wave function of the form

$$\psi \equiv \psi_{vib}^{\Gamma_1\Gamma_2}(\alpha_{20}, \alpha_{22}, \alpha_{3\nu}) R_{JM}^{\Gamma_3}(\Omega) = \psi_{vib,2}^{\Gamma_1}(\alpha_{20}, \alpha_{22})\, \psi_{vib,3}^{\Gamma_2}(\alpha_{3\nu})\, R_{JM}^{\Gamma_3} \qquad (1)$$

composed of products of the vibrational quadrupole $\psi_{vib,2}^{\Gamma_1}(\alpha_{20}, \alpha_{22})$, octupole $\psi_{vib,3}^{\Gamma_2}(\alpha_{3\nu})$ and rotational $R_{JM}^{\Gamma_3}(\Omega)$ solutions corresponding to uncoupled Hamiltonians. Each of those three $\psi$-functions belongs to only one irreducible representation

$\Gamma_i$ of the octahedral group $O$ or the tetrahedral group $T_d$. One should realize that both those groups are isomorphic, thus having the same set of the irreducible representation matrices. On the other hand, the states (1) span the collective space of our model in which a collective Hamiltonian should be constructed. It is the symmetry of that Hamiltonian which uniquely determines the symmetry properties of its eigensolutions built as the linear combinations of the basis functions (1). Therefore, at this stage, one is not able to unambiguously judge which of those two symmetries the underlying system really possesses.

As often assumed in simplistic collective approaches, the overall behavior of a low-lying state can be crudely reproduced by the zero- and one-phonon harmonic oscillator eigensolution. Since a collective Hamiltonian, able to reasonably reproduce the transitional probabilities is not known at this moment, we choose the physical states $\psi^{\Gamma_1}_{vib,2}(\alpha_{20},\alpha_{22})$, $\psi^{\Gamma_2}_{vib,3}(\alpha_{3\nu})$ of (1) to be the specific and complicated linear combinations of the zero- and one-phonon harmonic oscillator solutions transforming according to a given irreducible representation $\Gamma$ of the group $O$ (or $T_d$) and, in addition, having good parity. Notice that however the inversion operation does not belong to neither the octahedral group $O$ nor to the tetrahedral one $T_d$, it commutes with all elements of both groups. By consequence, the parity can be a good quantum number for the tetrahedrally or octahedrally symmetric states. The details of the procedures leading to such states and the way of constructing the rotational states $R^{\Gamma_3}_{JM}(\Omega)$ are presented in [1, 5, 8].

## RESULTS

The reduced transition probability $B(E\lambda)$ between the states (1), govern by the intrinsic transition operator $\hat{Q}_{\lambda\mu}$ can be calculated as

$$B(E\lambda, J\rightarrow J') = |\sum_{\mu}\langle\psi^{\Gamma'_1\Gamma'_2}_{vib}|\hat{Q}_{\lambda\mu}|\psi^{\Gamma_1\Gamma_2}_{vib}\rangle\,\langle R^{J'J';\Gamma'_3}||D^{\lambda\star}_{.\mu}||R^{J;\Gamma_3}\rangle|^2, \tag{2}$$

where $J$ and $J'$ are the angular momenta of the initial and final states, respectively. The symbol $.\mu$ as the sub-script of the Wigner function signifies that the considered reduced matrix element is reduced with respect to the first index. The meaning of the $\Gamma$–type symbols has been explained after (1).

Suppose that the initial $|i\rangle$ and final $|f\rangle$ states of a given collective Hamiltonian belong to the representations $\Gamma^i$ and $\Gamma^f$, respectively whereas the tensor transition operator $\hat{Q}_{\lambda\nu}$ transforms with respect to the irreducible representation $\Gamma^{\mathcal{Q}}$ of the octahedral group. The reduced probability of (2) can be non-zero if and only if $\Gamma^i\otimes\Gamma^{\mathcal{Q}}\supset\Gamma^f$, where the sign $\otimes$ denotes the Kronecker product of the irreducible representations.

Among all the five irreducible representations of the group $O$ (or $T_d$) there exist several pairs of representations corresponding to $\Gamma^i$ and $\Gamma^f$ which do not fulfill the above condition. The problem of the selection rules for the octahedral group $O$ has been discussed in details in [1].

Aware of those facts our task, at this stage, is to find out to which irreducible representation a given experimental level could possibly belong. The problem becomes even more challenging if one takes into account the symmetrization problem, usually solved

by introducing the so called *symmetrization group*, (for more details, see e.g. [1, 6]). It can be shown that for the here discussed collective space the symmetrization group is, in fact, the octahedral group $O$. Let us emphasize that, in general, one should clearly distinguish the *intrinsic symmetry group* acting on the intrinsic-component functions of (1) from the symmetrization group, however they coincide in this model. Each of those two types of groups influences different aspects of a collective model, (more details available e.g. in [5]).

Contrarily to the early simplistic considerations of the high-rank symmetries in atomic nuclei, based mainly on the tetrahedrally deformed mean-field, a realistic collective approach pretending to properly treat the problem of tetrahedral symmetry should comprise, apart from the simplest tetrahedral mode commonly recognized as the one which has zero quadrupole moment and represented in the lowest order by the $Y_{32}(\theta,\varphi)$ spherical harmonic alone, a possibility of incorporating the equivalent tetrahedral "combined modes" given by the characteristic superpositions of other than the $Y_{32}$ octupole modes, as done in [7]. It turns out that such a mode, coupled of the quadrupole, octupole and rotational motions, (see, [1]) can have arbitrarily large quadrupole moment, able to produce a substantial $B(E2)'$s.

## RESULTS

The calculation based on the above presented approach has been done in order to verify whereas a reasonable reproduction of the experimental reduced probabilities in $^{156}$Gd nucleus is, in general, possible in presence of the tetrahedral symmetry of the negative-parity states. The exact mathematical shape of the collective states used here to determine the transition probabilities can be found, e.g. in [2].

As shown in [4], the experimental values of the $Q_0$ moments of the ground state (6.83 $b$) and the octupole bands (7.10 $b$) are comparable. Therefore, in the following the quadrupole axial deformation of both those bands ($\beta_2 = 0.23$, $\gamma = 0.1^o$) is assumed to be identical. The experimental energies of the states of interest, taken from [4] are: 0.0 keV, 88.970(1) keV, 288.187(1) keV, 1276.138(2) keV, 1408.133(5) keV, respectively.

Below we write down the set of experimental transition probabilities $B(E\lambda)$ (in W.u.) of [4] between the states of spins $J_i$ and $J_f$ and the corresponding probabilities estimated within this work for relatively large, typical for the ground-state band, $\eta_3$ parameter. Here $\eta_3 = 12$, the experimental probabilities $B(E1,3^- \to 2^+) = 0.98 \cdot 10^{-3}$, $B(E2,2^+ \to 0^+) = 187$, $B(E2,4^+ \to 2^+) = 263$, $B(E2,5^- \to 3^-) = 293$.

$$
\begin{aligned}
&B(E1;(tA_1, J_i = 3^-, K_i = 0) \to (qA_1, J_f = 2^+, K_f = 0)) = 7.25 \cdot 10^{-6}\\
&B(E1;(tT_1, J_i = 3^-, K_i = 0) \to (qA_1, J_f = 2^+, K_f = 0)) = 7.25 \cdot 10^{-6}\\
&B(E1;(tT_2, J_i = 3^-, K_i = 0) \to (qA_1, J_f = 2^+, K_f = 0)) = 2.27 \cdot 10^{-1}\\
&B(E2;(qA_1, J_i = 2^+, K_i = 0) \to (qA_1, J_f = 0^+, K_f = 0)) = 86\\
&B(E2;(tA_1, J_i = 5^-, K_i = 0) \to (tA_1, J_f = 3^-, K_f = 0)) = 131\\
&B(E2;(tT_1, J_i = 5^-, K_i = 0) \to (tT_1, J_f = 3^-, K_f = 0)) = 130\\
&B(E2;(tT_2, J_i = 5^-, K_i = 0) \to (tT_2, J_f = 3^-, K_f = 0)) = 129.
\end{aligned}
$$

In the above the indeces "q" and "t" denote the ground-state and the tetrahedral octupole states belonging to a given irreducible representation $A_1$, $T_1$, $T_2$ (labeling taken from [9]) of the tetrahedral/octahedral symmetry group. Quantities $K_i$ and $K_f$ are the standard $K-$numbers of the initial and final states, respectively

The same reduced transition probabilities (in W.u.) estimated for relatively small $\eta_3$ parameter ($\eta_3 = 1$) have the following values:

$$
\begin{aligned}
&B(E1;(tA_1, J_i = 3^-, K_i = 0) \to (qA_1, J_f = 2^+, K_f = 0)) = 1.04 \cdot 10^{-3} \\
&B(E1;(tT_1, J_i = 3^-, K_i = 0) \to (qA_1, J_f = 2^+, K_f = 0)) = 1.04 \cdot 10^{-3} \\
&B(E1;(tT_2, J_i = 3^-, K_i = 0) \to (qA_1, J_f = 2^+, K_f = 0)) = 3.27 \cdot 10^{+1} \\
&B(E2;(qA_1, J_i = 2^+, K_i = 0) \to (qA_1, J_f = 0^+, K_f = 0)) = 86 \\
&B(E2;(tA_1, J_i = 5^-, K_i = 0) \to (tA_1, J_f = 3^-, K_f = 0)) = 131 \\
&B(E2;(tT_1, J_i = 5^-, K_i = 0) \to (tT_1, J_f = 3^-, K_f = 0)) = 130 \\
&B(E2;(tT_2, J_i = 5^-, K_i = 0) \to (tT_2, J_f = 3^-, K_f = 0)) = 9.42.
\end{aligned}
$$

The above simplistic estimates of the dipole and quadrupole transition probabilities in presence of the tetrahedral symmetry of the octupole states agree up to the order of magnitude with the experimental data if one assumes that the stiffness of the collective octupole potential is significantly smaller than the one corresponding to the quadrupole band ($\eta_3 \approx 1$). This suggests that above mentioned double-well potential in $^{156}$Gd is octupole "soft" contrarily to the one in, e.g. $^{156}$Dy nucleus, also supposed to possess the low-lying tetrahedral band. The quadrupole moment of the negative-parity band in $^{156}$Gd which experimentally turns out to be larger than the one of the ground-state band (see [4]) can be thus explained essentially by quite large dynamical deformation effects which may be strongly manifested in substantially soft octupole potentials. Hence, the advocated here hypothesis predicting the existence of the tetrahedrally symmetric octupole bands in $^{156}$Gd, whose states are described by above studied vibrational–rotational functions is not in contradiction with the empirical facts. This encourage us for further, more involved investigations for the presence of the high-rank symmetries in nuclear systems.

## REFERENCES


1. A. Dobrowolski, A. Szulerecka, A. Góźdź, *Phys. Scr.* **T154** (2013).
2. A. Dobrowolski, A. Szulerecka, A. Góźdź, *Acta Phys. Polon.* **B44**, 333, (2013).
3. M. Jentschel and L. Sengele, *private communication*.
4. M. Jentschel et al., *Phys. Rev. Lett.* 222502 (2010).
5. A. Góźdź, A. Szulerecka, A. Dobrowolski, J. Dudek, *Int. Jour. Mod. Phys.* **E20**, 199 (2011).
6. A. Góźdź, A. Szulerecka, A. Pedrak, A. Dobrowolski, *Nuclear Theory*, Vol. 31 (2012).
7. A. Góźdź, A. Dobrowolski, J. Dudek, K. Mazurek, *Int. Jour. Mod. Phys.* **E19**, 621 (2010).
8. A. Góźdź, A. Szulerecka, A. Dobrowolski, *Int. Jour. Mod. Phys.* **E20**, 565 (2011).
9. J.F. Cornwell, *G*roup theory in physics, Vol. 1, Academic Press, London, 1994.

# Binding energies and fission barrier heights of exotic nuclei

Krzysztof Pomorski and Bożena Pomorska

*Theoretical Physics Department, Maria Curie Skłodowska University, Lublin, Poland*

**Abstract.** The potential energy surfaces of fissioning nuclei are studied using the Lublin-Strasbourg Drop (LSD) for the macroscopic part of energy while the shell and pairing energy corrections were evaluated using eigenenergies of the Yukawa-folded single-particle hamiltonian. Four dimensional deformation parameter space containing the elongation, nonaxial, neck and mass asymmetry degrees of freedom was used to analyse ground and saddle points energies. The LSD estimates of the nuclear masses and the fission barrier heights are compared with predictions of other models and the experimental data.

**Keywords:** nuclear structure, binding energies, nuclear fission
**PACS:** 25.85.-w, 21.10.Dr, 21.10.Gv, 21.60.Jz

The nuclear liquid drop (LD) model composed of the volume, surface and Coulomb terms, proposed in 1935 by v. Weizsäcker, has described quantitatively the systematics of nuclear binding energies known at that time [1]. This model was extended in 1939 by Meitner and Frisch by adding the deformation dependence to the surface and Coulomb terms in the LD mass formula [2] in order to explain new phenomenon, nuclear fission discovered by Hahn and Strassman [3].

Another important step in evolution of the LD model was done by Myers and Świątecki who have added in 1966 the shell and pairing corrections to the liquid drop binding energy [5]. This new macroscopic-microscopic model became very successful in reproduction of nuclear data (masses, quadrupole moments, fission barrier heights, etc.) when the shell corrections were more precisely evaluated using a method proposed by Strutinsky [6] and the pairing correction obtained within the Bardeen-Cooper-Schrieffer (BCS) theory [7]. Later, it was shown that the standard liquid drop model failed in reproduction of measured fission barrier heights and some extensions of the LD like the droplet model (DM) [8] or the finite-range droplet model (FRDM) [11] have been proposed.

Parallel self-consistent theories of the Hartree-Fock plus BCS or the Hartree-Fock-Bogolubov types with the effective nucleon-nucleon Skyrme or Gogny interaction as well as the relativistic mean-field theory were successfully elaborated and implemented to the description of the nuclear binding energies and the fission barriers (for review see [9]). Nevertheless the macroscopic-microscopic model is still very popular as it gives the most accurate predictions of global nuclear properties.

Using the leptodermous expansion of the nuclear energy functional obtained e.g. within the self-consistent models one can easy obtain all terms (except the Coulomb one) which could appear in the nuclear liquid-drop mass formula. It was shown in Ref. [12] that the magnitude of the volume, surface, 1st and 2nd order curvature terms depends significantly on the surface radius constant $r_0$, where $R = r_0 A^{1/3}$ which choice is somehow arbitrary. This result has suggested to extend the original Myers and Świątecki LD model [5] by the first and second order curvature terms [12].

The coefficients of such extended liquid drop model were obtained by the least square fit to 2766 experimental binding energies taken from the compilation done in Ref. [10]. The microscopic (shell, pairing and deformation) corrections tabulated in Ref. [11] were added to our liquid drop energy when performing the fit. The resulting coefficients of this Lublin-Strasbourg-Drop (LSD) mass-formula [12]:

$$\begin{aligned} M(Z,N;\mathrm{def}) &= ZM_{\mathrm{H}} + NM_{\mathrm{n}} - b_{\mathrm{elec}}Z^{2.39} \\ &+ b_{\mathrm{vol}}(1-\kappa_{\mathrm{vol}}I^2)A + b_{\mathrm{surf}}(1-\kappa_{\mathrm{surf}}I^2)A^{\frac{2}{3}}B_{\mathrm{surf}}(\mathrm{def}) \\ &+ b_{\mathrm{cur}}(1-\kappa_{\mathrm{cur}}I^2)A^{\frac{1}{3}}B_{\mathrm{cur}}(\mathrm{def}) + \tfrac{3}{5}\tfrac{e^2Z^2}{r_0^{ch}A^{1/3}}B_{\mathrm{Coul}}(\mathrm{def}) \\ &- C_4\tfrac{Z^2}{A} + E_{\mathrm{cong}}(Z,N) + E_{\mathrm{micr}}(Z,N;\mathrm{def}) \ , \end{aligned} \tag{1}$$

with $Z$ and $N$ being the proton and neutron numbers, $I = (N-Z)/A$, are following:

$b_{\mathrm{vol}} = -15.4920$ , $\kappa_{\mathrm{vol}} = 1.8601$ , $b_{\mathrm{surf}} = 16.9707$ , $\kappa_{\mathrm{surf}} = 2.2938$
$b_{\mathrm{cur}} = 3.8602$ , $\kappa_{\mathrm{cur}} = -2.3764$ , $r_0 = 1.21725$ , $C_4 = 0.9181$ .

The rest of the coefficients in Eq. (1) are taken the same as in the mass table of Moller et al. [11]: $M_{\mathrm{H}}$=7.289034 MeV, $M_{\mathrm{n}}$=8.071431 MeV, $b_{\mathrm{elec}}$=1.433 eV. The congruence (Wigner) energy $E_{\mathrm{cong}} = -10\exp(-4.2|I|)$ MeV which plays in (1) a role of the Gauss curvature term is also taken from Ref. [11]. $E_{\mathrm{micr}}$ correction energy is composed of the shell and pairing parts.

Surprisingly, the quality of reproduction of the masses of the investigated 2766 isotopes with $Z,N > 8$ in Ref. [12] was better than that obtained within other more complex models like the Thomas-Fermi (TF) or the FRDM [11].

One has to mention here that the predictions of the TF [11] and the LSD [12] models differ significantly for nuclei close to the neutron drip line. The difference of the TF and LSD mass estimates for $\beta$-stable nuclei as well as for isotopes along the proton and neutron drip lines are plotted in Fig. 1 as functions of the charge number. It is seen that the both estimates are close to each other for the $\beta$-stable and neutron deficient nuclei, while the difference between the LSD and TF results reaches even 24 MeV for heavy nuclei along the neutron drip-line. The proper prediction of masses of neutron rich isotopes is very important for astrophysics, especially for the description of the rapid neutron capture processes.

The LSD formula was used in Ref. [12] to evaluate the fission barrier heights. The topographical theorem of Myers and Świątecki which says that in fissioning nuclei the microscopic energy correction at saddle points is negligible [13] is used to obtain the fission barrier heights.

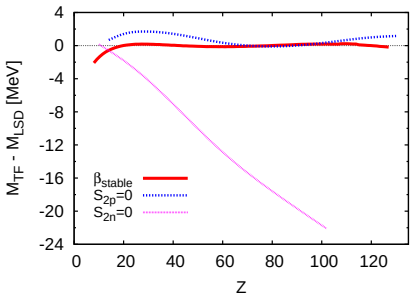


Figure 1: Difference of the TF and LSD mass estimates along the $\beta$-stability, proton and neutron drip lines.

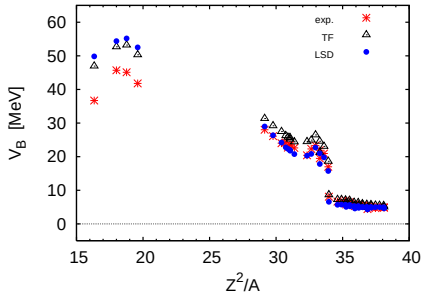


Figure 2: Comparison of the LSD and TF fission barrier heights with the experimental data in function of $Z^2/A$.

According to the topographical theorem the the barrier height is equal:

$$V_B = M^{\rm mac}_{\rm sadd} - M^{\rm exp}_{\rm g.s.} \tag{2}$$

where $M^{\rm mac}_{\rm sadd}$ and $M^{\rm exp}_{\rm g.s.}$ are the macroscopic saddle-point and the ground-state experimental masses, respectively.

The barrier height for nuclei the mass number $75 \leq A \leq 252$ were evaluated using the shape parametrisation independent model developed by Strutinsky and co-workers [14, 15]. The LSD estimates [12] are compared in Fig. 2 with the barrier heights obtained by Myers and Świątecki with the Thomas-Fermi (TF) model and the experimental data [13]. It is seen in Fig. 2 that except of four light isotopes ($^{75}$Br, $^{90,94,98}$Mo) the LSD estimates are closer to the data than the TF results. It was shown in Ref. [16] that this discrepancy in the light isotopes can be removed when one took into account the deformation dependence of the congruence and average pairing energies. The corrected by the above effects fission barriers $V_{\rm mac}$ for $^{75}$Br and $^{90,94,98}$Mo isotopes are shown in Fig. 3.

The obtained good agreement of the fission barrier heights proves that the LSD model with the parameters fitted to the ground-state binding energies only (not to the barrier heights!) can serve as a reliable and simple macroscopic model which is able to predict different properties of nuclei.

One has also to mention that in the last decade some other liquid drop models have been successfully used to reproduce the ground-state masses of nuclei but none of them is able to predict correctly the fission barrier heights in such a broad mass region as it is the case in the LSD model [17].

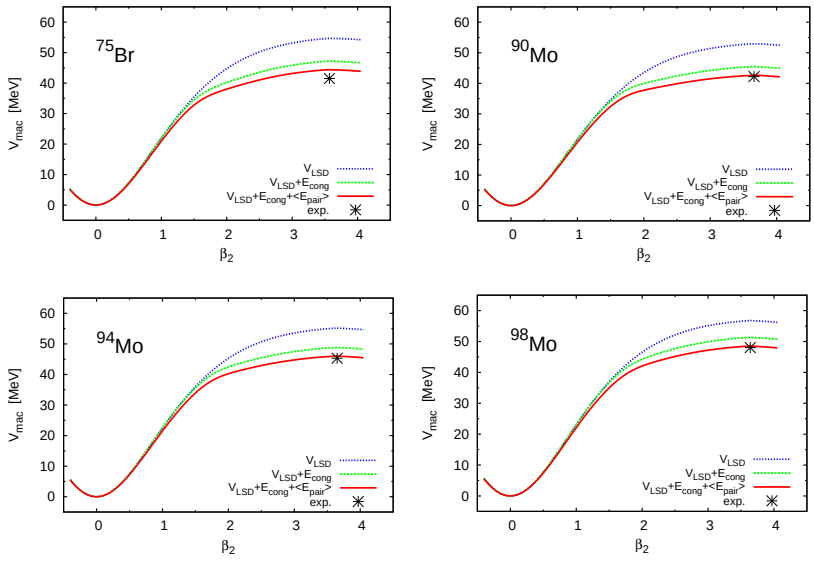


**FIGURE 1.** LSD fission barrier corrected by the deformation dependent congruence and average pairing energies as function of the relative elongation of nucleus. The experimental barrier heights are marked by crosses.

It is interesting to note that almost the same charge radius constant as in the LSD model can reproduce within the Gamow-like theory known half-lives for spontaneous emission of the alpha particles and light clusters [18]. This fact can be treated as an additional confirmation of the charge-radius fixed in the LSD model.

A continuous progress in the radioactive beam technique gives a hope for verification which model predictions are closer to reality for nuclei which are far from stability.

## REFERENCES


1. C. F. v. Weizsäcker, Z. Phys. **96**, 431 (1935).
2. L. Meitner and O. R. Frisch, Nature **143**, 239 (1939).
3. O. Hahn and F. Straßmann, Naturwiss. **27**, 11 (1939); Naturwiss. **27**, 89 (1939).
4. N. Bohr and J. A. Wheeler, Phys. Rev. **56**, 426 (1939).
5. W. D. Myers and W. J. Świątecki, Nucl. Phys. **81**, 1 (1966).
6. V. M. Strutinsky, Yad. Fiz. (USSR) **3** 614 (1966), [Sov. J. Nucl. Phys. **3**, 449 (1966)]; Nucl. Phys. **A95**, 420 (1967).
7. A. Bohr, B. R. Mottelson, D. Pines, Phys. Rev. **110**, 936 (1958)
8. W. D. Myers, *Droplet Model of Atomic Nuclei*, IFI/Plenum, New York, 1977.
9. H. J. Krappe and K. Pomorski, *Theory of Nuclear Fission*, Lecture Notes in Physics, vol. 843, Springer-Verlag, 2012.
10. M. S. Antony, *Nuclide Chart, Strasbourg 2002*, Impressions François, Haguenau, 2002.

11. P. Möller, J. R. Nix, W. D. Myers, and W. J. Świątecki, At. Data Nucl. Data Tables **59**, 185 (1995).
12. K. Pomorski and J. Dudek, Phys. Rev. C **67**, 044316 (2003).
13. W. D. Myers and W. J. Świątecki, Nucl. Phys. **A612**, 249 (1997).
14. V. M. Strutinsky, N. Ya. Lyashchenko, and N. A. Popov, Nucl. Phys. **46**, 639 (1963).
15. F. Ivanyuk and K. Pomorski, Phys. Rev. C **79**, 054327 (2009).
16. K. Pomorski and F. Ivanyuk, Int. Journ. Mod. Phys. **E18**, 900 (2009).
17. K. Pomorski, Phys. Scr. **T154**, 014023 (2013).
18. A. Zdeb, M. Warda, and K. Pomorski, Phys. Rev. C **87**, 024308, 2013.

# Entry distribution measurement: principles and the example of $^{254}$No

presented by Greg Henning

*GSI-Helmholtzzentrum fur Schwerionenforschung, Planckstrasse 1, D-64291 Darmstadt, Germany*

**Abstract.** One of the goals of nuclear structure research is to determine the limits of nuclear existence as a function of neutron and proton number, as well as excitation energy $E^\star$ and angular momentum $I$. In particular, it is important to understand the role that microscopic shell corrections play in enhancing and extending these limits. I will show how the determination of the spin and excitation energy at which a nucleus is formed, *i.e.* the entry point of a reaction, can contribute to our understanding of the stability of nuclei as well as their formation mechanism. Such measurements are performed since the 1980s and have been used to study highly elongated nuclei, and more recently, very heavy nuclei – both of which owe their existence to quantum shell effects. The method to performed such measurement will be presented and typical results will be discussed, with a focus on the recent measurement of the fission barrier of $^{254}$No.

## LIMITS OF NUCLEAR STABILITY

One of the current *hot* topics of nuclear structure research is to study the limits of nuclear stability. The stability of a nucleus in its ground state can be expressed, as a function of the neutron number N and proton number Z, by the nucleus' binding energy, given in the first order by the *liquid drop* mass model. However, the liquid drop model failed to explain simple experimental observations such as the natural abundance of elements in nature, which shows peaks for specific numbers of neutrons or protons: **2, 8, 20, 28, 50, 82, 126**. The so-called *magic numbers* arise from nucleons being organised in quantum levels within the nucleus potential, the spacing of the levels creates gaps in the density of single particle states. That is why one has to apply a **shell correction** to the liquid drop binding energy, to take into account this shell structure. When moving away from the magic nuclei, towards the limits of stability, an evolution of the density of single particle states is observed, that can be seen as a disappearance of magic numbers.

In nuclear reactions, it is of interest to also see the stability in term of dynamic properties: how much angular momentum and excitation energy can a nucleus sustain? The limit in $E^\star$ is a way to investigate *Q-values*, which give information on masses and shell stabilisation. The limits in angular momentum can be an effect of the reaction mechanism (angular momentum barrier) or fundamental properties of the nucleus.

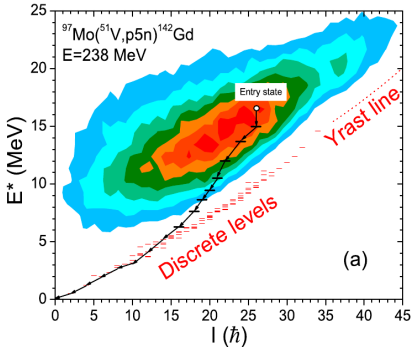


**Figure 1.** Entry state population distribution for the $^{97}$Mo($^{51}$V, $p5n$)$^{142}$Gd reaction channel and one simulated decay path from the entry state, indicated by a circle, to the ground states. The discrete levels observed in $^{142}$Gd are also shown. From [2].

## INTEREST OF ENTRY DISTRIBUTIONS

A great tool to investigate the limits in angular momentum and excitation energy of a nucleus in a reaction is the **entry distribution**: i.e. the distribution of I and $E^\star$ of the states populated in the reaction.

In *single particle reactions* like direct reactions or Coulomb excitation reactions, it is possible to access the excitation energy and angular momentum of populated states via kinematics measurements (energy and angular distribution). But in other types of reactions, like *fusion-evaporation* reactions, that follow a statistical process, it is not so easy. In consequence, finding the $E^\star$ and I of the nucleus formed in a reaction will give valuable information on all the subprocesses of the reaction: fusion, evaporation of particle, survival to fission, ... The entry distribution of fusion-evaporation products is therefore a good probe of reaction mechanism and nuclear properties.

To determine the starting excitation energy of the nucleus, one just has to sum the energies of the evaporated particles, typically $\gamma$ rays. The original spin of the nucleus is linked to the multiplicity of $\gamma$ rays emitted $M_\gamma$. Such entry distribution measurements are done in calorimetric experiments in which the total number of $\gamma$ rays and the total energy released by the nucleus are detected.

Entry distribution can be used to study reaction mechanism: in [1], the entry states for the products of the $^{54}$Ni+$^{100}$Mo reaction at c.m. bombarding energies from 141 to 128 MeV are studied via $\left(M_\gamma, E^\star\right)$ measurements. With increasing beam energy, the distributions are shifted to higher energy and spin and new exit channels are open.

In [2], the properties of complete or incomplete fusion reactions have been studied in $^{97}$Mo $+^{51}$ V, $^{100}$Mo $+^{48}$ Ti and $^{114}$Cd $+^{36}$ S reactions ; see figure 1.

In [3], the entry distributions leading to normal and super-deformed (SD) states in $^{192}Hg$ have been measured. The experimental results show how high in excitation energy the SD band is in respect to the normal yrast line.

## THE EXAMPLE OF $^{254}$NO

Super heavy elements (SHE) are at the limits of mass and Z in the nuclear chart. These elements are 25% heavier than the heaviest stable nucleus ($^{208}$Pb), which represent a huge extension of nuclear stability. They exist solely because of shell-effect stabilisation, which creates a sizeable fission barrier.

Studying the stability of those elements allows a precise investigation of the manifestation of shell effects and provides important information about SHE structure and formation mechanism.

The fission barrier can be deduced from the competition between $\gamma$ emission and fission. This feature has been exploited for the most direct determination of the fission barrier, namely by measuring the fission probability $P_{fission}(E^*)$ following transfer reactions [4]. Such reactions are not possible for nuclei with Z > 98, as there is no target to allow excitation function measurements by (n, f) or (d, pf) reactions for example. However, from the entry distribution one can instead determine the $\gamma$-decay probability $P_\gamma$ and, hence, $P_{fission}$ ($P_{fission} \approx 1 - P_\gamma$ below the neutron threshold).

Several models calculate the fission barrier of $^{254}$No. Density Functional Theory (DFT) calculations based on the Gogny D1S and Skyrme interactions give $B_f(I = 0\ \hbar)$ between 6 and 9.6 MeV [5, 6, 7, 8]. Calculations based on the macro-microscopic model give a distinctly lower value of $B_f(I = 0\ \hbar) = 6.8$ MeV [9, 10]. The liquid drop model predicts only $B_f\,(LD) \approx 0.9$ MeV. Hence, a measurement of $B_f$ provides a test of theory. A previous attempt at measurement of the fission barrier in $^{254}$No yielded a lower limit of 5 MeV for spin up to 22 $\hbar$ [11] – not enough to differentiate between theories.

We used the reaction $^{208}$Pb ($^{48}$Ca, 2n) at two beam energies: 219 MeV and 223 MeV. The beam was delivered by the Argonne Tandem Linac Accelerator System at Argonne National Laboratory. The $\gamma$-ray detector array Gammasphere [12] was used to perform the calorimetric measurement (as well as high resolution measurement of the $^{254}$No spectrum). In this type of measurement , the Bismuth Germanate (BGO) shields placed around the Ge detectors are used to measure the $\gamma$ rays energy and multiplicity – bringing an calorimetric efficiency of 63 %. The Gammasphere modules give the total energy released at the target position and the number of $\gamma$ rays emitted. The detection efficiency is taken into account by unfolding the measured multiplicity and energy with a statistical procedure [13] using the responses in energy and multiplicity which were constructed with $^{88}$Y source data [14]. The evaporation residues were separated from the non reacting and scattered beam by the Fragment Mass Analyzer (FMA) [15], according to their mass-to-charge ratio ($m/Q$). At the focal plane of the FMA evaporation residues were detected by a Parallel Plate Avalanche Counter (PPAC) measuring the energy loss and the position of the recoils. Finally, the evaporation residues were implanted in a Double-Sided Silicon Detector (DSSD).

The emitted $\gamma$-ray multiplicity $M$ obtained is transformed to a spin value using the expression $I = \Delta I(M - N_{\text{stat}}) + \Delta I_{\text{stat}} \cdot N_{\text{stat}} + I_{CE}$. $M$ is the measured multiplicity, $\Delta I$ the average spin carried by a $\gamma$ transition between nuclear levels, $N_{\text{stat}}$ the average number of statistical $\gamma$-rays, $\Delta I_{\text{stat}}$ the average spin carried by a statistical $\gamma$ ray and $I_{CE}$ the average spin carried by internal conversion electrons.

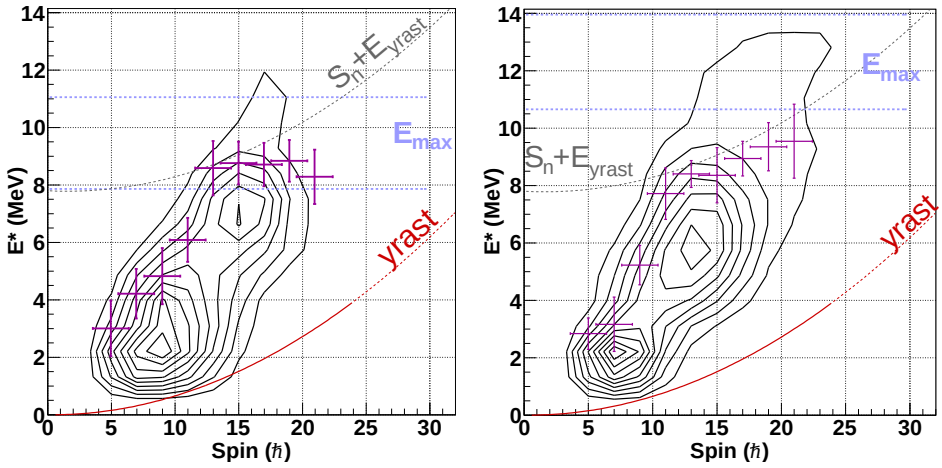


**Figure 2.** Entry distribution for $E_{\mathrm{beam}} = 219$ (top) and 223 MeV (bottom) obtained as described in the text. The yrast and neutron separation energy line are represented in red and grey. The maximum possible excitation energy range is represented by the blue dashed lines. The half-maximum point of each spin slice is marked in purple.

The value of the coefficients are determined through experimental data and the properties of the known level scheme – [16, 17, 18, 19, 20, 21, 22, 23, 24].

The entry distribution is analysed by examining the energy distribution at each spin and determining the energy $E_{1/2}$ where the distribution falls to 50 % of the maximum. Figure 2 shows the entry distributions for $^{254}$No measured at the 2 beam energies.

As the beam energy increases, one can see an increase in average $E^{\star}$ and spin by 1 MeV and 2 $\hbar$. The points where the distributions fall to 10 % of its maximum increases even more by 3.5 MeV and 4 $\hbar$. This shows that $^{254}$No still can sustain high average excitation energy and angular momentum at higher beam energy [11]. However, there is saturation of $E_{1/2}$ for I between 12 and 25 $\hbar$, which is attributed to the fission barrier resulting in depletion of $\gamma$-emitters states. The value of $B_f(0) = 6.6 \pm 0.9$ MeV, extrapolated from the data points is consistent with microscopic-macroscopic predictions $B_f^{\text{Mic-Mac}} = 6.76$ MeV [9, 10] and the previous experimental limit [11]. The fission barrier is $\approx 5$ MeV higher than the liquid-drop model value. These results show the strength and resilience of the shell effects, even at the highest spins.

## CONCLUSIONS

- Measurements of entry distributions can provide valuable information on nuclear properties such as fission barrier or the position of rotational bands. But also on reaction mechanisms.
- The current renewed interest for scintillator detectors will allow such measurements to be generalized and provide fresh sets of data.
- New, radioactive, beams will make new reactions possible and open a field of study for nuclear reactions and properties.

## ACKNOWLEDGEMENTS

This work was possible with the help of : T. L. Khoo[1], A. Lopez-Martens[2], D. Seweryniak[1], M. Alcorta[1], M. Asai[3], B. B. Back[1], P. Bertone[1], D. Boiley[4], M. P. Carpenter[1], C. J. Chiara[1,5], P. Chowdhury[6], B. Gall[7], P. T. Greenlees[8], G. Gurdal[9], K. Hauschild[2], A. Heinz[10], C. R. Hoffman[1], R. V. F. Janssens[1], A. V. Karpov[11], B. P. Kay[1], F. G. Kondev[1], S. Lakshmi[6], T. Lauristen[1], C. J. Lister[6], E. A. McCutchan[12], C. Nair[1], J. Piot[4], D. Potterveld[1], P. Reiter[13], N. Rowley[14], A. M. Rogers[1] and S. Zhu[1].

[1] Argonne National Laboratory,Argonne, IL, USA, [2] CSNSM, IN2P3-CNRS, Orsay, France, [3] Japan Atomic Energy Agency (JAEA), Japan, [4] GANIL, CEA-DSM and IN2P3-CNRS, B.P. 55027, F-14076 Caen Cedex, France, [5] University of Maryland, College Park, MD, USA, [6] University of Massachusetts Lowell, Lowell, MA, USA, [7] IPHC, IN2P3-CNRS and Universite Louis Pasteur, F-67037 Strasbourg Cedex 2, France, [8] University of Jyväskylä, Finland, [9] DePaul University, Chicago, IL, [10] Fundamental Fysik, Chalmers Tekniska Hogskola, 412 96 Goteborg, Sweden, [11] Flerov Laboratory of Nuclear Reactions, JINR, Dubna, Moscow Region, Russia, [12] Brookhaven National Lab., Brookhaven, NY, [13] Universität zu Köln, Germany, [14] IPNO, CNRS/IN2P3, Université Paris-Sud 11, F-91406 Orsay Cedex, France
This work is supported by the U.S. Department of Energy, under Contract Nos. DE-AC02-06CH11357, DE-FG02-91ER-40609 and DE-FG02-94ER40848


## REFERENCES


1. M. L. Halbert, J. R. Beene, D. C. Hensley, K. Honkanen, T. M. Semkow, V. Abenante, D. G. Sarantites, and Z. Li, *Phys. Rev. C* **40**, 2558–2575 (1989), URL http://link.aps.org/doi/10.1103/PhysRevC.40.2558.
2. R. Lieder, A. Pasternak, E. Lieder, W. Gast, G. Angelis, and D. Bazzacco, *The European Physical Journal A* **47**, 1–19 (2011), ISSN 1434-6001, URL http://dx.doi.org/10.1140/epja/i2011-11115-3.
3. T. Lauritsen, P. Benet, T. L. Khoo, K. B. Beard, I. Ahmad, M. P. Carpenter, P. J. Daly, M. W. Drigert, U. Garg, P. B. Fernandez, R. V. F. Janssens, E. F. Moore, F. L. H. Wolfs, and D. Ye, *Phys. Rev. Lett.* **69**, 2479–2482 (1992), URL http://link.aps.org/doi/10.1103/PhysRevLett.69.2479.
4. B. B. Back, O. Hansen, H. C. Britt, and J. D. Garrett, *Phys. Rev. C* **9**, 1924–1947 (1974), URL http://link.aps.org/doi/10.1103/PhysRevC.9.1924.
5. J. L. Egido, and L. M. Robledo, *Phys. Rev. Lett.* **85**, 1198–1201 (2000), URL http://link.aps.org/doi/10.1103/PhysRevLett.85.1198.
6. J.-P. Delaroche, M. Girod, H. Goutte, and J. Libert, *Nuclear Physics A* **771**, 103 – 168 (2006), ISSN 0375-9474, URL http://www.sciencedirect.com/science/article/pii/S0375947406001291.
7. L. Bonneau, P. Quentin, and D. Samsoen, *The European Physical Journal A - Hadrons and Nuclei* **21**, 391–406 (2004), ISSN 1434-6001, URL http://dx.doi.org/10.1140/epja/i2003-10224-x, 10.1140/epja/i2003-10224-x.
8. T. Duguet, P. Bonche, and P.-H. Heenen, *Nuclear Physics A* **679**, 427 – 440 (2001), ISSN 0375-9474, URL http://www.sciencedirect.com/science/article/pii/S0375947400003705.
9. P. Möller, A. J. Sierk, T. Ichikawa, A. Iwamoto, R. Bengtsson, H. Uhrenholt, and S. Åberg, *Phys. Rev. C* **79**, 064304 (2009), URL http://link.aps.org/doi/10.1103/PhysRevC.79.064304.
10. M. Kowal, P. Jachimowicz, and A. Sobiczewski, *Phys. Rev. C* **82**, 014303 (2010), URL http://link.aps.org/doi/10.1103/PhysRevC.82.014303.
11. P. Reiter, T. L. Khoo, T. Lauritsen, C. J. Lister, D. Seweryniak, A. A. Sonzogni, I. Ahmad, N. Amzal, P. Bhattacharyya, P. A. Butler, M. P. Carpenter, A. J. Chewter, J. A. Cizewski, C. N. Davids, K. Y. Ding, N. Fotiades, J. P. Greene, P. T. Greenlees, A. Heinz, W. F. Henning, R.-D. Herzberg, R. V. F.

Janssens, G. D. Jones, F. G. Kondev, W. Korten, M. Leino, S. Siem, J. Uusitalo, K. Vetter, and I. Wiedenhöver, *Phys. Rev. Lett.* **84**, 3542–3545 (2000), URL http://link.aps.org/doi/10.1103/PhysRevLett.84.3542.

12. I. Lee, *Nuclear Physics A* **520**, 641c (1990).
13. P. Benet, *Etude de l'émission de neutrons et distributions des moments angulaires du noyaux composé* $^{156}$*Dy dans les voies de sorties*, Ph.D. thesis, Université Louis Pasteur de Strasbourg (1988).
14. M. Jääskeläinen, D. Sarantites, R. Woodward, F. Dilmanian, J. Hood, R. Jääskeläinen, D. Hensley, M. Halbert, and J. Barker, *Nuclear Instruments and Methods in Physics Research* **204**, 385 – 405 (1983), ISSN 0167-5087, URL http://www.sciencedirect.com/science/article/pii/0167508783900686.
15. C. Davids, B. Back, K. Bindra, D. Henderson, W. Kutschera, T. Lauritsen, Y. Nagame, P. Sugathan, A. Ramayya, and W. Walters, *Nuclear Instruments and Methods in Physics Research Section B: Beam Interactions with Materials and Atoms* **70**, 358 – 365 (1992), ISSN 0168-583X, URL http://www.sciencedirect.com/science/article/pii/0168583X9295951M.
16. R. Clark, K. Gregorich, J. Berryman, M. Ali, J. Allmond, C. Beausang, M. Cromaz, M. Deleplanque, I. Dragojević, J. Dvorak, P. Ellison, P. Fallon, M. Garcia, J. Gates, S. Gros, H. Jeppesen, D. Kaji, I. Lee, A. Macchiavelli, K. Morimoto, H. Nitsche, S. Paschalis, M. Petri, L. Stavsetra, F. Stephens, H. Watanabe, and M. Wiedeking, *Physics Letters B* **690**, 19 – 24 (2010), ISSN 0370-2693, URL http://www.sciencedirect.com/science/article/pii/S0370269310005757.
17. S. Eeckhaudt, P. Greenlees, N. Amzal, J. Bastin, E. Bouchez, P. Butler, A. Chatillon, K. Eskola, J. Gerl, T. Grahn, A. Görgen, R. Herzberg, F. Hessberger, A. Hürstel, P. Ikin, G. Jones, P. Jones, R. Julin, S. Juutinen, H. Kettunen, T. Khoo, W. Korten, P. Kuusiniemi, Y. Le Coz, M. Leino, A. Leppänen, P. Nieminen, J. Pakarinen, J. Perkowski, A. Pritchard, P. Reiter, P. Rahkila, C. Scholey, C. Theisen, J. Uusitalo, K. Van de Vel, and J. Wilson, *The European Physical Journal A - Hadrons and Nuclei* **26**, 227–232 (2005), ISSN 1434-6001, URL http://dx.doi.org/10.1140/epja/i2005-10163-6, 10.1140/epja/i2005-10163-6.
18. F. Heßberger, S. Antalic, B. Sulignano, D. Ackermann, S. Heinz, S. Hofmann, B. Kindler, J. Khuyagbaatar, I. Kojouharov, P. Kuusiniemi, M. Leino, B. Lommel, R. Mann, K. Nishio, A. Popeko, S. Saro, B. Streicher, J. Uusitalo, M. Venhart, and A. Yeremin, *The European Physical Journal A - Hadrons and Nuclei* **43**, 55–66 (2010), ISSN 1434-6001, URL http://dx.doi.org/10.1140/epja/i2009-10899-9, 10.1140/epja/i2009-10899-9.
19. M. Leino, H. Kankaanpää, R.-D. Herzberg, A. Chewter, F. Heßberger, Y. Le Coz, F. Becker, P. Butler, J. Cocks, O. Dorvaux, K. Eskola, J. Gerl, P. Greenlees, K. Helariutta, M. Houry, G. Jones, P. Jones, R. Julin, S. Juutinen, H. Kettunen, T. Khoo, A. Kleinböhl, W. Korten, P. Kuusiniemi, R. Lucas, M. Muikku, P. Nieminen, R. Page, P. Rahkila, P. Reiter, A. Savelius, C. Schlegel, C. Theisen, W. Trzaska, and H.-J. Wollersheim, *The European Physical Journal A - Hadrons and Nuclei* **6**, 63–69 (1999), ISSN 1434-6001, URL http://dx.doi.org/10.1007/s100500050318, 10.1007/s100500050318.
20. P. Reiter, T. L. Khoo, C. J. Lister, D. Seweryniak, I. Ahmad, M. Alcorta, M. P. Carpenter, J. A. Cizewski, C. N. Davids, G. Gervais, J. P. Greene, W. F. Henning, R. V. F. Janssens, T. Lauritsen, S. Siem, A. A. Sonzogni, D. Sullivan, J. Uusitalo, I. Wiedenhöver, N. Amzal, P. A. Butler, A. J. Chewter, K. Y. Ding, N. Fotiades, J. D. Fox, P. T. Greenlees, R.-D. Herzberg, G. D. Jones, W. Korten, M. Leino, and K. Vetter, *Phys. Rev. Lett.* **82**, 509–512 (1999), URL http://link.aps.org/doi/10.1103/PhysRevLett.82.509.
21. W. Reviol, C. J. Chiara, M. Montero, D. G. Sarantites, O. L. Pechenaya, M. P. Carpenter, R. V. F. Janssens, T. L. Khoo, T. Lauritsen, C. J. Lister, D. Seweryniak, S. Zhu, and S. G. Frauendorf, *Phys. Rev. C* **74**, 044305 (2006), URL http://link.aps.org/doi/10.1103/PhysRevC.74.044305.
22. P. Greenlees, private communication (2012).
23. S. K. Tandel, T. L. Khoo, D. Seweryniak, G. Mukherjee, and et al., *Phys. Rev. Lett.* **97**, 082502 (2006), URL http://link.aps.org/doi/10.1103/PhysRevLett.97.082502.
24. R.-D. Herzberg, P. T. Greenlees, P. A. Butler, G. D. Jones, M. Venhart, I. G. Darby, S. Eeckhaudt, K. Eskola, T. Grahn, C. Gray-Jones, F. P. Hessberger, P. Jones, R. Julin, S. Juutinen, S. Ketelhut, W. Korten, M. Leino, A.-P. Leppanen, S. Moon, M. Nyman, R. D. Page, J. Pakarinen, A. Pritchard, P. Rahkila, J. Saren, C. Scholey, A. Steer, Y. Sun, C. Theisen, and J. Uusitalo, *Nature* **442**, 896–899 (2006), ISSN 0028-0836, URL http://dx.doi.org/10.1038/nature05069.

# Excitation-energy sorting in low-energy fission

Beatriz Jurado and Karl-Heinz Schmidt

*CENBG, CNRS/IN2P3, Chemin du Solarium, B. P. 120, 33175 Gradignan, France*

**Abstract.** In fission, on the way to scission, the nascent fragments form a system of two nuclei in thermal contact through the neck. At low excitation energies, energy sorting takes place where the intrinsic excitation energy flows from the light to the heavy fragment until the excitation energy in the light fragment is practically exhausted. The excitation-energy sorting process explains in a transparent way why an increase of excitation energy in the fissioning nucleus leads to an increase of the number of neutrons emitted by the heavy fragment only. This observation remained unexplained over decades. It also explains complex features observed in the even-odd staggering of fission-fragment Z yields that have been a puzzle since many years. The opportunity to further explore the energy sorting process with EURISOL beams is discussed.

## INTRODUCTION

Fission is a large-scale collective motion where a heavy nucleus evolves into two individual nuclei with nuclear properties that considerably differ from those of the initial nucleus. This transition from a mononuclear to di-nuclear system involves a drastic rearrangement of nucleons and energy. At scission, right before the emerging fission fragments separate, the fissioning system consists of two nuclei in contact through a neck. Because of the mutual Coulomb repulsion, the two emerging fragments are generally highly deformed. After scission, the fragments fly apart with high kinetic energies and snap back to a smaller deformation. The deformation energy transforms into intrinsic excitation energy of the fully accelerated fragments. Since fission fragments are neutron-rich, the deexcitation proceeds almost exclusively by neutron evaporation and, subsequently, by gamma emission. The neutron-induced fission of $^{237}$Np has been studied very carefully at two different neutron energies [1]. The left of Fig. 1 shows the average number of evaporated neutrons as a function of fragment mass. The well known saw-tooth-like behaviour of this curve is attributed to the deformation energy. The minimum close to A=130 is due to the shell closures N=82, Z=50 that lead to spherical fission fragments. An increase of incident neutron energy translates into an increase of the initial excitation energy of the fissioning nucleus. For the more asymmetric mass splits, we observe a very peculiar feature: the increase of excitation energy leads to an increase of the number of evaporated neutrons for the heavy fragment, only.

The most prominent manifestation of pairing correlations in nuclear fission is the enhanced production of even-Z elements in low-energy fission of an even-Z compound nucleus. It was proposed in ref. [2] to quantify the even-odd staggering observed in fission yields by the local even-odd effect $\delta_p(Z)$, which corresponds to the

third differences of the logarithm of the yields. $\delta_p(Z)$ filters out from the yields the variations that extend over a significant number of charges and are caused by the global shape of the potential energy. The right part of Fig. 1 shows experimental data on $\delta_p(Z)$ as a function of charge asymmetry for different fissioning nuclei measured at ILL Grenoble where fission was induced by thermal neutrons. These data and the systematics compiled in [3] clearly illustrate several features:

(i) The amplitude of $\delta_p$ decreases with increasing mass of the fissioning system.

(ii) For a given fissioning nucleus $\delta_p$ increases with asymmetry.

(iii) Also odd-Z fissioning systems like $^{243}$Am show an even-odd effect at large asymmetry whose magnitude is about the same as for even-Z systems of comparable mass.

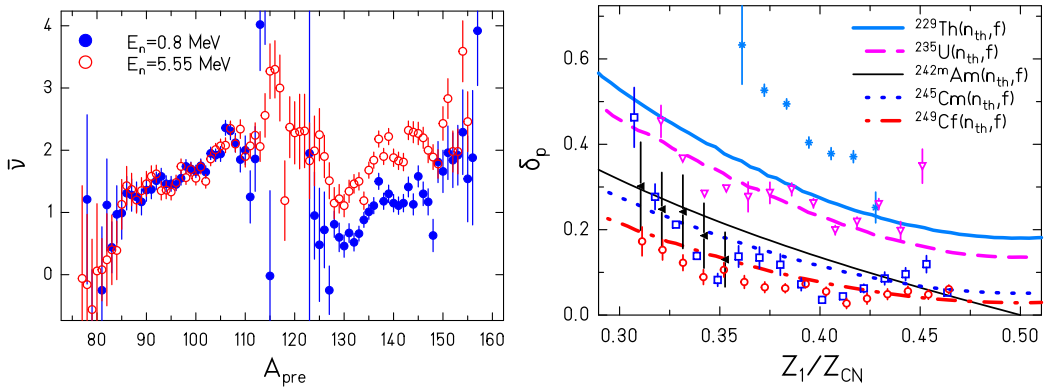


**FIGURE 1.** (Left) Average number of prompt neutrons as a function of fragment mass for the neutron-induced fission of $^{237}$Np at two incident neutron energies [1]. (Right) Local even-odd effect as a function of asymmetry, parameterized as the ratio of the charge of the light fragment $Z_1$ and the charge of the fissioning nucleus $Z_{CN}$. The symbols represent the experimental data which are taken from the compilation shown in ref. [3]. The lines correspond to the statistical calculation developed in this work.

Presently, there is no consistent explanation for the features shown in Fig. 1. In this contribution, we present a simple model based on statistical mechanics that describes these features.

## MODEL BASED ON STATISTICAL MECHANICS

We assume statistical equilibrium among the different types of degrees of freedom (intrinsic and collective) in the region around the outer saddle point. The intrinsic excitation energy at the outer saddle is essentially equal to the initial excitation energy of the nucleus minus the height of the outer fission barrier. The intrinsic excitation energy grows on the way from saddle to scission because part of the potential-energy release is dissipated into intrinsic excitations. Two-centre shell-model calculations shown in Fig. 12 of [4] show that there are many level crossings on the first section behind the outer saddle. Afterwards, the single-particle levels change only little. Level crossings lead to intrinsic excitations. This implies that the additional excitation energy is mostly dissipated in the vicinity of the outer saddle. The dissipated energy increases with the mass of the fissioning nucleus because the fission barrier is located

at smaller deformations and the range with a high number of level crossings is extended.

Theoretical investigations of the gradual transition from the mononucleus regime to the dinuclear system concerning shell effects [4], pairing correlations [5] and congruence energy [6] show that the properties of the individual fission fragments are already very well established in the vicinity of the outer saddle. Therefore, close to the outer saddle the fissioning system consists of two well-defined nuclei in contact through the neck and a total amount of excitation energy $E_{tot}$ that is equal to the intrinsic excitation energy above the outer saddle plus the energy acquired by dissipation on the first section behind the outer saddle. The partition of $E_{tot}$ among the two fragments at statistical equilibrium is thus ruled by the level densities of both fragments. At low excitation energies, nuclear level densities are well described by the constant-temperature level density. We assume a transition to the Fermi-gas level density at energies of about 8-9 MeV [7]. It was shown that the constant-temperature behavior of the nuclear level density in the low-energy regime leads to an energy-sorting process if two nuclei are in thermal contact. In the absence of strong shell effects, the light fragment will transfer essentially all its excitation energy to the heavy one [8]. This process of energy sorting explains why the increase of the initial excitation energy leads to an increase of the number of emitted neutrons from the heavy fission fragment, only (see left side of Fig. 1).

Nucleon exchange between the fragments establishes also an equilibrium between even-even, odd-A, and odd-odd light and heavy nascent fragments with a restriction on the gross mass asymmetry given by the bottom of the potential in the fission valleys and on the total intrinsic excitation energy $E_{tot}$. To obtain the probability of populating a given configuration at statistical equilibrium and derive the local even-odd effect $\delta_{p,}$ we have to consider the level densities of neighboring even-even, even-odd, odd-even or odd-odd nuclei in an absolute energy scale. However, as said above, the quantity $\delta_p$ filters out the slowly-varying components of the yields. Therefore, we have to use level densities where these effects are filtered out as well. This can be done by placing the level densities in an excitation-energy scale that is reduced by $2\Delta$ for even-even nuclei, by $\Delta$ for even-odd and odd-even nuclei and is left unchanged for odd-odd nuclei. We have done this on Fig. 2 with the experimental level densities determined by the Oslo method [9] for various even-even, odd-A and odd-odd nuclei located in two distinct mass regions around $A$=165 and 45. These two groups of nuclei are representative of the complementary fission fragments produced in very asymmetric fission. Within the heavy group, the level densities of neighboring even-even and even-odd nuclei are almost identical. Sizeable differences appear only in the energy interval $-2\Delta_2 < E < -\Delta_2$, where only even-even nuclei have states. For the light-mass group, the level densities converge well at positive energies. The features shown on the right of Fig. 1 can be explained by simple inspection of Fig. 2. Indeed, Fig. 2 shows that the logarithmic slope of the level densities is nearly constant and that the logarithmic slope of the heavy group is much larger than the one of the light group. The total amount of possible configurations with particular values of $Z_1$ and $Z_2$ is directly related to the integral of the total level density for that particular split over the excitation energy. This integral runs over the excitation energy of one fragment $E_i$, with the condition that $E_1 + E_2 = E_{tot}$, and reflects the freedom of the system in the

division of excitation energy. The total level density is given by the product of the level densities of the two fragments $\rho_1(E_1)\rho_2(E_2)$. The most probable configuration is the one that provides the highest total level density. Due to the very different logarithmic slopes of the level densities for the heavy and the light fragment group, the most favorable configurations are those that minimize the excitation energy of the light fragment. In other words, energy sorting takes place [8]. Only at the end of the energy sorting, when $E_1 \approx 0$ and $E_2 \approx E_{tot}$, the benefit of transferring the unpaired nucleons to the heavy fragment to form an even-odd or an even-even light fragment becomes apparent because only for these configurations there are states available. If an even-even light fragment in the ground state is formed, instead of an odd-odd one, the energy in the heavy fragment increases to $E_{tot} + 2\Delta_1$, which for the nuclei considered in Fig. 2 corresponds to an increase of the level density of the heavy fragment of more than three orders of magnitude. It becomes clear that configurations with fully paired light fragments are strongly favored for very asymmetric fission. Because the logarithmic slope of the constant-temperature level densities is roughly proportional to $A^{2/3}$ [10], for less asymmetric splits the logarithmic slopes of the level densities of the two fragments will become closer. Therefore, the probability to populate the ground states of even-even or even-odd light fragments decreases with decreasing asymmetry. Since the logarithmic slope of the Fermi-gas level density becomes more gradual with increasing excitation energy, the relative statistical weight of configurations with a fully-paired light fragment is less important than in the constant-temperature regime. Therefore, the transition from the constant-temperature to the Fermi-gas regime that may occur when $E_{tot}$ increases will lead to a considerable decrease of $\delta_p$.

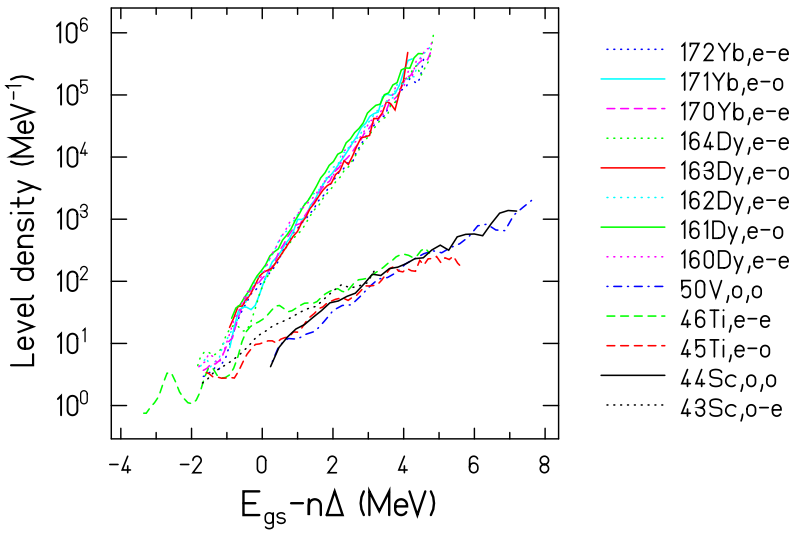


**FIGURE 2.** Experimental level densities of various nuclei [9]. The excitation energy is reduced by $2\Delta$ for even-even (e-e) nuclei, by $\Delta$ for even-odd (e-o) or odd-even (o-e) nuclei and left unchanged for odd-odd (o-o) nuclei.

We have put the previous ideas into equations, leading to a simple model [11]. The results of our calculation are compared with experimental data on the right part of Fig. 1. Except for $^{230}$Th, the agreement with the data is fairly good. In our calculation, we consider that 40% of the potential energy difference from saddle to scission is

dissipated. When $E_{tot}$ is small, as is the case for $^{230}$Th, $\delta_p$ varies very rapidly with $E_{tot}$. Therefore, $^{230}$Th is particularly sensitive to the uncertainties on the dissipated energy. The disagreement found for $^{230}$Th may be caused by the neglect of fluctuations in the dissipated energy acquired on the way from saddle to scission that are due to shape variations and the threshold character of the first quasi-particle excitation in a fully paired system.

## CONCLUSIONS AND PERSPECTIVES

The fission process offers a unique possibility to investigate the behaviour of two warm nuclei in thermal contact. Application of statistical mechanics shows that the process of excitation-energy sorting takes place where excitation energy and unpaired nucleons are predominantly transferred to the heavy fragment. The energy sorting process explains in a transparent way the excitation-energy dependence of the prompt-fission neutron yields [8] and the complex features of the even-odd effect [11]. To further explore the energy-sorting process, new experimental data are needed on these two observables. In particular, a systematic study on the evolution of prompt-neutron yields and the even-odd effect with excitation energy for different fissioning nuclei is required. This study can be performed in experiments with EURISOL actinide beams at medium energies where fission is induced by few-nucleon transfer reactions.

## ACKNOWLEDGMENTS

This work was supported by the European Commission within the Sixth Framework Programme through EFNUDAT (project no. 036434) and within the Seventh Framework Programme through Fission-2010-ERINDA (project no.269499).

## REFERENCES

1. A. A. Naqvi, F. Käppeler, F. Dickmann, R. Müller, *Phys. Rev. C* **34**, 218 (1986)
2. B. L. Tracy et al., *Phys. Rev. C* **5**, 222 (1972)
3. M. Caamano, F. Rejmund, K.-H. Schmidt, *J. Phys. G: Nucl. Part. Phys.* **38**, 035101 (2011)
4. U. Mosel and H. W. Schmitt, *Nucl. Phys. A* **165**, 73 (1971)
5. H. J. Krappe, *Int. J. Mod. Phys. E* **16**, 396 (2007)
6. W.D. Myers and W. J. Swiatecki, *Nucl. Phys. A* **612**, 249 (1997)
7. K.-H. Schmidt, B. Jurado, *Phys. Rev. C* **86**, 044322 (2012)
8. K.-H. Schmidt, B. Jurado, *Phys. Rev. Lett.* **104**, 212501 (2010); *Phys. Rev. C* **83**, 061601 (2011)
9. A. C. Larsen et al., *Phys. Rev. C* **83**, 034315 (2011)
10. T. von Egidy, D. Bucurescu, *Phys. Rev. C* **72**, 044311 (2005)
11. K.-H. Schmidt, B. Jurado, to be published

# Beta-delayed fission: from neutron-deficient to neutron-rich nuclei

Andrei Andreyev[a,b]

[a]*Department of Physics, University of York, York, YO10 5DD*
[b]*Advanced Science Research Center (ASRC), Japan Atomic Energy Agency (JAEA), Tokai, Japan*

**Abstract.** Beta-delayed fission is a rare decay mode which can probe phenomena near and beyond the fission barrier. The status and perspectives for studies of beta-delayed fission in neutron-deficient and neutron-rich nuclei are discussed.

**Keywords:** low-energy fission, fission fragments mass distribution
**PACS:** 28.50.-k, 25.85.-w

## BETA-DELAYED FISSION: A RARE DECAY MODE AS PROBE FOR PHENOMENA NEAR AND BEYOND THE FISSION BARRIER

Beta-delayed fission (βDF), discovered in 1965-1966 in Dubna, is a two-step nuclear decay process that couples beta decay and fission, see Fig.1. Similar to other beta-delayed decay processes, in βDF a parent nucleus (a precursor) first undergoes β decay, populating excited state(s) in the daughter nuclide.

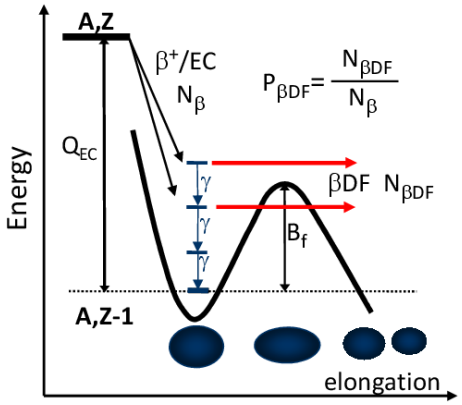


**FIGURE 1.** Simplified diagram for the $\beta^+$/EC delayed fission in the neutron-deficient nuclei. Shown are the ground states of the parent (A,Z) and daughter (A,Z-1) nuclei, and as a function of elongation, the potential energy of the daughter nucleus. $Q_{EC}$ value of the parent and fission barrier $B_f$ of the daughter nuclei are indicated by vertical arrows. The βDF of excited states with $E^* \sim B_f$ in the daughter nucleus is shown by horizontal arrows (see text).

In the case of neutron-deficient nuclei, electron capture (EC) or $\beta^+$ decay is considered, while $\beta^-$ decay happens on the neutron-rich side of the Nuclidic Chart. The

term "βDF" is used in this text for both the neutron-rich and neutron-deficient nuclei. In βDF, the *maximum* excitation energy of the daughter nucleus is limited by the $Q_{EC}$ ($Q_{\beta-}$ in case of neutron-rich nuclei) of the parent. The typical $Q_{EC}$ values are in the range of 3-6 MeV and 9-12 MeV for the known βDF nuclei in the trans-uranium and lead regions, respectively. If the excitation energy of these states, E*, is comparable to or greater than the fission barrier height, $B_f$ , of the daughter nucleus ($E^* \sim B_f$) then fission may happen in competition with other decay modes, e.g. γ decay and/or particle emission. Therefore, the special feature of βDF is that fission proceeds from excited state(s) of the daughter nuclide, but the time scale of the βDF events is determined by the half-life of the parent nucleus. As in most cases the β-decay half-lives are longer than tens of ms, it makes βDF more easily accessible for experimental studies. The importance of βDF is highlighted by its ability to provide *low-energy* fission data for very exotic nuclei which do not decay by spontaneous fission and which are difficult to access by other techniques. The βDF nuclei are situated in three regions of the Nuclidic Chart, see Fig.2, taken from the recent review on βDF [1].

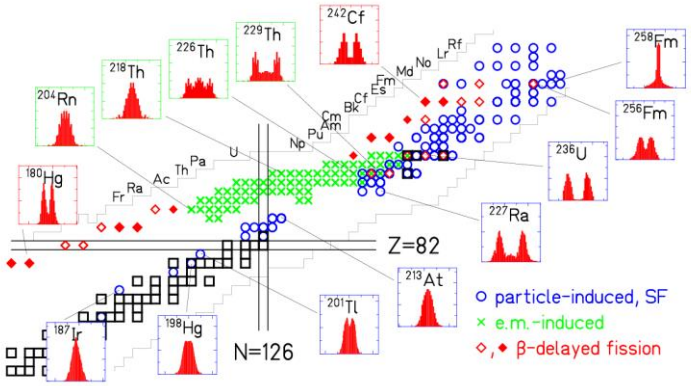


**FIGURE 2.** The nuclei for which fission fragments mass or nuclear-charge distributions have been measured by low-energy fission. The mass distributions are shown for selected systems. Blue open circles: distributions, measured in conventional particle-induced fission experiments and spontaneous fission. Green crosses: nuclear-charge distributions, measured by Coulex-excitation. Open and closed diamonds show 26 known βDF cases, the fissionning daughter is indicated. Filled diamonds mark 11 daughter nuclides for which mass distribution was measured, two of them - $^{180}$Hg and $^{242}$Cf are shown in the plot. The references to all data in the plot can be found in [1].

Historically, the first cases of βDF were discovered in Dubna in the neutron-deficient precursors $^{232,234}$Am (thus, $^{232,234}$Pu are fissionning daughter nuclides). This region is relatively easily accessible by complete fusion reactions with heavy ions but the initial experiments used quite unselective production and detection techniques (e.g. the fission track mica foils). The second region of βDF nuclei includes six neutron-rich nuclei of Ac-Pa (e.g. $^{228,230}$Ac) mostly produced by transfer reactions on the heaviest stable targets. However, although these measurements are more relevant for the r-process, due to the extreme difficulties to produce neutron-rich nuclei quite uncertain data exist in the literature.

Recently, extensive βDF studies in the very neutron-deficient nuclei between Tl and Fr (the third region of βDF nuclei) have been performed by our collaboration. As shown in Fig. 2, these βDF nuclides lie very close to the border of known nuclei.

Fissioning nuclei in this region possess very unusual neutron-to-proton ratios, e.g. N/Z=1.23-1.25 for $^{178,180}$Hg in contrast to a typical ratio of N/Z=1.55-1.59 in the uranium region, where numerous spontaneous fission and βDF cases are known. This allows to investigate potential differences in the βDF process and its observables in the two regions, which differ in many nuclear-structure properties.

Since 2008, our collaboration performed dedicated βDF studies at the SHIP velocity filter at GSI (Darmstadt) and at the ISOLDE mass separator at CERN (Geneva) [2]. In particular, the coupling of the Resonance Ionization Laser Ion Source (RILIS) [3] to ISOLDE opened up new possibilities for βDF studies. The uniqueness of this technique is the unambiguous A and Z identification of the precursor, via the combination of the mass selection by ISOLDE and Z selection by the RILIS. With the help of this techniques, detailed βDF studies of $^{178,180}$Tl and of $^{194,196}$At were recently performed at ISOLDE [1,4]. The laser ionization also allows unique *isomer* separation, which is especially important for the odd-odd βDF precursors, many of which have more than one nuclear state capable of βDF.

## FUTURE PROSPECTS FOR BETA-DELAYED FISSION STUDIES

To date, 26 βDF isotopes are known in three regions of the Chart of Nuclides, see Fig. 2: the neutron-rich Ac and Pa isotopes, and the neutron-deficient isotopes in the trans-uranium and lead regions. However, in many cases only scarce information is presently available. Substantial progress can be expected in all three regions, due to developments of new and/or improved production and detection methods. Below we highlight some of the interesting βDF studies feasible in the near future.

The main efforts in all three βDF regions should concentrate on detailed experiments to reliably measure βDF probabilities, partial half-lives, and energy/mass distributions of fission fragments, similar to those, performed for e.g. $^{180}$Hg in [4]. A direct measurement of the Z values is also needed to firmly establish the A and Z distributions of the fission fragments. The experiments with the laser-ionized isomerically-pure beams of $^{192,194}$At, $^{186,188}$Bi, and $^{202}$Fr should determine whether both isomers of each isotope undergo βDF and whether any difference exists in the βDF process of different isomers. The search for new βDF cases is another important task. For example, with the presently-available beam intensities dedicated searches for βDF of the neutron-rich $^{228,230,232}$Fr and of $^{228,230,232}$Ac are possible at ISOL facilities, such as e.g. ISOLDE or ISAC (TRIUMF). Furthermore, in the past, by using the multinucleon-transfer reactions of 11.4 MeV/u $^{238}$U ions with W/Ta targets at the GSI ISOL mass-separator, new isotopes $^{232}$Ra and $^{233,234}$Ac were produced. The use of this method to search for βDF of $^{232,234}$Ac could be an interesting extension of the βDF studies of $^{230}$Ac, also produced in the transfer reaction. In the lead region, a search for βDF of the odd-A precursors should be performed.

These goals require improved production and detection techniques. The new in-flight recoil separators, such as $S^3$ (GANIL) [5] should provide unique opportunities to access the neutron-deficient nuclei in the trans-uranium region, which are not accessible using the fragmentation-based ISOL techniques. Due to a substantial beam intensity increase, a gain by at least an order of magnitude in

production rates can be expected. Combined with better separation capabilities and improved detection systems, these facilities will certainly open a new era in βDF studies in the trans-uranium region. The same technique can also be used to study the shortest-lived βDF nuclides in the lead region, such as $^{192}$At ($T_{1/2}$~20-100 ms), which is not yet accessible at ISOL facilities due to its short half-life compared to the relatively long release time from the target-ion source.

Laser-based techniques, such as RILIS@ISOLDE [2,3], CRIS@ISOLDE [6] and the recently-developed IGLIS method [7], coupled to the $S^3$ separator, will further increase the sensitivity of the experiments and allow to address the problem of existence of two isomers in a βDF precursor.

More generally, as far as *low-energy* fission studies are concerned, several promising projects are presently being developed. As a continuation of the Coulex-induced fission experiments with relativistic secondary beams the next generation of such studies has recently been initiated by the SOFIA collaboration at GSI [8]. These experiments will benefit from the improved beam intensity of the initial $^{238}$U beam and from detector developments which should enable the unique mass and charge identification of fission fragments with a precision of one unit. In another recent approach, the VAMOS spectrometer (GANIL) was used to study fission initiated by multi-nucleon transfer reactions in inverse kinematics between a $^{238}$U beam and a $^{12}$C target. The first experiments produced different minor actinides, within a range of excitation energies below 30 MeV [9].

A new ambitious method to study low-energy fission exploits the inelastic electron scattering off exotic radioactive beams in a colliding beam kinematics. Two such projects are currently underway: ELISe (FAIR) [10] and SCRIT (RIKEN) [11]. Overall, substantial progress in βDF and low-energy fission studies is certainly expected in the near future.

## ACKNOWLEDGMENTS

This work is based on the recent review of βDF to be appear in Review of Modern Physics [1]. Extensive discussions with Mark Huyse and Piet Van Duppen are highly appreciated.

## REFERENCES

1. A. N. Andreyev, M. Huyse and P. Van Duppen, Rev. Mod. Phys., in print (2013).
2. E. Kugler, Hyp. Int. 129 (2000) 23.
3. V. N. Fedosseev et al., Rev. Sci. Instr. 83 (2012) 02A903.
4. A.N. Andreyev et al., Phys. Rev. Lett. 105 (2011) 252502.
5. A. Drouart et al., EPJ Web of Conferences 17, (2011) 14004.
6. K. M. Lynch et al., J. Phys.: Conf. Ser. 381 (2012) 012128.
7. R. Ferrer et al., Nucl. Instrum. Methods. B291(2012) 29.
8. J. Taieb, Private Communication.
9. X. Derkx et al., EPJ Web of Conferences, 2, (2010) 07001.
10. H. Simon, Nucl. Phys. A 787 (2007) 102.
11. T. Suda et al., Phys. Rev. Lett. 102, (2009) 102501.

# The Use of On-line Isotope Separators for the Direct Production of Medically Relevant Alpha-Emitters

Itzhak Kelson and Michael Schmidt

*School of Physics and Astronomy, Tel Aviv University*
*Tel Aviv 69978, Israel*

The efficacy of alpha particles against cancer cells is well established. Typically, only a few alpha particle hits to the cell nucleus are required to inactivate its reproductive mechanism [1, 2]. In addition, compared to photons or electrons, the effect of alpha radiation is significantly less sensitive to the oxygenation state of the cell, its position in the cell cycle or the administered dose rate [1]. The short range of alpha particles in tissue (50-90 μm) ensures that cells lying outside of the targeted region are spared. However, it also requires that the alpha emitting atoms are brought to the immediate vicinity of the cancer cells, or be otherwise ineffective. Previous work on the therapeutic utilization of alpha particles in the treatment of cancer has focused on targeted alpha therapy and has recently reached the stage of clinical trials. This includes a treatment of bone metastases with $^{223}$Ra and alpha-radio-immunotherapy (α-RIT) trials, involving monoclonal antibodies or peptides labeled with $^{213}$Bi or $^{211}$At for myeloid leukemia, melanoma, lymphoma and glioma. α-RIT is generally considered to be best suited for the treatment of isolated cells, small cell clusters and micro-metastases, rather than solid tumors. This is largely because of physical barriers that exist in solid tumors such as the elevated interstitial fluid pressure, which preclude efficient delivery of the labeled molecules into the tumor.

Diffusing Alpha-emitters Radiation Therapy (DART) represents a different approach for the application of alpha particles, which enables the treatment of solid tumors [3]. The basic idea is to insert into the tumor a number of radioactive sources, which continually release short lived alpha emitting atoms from their surface. The released atoms spread within the tumor by the combined effects of thermal diffusion and advection (vascular and interstitial), forming a region of tumor cell destruction, where a lethal dose is delivered through their alpha decays. The special characteristics of malignant tumors, such as the high concentration of blood vessels and their chaotic nature, play a special role in this dispersion process.

The implementation of the idea relies on the alpha decay chain beginning with $^{228}$Th. The source – a thin conducting wire bearing a relatively small activity of $^{224}$Ra ($t_{1/2}$ = 3.66 d) – is inserted through a fine-gauge needle into the tumor. Once inside the tumor the source releases $^{220}$Rn ($t_{1/2}$ = 55.6 s), $^{216}$Po ($t_{1/2}$ = 0.15 s) and $^{212}$Pb ($t_{1/2}$ = 10.64 h) atoms. A key requirement is that $^{224}$Ra remains fixed on the source, with a minimal residual release of radium atoms into the body. The diffusing atoms are

released from the source by virtue of their recoil energy: when a decaying atom emits an alpha particle with a kinetic energy of 5-10 MeV, its daughter recoils in the opposite direction with a typical kinetic energy of 100-200 keV. This energy is sufficient for the recoiling daughter to traverse 10-30 nm in solid materials (depending on the density). Thus, if the parent atom lies several nanometers below the source surface, the recoiling daughter may leave the source with a considerable probability. The entire progeny [4] of this desorbing nucleus is then dispersed throughout the tumor. Some $^{212}$Pb atoms cleared from the tumor through the blood redistribute throughout the body at low concentration.

$^{224}$Ra-bearing sources are produced by using a $^{228}$Th ($t_{1/2}$ = 1.91 y) generator - a surface covered with a layer containing $^{228}$Th, which is thin enough to enable considerable release of $^{224}$Ra atoms which recoil during the $^{228}$Th alpha disintegration. $^{224}$Ra atoms lose some electrons from their outer shells as they recoil [5]. They escape the generator positively charged with energies up to 100 keV. The generator-source setup comprises an electrically isolated, gas filled enclosure, with the $^{228}$Th generator as an anode and a thin conducting wire, which subsequently becomes the DART source, as a cathode. $^{224}Ra^{+}$ ions escaping the generator are thermalized by collisions with the gas molecules and drift along the focusing field lines to the wire, on whose surface they settle. The duration of the electrostatic collection stage is dictated by the half-life of $^{224}$Ra (3.66 d).

An alternative potential chain, very similar to this, begins with an $^{227}$Ac/$^{227}$Th generator and proceeds with an identical decay chain with one neutron less for all isotopes and with appropriately different half-lives.

The implementation of this new treatment modality clearly depends on the availability of the primary isotopes - $^{228}$Th and $^{227}$Ac. $^{227}$Ac can be produced by irradiating $^{226}$Ra in a high flux of thermal neutrons. Following neutron capture, $^{227}$Ra is produced with a cross section of 8 barns, decaying with a half-life of 42 minutes to $^{227}$Ac. Note, that $^{227}$Ac itself has a very high cross section for thermal neutron capture (about 900 barns), so that by continuing the irradiation long enough it will be transmuted into $^{228}$Th through the formation of the beta decaying isotope $^{228}$Ac ($t_{1/2}$ = 6.1 h). An alternative way of producing $^{228}$Th is through its chemical separation from a solution containing the 72 years half-life isotope $^{232}$U. The alpha decaying $^{232}$U may be produced by a number of available reactions.

The production of generators from the primary raw material supplied in a solution poses practical problems, particularly when large scale activity is considered. Furthermore, the primary isotope is mostly deposited on the surface of the generator and is thus susceptible to undesirable sputtering during the therapeutic source charging phase, a phenomenon unacceptable from the regulatory point of view.

The future availability of very high output isotope production facilities such as EURISOL opens new and improved ways of producing the generators required for the implementation of the DART modality. $^{227}$Ac is produced by collecting the A=227 isobars $^{227}$Fr ($t_{1/2}$ = 2.5 m) and $^{227}$Ra ($t_{1/2}$ = 42 m). $^{228}$Th is produced by collecting the A=228 isobars $^{228}$Fr ($t_{1/2}$ = 39 s) and $^{228}$Ra ($t_{1/2}$ = 5.8 y). By adjusting the acceleration energy appropriately the produced isotopes can be implanted at an optimal depth in the generators-to-be. The net result of this procedure is a generator in its finalized form, ready to be used with any further manipulation. The $^{228}$Th case is characterized by

important further advantages. First, the long half-life of $^{228}$Ra allows its parasitic accumulation in a target which is used as a beam dump, from which it is eventually extracted. The fact that the generator is now based on $^{228}$Ra means a longer half-life and less replacement cycles of the generators in the source preparation facility. Both primary isotopes were actually collected on a small scale at ISOLDE for initial testing and verification.

Since cost considerations play a significant role in the development and implementation of therapeutic modalities, it is interesting to get an estimate of how many patients might be treated by the isotopes produced in a 24 hour period in the facility. Assuming an average tumor burden of a few grams per patient, a required number of primary radioactive atoms of a few times $10^{11}$ per gram of tumor and a production rate of a few times $10^{10}$ per second, the 24 hour output provides treatment for a few thousands patients.

## REFERENCES


1. J. E. Hall, *Radiobiology for the radiologist*, Philadelphia: Lippincott, Williams and Wilkins, 2000.
2. J. Rotmensch, R. W. Archer, J. Hines, M. Toolhill and A. L. Herbst, *Gynecol. Oncol.* **35**, 297-300 (1989).
3. L. Arazi, T. Cooks, M. Schmidt, Y. Keisari and I. Kelson, *Phys. Med. Biol.* **52**, 5025-5042 (2007).
4. C. M. Lederer and V. S. Shirley, *Table of Isotopes, 7th Edition*, New York, Wiley, 1977.
5. G. L. Cano and R. W. Dressel, *Phys. Rev.* **139**, 1883-1885 (1965).

# Optimization of multiple-frequency heating and gas mixing in ECR charge breeders.

Ł. Standyło[a], H. Koivisto[b], O. Tarvainen[b], V. Toivanen[b], J. Komppula[b], T. Lamy[c], J. Angot[c], P. Delahaye[d], L. Maunoury[d], P. Gmaj[a], A. Galata[e], O. Steczkiewicz[a] and J. Choiński[a]

[a]*Heavy Ion Laboratory, University of Warsaw, Warsaw, Poland*
[b]*Department of Physics, University of Jyväskylä, Jyväskylä, Finland*
[c]*LPSC Grenoble, 53, rue des Martyrs, 38026 Grenoble Cedex, France*
[d]*GANIL, CEA/DSM-CNRS/IN2P3, Caen Cedex 05, France*
[e]*INFN-Laboratori Nazionali di Legnaro, Legnaro, Padova, Italy*

**Abstract.** The ECR charge breeders have successfully been used to produce intensive beams of highly charged ions. The further improvements of boosters like PHOENIX, installed at LPSC, will benefit many Radioactive Ion Beam (RIB) facilities like SPES, SPIRAL1 Upgrade and SPIRAL2 but even more for those like EURISOL that foresee the production of high intensity radioactive beams. In order to respond to these requirements the effect of multiple-frequency heating and gas mixing techniques on the optimization of charge state distribution (CDS) and ionization process was studied. These techniques are powerful tools to improve the intensity of highly charged ion beams. Measurements performed at JYFL investigated the effect of the gas mixing and 2-frequency heating on the production efficiency of highly charged ion beams. The experiments were performed using conventional ECRIS with argon, krypton and xenon gases and oxygen as a support gas. The main microwave source was 14 GHz Klystron and the additional heating frequency was fed into the plasma chamber using TWTA (oscillator 10.75 – 12.75 GHz). In order to limit variables during the experiment the total microwave power was kept constant at 600 W. Results showed that the 2-frequency heating and gas mixing have an enormous effect on beam intensities when they are used simultaneously - their effect seems to be additive. As an example, the intensity of $Xe^{22+}$ ion beam increased by a factor of 10. Experiments have also shown that the gas mixing is superior when the production efficiency has to be increased. The efficiency of $Kr^{20+}$ increased from 0.5% to 2.5%, when support gas has been added. The next step was to measure 2-frequency and the gas mixing effect on the charge breeder. Main goal was to confirm the effects observed by the conventional ECRIS and to optimize the breeding efficiency of the PHOENIX booster. The experiment was performed at LPSC. Primary 1+ beam was produced by the COMIC source (2.45 GHz) and subsequently injected into the PHOENIX charge breeder. The measurements were carried out using argon and krypton with and without the use of oxygen mixing gas. The plasma was heated by the 14.51 GHz Klystron and additional TWTA with tuned frequency. Obtained data is still under analysis and discussion. *This work is supported by NuPNET as part of the EMILIE project.*

**Keywords:** ECR ion sources, charge breeder, multiple-frequency heating.
**PACS:** 07.77.Ka, 52.50.Sw.

## INTRODUCTION

The study and development of charge breeding techniques is of primary interest for the post-acceleration of intense beams from a second generation ISOL facility.

Extracted as singly charged ions from the target-ion source units, the radioactive isotopes have to be bred to an n+ charge state prior to their post-acceleration, for an optimized efficiency and compactness of the post-accelerator [1]. The principle of the $1^+ \rightarrow n^+$ method (charge breeding with an ECR ion source) consists in capturing ions from radioactive or stable elements in the plasma of an ECRIS, after which high-charge states can be produced with optimal beam intensities [2]. With techniques, such as multiple-frequency plasma heating, better surface coating to provide extra cold electrons and higher magnetic mirror fields, ECRIS performance on ion charge state and beam intensity both have been greatly enhanced. Microwaves of various frequencies can be simultaneously launched into and absorbed by a high charge state ECR plasma. The minimum-B magnetic field configuration in an ECRIS can provide many closed and nested ECR heating surfaces [3].

## Experiments with conventional ECRIS

The first set of experiments was carried out at JYFL (August, 2012) using the JYFL 14 GHz ECRIS. The additional second heating frequency was fed into the plasma chamber using TWTA (oscillator 10.75 – 12.75 GHz). In addition to 2-frequency heating the impact of the well-known gas mixing effect alone and when combined with the 2-frequency heating on the production efficiencies of some gaseous elements was studied.The measurements were carried out using argon, krypton and xenon with and without the use of oxygen mixing gas. The total microwave power was kept constant (600 W) in order to limit the variables during the experiment.

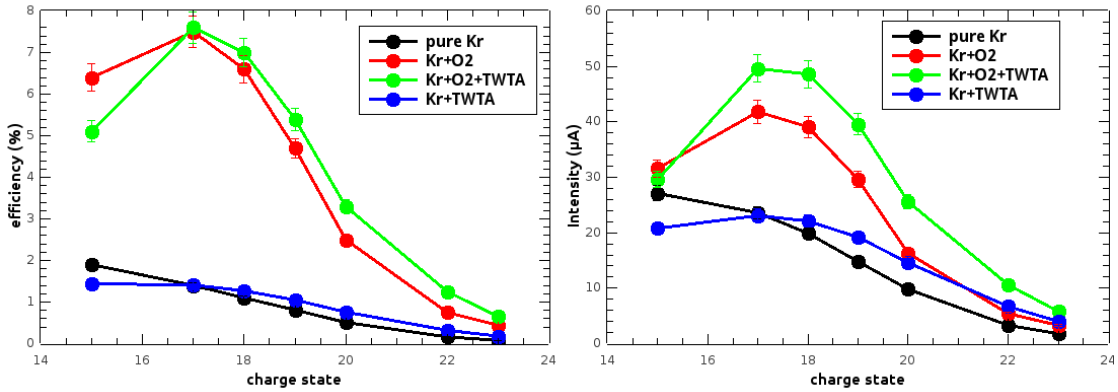


**FIGURE 1.** Production efficiencies (*left*) of different krypton charge states (in %) when different methods have been applied. Tuning for $Kr^{20+}$. The intensities (*right*) of krypton ion beams as a function of charge state when different methods.

According to the results, the combined effect, i.e when the gas mixing and the 2-frequency heating are applied simultaneously, seems to be additive. The tendency indicates that the gas mixing and the 2-frequency method have different mechanisms to improve the intensity of highly charged ions. The intensity of highly charged ion beams increased remarkably when the 2-frequency heating was applied – as was expected. This effect is practically negligible for medium charge states (like $Xe^{22+}$) but the method at least doubles the intensity of very high charge states (like $Xe^{28+}$).

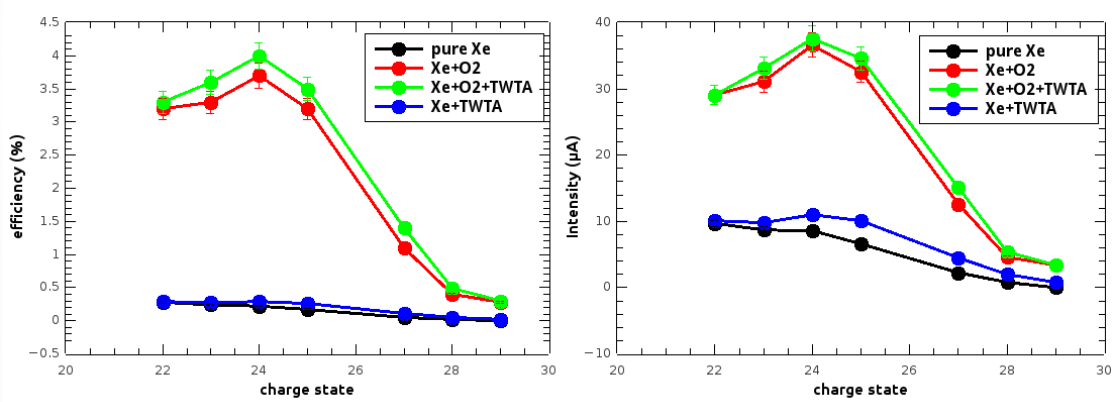


**FIGURE 2.** Production efficiencies (*left*) of different xenon charge states (in %) when different methods have been applied. Tuning for $Kr^{20+}$. The intensities (*right*) of xenon ion beams as a function of charge state when different methods.

## Experiments with charge breeder

The second set of the experiments was performed with the Phoenix charge breeder [4] on the LPSC test stand. The 1+ beam injected into the breeder was produced with the COMIC ion source [5]. Measurements were performed with $^{40}Ar^{+}$ and $^{78}Kr^{+}$ ion beams. The breeder was optimized for high charge states of argon (or krypton) and the intensities of all charge states were subsequently measured. The optimization was done with and without 2-frequency heating (14.5 GHz klystron + adjustable frequency TWTA). Frequency tunning on argon beam was performed to find optimal frequencies with high efficiency and beam intensity – Figure 3.

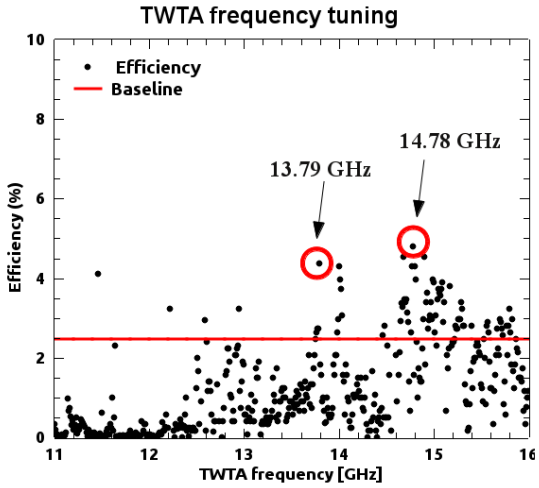


**FIGURE 3.** Production efficiencies of $Ar^{11+}$ ion beams as a function of TWTA frequency and power. Red baseline corresponds to the results when the plasma was heated using the klystron alone with the equivalent total power.

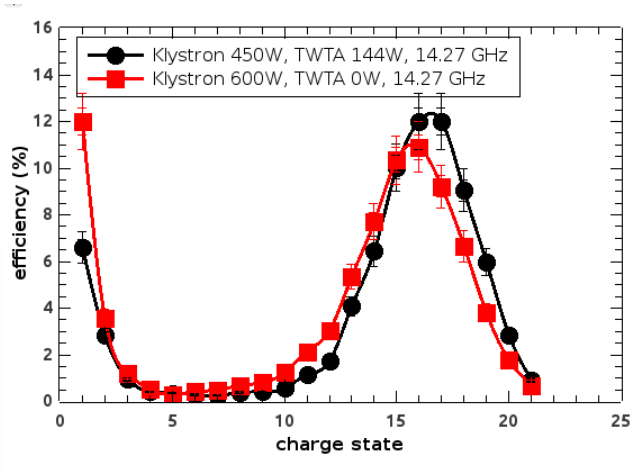


**FIGURE 4.** Results for krypton – tuned for $^{78}Kr^{18+}$. There is an increase with the efficiency (*black dots*) when 2-frequency is applied.

Figure 4. shows results for krypton with measured production efficiency with and without 2-frequency heating. The production efficiency performed with charge breeder is higher than for conventional ECRIS. In both cases the charge state is peaked at $Kr^{+17}$ and for this state with 2-frequency heating we get almost 4.5 % higher efficiency on charge breeder.

## ACKNOWLEDGMENTS

This work has been supported by the EU 7th framework program ”Integrating Activities - Transnational Access”, project number: 262010 (ENSAR), by the ERA-NET NuPNET and by the Academy of Finland under Finnish Centre of Excellence Programme 2012 - 2017 (Nuclear and Accelerator Based Physics Research at JYFL).

## REFERENCES

1. The EURISOL report, http://www.ganil.fr/eurisol/Final_Report.html, and the final report of the RTD-project HPRI-CT-1999-500003, http://www.ha.physik.uni-muenchen.de/jra03cb/
2. P. Sortais et al., Nuclear Physics A 701 (2002) 537c–549c
3. Z. Q. Xie, Rev. of Scien. Instr. Vol. 69, nr 2, February 1998
4. P. Sortais, et al., Rev. Sci. Instrum. 71, (2000), p.617.
5. P. Sortais et al., Rev. Sci. Instrum. 81, (2010), p. 02B314.

# Rare Isotope Beams Production & ELI-NP

Livius Trache

*"Horia Hulubei" Institute for Physics and Nuclear Engineering, Bucharest, Romania*
*Cyclotron institute, Texas A&M University, College Station, TX 77843, USA*

**Abstract.** Rare Isotope Beams (RIB) are typically produced by two methods: ISOL (as in EURISOL) and projectile fragmentation. I touch here upon two different production mechanisms. An existing one: in-flight production and separation in inverse kinematics, with emphasis on the production of a 67% pure isomeric $^{26m}$Al beam at the MARS separator of Texas A&M University. The isomeric beam is obtained by choosing the reaction mechanism, not by separation. Then I will present briefly the Extreme Light Infrastructure – Nuclear Physics (ELI-NP) facility currently under construction in Bucharest, speculating about its possible use as a RIB production facility and its use for nuclear astrophysics studies.

**Keywords:** nuclear reactions; rare isotope beams; experimental methods.
**PACS:** 24; 24.50.+g; 26.60.-t; 25.60.Bx; 25.60.Je; 29.

## INTRODUCTION

I changed the title and content of my presentation from the ones initially announced as I believe these two topics, put together will be of a more general interest to this audience than the original one, presented in detail. Typical RIB production techniques are ISOL and projectile fragmentation. One less used is the production of unstable nuclei in some not-so-exotic reaction mechanisms, like fusion-evaporation or transfer induced by light particles, in inverse kinematics and followed by selection in mass separators like MARS at Texas A&M University [1]. This mechanism (mostly (p,n) and (p,2n) reactions) was used successfully for more than 15 years to obtain dozens of RIBs of high purity (typically over 95%, some close to 100% pure), moderate intensity ($10^4$ to $10^6$ pps) and intermediate energies 10-40 MeV/nucleon. The beams were used to induce secondary reactions for nuclear astrophysics with indirect methods (proton transfer reactions to determine astrophysical S-factors for proton radiative capture reactions), for precision studies of beta-decay, for resonance reactions, for beta-delayed proton emission studies, etc. Here I will show briefly the results we obtained in an effort to obtain an isomeric beam: a beam of $^{26m}$Al and the results of the $^{26m}$Al(d,p) reaction in inverse kinematics. Then I will describe briefly the new European facility ELI-NP under construction in Bucharest, Romania, and talk about its possible use as a RIB production facility. If successful, this RIB facility will use a production mechanism different from ISOL or fragmentation.

# ISOMERIC $^{26M}$AL BEAM

The isotope $^{26}$Al is unstable with a long half-life of 0.72 million years for its $J=5^+$ ground state and has an isomeric state $J=0^+$ only 228 keV above with a much shorter half-life of 6.34 sec. The isotope is known to be important in nuclear astrophysics: the gamma-ray line of 1809 keV following the beta-decay of its long-lived ground state was the first discrete line to be detected by gamma-ray satellite telescopes and is taken as a proof of on-going nucleosynthesis. Its origin is not well known, however, and the comparison of observations with nucleosynthesis model predictions is hindered by the lack of precise nuclear data for some reactions in the reaction networks used in calculations. For all temperatures below 2 GK, $^{26g}$Al and $^{26m}$Al behave like separate, different isotopes and can be treated as such in calculations, but for higher temperatures, reached in some explosive scenarios, they will mix. It becomes important to evaluate reactions on $^{26m}$Al and those can only be studied experimentally with an isomeric beam. The two states, g.s. and isomer, cannot be separated by current mass separators, because resolutions of 228 keV at masses of about 26 GeV are not available at current accelerators, and different methods must be found. We tried the use of a selective reaction mechanism at the MARS separator of the Cyclotron Institute of Texas A&M University. We started with a $^{26}$Mg primary beam of 16 MeV/nucleon from the superconducting cyclotron K500 bombarding a $H_2$ cryotarget. With it $^{26}$Al can be produced by $^{26}$Mg(p,n) reaction by two mechanisms: fusion-evaporation and charge exchange. The first should not be selective and produce a mixing of g.s. ($J=5^+$) and isomeric state ($J=0^+$) around the velocity of the compound system, while charge-exchange should select the isomeric state through the GT transition: $(\nu d_{5/2} * \nu d_{5/2})_{0+} \rightarrow (\nu d_{5/2} * \pi d_{5/2})_{0+}$ at velocities close to that of the projectile. By tuning MARS for the appropriate magnetic rigidities we can separate the two. Indeed, when we tuned MARS for the fusion-evaporation products we obtained a pure $^{26}$Al beam of $3*10^6$ pps with 33% $^{26m}$Al content. When we changed the rigidity to that of the transfer reaction, we increased the $^{26m}$Al content of the beam to 67%, but the intensity decreased 10 times to about $3*10^5$ pps.

The intensities were sufficient in the two cases to study (d,p) reactions in inverse kinematics using TECSA detection system [2]. The comparison of the results show that the two beams can populate same or different excited states in the final nucleus $^{27}$Al. Details of the experiment and the results will be published elsewhere [3]. It follows from the experiment that the production of the isomeric beam using a selective population mechanism like charge-exchange is possible. A better isomeric purity can be obtained by increasing the bombarding energy of the primary beam to 25-40 MeV/nucleon. The isomer production through charge-exchange will be favored by the larger energy and at the same time the fusion-evaporation mechanism will lead mostly to $^{25}$Al through (p,2n). Also the rigidity separation between the two components will increase, favoring a better separation.

# ELI-NP FOR RIB PRODUCTION

Extreme Light Infrastructure (ELI) in Europe is on the ESFRI roadmap since 2009 and in its Preparatory Phase has proposed three facilities with large power lasers (three pillars) to be built in Eastern European countries: the Czech Republic, Hungary and Romania. The one in Romania, which is already under construction, is dedicated to studies of the ultra-high fields generated by two powerful lasers of 10 PW each on nuclei and the nuclear physics that can be made with them. Another part of the facility will be a brilliant gamma-ray beam which will be produced through Compton back-scattering of a laser beam on an intense 6-700 MeV electron beam from a linear accelerator. Gamma-ray energies up to about 20 MeV with bandwidth down to 0.1% and intensities to $10^{13}$ photons/s will be available for experiments with gamma-beam or with gamma and laser beams. It will be the most powerful facility of its kind planned so far (see www.eli-np.ro [4] for details).

## Rare Ion Beams at ELI-NP

To a large extent the facility will be unique and will present opportunities to research in areas barely touched so far [5]:

- *Nuclear Physics experiments to characterize laser – target interaction at large powers/ultra-high fields*
- *Photonuclear reactions – most brilliant gamma-beam, good resolution*
- *Exotic Nuclear Physics and Astrophysics studies* - ***complementary to other NP large facilities (FAIR, SPIRAL2, EURISOL)***.
- *Physics with laser and gamma or e- beams*
- *Applications based on high intensity laser and very brilliant γ beams.*

The research at this ELI-NP facility will be complementary to those at the other ELI pillars.
Of interest for today's subject, the RIB production, studies will be done on:

- Laser Acceleration of very dense Electrons, Protons and Heavy Ions Beams
- Laser-Accelerated Th Beam to produce Neutron-Rich Nuclei around the N = 126 Waiting Point of the r-Process via the Fission-Fusion Reaction
- ***RIB production and separation.***

Parts of these are discussed in more detail in [5, 6].

## Laser induced stellar plasma

One additional observation I want to make is that at these high powers, for very short times, but sufficient to be relevant, laser produced plasmas will simulate stellar plasmas. That is a unique opportunity to make studies important for strophysics, for nuclear astrophysics in particular. Several questions will be of interest:

- Characterization of plasmas: temperatures, densities, lifetimes,…
- Nuclear reaction rates measured directly.
- Nuclear astrophysics: capture reactions on excited states – very important for quantitative descriptions of stellar nucleosynthesis, but out of the range of our current experimental possibilities. Can we do that?!

- How?! What setups?!

I conclude with the belief that ELI-NP will actually raise as the above questions and some we do not imagine at this time. And this is how it should be! Thanks you for your attention!

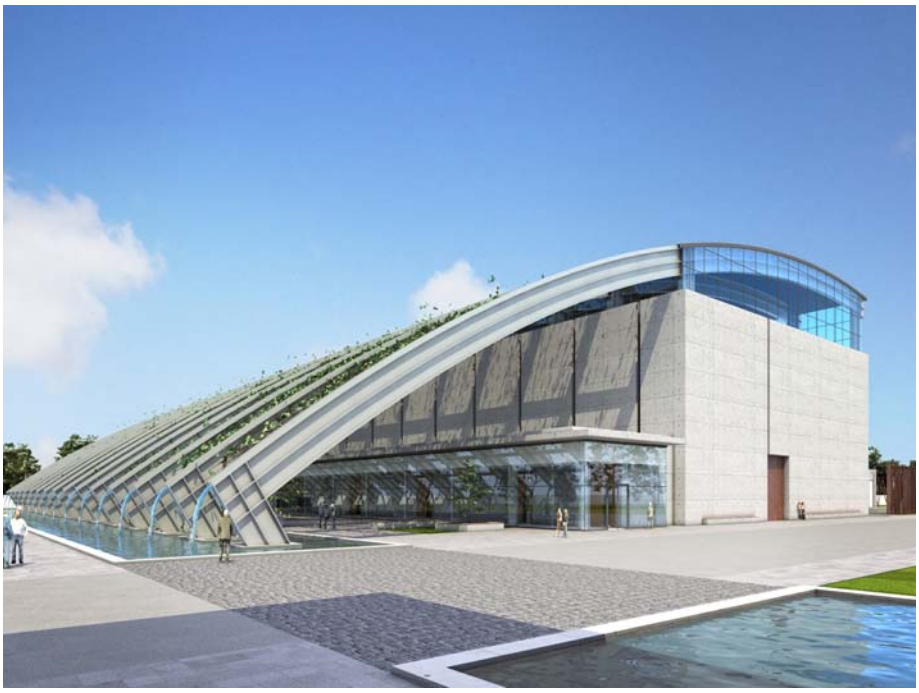

**Figure 1.** Artist view of the projected ELI-NP facility at IFIN-HH Bucharest-Magurele.

## ACKNOWLEDGMENTS

The first part of the talk is based on work done with my colleagues from the TECSA collaboration (Texas A&M University, University of Edinburg, LNS Catania). The original articles or planned publications are cited throughout this paper. The work was supported by U.S. Department of Energy under Grant No. DE-FG03-93ER40773. N.V. Zamfir and I.I. Ursu contributed with material for this presentation. The ELI-NP is a project co-financed by the European Regional Development Fund and the Government of Romania.

## REFERENCES

1. R.E. Tribble et al., *Nucl. Instr. Meth. A* **285**, 441 (1991).
2. B.T. Roeder, M. McCleskey, L. Trache, A.A. Alharbi, A. Banu, S. Cherubini, T. Davinson, V.Z. Goldberg, M. Gulino, R.G. Pizzone, E. Simmons, R. Sparta, A. Spiridon, C. Spitaleri, J.P. Wallace, R.E. Tribble and P.J. Woods, *Nucl. Instr. Meth. A* **634**, 71 (2011).
2. B.T. Roeder et al, to be published.
3. http://www.eli-np.ro/.
5. D. Habs et al. (eds.) *The White Book of ELI Nuclear Physics, Bucharest, 2010*
6. D. Habs and P.G. Thirolf, in *ELI-NP white book*, Bucharest 2010, and P.G. Thirolf et al., presentation at the *ELI-NP Workshop: Laser Experiments*, Bucharest, June 27/28, 2013.

# EAGLE - the central European Array for Gamma Levels Eavaluation at Heavy Ion Laboratory, University of Warsaw.

J. Srebrny[a], J. Mierzejewski[a] and M. Kowalczyk[a,b] on behalf of the EAGLE collaboration[c]

[a] *Heavy Ion Laboratory, University of Warsaw, ul. Pasteura 5a, 02-093 Warszawa, PL*
[b] *Institute of Experimental Physics, University of Warsaw, ul. Hoża 69, 00-681 Warszawa, PL*
[c] *see the collaboration webpage: http://www.slcj.uw.edu.pl/en/97.html*

**Abstract.** The EAGLE array is presented together with an ancillary detectors, scientific program and highlights from the last campaigns. The new electron conversion spectrometer and a prototype of digital electronics for ACS Ge detectors are also presented.

**Keywords: Ge ACS, plunger, RDDSM, coulomb excitations, Si-ball, chiral symmetry spontaneous braking, shape coexistence, electron conversion, K-isomers, incomplete fusion**.
**PACS:** 21.10.-k, 21.10.Re, 23.20.Lv, 21.10.Tg, 21.60.Ev, 25.70.Jj, 29.30.Kv

## THE EAGLE ARRAY AND ANCILARY DEVICES

The EAGLE array became operational in 2010 [1] replacing the OSIRIS-II [2] array at Heavy Ion Laboratory. The EAGLE can accommodate a maximum number of 30 Ge ACS detectors coupled to various ancillary devices, such as:

- Internal Conversion Electron (ICE) spectrometer.
- Bucharest-Köln Plunger.
- Compact scattering chamber equipped with 110 PIN diodes placed at backward angles.
- $4\pi$ inner ball consisting of 60 $BaF_2$ crystals.
- 30 element $4\pi$ silicon detector array Si-ball.
- Recoil Filter Detector.

Until June 2011 OSIRIS-II and EAGLE arrays were equipped with 12 ACS HPGe detectors, resulting in a total photo-peak efficiency equal to 0.5% at 1.3 MeV. This configuration was replaced by the configuration with 15 Eurogam Phase-1 ACS HPGe detectors loaned by the GAMMAPOOL, increasing the efficiency to 1.8%.

## THE SCIENTIFIC PROGRAM

The scientific program of the OSIRIS and EAGLE arrays focused on the phenomenon of spontaneous symmetry breaking in atomic nuclei. It includes:
1. The experimental study of spontaneous chiral symmetry breaking by DSAM lifetime measurements of partner bands in $^{132}$La and $^{122,124,126,128}$Cs nuclei [3-5].

2. The shape coexistence and shape evolution studied by the measurements of transition probabilities by COULEX and RDDS measurements, seeking for the shape coexistence of 0+ states. The following experiments were performed:
- super-deformation in $^{42}$Ca [6]. The first AGATA experiment in LNL Legnaro, where the COULEX of $^{42}$Ca on $^{208}$Pb target was performed, required a separate experiment for the refinement of the level scheme in $^{42}$Ca. The $^{12}$C($^{32}$S,2p)$^{42}$Ca reaction was studied.
- The first successful production run with the Koeln-Bucharest Plunger in the frame of Warsaw-Oslo-Bucharest collaboration. The lifetimes of low spin levels in $^{140}$Sm were investigated using RDDS method. The data are being analyzed.
- COULEX of $^{107}$Ag and $^{70}$Zn using $^{32}$S beam. The data are being analysed.
- determination of quadrupole deformation and triaxiality for coexisting two 0+ levels in $^{100}$Mo by COULEX on $^{32}$S beam[7].
3. The studies of K-isomers, as a test of K-quantum number conservation, by the combined gamma and internal conversion electron spectroscopy of $^{132}$Ce, $^{130}$Ba, $^{134}$Nd and $^{184}$Pt nuclei [8,9]. During the last EAGLE campaign with GAMMAPOOL detectors, the new ICE spectrometer was designed, built and tested (see Fig. 1).

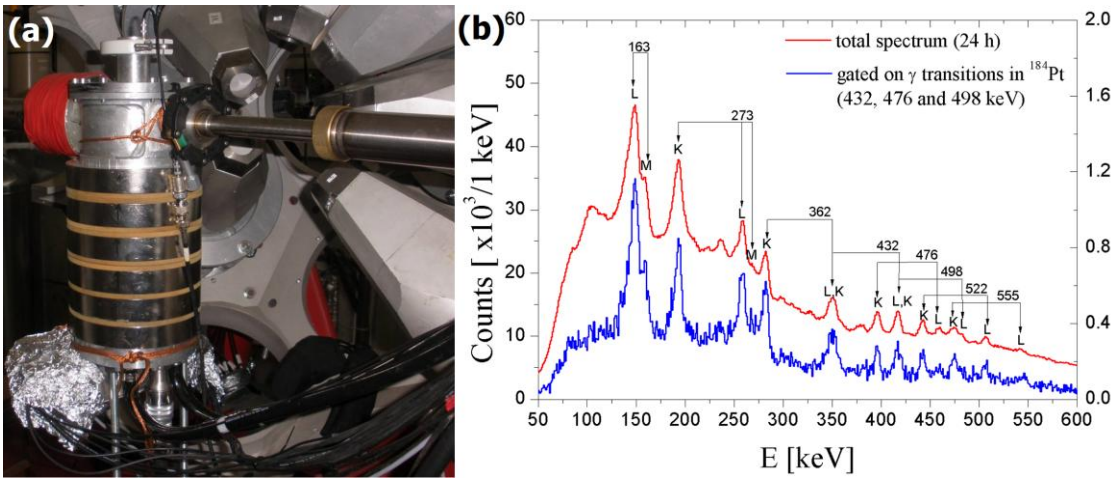


**FIGURE 1.** The new ICE spectrometer inside the EAGLE array (a) and in-beam measured electron spectra (b): inclusive one (red line) and exclusive one (blue line) gated on γ–transitions in $^{184}$Pt. The transitions energies and corresponding electron lines are labeled.

4. The incomplete fusion reaction mechanism studied by the γ–α coincidences measurements [1]. The $^{122}$Sn($^{20}$Ne, αxn)$^{138-x}$Ce reaction at 141 and 150 MeV beam energies was studied. The preliminary results point to the important role of the incomplete fusion, which contributes significantly (at least 30% at 141 and 50% at 150 MeV) to the cross section for the production of $^{132,133}$Ce nuclei.
5. Beside the rich scientific program, the EAGLE array is also used for teaching and training purposes. During the EAGLE campaign more than 80 students took part in one of the three major training programs at HIL: International Workshop on Acceleration and Applications of Heavy Ions (II and III edition, 2 weeks each), I Summer School on Acceleration and Applications of Heavy Ions (1 week) and Polish Workshop on Acceleration and Applications of Heavy Ions (VII and VIII editions, 1 week each) [10].

# THE NEW DIGITAL MODULE FOR ACS Ge DETECTORS

The prototype of a new acquisition module for 4 ACS Ge detectors was designed, built and tested (see Fig. 2). It consists of a motherboard, data acquisition mezzanine board and a communication module. The signals from Ge detectors are connected to the acquisition board on which two dual channel 16-bit ADC16DV160 ADC's from National Semiconductor are installed. Each input track is equipped with a programmable DAC for the offset modification and a programmable amplifier for the range modification. The LMK04031 clock can be synchronized with the external source or/and used as a synchronization source. All the data and control signals from acquisition mezzanine board are connected to the Virtex-4 LX25 FPGA, placed on the motherboard, which is responsible for the data preprocessing and buffering. The logical NIM signals from ACS together with additional general purpose two NIM input and two NIM output signals are connected to the motherboard and controlled by the same FPGA module. A separate mezzanine board is used for the communication purposes. It consists of Virtex-4 FX12 Mini Module designed by MEMEC. The embedded PowerPC CPU, 64 MB on-board RAM and a gigabit Ethernet interface allows to use C language and TCP libraries in communication with the external computers for data transfer and acquisition board setup.
The presented solution gives the full control over the acquisition hardware and low level software, allowing to adapt the system for a cooperation with the external devices. The clock time stamp together with LVDS and NIM signals can be used for the synchronization and data exchange.
The module was tested using both calibration sources and during the in-beam measurements with EAGLE array coupled with the ICE spectrometer (see Fig. 1a). The energetic linearity obtained with the presented module is better than in the case of standard ORTEC analog amplifier and ADC (see Fig. 2b.)

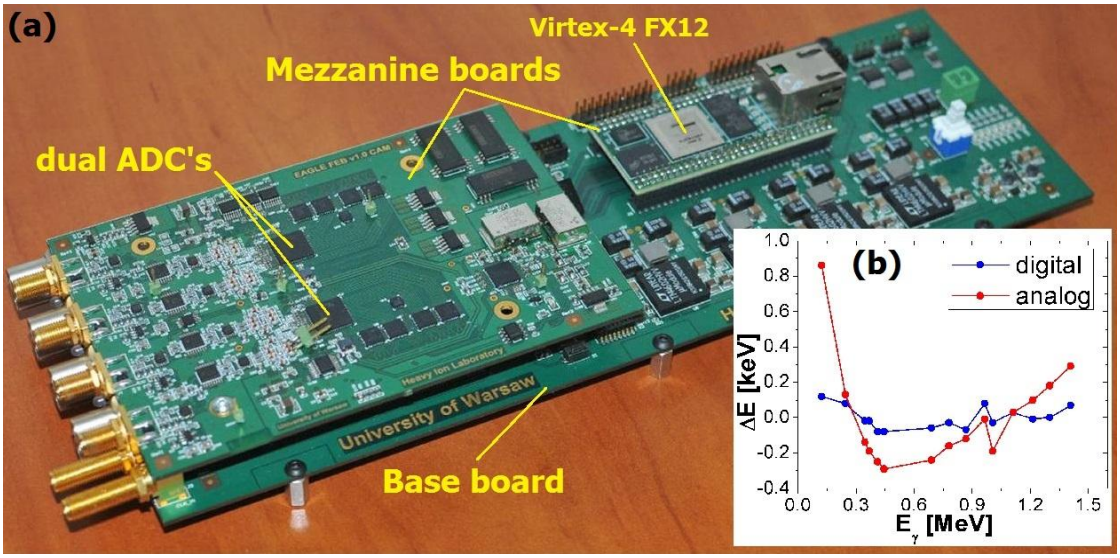


**FIGURE 2.** a.) The new acquisition module for 4 ACS Ge detectors; the most important components are labeled; b.) The energy difference between actual γ energy and the one calculated with linear calibration using $^{152}$Eu source for the presented digital module (blue) and standard ORTEC analog amplifier and ADC(red). The lines are drawn only to guide an eye.

## SUMMARY

The EAGLE set-up on beam of Warsaw's heavy ion cyclotron is the biggest array of Germanium detectors in the new countries of the European Union. A high standard equipment provides an opportunity for measurements of valuable and attractive subjects. Our results prove that we can provide a precise information on nuclear structure, particularly on electromagnetic matrix elements measured with COULEX, DSA and RDDS methods, with an intense and stable beams, complementing results obtained with radioactive beams. In the frame of the EAGLE collaboration a relatively young experts were educated. An innovative digital electronics for ACS Ge detectors and a new conversion electron spectrometer were designed and manufactured. The new experimental as well as theoretical evidences of spontaneous time reversal (equivalent of chiral) symmetry breaking phenomenon in atomic nucleus were found. The EAGLE array on beam of U200-P heavy ion cyclotron is a perfect training ground for young scientists expected to work with the future EURISOL beams.

## ACKNOWLEDGMENTS

The authors would like to express their thanks to young leaders of the EAGLE collaboration: E. Grodner, K. Hadyńska – Klęk , P. Napiorkowski, W. Okliński and J. Perkowski, for help in the preparation of this work. We express our gratitude to the Heavy Ion Laboratory technical staff for their contribution at the development stage of the project. Some difficulties would not have been overcome without their competence and skills. We would like to acknowledge the crew of the cyclotron for providing valuable ion beams. Finally, we would like to express our thanks to the Polish Ministry of Science and Higher Education for its financial support of the project (no.589/N-G-POOL/2009/0).

## REFERENCES

1. J. Mierzejewski et al., **Nuclear. Instruments and Methods A 659, 84 (2011)**
2. M. Kisieliński et al. for the OSIRIS-II Collaboration, HIL Annual Report 2004, 32 p
3. E. Grodner et al., **Phys. Rev. Lett. 97, 172501 (2006)**
4. E. Grodner et al., **Physics Letters B 703, 46 (2011**)
5. E. Grodner et al., J. Phys.: Conference Series 381, 012067 (2012)
6. K. Hadyńska-Klęk et al., **Acta Physica Polonica B 44, 617 (2013)**
7. K. Wrzosek-Lipska et al. **Phys. Rev. C 86, 064305 (2012**)
8. J. Perkowski et al. **European Physical Journal A 42, 379 (2009)**
9. J. Perkowski, et al., Acta Physica Polonica B 43, 273 (2012)
10. Workshop webpage: <http://www.slcj.uw.edu.pl/en/66.html>

# Symmetry Breaking at High Temperature and Spin: Nuclear Jacobi and Poincaré Transitions

J. Dudek*, K. Mazurek†, A. Maj† and D. Rouvel*

*IPHC/DRS and Université de Strasbourg, 23 rue du Loess, B.P. 28, F-67037 Strasbourg, France
†Institute of Nuclear Physics PAN, ul. Radzikowskiego 152, Pl-31342 Kraków, Poland

**Abstract.** We discuss a research strategy focussed around the so-called Jacobi and Poincaré shape transitions at high temperatures and angular momenta. As discussed in the text, these transitions offer unique opportunities of studying global, i.e. varying little from one nucleus to another, nuclear properties related to both the nuclear stability, thus the very existence of nuclei – one of the fundamental goals in Physics of Exotic Nuclei – and to the symmetry breaking phenomena.

**Keywords:** Nuclei at High Temperatures, Symmetry Breaking in Nuclei, Collective Rotation
**PACS:** 21.10.Dr, 21.10.Re, 24.75.+i, 25.85.-w, 21.10.Dr

## IMPORTANCE OF THE PHYSICS CASE VS. EURISOL

Atomic nuclei belong to those systems whose bulk excited-state *collective properties* such as rotational ones, are often predetermined by the properties of *a few single-nucleonic states* with energies close to the Fermi energy. Experimental evidence, among the best known in the literature, is provided by the structure of rotational bands, backbending, blocking and associated phenomena studied intensively in the 80'ies and since. Strongly excited states can often be described within the nuclear mean field theory as high-temperature configurations. At sufficiently high temperatures, one says, the quantum (shell) effects disappear and the nuclei can be described by classical 'macroscopic' models such as the Liquid Drop Model. The successful classical parameterisation of the nuclear energy remains an important both technical and practical factor which can be used to simplify the analysis of the experimental facts as long as the fully microscopic theory is not (or cannot be) used.

The nuclear Jacobi transitions taking place when the angular momentum increases, consist in an increase of the nuclear axial oblate deformation, followed by breaking the axial symmetry, the tri-axial shapes replacing the axial ones. The Poincaré transitions in turn correspond to the evolution of the originally left-right symmetric shapes into the left-right asymmetric ones starting at a certain critical spin value. Usually such transitions are described with the help of their critical spin values, say $I_J^{\rm crit.}$ and $I_P^{\rm crit.}$, respectively. The nuclear Jacobi and Poincaré shape transitions offer a unique background for studying these symmetry breaking phenomena precisely because of the 'incidental' simplicity of the macroscopic parametrisation techniques which will allow to exploit the corresponding research strategies also in the absence of the adequate microscopic, fully quantum-mechanical tools. In what follows we will describe in a few words the techniques and the results based on the LSD (Lublin-Strasbourg Drop) model of Ref. [1].

EURISOL Radioactive Ion Beam Facility is expected to deliver beams of nuclei very

rich in neutrons with intensities comparable to those of the stable beams ($10^9$-$10^{10}$ pps). This will allow exploring, the exciting field of high spin physics in unexplored, very exotic regions of the nuclear chart, using fusion reactions. This is related to the fact that the fission limit for very neutron-rich nuclei, produced via fusion-evaporation reaction, is higher at least by 10 units of spins, as a consequence of the significant increase of the fission barrier with the increasing neutron number [see below].

Theoretical calculations strongly suggest that neutron-rich nuclei in the mass range A$\sim$120-140 are good candidates for producing hyper-deformed nuclear states in fusion reactions. This arises because of both the favourable shell-effects at low temperatures *and* the contribution from liquid drop energy term showing, at spins even higher than (80-90) $\hbar$, a well-defined minimum associated with very large deformations. At sufficiently high spins, such minima eventually become yrast, Ref. [2]. Particularly interesting are neutron-rich Barium nuclei, since already with the stable beam experiments indications of hyper-deformation were obtained by the analysis of quasi-continuum ridge-structure in $\gamma$-coincidence spectra, following the population of the compound nucleus $^{128}$Ba, Ref. [3]. In this connection, it is worth noticing that the first indication of super-deformed structures in $^{152}$Dy was also obtained from the analysis of the ridge structures.

The Barium compound nuclei can be obtained using neutron rich Krypton beams delivered by EURISOL by bombarding the $^{48}$Ca target. As it is expected, [4], even $^{96}$Kr will be produced with intensity $10^{10}$ pps, so that one may have a possibility of forming very exotic Barium compound nuclei up to mass A$\sim$144, or even higher.

## REALISTIC CALCULATIONS USING LSD MODEL: THEORY INTERESTS AND ILLUSTRATION

In principle the correct quantum description of the nucleonic motion in nuclei should be based on the microscopic Hamiltonian of the general structure

$$\hat{H}_{\text{nucl.}} = \sum_i \hat{t}_i + \frac{1}{2}\sum_i\sum_j \hat{v}^{(2)}_{i\leftrightarrow j} + \frac{1}{6}\sum_i\sum_j\sum_k \hat{v}^{(3)}_{i\leftrightarrow j\leftrightarrow k}, \tag{1}$$

where $\hat{t}_i$ are nucleonic kinetic energy operators, whereas $\hat{v}^{(2)}$ and $\hat{v}^{(3)}$ denote the nuclear two-body and three-body interactions [Studies of the interactions of this generic structure are intensively pursued at present]. This being said, it is not at all evident in which respect the nuclear systems described, at least in principle, by the above many-body Hamiltonians should lead to the liquid-drop type behaviour and even less so, why a few-parametric Liquid Drop Model formulae like the LSD one, could be treated as 'explanation' of the corresponding behaviour. Part of the 'puzzle' lies in the fact that whereas Hamiltonians of the general above structure are expected to describe and explain the microscopic origin of various phenomena, e.g. by relating the critical spin values to the interplay between various terms in the nuclear Hamiltonian – the macroscopic energy formulae merely 'intelligently parametrize' the experimental data. However, despite the fact that such parametrizations do not explain the fundamental nuclear processes behind the shape transitions, they are nevertheless extremely important in guiding the experiments, the latter in charge of efficiently collecting the 'physical truth' and the experimen-

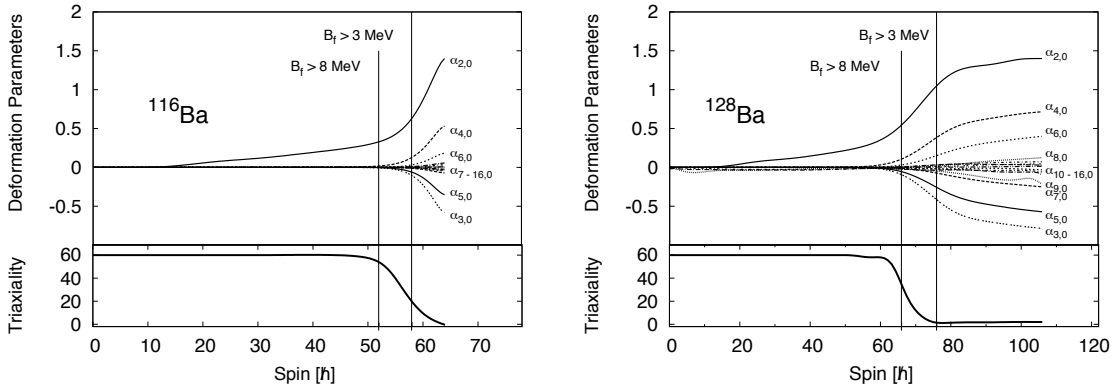


**FIGURE 1.** Shape evolution accompanying the spin increase for $^{116}$Ba and $^{128}$Ba, representing the stable nuclei in the present illustration. Deformation parameters are represented in terms of the standard multipole expansion $\alpha_{\lambda\mu}$; odd $\lambda$ represent mass-asymmetric degrees of freedom. The latter values are plotted by convention as negative. The first from the left vertical lines give the spin at which calculated fission barrier is equal to 8 MeV, whereas the next one – the spin at which the fission barrier equals 3 MeV. It is expected that, roughly, for spins in between the two lines the nucleon evaporation channels compete with fission whereas for the spins 'to the right from the second straight line, the fission decay channel dominates. The bottom frame illustrates the evolution of the tri-axiality represented by the Bohr angle $\gamma$, varying from $60^\circ$ (oblate axially symmetric shapes) towards $\gamma = 0^\circ$, the latter representing elongated, axially symmetric shapes. The areas between the two asymptotically constant $\gamma$-values, i.e. $60^\circ$ and $0^\circ$ describe the Jacobi shape transitions. [From [5].]

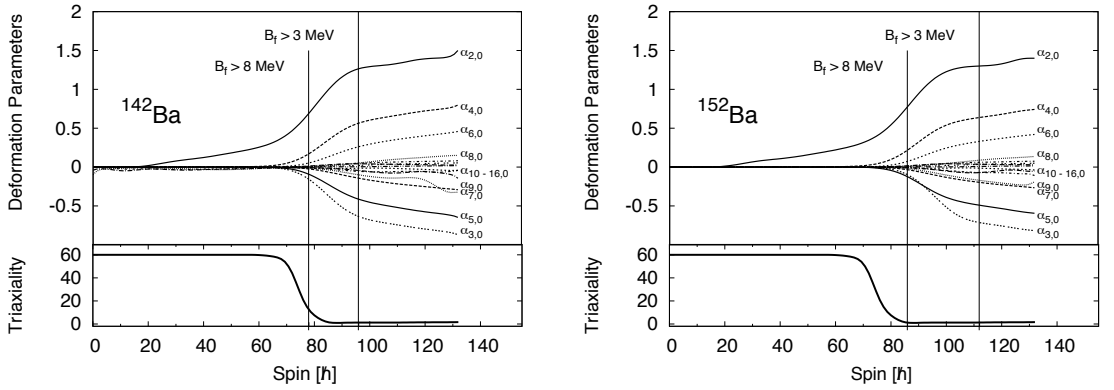


**FIGURE 2.** Similar to the preceding one but for the increasingly exotic, neutron rich Barium isotopes $^{142}$Ba and $^{152}$Ba, the possible realm of the experiments with EURISOL. Observe the systematic shift to the higher and higher critical spin values, the latter marked with the vertical straight lines. The presence of this shift emphasises the uniqueness of the nuclei in this mass range when intending to study the highest spin-states the finite nuclei can withstand. Recall that the highest spins (the 'fastest' collective rotation) implies for theory one of a few most valuable ways of examining the effective time-reversal symmetry breaking phenomena in microscopic nuclear theories of the nucleon-nucleon forces. [From [5].]

tal facts. When the experimental information about Jacobi and Poincaré shape transitions will be fully available it will also be possible to *investigate and test* the advanced theoretical tools as the ones schematised in Eq. (1), importantly, at the extremely high-spin

limit at which the time-reversal symmetry-breaking effective-interactions are expected to be at their extreme. But even before these theoretical investigations will be technically possible – the present studies, whose results are illustrated here – are of high importance for improving the Macroscopic energy-term alone in the so-called Macroscopic-Microscopic methods, the latter using simultaneously the 'classical' (Macroscopic) and 'quantum' (Microscopic) energy terms. The possibility of testing against experiment one of these two elements alone rather than the combination of both has valuable advantages. Shape transitions at high temperatures are the unique terrain to obtain this type of the information and the experimental tests.

In obtaining the illustrative results in Figs. (1-2), the macroscopic energy formula of the LSD model, Ref. [1], has been used. We employ the nuclear surface parameterization in terms of spherical harmonic basis-expansions using the standard $\alpha_{\lambda\mu}$-parameters, minimising the total energy landscapes over up to 16 deformation parameters at each spin after having tested the adequacy of the applied basis selection (cut off). As it can be seen from the Figures the elongation (quadrupole deformation $\alpha_{20}$) plays also numerically a dominant role. Let us notice that in the extremely neutron rich Barium isotopes studied, $^{142}$Ba and $^{152}$Ba, the Poincaré shape transitions are predicted *to follow* the Jacobi shape transitions in the spin windows within which the fission barriers decrease from 8 MeV to 3 MeV, i.e. within an experimentally observable conditions. In experiments capable of providing the fission-fragment mass-distributions such phenomena can be perfectly studied and tested.

## EXPERIMENTAL TESTS AND BIBLIOGRAPHICAL NOTES

The measurement of the fission-fragment mass-asymmetry at varying spin provides a direct test of the Poincaré shape transitions. The experimental studies of the Jacobi shape transitions are less direct and may be performed analysing e.g. Coriolis splitting of the Giant Dipole Resonances. Interested reader may consult Refs. (10-21) in [7] for more information. A short overview of XVII-to-XX century astrophysical studies of the Jacobi and Poincaré transitions can be found in "Part I" of [8], whereas the realistic calculations using the LSD model in the spirit of the present discussion can be found in "Part II" (ibid.) and in [7]. The mathematical background of the LSD model is discussed in "Part IV" while large amplitude motion aspects in "Part III" (ibid.) and in [7].

## REFERENCES


1. K. Pomorski and J. Dudek, *Phys. Rev.* **C 67**, 044316 (2003) [Lublin Strasbourg Drop (LSD) model].
2. J. Dudek, N. Schunck, N. Dubray, Acta Phys. Polon. **B 36**, 975 (2005).
3. B. Herskind et al., Acta Phys. Polon. **B 38**, 1421 (2007);
   B. Herskind et al., Phys. Scr. **T 125**, 108 (2006).
4. M. Lewitowicz, private communication;
5. K. Mazurek, J. Dudek, M. Kmiecik, A. Maj, J. P. Wieleczko and D. Rouvel,
   Acta Phys. Polon. **B 42**, 471 (2011).
6. S. Chandrasekhar, *Communications on Pure and Applied Mathematics*, **XX**, 251 (1967).
7. K. Mazurek, J. Dudek and A. Maj, *Submitted for publication, 2013*; XArchiv ... .

8. J. Dudek, EURISOL Topical Meeting 2013, Cracow, Poland;
http://eurisol.ifj.edu.pl/download/dudek_eurisol.pdf.

# Nuclear Shapes at the Highest Spins

John Simpson[a]

[a]*STFC Daresbury Laboratory, Daresbury, Warrington, WA44AD, UK*

**Abstract.** One of the most interesting and intriguing aspects of atomic nuclei is the generation of angular momentum through the delicate interplay between collective and single-particle degrees of freedom. Nuclei are studied to the extremes of angular momentum to probe these competing modes of excitation and the rich variety of shapes that occur. The quest to observe nuclear behaviour at such high spin has driven the development of ever more sensitive multidetector γ-ray spectrometers for many decades. This talk will discuss recent discoveries from investigations of high spin behaviour in the light rare earth neutron deficient Er, Tm and Yb nuclei utilising the Gammasphere gamma-ray spectrometer. In particular it will include discussion of the shape evolution and coexistence observed in these nuclei including the discovery of weakly populated rotational sequences with high moment of inertia that bypass the classic terminating single-particle configurations near spin 40–50ħ, marking a return to collectivity that extends discrete γ-ray spectroscopy to well over 60ħ. Cranking calculations suggest that these new structures most likely represent stable triaxial strongly deformed bands, however the exact nature of the triaxiality remains a puzzle. The latest lifetime measurements to determine the deformation of these bands will be presented along with recent theoretical speculations. Spectroscopy at the highest spins is generally limited to the neutron deficient region of the nuclear landscape. Intense beams of radioactive ions from EURISOL offers the promise of similar investigations in neutron-rich nuclei where other exotic shapes may be discovered.

**Keywords:** nuclear shapes, angular momentum, gamma-ray detection systems
**PACS:** 21.10.Re, 21.10.Pc, 23.20.Lv

In this talk I will review the development of discrete-line high-spin γ-ray spectroscopy up to the present day where it is now possible to identify structures in the atomic nucleus at an intensity level of ~$10^{-5}$. The nucleus $^{158}$Er has become a textbook example in terms of the evolution of nuclear structure with increasing excitation energy and angular momentum [1,2,3]. I will therefore use $^{158}$Er as the central example of how high spin physics has developed and how the nuclear shape along the yrast line has evolved. The discoveries in $^{158}$Er illustrated in Fig. 1 have benefited much from the progression of detector technologies, indeed new physics and technological improvements go hand in hand. As displayed in Fig. 1, many fascinating phenomena have been observed in $^{158}$Er. As the angular momentum increases, this nucleus first exhibits Coriolis induced alignments of both neutron and proton pairs along the yrast line. It was among the first in which backbending was discovered [4] ($I$~14), and it was also the first nucleus where the second ($I$~28) and third ($I$~38) discontinuities along the yrast line were identified [5,6]. At spins 40−50$h$, the yrast line is crossed by a very different structure, where the nucleus undergoes a dramatic shape transition from a prolate collective rotation to non-collective oblate configurations [7,8]. This transition manifests itself as favoured, fully aligned band termination [9,10,11] and in $^{158}$Er three terminating states, have been observed [12].

There is a huge drop in intensity of γ rays above the terminating states as is evident in Fig. 2(a), and it had been a goal for many years to establish the nature of the states well beyond these very favoured band-termination states. In 2007, a new frontier of discrete-line γ-ray spectroscopy in the spin 50−70*h* range (the so-called "ultrahigh-spin regime") was opened. Four rotational structures in $^{158}$Er and $^{157}$Er (two in each nucleus), displaying high dynamic moments of inertia and possessing very low intensities (~ $10^{-4}$ of the respective channel intensity), were identified and extended up to spin ~ 65*h* [13]. These structures were observed using Gammasphere [14], located at Lawrence Berkeley National Laboratory. This spectrometer, which has 100 suppressed Ge detectors and with a photopeak efficiency of ~9.5%, is currently the best device to perform these high γ-ray multiplicity experiments.

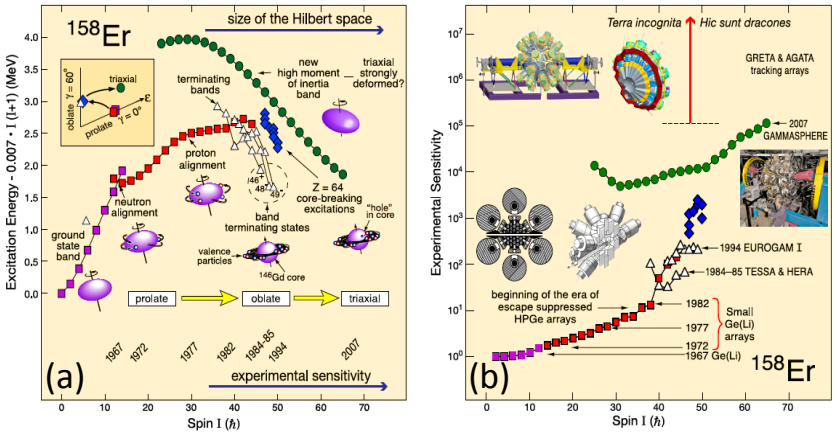


**FIGURE 1.** (a) the evolution of nuclear structure in $^{158}$Er with excitation energy and angular momentum (spin). The inset illustrates the changing shape of $^{158}$Er with increasing spin within the standard (ε, γ) deformation plane. (b) the experimental sensitivity of detection (proportional to the inverse of the observed gamma-ray intensity) is plotted as a function of spin showing the progression of gamma-ray detector technologies with time that are associated with nuclear structure phenomena in $^{158}$Er.

The structures observed bypass the well-known "band-terminating" states, marking a return to collectivity at spins beyond band termination. These bands were proposed to be triaxial strongly deformed (TSD) structures [13], consistent with the predictions of the early cranking calculations [10, 11]. In a rotating triaxial [14] nucleus collective rotation about the short axis, corresponding to a positive γ value ($0^\circ < \gamma < 60^\circ$), usually has the lowest excitation energy based on moment of inertia considerations [16, 17]. Thus, this mode is expected to be favoured over rotation about the intermediate axis ($-60^\circ < \gamma < 0^\circ$). In $^{158}$Er, configurations with $\varepsilon_2 \sim 0.34$ and a positive value of $\gamma = 20^\circ - 25^\circ$ were predicted to be low in energy theoretically and, were thus initially adopted to interpret the collective bands at ultrahigh spin [13].

In order to confirm this assignment an experiment to measure the transition quadrupole moments was carried out using the Doppler Shift Attenuation Method to determine the deformation. This experiment was performed using Gammasphere located at Argonne National Laboratory [18,19]. In spite of their extremely low intensities, an analysis of fractional Doppler shifts $F(t)$ was conducted for three bands in $^{158}$Er [18,19]. This enabled the transition quadrupole moments $Q_t$ of the three collective bands at ultrahigh spin in $^{158}$Er to be measured and they are ~ 9−11 eb. This

demonstrates that they are all associated with strongly deformed shapes. However, the measured $Q_t$ values appear too large for the energetically favoured positive-γ (rotation about the short axis) triaxial shape ($\varepsilon_2 \sim 0.34$). Rather, they appear to be more compatible with a negative-γ (rotation about the intermediate axis) triaxial deformed minimum ($\varepsilon_2 \sim 0.34$) or a positive-γ minimum with larger deformation ($\varepsilon_2 \sim 0.43$) within the cranked Nilsson-Strutinsky (CNS) theoretical framework [20].

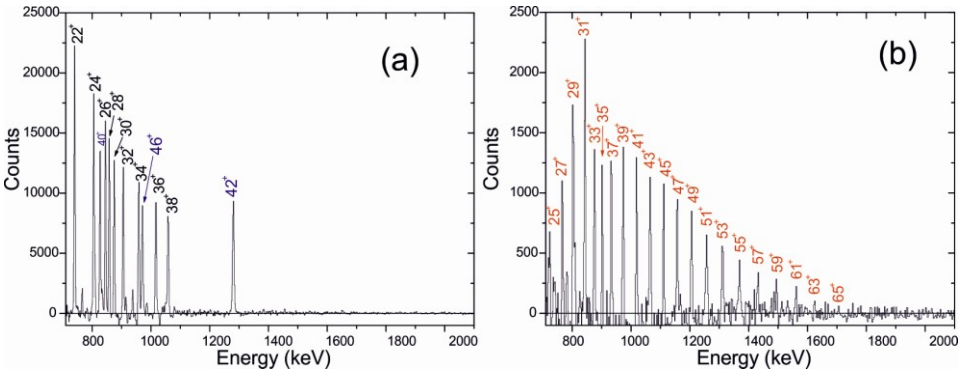


**FIGURE 2.** (a): Sample spectrum highlighting the high spin γ-ray transitions of the yrast band in $^{158}$Er (in coincidence with the $44^+ \rightarrow 42^+$ transition and any one of the transitions between the $38^+$ and the $22^+$ states in the yrast band). (b): Coincidence spectrum representative of the strongest collective band at ultrahigh spin (band 1) observed in $^{158}$Er.

This puzzle led us to perform an additional lifetime experiment to "calibrate" our results by measuring the $Q_t$ of the previously reported bands in $^{154}$Er that were suggested to correspond to superdeformed axial and triaxial strongly deformed shapes [21, 22]. In this experiment quadrupole moments were extracted for the two known high-spin collective bands in $^{154}$Er, in addition to a third newly identified band. The results are consistent with coexisting TSD and axial SD nuclear shapes in this nucleus at high spin [23]. Similar to the TSD bands in $^{157,158}$Er [13], the measured $Q_t$ moments are significantly larger than the value predicted for favoured CNS configurations.

This puzzling discrepancy in our Er work has motivated further theoretical interest [24,25,26]. In a study using the 2-dimensional tilted axis cranking method [24] based on a self-consistent Skyrme-Hartree-Fock model, configurations associated with triaxial shapes at ultrahigh spin in $^{158}$Er were investigated. In this work, the negative-γ minimum becomes only a saddle point when titled cranking is considered and was removed from consideration. The calculated $Q_t$ value for a candidate positive-γ triaxial minimum with large deformation (~ 10.5 eb) agrees well with experiment, nevertheless, this minimum is not yrast until spin ~ 70$\hbar$. In general theory predicts higher spins than indicated by the experiment. Indeed, in [25] it is even stated that if the theoretical spins are correct then the bands observed are the highest spins ever observed in discrete line spectroscopy. Thus, a fully consistent picture between experiment and theory as to the nature of the nucleus in the ultrahigh spin triaxial world remains to be uncovered. These results point to the need for further measurements in this region of triaxial strongly deformed structures to provide more precise $Q_t$, excitation energies and spin values for these bands.

This journey to the highest spins continues to reveal new physics and ever exotic nuclear shapes, and this fascinating story was recently recognised as one of the science highlights of 2013 [27]. The systematic experimental study in a range of

nuclei and the new detailed calculations [24,25,26] are enabling a detailed spectroscopic study of the key single-particle orbitals to start in this new spin domain. This type of physics requires a highly efficient γ–ray spectrometer and relatively intense beams to be able to observe structures at the ~$10^{-5}$ intensity level. This combination will facilitate the search for even weaker structures on the path to fission such as hyperdeformation. Particular regions of the nuclear landscape, such as in the heavy Cd and Yb isotopes where such shapes of expected, can be preferentially populated by neutron rich radioactive beams. A facility such as EURISOL must have such state of the art instrumentation and the new generation of tracking arrays such as AGATA and GRETA [28] are ideal.

## ACKNOWLEDGMENTS

This work would not be possible without the hard work of a huge number of colleagues and good friends who have participated in this programme of research over the last 30 years. In particular I'd like to thanks all those involved in the recent experiments using Gammasphere at Berkeley and Argonne.

## REFERENCES

1. K.S. Krane, *Introductory Nuclear Physics* (John Wiley and Sons, New York, 1988)
2. S.G. Nilsson and I. Ragnarsson, *Shapes and Shells in Nuclear Structure* (Cambridge University Press, Cambridge, England, 1995)
3. K. Heyde, *Basic Ideas and Concepts in Nuclear Physics* (Institute of Physics, Bristol, 1999)
4. H. Beuscher *et al.*, *Phys. Lett*. B **40**, 449 (1972)
5. I.Y. Lee *et al.*, *Phys. Rev. Lett.* **38**, 1454 (1977)
6. J. Burde *et al.*, *Phys. Rev. Lett*. **48**, 530 (1982)
7. J. Simpson *et al.*, *Phys. Rev. Lett.* **53**, 648 (1984)
8. P.O. Tjøm *et al.*, *Phys. Rev. Lett*. **55**, 2405 (1985)
9. T. Bengtsson, I. Ragnarsson, *Phys. Scr.* **T5**, 165 (1983)
10. J. Dudek, W. Nazarewicz, *Phys. Rev.* C **31**, 298 (1985)
11. I. Ragnarsson *et al.*, *Phys. Scr*. **34**, 651 (1986)
12. J. Simpson *et al.*, *Phys. Lett.* B **327**, 187 (1994)
13. E.S. Paul *et al.*, *Phys. Rev. Lett.* **98**, 012501 (2007)
14. R.V.F. Janssens, F.S. Stephens, *Nucl. Phys. News* 6, 9 (1996)
15. G. Andersson *et al.*, *Nucl. Phys.* A **268**, 205 (1976)
16. Z. Szyma´nski, *Fast Nuclear Rotation* (Clarendon Press, Oxford, England, 1983)
17. B.G. Carlsson *et al.*, *Phys. Rev.* C **78**, 034316 (2008)
18. X. Wang et al., *Phys. Lett.* B **702**, 127 (2011)
19. X. Wang et al., J. Phys. Con. Ser. 832, 012065 (2012)
20. B. G. Carlsson, I. Ragnarsson, *Phys. Rev.* C **74(3),** 011302(R) (2006)
21. L. A. Bernstein et al., *Phys. Rev*. C **52**, R1171 (1995)
22. K. Lagergren et al., *Phys. Rev. Lett.* **87**, 022502 (2001)
23. J.P. Revill et al., *Phys. Rev.* C, in press
24. Y. Shi et al., *Phys. Rev. Lett.* **108**, 092501 (2012)
25. A. V. Afanasjev, Y. Shi, W.Nazarewicz, *Phys. Rev.* **C** 86, 031304 (R) (2012)
26. A. Karden, I. Ragnarsson, H. Miri-Hakimabad, R. Rafat-Motevali, *Phys. Rev.* **C** 86, 014309 (2012)
27. X. Wang, M.A. Riley, J. Simpson and E.S. Paul, McGraw Hill 2013 Yearbook of Science and Technology, p 119
28. I.Y. Lee and J. Simpson, Nucl. Phys. News **20**(4), 23 (2010)

# Opportunities in shape coexistence studies using in-beam $\gamma$-ray spectroscopy

E. Clément

*GANIL, CEA/DSM - CNRS/IN2P3, Boulevard Henri Becquerel, BP 55027 - F-14076 CAEN Cedex 05, France*

**Abstract.** The study of shape coexistence in exotic nuclei has recently been a subject of intense experimental work thanks to the first generation of post-accelerated Radioactive Ions Beams facilities which became operational and by using the well established Coulomb excitation technique. Several experiments performed at the GANIL-SPIRAL1 facility, Caen-France, or REX-ISOLDE, CERN, brought new experimental probes in this topic. In this contribution a brief introduction to the phenomena will be followed by a review of the standard techniques used in stable facilities. Features from ISOL facilities will be described and few prospective toward EURISOL will be given.

**Keywords:** Shape coexistence, Coulomb excitation reaction, wave function mixing, ISOL facilities
**PACS:** 21.10.Re, 21.10.-k, 23.20.Lv, 21.10.Tg, 21.60.Ev, 25.70.-z

## INTRODUCTION

Along the shell closures, nuclei are usually spherical. As soon as one goes away from the major shell closures, nuclei become deformed and excitations are of a collective character. The deformation of nuclei between closed shells takes its origin from macroscopic and microscopic effects. Prolate deformations occur far more abundantly than oblate shapes, and there are only few examples throughout the nuclear chart that are predicted to have a large oblate ground-state deformation. In most of the case, the ground state deformation is unique and other shapes with significant variation of the deformation parameter, corresponding to different microscopical configurations, appear at higher excitation energies in the potential energy. However, in particular regions of the nuclear chart, several microscopical configurations, associated to different shapes, might compete in a very narrow energy range for the ground state. In the potential energy surface these configurations appear as local minima close to the ground state and are separated by a barrier high enough to exclude a too high mixing of the configurations. In even-even nuclei, these local minima correspond to low lying $0^+$ states. An overview of the shape coexistence phenomena along the nuclear chart can be seen from the P. Möller calculations that show the number of minima in the potential energy surface of the even-even nuclei [1]. Area of shape competition can be seen in neutron deficient nuclei along the N=Z line between the Z=28 and Z=50 shell closures, in the neutron rich Zr, Sr and Mo isotopes at N=60, in neutron deficient Hg, Pb and Po, in the mid-shell Sn isotopes, below $^{68}$Ni in the so-called third island of inversion and at N=28 below $^{48}$Ca. These mass regions have been intensively discussed and experimentally investigated since decades and a complete overview can be found in the recent review by Kris Heyde and John L. Wood [2]. From the systematics, shape coexistence occurs

close to shell or sub-shell closure closed by high j-orbitals and results from a strong gain in the binding energy thanks to the proton-neutron correlation energy. In the unified view of Heyde and Wood, the appearance of shape coexistence at low energy is a competition between energy gap and a residual interaction that lower the energy of such configuration. In this description, the excitation energy of the low lying $0_2^+$ state results from the cost in energy to create a 2p-2h excitation (usually across a proton gap) and the gain in binding energy from the pairing and the proton-neutron residual energy that includes monopole correction and p-n quadrupole binding energy. These low lying $0_2^+$ states include therefore all the ingredients describing nuclear structure at low excitation energy. As a result, the experimental investigation and spectroscopic data in mass region where shape coexistence occurs bring important constraint for modern nuclear models.

From a theoretical point of view, shape coexistence appears first in the potential energy, where two minima of significatively different $\beta_2$ values are predicted. Each of these minima correspond to an isomeric $0_2^+$ state in even-even nuclei. First experimental evidences for shape coexistence are the observation of a low lying $0_2^+$ state and collective structure built on top of it. The collective character can be assessed through the measurement of the reduced transition probabilities B(E2) and the direct evaluation of the deformation can be obtained by the measurement of the spectroscopic quadrupole moment $Q_s$. The $0^+$ states are usually separated by only few hundred of keV and can therefore mix. The degree of mixing can be assessed via the monopole transition strength between the $0^+$ states, $\rho^2$(E0), or from the full set of B(E2)'s connecting the different configurations. This degree of mixing might reveal the difference in microscopical configuration of the different structures. Low lying $0_2^+$ state can be observed by electron conversion spectroscopy via the search of E0 decay. From the lifetime of the $0_2^+$ state and the E2/E0 branching ratio, the monopole transition strength to the ground state can be extracted. This quantity is proportional to the mixing of the $0_2^+$ and $0_{gs}^+$ wave functions and the difference in deformation. A strong $\rho^2$(E0) ($\geq$50 m.u ) can be the sign of a large mixing as observed in the light Kr isotopes [4] or a large difference in the quadrupole deformation as observed in the neutron rich Sr and Zr at N=60.

From fusion-evaporation reactions in neutron deficient nuclei or from fusion-fission, fission source or deep inelastic collisions in neutron rich nuclei, excited states above the $0^+$ band heads can be established. Assuming that the high spin states are weakly mixed, one can extract from collective models the *unperturbated* excitation energies of the $0^+$ states. Deviation from the extrapolated position or from the standard tendency of the static moment of inertia or of reduced transition probabilities, might reveal shape coexistence and mixing of configurations. See for instance in the light Kr isotopes [4, 5]. These spectroscopic observables have been used since decades to investigate the mass regions cited above [2]. Experiments have established in these unstable nuclei one or several low lying $0^+$ states and observed significant deviations from the standard collective trends in the level scheme and in the B(E2)'s close to the ground state. These observations are all evidences for shape coexistence and used to constraint the theoretical models. However, as soon as direct measurements of the shape associated to each configuration were not possible, no final conclusion can be drawn.

## USING ISOL FACILITIES

Since Radioactive Ions Beams facilities offer post-accelerated beams at 3-5 MeV/A with intensities greater than $10^3$ pps, an intensive experimental work is performed on the study of shape coexistence by safe Coulomb excitation (see the review [3]). The experimental output are B(E2)'s for yrast and non-yrast states, algebric $Q_s$ (prolate, oblate), mixing angles and deformation parameters. This large set of experimental output allows fully mapping the collectivity of the nucleus under investigation. At the first order, the Coulomb excitation cross section is proportional to the B(E2) and in a second order effect to the diagonal matrix element of the quadrupole operator for a given state, ie its electric quadrupole moment. Using the differential Coulomb excitation cross section, one can extract both quantities in a single experiment. The experimental setup consists in an annular silicon strip detector and a high efficient HPGe array as EXOGAM at GANIL/SPIRAL1 [6] or Miniball at REX-ISOLDE [7]. The Coulomb excitation cross section is then analyzed using the GOSIA code [8]. For the first time in unstable nuclei, from the spectroscopic quadrupole moments, the sign and the amplitude of the deformation are determined. A soon as the non-yrast band is populated, the B(E2)'s within and between bands can be measured. These informations are used to estimate from simple models the mixing between the configurations. In a two levels mixing approach, the observed states wave functions can be written as a linear combination of *unperturbated* wave functions. From the measured B(E2)'s, mixing angles can be deduced. See for instance the case of the light Kr isotopes [9]. This complete picture in terms of collectivity (full set of B(E2), $Q_s$ and mixing angles) has been obtained thanks to the ISOL facilities and so far only in the light Kr isotopes. Further detailled results will be soon available in neutron rich $^{96,98}$Sr [10] and in the neutron deficient Hg [11]. As a consequence, referring to the nuclear chart calculated by P. Möller [1], only a small fraction of the cases have been covered by the present ISOL facilities. Post-accelerated beams with intensities greater than $10^4$ pps and energies greater than 4 MeV/A are requested to reach the level of description.

## PROSPECTIVE TOWARD EURISOL

The next generation of ISOL facilities with post-accelerated beams at 5 MeV/A has chemical challenges in order to extract new elements in mass regions covered by GANIL-SPIRAL1 and REX-ISOLDE. Very few cases have been investigated with sufficient details using the Coulomb excitation technique. Almost all elements from Se to Cd isotopes along the N=Z line, both odd and even mass, deserve new experiments with more statistic. The new island of inversion below $^{68}$Ni might present a scenario of shape coexistence [12, 13]. Post-accelerated beams of Co, Fe and Mn isotopes around N=40 will be mandatory. On the neutron rich side, close to N=60, the development of post-accelerated Zr beams at high intensity will allow understanding the complex scenario of shape change. As already mentioned, shape coexistence occurs close to shell or sub-shell closures. It means that the search for new shape coexistence area is intimately related to the search for new shell or sub-shell closures far from stability. As an

example, shape isomerism and shape coexistence should be investigated around $^{60}$Ca, in the neutron rich Ni beyond N=50 and in the Sn isotopes at the mid-shell between N=82 and N=126. In the very neutron rich matter, shell gaps arising from the spin-orbit might disappear, favoring the oscillator gaps. In this framework, shape coexistence close to N, Z=70 in very neutron rich nuclei could be investigated. Superdeformation (SD) has been a major facet of nuclear structure and is a dramatic form of shape coexistence. It occurs at relatively high energy and high spin in opposition to the low spin and low excitation energy regime described previously. However, the connection between SD configuration and low excitation energy structure remains to be understood. New area might be in heavy nuclei close to stability and will be populated by fusion evaporation reactions using neutron rich radioactive beams provided by facilities like SPIRAL2 or in a longer term by EURISOL and will make use of HPGe arrays like AGATA or GRETINA. More transverse open questions remain in the field of shape coexistence. In the $0_2^+$ energy, the pairing energy plays a key role and is a long standing motivation for the study of N=Z nuclei in order to determine the strength of the pairing. Mixing of coexisting structures always occurs but with varying strengths as a function of the mass region or spin and deserves a systematic study. The wave function mixing and shape transition request a better microscopical description through the $2^+$ and $0^+$ states wave functions decomposition. The use of transfer reactions, ($^6$Li,$^8$Be) (t,p) (t,$^3$He), requesting higher energies and higher beam intensities could be investigated. Finally nuclei with a large excess of neutrons may be deformed in novel ways and hence may adopt unusual shapes. Indeed the neutron skin might adopt a different deformation than the core.

## CONCLUSION

The first generation of ISOL facilities has shown that new spectroscopic data can be extracted in order to obtain a detailed description of the shape coexistence. These data have been widely compared to the most recent theoretical models with great success. Next generation of facilities like EURISOL opens new area with more details thanks to higher beam intensities and higher beam energies. For the most exotic case, first evidences based on B(E2)'s and level scheme will be discovered.

## REFERENCES


1. Peter Möller Phys. Rev. Lett 103, 212501 (2009)
2. Kris Heyde and John L. Wood Rev. Mod. Phys. 83, 1467 (2011)
3. Andreas Görgen J. Phys. G: Nucl. Part. Phys. 37, 103101 (2010)
4. E. Bouchez *et al.* Phys. Rev. Lett., 90 (2003)
5. A. Görgen *et al.* Eur. Phy. J A 26, 153 (2005)
6. J. Simpson *et al.* Acta Physica Hungarica, New Series, Heavy Ion Physics 11 (2000) 159-188
7. N. Warr for the Miniball Collaboration Eur.Phys.J. A 49, 40 (2013)
8. T. Czosnyka,D. Cline, and C.Y.Wu, GOSIA manual, University of Rochester, unpublished
9. E. Clément *et al.* Phys. Rev. C 75, 054313 (2007)
10. E. Clément *et al.* Int.J.Mod.Phys. E20, 415 (2011) and in preparation
11. K. Wrzosek-Lipska *et al.* in preparation
12. A. Dijon *et al.* Phys.Rev. C 85, 031301 (2012)
13. D.Pauwels *et al.* Phys.Rev. C 78, 041307 (2008)

# Shape Coexistence In The Neutron-Deficient, Even-Even $^{182-188}$Hg Isotopes

Katarzyna Wrzosek-Lipska[a] and Nick Bree[a]
and the Miniball collaboration

[a]*Instituut voor Kern- en Stralinsfysica, KU Leuven, BE-3001 Leuven, Belgium*

## INTRODUCTION AND PHYSICS CASE

Shape coexistence whereby two or more shapes coexist at low excitation energy in the atomic nucleus is an intriguing phenomenon [1,2,3]. Its manifestation in the neutron-deficient nuclei in the Z=82 region has been first observed through optical spectroscopy measurements whereby a sharp transition in the mean-square-charge-radii was discovered between $^{187}$Hg and $^{185}$Hg [4] and since then a wide spectrum of experimental tools has been used to understand shape coexistence in this mass region (decay studies, laser spectroscopy and in-beam spectroscopy studies, and more recently Coulomb excitation experiments using post-accelerated beams from REX-ISOLDE). This resulted, amongst others, in the discovery of triple shape coexistence in $^{186}$Pb [5] and an early onset of deformation in the light polonium isotopes as evidenced through laser spectroscopic studies [6]. Understanding the evolution and microscopic origin of quadrupole collectivity and shape coexistence is important as it highlights the subtle interplay between the individual nucleon behavior sharpened by the strong Z=82 shell closure and collective degrees of freedom in the atomic nucleus. These experimental observations, therefore, form ideal testing grounds of different theories. Several contemporary theoretical models have been applied to describe the structure of the nuclei around Z=82, such as phenomenological shape mixing calculations, symmetry guided models like e.g. the interacting boson model truncations [7], and beyond mean-field approaches [6,8]. These models do reproduce the global trends of the experimental findings, however important elements, especially on the subtle mixing of the different configurations remain not understood.

In the neutron-deficient mercury isotopes with neutron number around mid-shell (N=104, $^{184}$Hg) the intruding deformed states come low in excitation energy and mix with the normal more spherical states (see Fig. 1). On the other hand the mixing of deformed states in the ground states of the even-even nuclei is limited as evidenced by the charge radii results that are summarized in Ref [6].

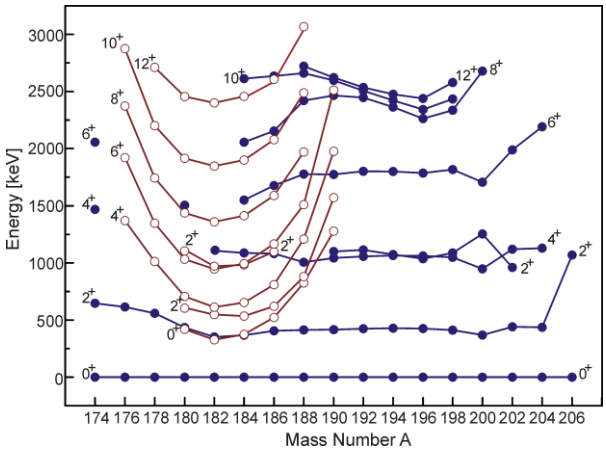


**FIGURE 1.** Energy level systematics of even-even Hg isotopes, taken from reference [1,9]. The full circles are associated with the weakly oblate band and the open circles are those related to excited prolate deformed structures in even – even Hg isotopes.

The mixing between the different states gives rise to strongly converted $2^+_2 \rightarrow 2^+_1$ transitions as recently deduced from beta-decay studies of $^{182,184}$Tl performed at ISOLDE [9,10]. Moreover life times of several states have been obtained in in-beam studies (recoil distance Doppler-shift (RDDS) method [11,12,13]), these are essential to extract reliable quadrupole matrix elements from the Coulomb excitation (Coulex) analysis.

## Coulomb Excitation Experiments at REX-ISOLDE

The Coulomb excitation of even-even $^{182-188}$Hg was carried out at the REX-ISOLDE facility at CERN [21, 22]. Protons from the CERN Proton Synchrotron booster, with an energy of 1.4 GeV, impinging on a molten lead primary target producing a wide spectrum of different nuclei including the mercury isotopes of interest. Using a cold transfer line and after mass separation a high-purity radioactive Hg beam was produced and further accelerated with the REX postaccelerator to an energy of 2.85 MeV/A and delivered to the MINIBALL set-up [23]. Coulomb excitation of $^{182-188}$Hg was induced in $^{120}$Sn, $^{107}$Ag, and $^{112,114}$Cd targets of thicknesses of 2.3 mg/cm$^2$, 1.1 mg/cm$^2$ and 2 mg/cm$^2$ respectively. A summary of the Hg beam particle rates at the secondary target are listed in Table I.

**TABLE 1.** Experimental parameters of the neutron-deficient, even-even 182-188Hg breams.

| Isotope | Year | Intensity [pps] |
|---|---|---|
| $^{182}$Hg | 2008 | $4.9 \cdot 10^3$ |
| $^{184}$Hg | 2007 | $1 \cdot 10^3$ |
| | 2008 | $1 \cdot 10^5$ |
| $^{186}$Hg | 2007 | $2 \cdot 10^5$ |
| | 2008 | $2.5 \cdot 10^5$ |
| $^{188}$Hg | 2007 | $2.5 \cdot 10^5$ |
| | 2008 | $3.1 \cdot 10^5$ |

The γ-rays depopulating Coulomb excited states, of the projectile as well as the target nuclei, were detected with the high-efficiency MINIBALL spectrometer containing 8 triple clusters. The energies of scattered target recoils and mercury ejectiles were measured with a double-sided silicon strip detector (DSSSD) [25]. The DSSSD detector covers the angular range from 15 to 51 degrees in the laboratory frame. It is subdivided into four quadrants with 16 annular and 12 radial strips per quadrant what allows to measure the angular distribution of both mercury ejectiles and target recoils. The high granuality of the DSSSD particle detector as well as the MINIBALL array allowed to perform event-by-event Doppler correction of the observed γ-rays.

The low-energy part of the level schemes of $^{182-188}$Hg that were populated in the experiment, together with the observed electromagnetic transitions is presented on Fig.2.

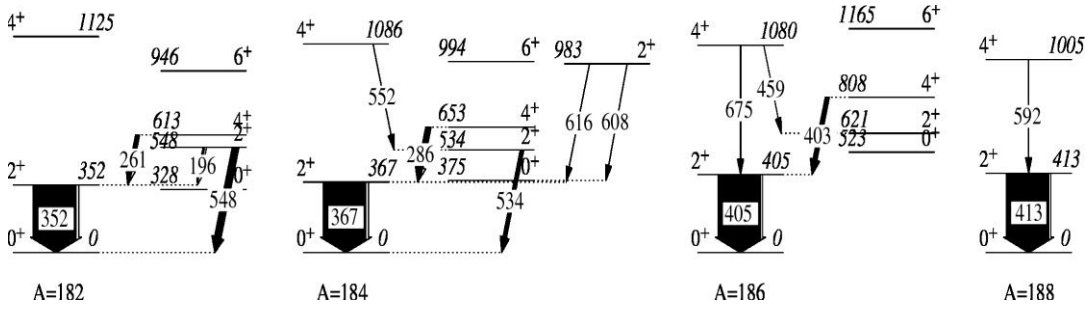


**FIGURE 2.** Low-energy part of level schemes of $^{182-188}$Hg populated in the experiment. Level energies and energies of the γ-ray transitions are given in keV. Widths of arrows are proportional to the measured γ-ray intensities.

Moreover an intense KX-ray peak was observed in low-energy part of the gamma spectrum of the mercury isotopes. It stems from atomic X-rays produced when the Hg beam passes the target, from the electron conversion of the observed gamma rays and the de-excitation of the $0^+_2$ and $2^+_2$ states.

Detailed analysis of the observed γ-ray transitions depopulating Coulomb excited states of investigated nuclei, in coincident with scattered projectile particle – target particle, combined with recent results from life-time measurements and beta decay studies of Tl isotopes enable to extract, for a first time, a set of E2 reduced matrix elements coupling low-lying yrast and non-yrast states of $^{182-188}$Hg. Based on the experimentally obtained magnitudes and relative signs of E2 matrix elements information on the deformation of the ground and first excited $0^+$ states was obtained in a nuclear model independent way. Results show that the ground state of light mercury isotopes is slightly deformed, and of oblate nature, while the deformation of the excited $0^+$ states of $^{182,184}$Hg is larger and hinting towards a triaxial character.

Experimental results were compared to the state-of-the-art beyond mean field and interpreted within a two-state mixing model. This firmly establish the presence of two different topographies in the light mercury isotopes that coexist and mix at low excitation energy. The results will soon be published.

# OUTLOOK

The present experiment of Coulomb excitation of $^{182\text{-}188}$Hg isotopes is a part of a larger campaign to probe shape coexistence in the neutron-deficient lead region. Using beams from REX-ISOLDE, Coulomb excitation studies have been performed as well on a lead ($^{188\text{-}192}$Pb), polonium ($^{196\text{-}206}$Po) and radon ($^{208\text{-}212}$Rn, $^{220\text{-}224}$Rn) isotopes. Shape coexistence studies in the lead region will be further continued with HIE ISOLDE beams using Coulex and transfer reaction techniques. All these experiments need the improvements and the new possibilities offered by the HIE-ISOLDE project: a higher beam energy, higher intensity and better purity and phase space definition of the beam.

With the higher beam energy (5 meV/A) the multiple Coulex cross section will be enhanced and the unknown transitional probabilities mainly in the non-yrast band in these nuclei will be possible to measure for a first time. The higher beam intensity and purity will bring us further out from stability towards the N=104 region where the shape coexisting states become lowest in energy (this is especially needed for the lead, polonium and radon isotopes). Better understanding of shape coexistence in the lead region requires to extend studies to odd mass nuclei, e.g. the Coulomb excitation on selected isomers from the odd mass isotopes (e.g. on the $13/2^+$ and $1/2^-$ isomers in the Hg isotopes) will allow a study of the collective properties of these isotopes and of the bands built on top of them.

# REFERENCES


1. R. Julin, K. Helariotta and M. Muikku, 2001 J. Phys. G. 27 R109
2. J. L. Wood, K. Heyde, W. Nazarewicz, M. Huyse and P. Van Duppen, Phys. Rep. 215, 101 (1992).
3. K. Heyde and J.L. Wood, Reviews of Modern Physics 83 (2011) 1467
4. J. Bonn et al. 1972 Phys. Lett. B 38 308
5. A. N. Andreyev et al. 2000 Nature 405 430
6. T. Cocolios et al., Phys. Rev. Lett. 106 (2011) 052503
7. Garcia-Ramos Physical Review C84 (2011) 014331
8. Y. M. Yao, P.-H. Heenen, M. Bender Phys.Rev. C 87, 034322 (2013)
9. J. Elseviers et al. Phys. Rev. C 84 (2011) 034307
10. E. Rapisarda et al., to be published
11. M. Scheck et al. Phys. Rev. C 81, (2010) 014310
12. T. Grahn et al. Phys. Rev. C 80, (2009) 014324
13. L. Gaffney et al. to be published
21. D. Habs and et al., Nucl. Instr. Met. Phys. Res., Sect. B 139, 128 (1998).
22. O. Kester and et al., Nucl. Instr. Met. Phys. Res., Sect. B 204, 20 (2003).
23. N. Warr and et al., Eur. Phys. J. A 49, 40 (2013).
25. A. N. Ostrowski and et al., Nucl. Instr. Meth. A 480, 448 (2002).

# Yrast Structure of the $^{205,206,210}$Bi Isotopes Produced in Deep-inelastic Reactions

N. Cieplicka[a], B. Fornal[a], K. H. Maier[a], B. Szpak[a], M. Alcorta[b], M. Bowry[c], R. Broda[a], M. Bunce[c], M. P. Carpenter[b], C. J. Chiara[b,d], A. Y. Deo[e], G. D. Dracoulis[f], W. Gelletly[c], C. R. Hoffman[b], R. V. F. Janssens[b], B. P. Kay[b,g], R. Kempley[c], F. G. Kondev[b], W. Królas[a], G. J. Lane[f], T. Lauritsen[b], C. J. Lister[b], E. A. McCutchan[b,h], T. Pawłat[a], Zs. Podolyák[c], M. Reed[c,f], P. H. Regan[c], C. Rodriguez-Triguero[h], A. M. Rogers[b], D. Seweryniak[b], N. Sharp[d], P. M. Walker[c], W. B. Walters[d], E. Wilson[c], J. Wrzesiński[a], and S. Zhu[b]

[a]*The Henryk Niewodniczański Institute of Nuclear Physics PAN, 31-342 Kraków, Poland*
[b]*Physics Division, Argonne National Laboratory, Argonne, IL 60439, USA*
[c]*Department of Physics, University of Surrey, Guilford, GU2 7XH, UK*
[d]*Department of Chemistry and Biochemistry, University of Maryland, College Park, MD 20742, USA*
[e]*Department of Physics, University of Massachusetts Lowell, Lowell, MA 01854, USA*
[f]*Department of Nuclear Physics, Australian National University, Canberra, ACT 0200, Australia*
[g]*Department of Physics, University of York, Heslington, YO10 5DD, UK*
[h]*National Nuclear Data Center, Brookhaven National Laboratory, Upton, NY 11973, USA*
[i]*School of Computing, Engineering and Mathematics, University of Brighton, BN2 4GL, Brighton, UK*

**Abstract.** High-spin yrast structures of $^{205,206,210}$Bi isotopes were investigated using γ-ray coincidence spectroscopy and deep-inelastic reactions technique with the $^{76}$Ge+$^{208}$Pb and $^{208}$Pb+$^{208}$Pb systems. Newly found states are well suited for testing shell-model realistic calculations. The use of radioactive beams provided by EURISOL will allow to extend this testing ground to heavier bismuth isotopes.

**Keywords:** nuclear structure $^{205,206,210}$Bi, isomers, conversion coefficients, angular distributions, shell-model calculations
**PACS:** 27.80.+w, 23.20.Lv, 23.20.En, 21.60.Cs

## INTRODUCTION

Nuclei around doubly closed shells play a crucial role in determining both the nucleonic single-particle energy levels and the two-body matrix elements of the effective nuclear interactions. Of particular importance is a comparison of experimental data with calculations which may deliver information on some basic aspects of the nucleon-nucleon interaction. The region around doubly magic $^{208}$Pb is particularly attractive in this respect as the $^{208}$Pb nucleus is considered one of the best doubly closed cores. The object of the presented work are Bi isotopes: $^{205,206,210}$Bi, which belong to this region. Investigated structures involve states arising from the valence particles/holes couplings as well as the states originating from core

excitations. Such high-spin yrast states often arise from the maximum spin couplings of the valence particles/holes and their wave functions involve usually one well-defined configuration. This makes them well suited for comparisons between experimental results and theory.

## EXPERIMENT

The experimental γ-ray data were collected in the two measurements performed at Argonne National Laboratory with the Gammasphere [1] detection system that consists of 101 Compton-suppressed Ge detectors. Two reactions with beams of $^{76}$Ge (450 MeV) and $^{208}$Pb (1446 MeV) on a thick $^{208}$Pb target have been investigated. Deep-inelastic processes occurring in those reactions allowed to reach high-spin yrast states in the products around $^{208}$Pb, including $^{205,206,210}$Bi. Conditions on time parameter were set to obtain various versions of prompt and delayed (emitted between beam bursts separated by ca. 412 ns) matrices and cubes. By gating on yrast transitions known in the investigated Bi isotopes from previous studies and by analyzing the γ-coincident spectra (which covered energy range up to 4 MeV), we significantly extended the level schemes of the $^{205,206,210}$Bi nuclei. Moreover, we noticed that the spin of deep-inelastic reaction products around $^{208}$Pb exhibits an appreciable alignment in the plane perpendicular to the beam direction. This is the same situation as in fusion-evaporation reactions and, in consequence, γ-ray angular distributions can be applied for the transition multipolarity analysis using the well known formalism. Indeed, to make spin-parity assignments to the newly identified states we used γ-ray angular distribution information as well as information on the decay pattern and the data on transitions conversion coefficients extracted from the transition intensity balances.

## RESULTS

In the $^{205}$Bi nucleus, which is one-proton, four-neutron holes system with respect to doubly magic $^{208}$Pb core, the yrast level scheme was known up to 6719 keV, while the highest spin $39/2^+$ was assigned to a state at 5931 keV [2]. Results from the deep-inelastic reaction experiments allowed us to extend the level scheme of $^{205}$Bi up to an isomeric level at 7974-keV. $T_{1/2}$ of this state has been estimated to be longer than 2 μs (the electronics setup allowed to construct the time spectrum only in the 400 ns range and lifetimes longer than 2 μs could not be measured). The newly identified isomer decays by two transitions: 385 keV to a 7589-keV level and an unobserved (most likely because of the strong internal conversion) 58 keV γ-ray populating the 7916-keV state. The conversion coefficient extracted from the intensity balance for the 385-keV line is $\alpha = 0.21(8)$, which suggests M1 multipolarity for this transition. In addition, 16 new levels have been located below the new isomer.

Shell-model calculations with effective interactions predict in the considered energy range states which arise from the excitations of valence proton particle and three neutron holes. The comparison between results of those calculations and

experiment may be used to tentatively assign spins and parities to the newly found states. Such analysis yields the spin-parity of $51/2^-$ for the 7974-keV isomer.

In $^{206}$Bi, new high-spin microsecond isomers have been identified as well. This includes the states with $J^\pi=(31^+)$ and $J^\pi=(28^-)$, at 10170 ($T_{1/2}>2$ μs) and 9233 keV ($T_{1/2}=155$ ns), respectively [3]. Yrast and near-yrast levels populated in the decay of these isomers have been located. The states identified at energies up to approximately 7 MeV can be described well in terms of one-proton particle, three-neutron-hole couplings, while the higher-spin structures should originate from core excitations. Spin-parity assignments were based on comparisons with the results of shell-model calculations and the decay pattern for the levels arising from the valence particle-holes excitations (up to $J^\pi=23^+$). For the states involving core excitations, the spin-parity assignments were based on γ-rays angular distributions and the transitions conversion coefficients extracted from the intensity balances.

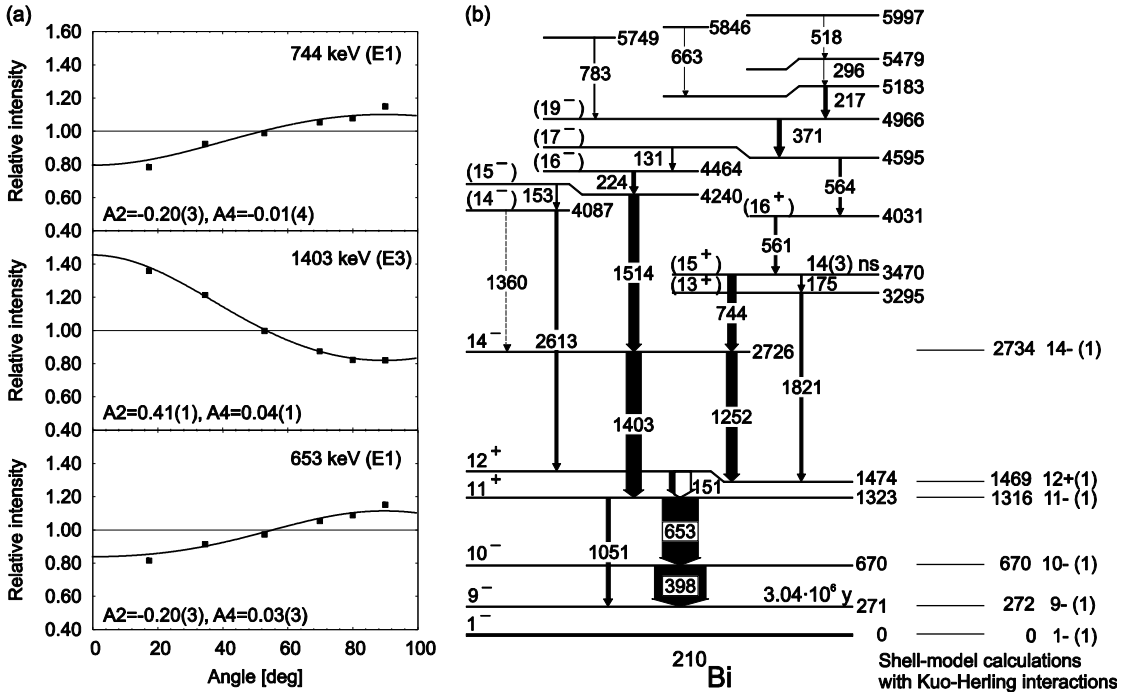


**FIGURE 1.** Level scheme for yrast states in $^{210}$Bi compared with the results of shell-model calculation (b). Widths of the arrows indicate observed intensity. Examples of angular distributions (measured points and fitted curves) obtained for the strong transitions (a).

The $^{210}$Bi nucleus (one-proton, one-neutron system) was another object of our study. In this case, the investigation fully confirmed known thus far level scheme [4] and resulted in adding new prompt lines: 371, 217, 296, 518, 783, and 663 keV, which could be used to locate levels at 4966, 5183, 5479, 5749, and 5997 keV. The ordering of these transitions was determined based on their intensities. Moreover, the existence of a 4087-keV state was confirmed by the parallel 1360-keV branch connecting it with the level at 2726-keV. A series of higher-lying γ-rays observed in the delayed spectra indicate the presence of an unknown isomeric state at some higher excitation energy, but the exact placement of this isomer could not be done.

For the states arising from valence particles couplings, the comparison of the experimental results with theoretical calculation using the modified Kuo-Herling interaction is presented in Fig. 1(b). To describe higher lying states, the calculations must involve excitations of proton or neutron across the energy gap. At present we can estimate spins and parities values for some of those levels by using angular distributions of γ-rays. According to the Yamazaki formalism [5], the angular distribution function is parametrized by the coefficients $A_2$ and $A_4$ of the Legendre polynomials $P_n(\cos\Theta)$, where Θ is an angle between the beam direction and direction of γ-ray emission. As these coefficients depend on the angular momentum alignment, the spins of the two levels involved in the γ decay, and multipolarity of the transition, we could confirm spins and parities for the previously known levels as well as make assignments for the new ones. This procedure will also allow to extract the mixing ratios. Additional source of information for low-energy lines are conversion coefficients, which also were obtained. The results of this analysis are showed in Fig. 1(b) together with the examples of angular distributions for the strong lines in $^{210}$Bi – Fig. 1(a). As the further steps, we are going to perform shell-model calculations with core excitations for which the newly identified states will serve as an excellent material for comparisons.

## CONCLUSION

The level schemes of $^{205,206,210}$Bi produced in deep-inelastic reactions have been significantly extended. They include states arising from couplings of valence particles/holes as well as core excitations, some of which are isomers. The experimental outcomes on new yrast structures in presented nuclei will be compared with the results of the shell model calculations based on the realistic shell-model interaction, named $V_{low\text{-}k}$, derived from the free nucleon-nucleon potential without adjustable parameters.

The use of radioactive ion beams of neutron-rich $^{212\text{-}214}$Bi isotopes from EURISOL, in combination with the technique employing discrete γ-ray spectroscopy of deep-inelastic reaction products, as presented here, will certainly allow the investigation of heavier Bi isotopes, e.g., $^{212,213}$Bi. With this, the testing ground for the realistic, effective shell-model interactions will be also extended.

## ACKNOWLEDGMENTS

This work is supported by the National Science Centre under Contract No. DEC-2011/01/N/ST2/04612.

## REFERENCES

1. I.-Y. Lee, *Nuclear Physics A* **520**, 641c (1990).
2. R. Brock et al., *Nuclear Physics A* **278**, 45 (1977).
3. N. Cieplicka et al., *Physical Review C* **86**, 054322 (2012).
4. B. Fornal, Habilitation thesis, Raport No. 1939/PL (2004).
5. T. Yamazaki, *Nuclear Data A* **3**, 1 (1967).

# Isomers in Heavy Neutron-Rich Nuclei

P.M. Walker

*Department of Physics, University of Surrey, Guildford GU2 7XH, UK*

**Abstract.** The long half-lives of isomers enable purification techniques to be applied, leading to enhanced sensitivity. This gives isomers an important experimental role in the study of exotic nuclei with ISOL and projectile-fragmentation techniques. Recent storage-ring isomer results for $^{184}$Hf, $^{192}$Re and $^{212}$Bi are compared with γ-ray and other measurements for the same nuclides.

**Keywords:** isomers, nuclear structure, exotic nuclei.
**PACS:** 21.10.-k, 27.70.+q, 27.80.+w, 29.20.Dh.

## INTRODUCTION

The nuclear structure motivation for the study of isomers in heavy, neutron-rich nuclei is at least two-fold. First there is the wish to determine the degree to which the strength of the N = 126 shell gap is maintained as protons are removed from the Z = 82 closed shell. When modelling *r*-process nucleosynthesis, a weakened shell closure could account better for the measured isotopic abundances in the A = 180 mass region [1], but the experimental situation is unknown.

Second, as the N = 126 shell closure is approached from the well deformed A = 170 region, by the addition of neutrons, there is predicted to be a prolate-to-oblate shape transition [2], with N = 116 being the critical neutron number. For N ≤ 116, angular momentum induces the same shape transition, due to rotation alignment in the oblate well [3,4]. While there is evidence for this effect in the well deformed, Z = 72 nuclide $^{180}$Hf [5], the clearest manifestation to date has been found in the γ-soft, Z = 76 nuclide $^{192}$Os [6]. Additional data are needed for well deformed cases, such as the neutron-rich hafnium isotopes.

For both these situations, N ≈ 126 and N ≈ 116, the observation of isomeric states is expected to provide key information. Isomerism is well known in closed-shell regions, such as N ≈ 126; and, at least for the neutron-rich hafnium isotopes, prolate high-K isomers are expected to co-exist with oblate rotational states for N ≈ 116 [4,7]. From an experimental perspective, therefore, the ability to physically separate isomers from the reaction region leads to the possibility of sensitive observations. This selectivity appears to be particularly important for the study of heavy, neutron-rich nuclides, since the production reactions (deep-inelastic and fragmentation) are themselves non-selective.

With the isotope separation on-line (ISOL) method, physical mass selection is achieved at low beam energy (about 50 keV) with a dipole magnet. In contrast, with the in-flight projectile-fragmentation method, the mass-to-charge ratio and atomic number can be determined electronically on an ion-by-ion basis using magnetic, energy-loss and time-of-flight analysis, with ion energies of several hundred MeV per nucleon. In the following, comparative examples of the application of these techniques at GSI are given, for the study of isomers in heavy, neutron-rich nuclides.

## ISOTOPE SEPARATION WITH GAMMA-RAY DETECTION

Using the GSI on-line isotope separator, with magnetic mass analysis of ionised reaction products, and detecting γ-rays, an isomer with a half-life of approximately one minute was discovered in $^{184}$Hf [8]. The γ-ray spectrum is shown in fig. 1. This is the most neutron-rich hafnium isotope for which excited-state structure has been reliably determined. The observed γ-ray transitions can be interpreted as cascading from a $K^{\pi} = 8^{-}$ isomer to the $K^{\pi} = 0^{+}$ ground state.

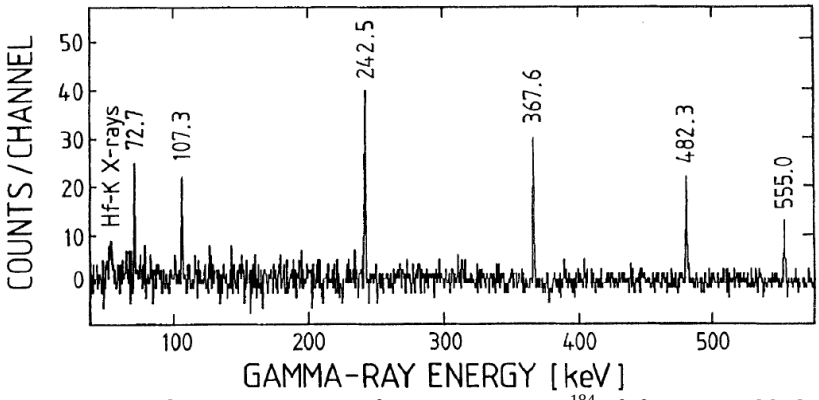


**FIGURE 1.** Spectrum showing transitions from an isomer in $^{184}$Hf, from Krumbholz et al. [8].

## FRAGMENTATION WITH GAMMA-RAY DETECTION

In conjunction with an array of γ-ray detectors, the FRagment Separator (FRS) at GSI has been widely used for isomer identifications in heavy, neutron-rich nuclei [9-11]. Due to the need to correlate ion and γ-ray events, the sensitivity for γ-ray detection is optimal for isomer half-lives in the range 100 ns to 100 μs. The lack of isomer discoveries in neutron-rich hafnium isotopes, by this method, probably arises from their long half-lives, such as the above case of $^{184}$Hf.

A positive example, in the same mass region, is the observation of a 160 keV γ-ray transition in $^{192}$Re (Z = 75) with a half-life of approximately 100 μs [9]. This will be discussed in the next section.

## FRAGMENTATION WITH STORED-ION DETECTION

A relatively new isomer-detection technique involves injecting highly charged ions from the FRS into the 108 m circumference Experimental Storage Ring (ESR) at GSI. Ions with different mass-to-charge ratios have different revolution frequencies, which can be used to distinguish between an isomer and its ground state, providing the half-life is greater than 1 s, and the isomer excitation energy is greater than 100 keV. Three different injections of A = 184 isobars with charge state q = 72+ are illustrated in fig. 2. A single ion of the ground state of $^{184}$Hf is seen in the second and third injections, while the m1 isomer is seen in the third injection, and a previously unknown m2 isomer is seen in the first and second injections.

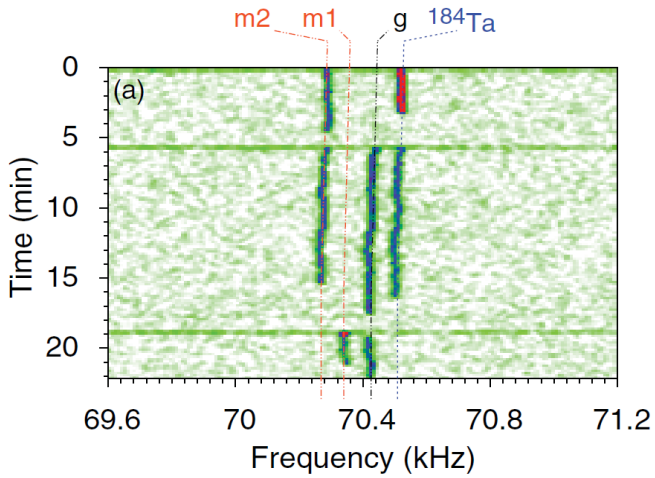


**FIGURE 2.** A = 184 isobars and isomers with q = 72+ observed in the ESR. The figure is from Reed et al. [12]. The labels g, m1 and m2 refer to $^{184}$Hf. The frequency scale has an offset.

It is notable that the excitation energy of the m1 isomer is 1272(1) keV from the γ-ray measurement [8] and 1264(10) keV from the ESR measurement [12]. The ESR confirmation has particular value because there was an ambiguity in the γ-ray data due to possible feeding from $^{184}$Lu β decay. In the ESR, the q = 72+ charge state rules out any $^{184}$Lu (Z = 71) contamination. The second $^{184}$Hf isomer, observed only in the ESR, is at 2477(10) keV and is interpreted as a $K^{\pi} = 15^{+}$ state [12].

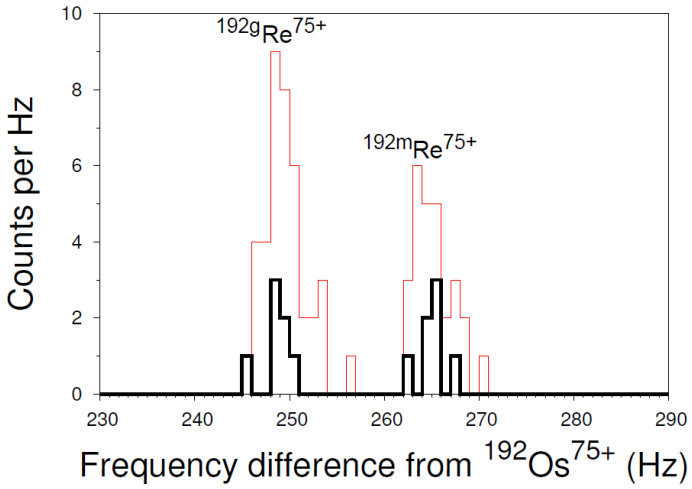


**FIGURE 3.** Ground-state and isomeric ions of $^{192}$Re. Each count represents a single ion with q = 75+. The subset shown by the bold trace (seven counts in total) is for ions that γ decayed during the observation time, so that their revolution frequency could be determined both before and after decay. The isomer excitation energy is 267(10) keV. The figure is from Reed et al. [13].

The $^{184}$Hf measurements give little idea of the sensitivity to low isomer excitation energies. In this respect, a clearer example is observed in $^{192}$Re, which is illustrated in fig. 3. The newly found isomer is at an excitation energy of 267(10) keV, with a half-life of 16(1) s [12,13]. This isomer is clearly different from the 100 μs state determined from the observation of 160 keV γ radiation [9] mentioned above. The γ-ray and ESR data complement one another.

A remarkable case, that brings together ESR data [14] and β-delayed α-decay data [15], is that of $^{212}$Bi. The new ESR results, shown in fig. 4, agree with earlier shell-model calculations of the m2 isomer excitation energy [16], which have been in long-standing conflict with the experimental interpretation. The ESR data now imply that strong (>75%) internal decay from the second isomer competes with β decay, but the internal decay remains to be observed. In this instance, it is clear that the ESR data add essential ingredients for understanding the nuclear structure.

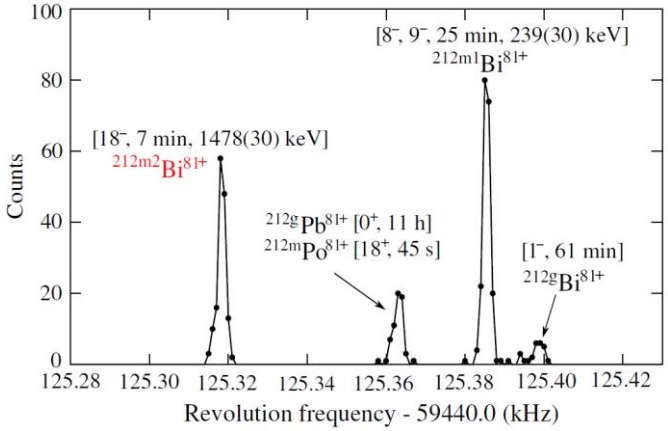


**FIGURE 4.** A = 212 isobars and isomers with q = 81+ observed in the ESR, from Chen et al. [14].

## DISCUSSION

It has been shown that storage-ring data complement decay-spectroscopy data. It needs to be carefully considered if EURISOL should be equipped with a storage ring. There is a choice of location for such a ring, with beams either at Coulomb-barrier energies, similar to the TSR being installed at HIE-ISOLDE [17], or at high energies to take advantage of secondary fragmentation.

## REFERENCES


1. K-L. Kratz et al., *Hyp. Int.* **129**, 185 (2000).
2. L.M. Robledo et al., *J. Phys. G: Nucl. Part. Phys.* **36**, 115104 (2009).
3. R.R Hilton and H.J. Mang, *Phys. Rev. Lett.* **43**, 1979 (1979).
4. F.R. Xu, P.M. Walker and R. Wyss, *Phys. Rev.* **C62**, 014301 (2000).
5. U.S. Tandel et al., *Phys. Rev. Lett.* **101**, 182503 (2008).
6. G.D. Dracoulis et al., *Phys. Lett.* **B720**, 330 (2013).
7. H.L. Liu et al., *Phys. Rev.* **C83**, 067303 (2011).
8. K. Krumbholz et al., *Z. Phys.* **A351**, 11 (1995).
9. M. Caamano et al., *Eur. Phys. J.* **A23**, 201 (2005).
10. S.J. Steer et al., *Phys. Rev.* **C84**, 044313 (2011).
11. A. Gottardo et al., *Phys. Rev. Lett.* **109**, 162502 (2012).
12. M.W. Reed et al., *Phys. Rev.* **C86**, 054321 (2012).
13. M.W. Reed et al., *J. Phys. Conf. Series* **381**, 012058 (2012).
14. L. Chen et al., *Phys. Rev. Lett.* **110**, 122502 (2013).
15. P.A. Baisden et al.,, *Phys. Rev. Lett.* **41**, 738 (1978); K. Eskola et al., *Phys. Rev.* **C29**, 2160 (1984).
16. E.K. Warburton, *Phys. Rev.* **C44**, 261 (1991).
17. M. Grieser et al., *Eur. Phys. J. Special Topics* **207**, 1 (2012).

# Nuclear Moments With Neutron-Rich Radioactive Beams.

Georgi Georgiev[a]

[a]*CSNSM, CNRS/IN2P3; Université Paris-Sud, UMR8609, F-91405 ORSAY-Campus, France.*

**Abstract.** Nuclear moments are among the experimental observables that provide very high sensitivity both towards single-particle and collective properties of the nuclei. They can serve as stringent tests to the nuclear models especially in regions far from stability where the appearance of new shell closures or built-up of collectivity are being discussed. The nuclear moment studies with radioactive beams require some substantial developments of the applied techniques. Few examples of ongoing, and plans for future investigations of techniques, to be applied with EURISOL beams, will be discussed.

**Keywords:** Nuclear **s**tructure, Electromagnetic moments, Radioactive beams.
PACS: **21.10.-k; 21.10.Ky; 29.27.Hj; 29.38.-c.**

Nuclear moment investigation methods are strongly dependent on the lifetime of the state of interest. For example isomeric ($t_{1/2}$ > few ns) and longer-lived states would require stopping of the nuclei in a perturbation-free environment, e.g. cubic crystal. This might appear in contradiction with the use of radioactive beams, especially for "in-beams" techniques, in which the stopping of the beam in the center of the detection setup would build up huge background activity. Therefore, for the nuclear moment studies of longer-lived states, the beam, stopped at the implantation point, needs to contain at least few percents of the state of interest, as e.g. in projectile-fragmentation reactions. In the first section an example of nuclear moment measurement of an isomeric state in two-step projectile fragmentation will be given.

The nuclear moment studies of very short-lived states (~ ps) are usually performed using hyperfine fields, produced in-matter or by free ions. The interaction times, comparable to the nuclear lifetimes, are of the same order as the times for the passage of the ions through the target materials. Therefore there is no requirement that the nuclei are stopped. This allows for the use of techniques as e.g. Recoil In Vacuum. An example of the development of the Time Dependent Recoil In Vacuum (TDRIV) technique, providing high-accuracy, model independent results for picosecond states, will be given in the second section.

The interaction between polarized atomic states and nuclear spins in tilted-foil geometry (Tilted Foils technique) could be used in order to provide nuclear spin-polarized ensembles. Some recent results from the application of this technique at ISOLDE, using low-energy post-accelerated beams, will be mentioned in the third section.

# NUCLEAR MOMENTS OF ISOMERIC STATES IN PROJECTILE-FRAGMENTATION REACTIONS

Nuclear spin alignment in projectile fragmentation reactions has been investigated for many years [1, 2, 3]. It provides a unique opportunity to study microsecond isomeric states in neutron-rich nuclei, inaccessible by other means. Significant amount of spin orientation is observed for species few nucleons away from the projectile, although some alignment could still be observed for fragments removed further away from the primary beam [4]. The nuclei of interest need to be transported through the fragment separator in a fully-stripped charge state in order to preserve the spin-orientation.

As one of the extreme examples in which the nuclear moment studies in projectile-fragmentation were applied could be mentioned the investigation of the $I^{\pi} = 12^{+}$ isomeric state in $^{192}$Pb [4]. The spin-aligned isomeric states were produced starting from $^{238}$U at 1 GeV/u (46 nucleons away from the isotope of interest) and were implanted at the final focal point with a remaining energy of ~290 MeV/u that was sufficient to get 90 % of the secondary beam fully stripped.

A further development of the method has been performed in a recent study by Ichikawa *et al.* [5] using a two-step projectile fragmentation in combination with a dispersion-matching technique. The isomeric state of interest, $^{32m}$Al, has been populated through the fragmentation of 345 MeV/u $^{48}$Ca beam. The level of spin alignment, observed when using a single-step reaction, was determined as < 0.8%. In a second approach a beam of radioactive $^{33}$Al has been selected and further fragmented at 200 MeV/u in order to populate the same isomeric state in $^{32}$Al. The two-step fragmentation, producing nucleus just one nucleon away from the secondary projectile, yielded much higher level of spin orientation, 8(1) %, at a production rate suitable for nuclear moment measurement. The overall figure-of-merit from the application of the two-step fragmentation reaction, combined with the dispersion-matching technique, was estimated to be higher than 50. This approach should further open the possibility of nuclear moment studies further away from stability using projectile-fragmentation reactions.

At EURISOL it is foreseen that radioactive beams could be accelerated up to 150 MeV/u, which should allow performing projectile-fragmentation studies up to Z~50 and obtaining the fragments in fully-stripped charge state. Taking into account that the radioactive beams would have intensities lower than the presently available stable beams a projectile as close as possible to the nuclei of interest would be looked for in most of the cases. However, considering that the ISOL beam intensities are strongly chemically dependent, there could be cases in which choosing a projectile further away from the nucleus of interest might appear more advantageous. For similar cases it might be necessary to consider whether the presently foreseen 150 MeV/u are sufficient or higher beam energies might be required. The higher beam energies would be advantageous not only for applying the above presented approach of two-step fragmentation in combination with the dispersion matching technique for nuclear moment measurements, but as well for the production of more exotic species. For example the higher beam energies would allow for higher effective target thicknesses and provide more important forward focusing of the reaction products.

# NUCLEAR MOMENTS OF SHORT-LIVED STATES THROUGH TDRIV MEASUREMENTS

One of the main challenges in the nuclear moment measurements of very short-lived (picosecond) states is to obtain a sufficiently strong magnetic field that would allow for a measurable rotation of the nuclear spin ensemble within the nuclear lifetime. Although the Transient Field technique has advanced considerably in the last years [6] it still relies on calibration measurements on known cases since the obtained fields could not be determined from first principles. This shortcoming could be overcome by applying the Time Dependent Recoil In Vacuum (TDRIV) method using H-like charge states [7]. The magnetic field, produced by a hydrogen-like ion at the nuclear site, can be calculated by first principles and the use of a time-dependent method could provide a high-accuracy results.

When applying the TDRIV method with radioactive beams the ions would not be stopped in a thick perturbation-free host as is the case for stable beams [7]. Letting the excited states decay in vacuum would cause a reduction of the amplitude of the observed oscillation pattern. A new method, using a thin electron reset foil, has been proposed by Stuchbery *et al.* [8]. This would preserve some significant amplitude of the oscillations (see FIG. 1) even though the two components (decay-after-target and decay-after-reset-foil) are not resolved.

An experiment, applying the technique proposed in REF. [8] has been performed at ALTO, Orsay, France. The ORGAM Ge γ-ray array has been used for detecting the γ-rays of interest. It was combined with an annular segmented particle, used for the detection of the recoiling beam particles. The angular distribution of the γ-ray of the $2^+ \rightarrow 0^+$ transition of $^{24}$Mg, obtained using $^{93}$Nb target and $^{197}$Au reset foil, is presented in FIG. 1.

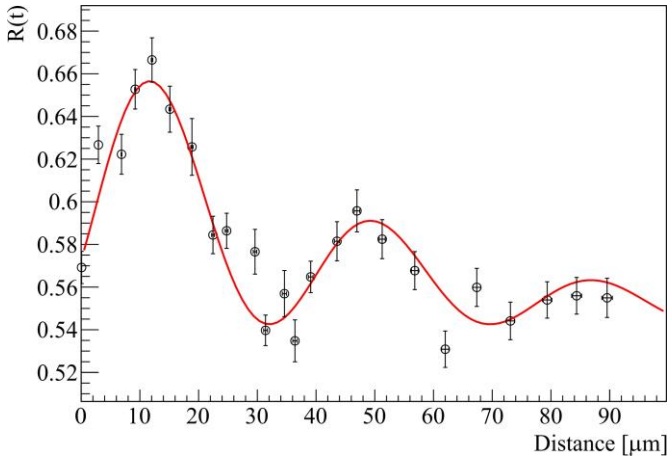


**FIGURE 1.** Time-dependent angular correlations (as a function of distance) for H-like $^{24}$Mg ions as obtained in radioactive beam geometry.

The preliminary results confirm the applicability of the approach and open the possibility for high-precision g factor measurements of light radioactive nuclei. A point that still needs further investigation is *what is the highest-Z value for which the TDRIV method on H-like could be applied*. The use of heavier alkali-like charge states might be envisaged as well.

# SPIN POLARIZATION OF RADIOACTIVE NUCLEI USING THE TILTED FOILS TECHNIQUE

Nuclear spin-polarized ensemble is a requirement for nuclear moment investigations but it can represent some important advantages as well for studies in solid state physics, biophysics, chemistry etc. Therefore reliable and widely applicable methods for nuclear polarization are needed. One such method that requires a relatively simple experimental setup, and does not show a dependence of the obtained polarization on the chemical properties of the polarized elements, is the Tilted Foils (TF) technique, see e.g. [9]. It is based on the passage of ions through a stack of very thin foils, positioned at oblique angle with respect to the beam direction. Some sizeable atomic polarization (up to 50% for specific configurations) is produced at the exit of each of the foils. It is subsequently transferred to the atomic spin ensemble through the hyperfine interaction. A strong dependence of the amount of polarization as a function of the beam energy has been figured out, with a maximum presently observed around few tens of keV/u.

Radioactive beams at similar energies were no available until few years ago, which hampered considerably the application of the TF technique. Some recent studies at TRIAC, Japan [10], using post-accelerated $^{8}$Li beam, have allowed for a more detailed investigation of the TF polarization as a function of beam energy and charge state. However, the TRIAC facility has recently been closed for radioactive ion beams.

A β-NMR+TF setup was installed at REX-ISOLDE. Its test in 2012, using conditions very similar to the TRIAC's study, has shown an excellent reproducibility, providing 3.6 (3) % polarization for $^{8}$Li beam. This opens the possibilities for further studies using polarized beams at ISOLDE for nuclear-, solid-state- and bio-physics.

A further step, to be considered at HIE-ISOLDE in near future and further on at EURISOL, is the post-acceleration of polarized beams to few MeV/u or higher. A similar approach, presently under consideration at ISOLDE, could provide an access to nuclear reaction studies with polarized beams.

## ACKNOWLEDGMENTS

Partial support from ENSAR FP7 framework under contract no. 262010 is acknowledged.

## REFERENCES

1. W.-D. Schmidt-Ott *et al., Z. Phys.* **A 350**, 215 (1994).
2. G. Georgiev *et al., J. Phys.* **G 28**, 2993 (2002).
3. I. Matea *et al., Phys. Rev. Lett.* **93**, 142503 (2004).
4. M. Kmiecik *et al., Eur. Phys. Journ.* **A 45**, 153 (2010).
5. Yu. Ichikawa *et al., Nature Physics* **8**, 918 (2012).
6. N. Benczer-Koller and G.J. Kumbartzki, *Jour. Phys.* **G34**, 321 (2007).
7. R.E. Horstman *et al., Nucl. Phys.* **A248**, 291 (1975).
8. A.E. Stuchbery *et al., Phys. Rev.* C71, 047302 (2005).
9. M. Hass *et al., Nucl. Phys.* **A414**, 316 (1984).
10. Y. Hirayama *et al., Eur. Phys. Journ.* **A48**, 54 (2012).

# Beta decay and isomer spectroscopy in the $^{132}$Sn region: Present status and future perspectives

A. Jungclaus[*], G.S. Simpson[†], G. Gey[†,‡], J. Taprogge[*,‡], S. Nishimura[‡], P. Doornenbal[‡], G. Lorusso[‡], P.-A. Söderström[‡], T. Sumikama[¶], Z. Xu[‖], H. Baba[‡], F. Browne[††,‡], N. Fukuda[‡], N. Inabe[‡], T. Isobe[‡], H.S. Jung[‡‡], D. Kameda[‡], G.D. Kim[§§], Y.-K. Kim[§§,¶¶], I. Kojouharov[***], T. Kubo[‡], N. Kurz[***], Y.K. Kwon[§§], Z. Li[†††], H. Sakurai[‡,‖], H. Schaffner[***], H. Suzuki[‡], H. Takeda[‡], Z. Vajta[‡‡‡,‡], H. Watanabe[‡], J. Wu[†††,‡], A. Yagi[§§§], K. Yoshinaga[¶¶¶], S. Bönig, J.-M. Daugas, F. Drouet[†], R. Gernhäuser, S. Ilieva, T. Kröll, A. Montaner-Pizá, K. Moschner, D. Mücher, H. Nishibata[§§§], R. Orlandi, K. Steiger and A. Wendt

[*]*Instituto de Estructura de la Materia, CSIC, E-28006 Madrid, Spain*
[†]*LPSC, Université Joseph Fourier Grenoble 1, CNRS/IN2P3, Institut National Polytechnique de Grenoble, F-38026 Grenoble Cedex, France*
[**]*Institut Laue-Langevin, B.P. 156, F-38042 Grenoble Cedex 9, France*
[‡]*RIKEN Nishina Center, RIKEN, 2-1 Hirosawa, Wako-shi, Saitama 351-0198, Japan*
[§]*Departamento de Física Teórica, Universidad Autónoma de Madrid, E-28049 Madrid, Spain*
[¶]*Department of Physics, Tohoku University, Aoba, Sendai, Miyagi 980-8578, Japan*
[‖]*Department of Physics, University of Tokyo, Hongo 7-3-1, Bunkyo-ku, 113-0033 Tokyo, Japan*
[††]*School of Computing, Engineering and Mathematics, University of Brighton, Brighton BN2 4JG, United Kingdom*
[‡‡]*Department of Physics, Chung-Ang University, Seoul 156-756, Republic of Korea*
[§§]*Rare Isotope Science Project, Institute for Basic Science, Daejeon 305-811, Republic of Korea*
[¶¶]*Department of Nuclear Engineering, Hanyang University, Seoul 133-791, Republic of Korea*
[***]*GSI Helmholtzzentrum für Schwerionenforschung GmbH, 64291 Darmstadt, Germany*
[†††]*School of Physics and State key Laboratory of Nuclear Physics and Technology, Peking University, Beijing 100871, China*
[‡‡‡]*Institute of Nuclear Reserach of the Hungarian Academy of Sciences (ATOMKI), Debrecen, H-4011 Hungary*
[§§§]*Department of Physics, Osaka University, Machikaneyama-machi 1-1, Osaka 560-0043 Toyonaka, Japan*
[¶¶¶]*Department of Physics, Faculty of Science and Technology, Tokyo University of Science, 2641 Yamazaki, Noda, Chiba, Japan*
*Institut für Kernphysik, Technische Universität Darmstadt, D-64289 Darmstadt, Germany*
*CEA, DAM, DIF, 91297 Arpajon cedex, France*
*Physik Department E12, Technische Universität München, D-85748 Garching, Germany*
*Instituto de FŠsica Corpuscular, CSIC-Univ. of Valencia, E-46980 Paterna, Spain*
*IKP, University of Cologne, D-50937 Cologne, Germany*
*Instituut voor Kern- en StralingsFysica, K.U. Leuven, B-3001 Heverlee, Belgium*

**Abstract.** The first EURICA campaign with high intensity Uranium beams took place at RIKEN in November/December 2012. Within this campaign experiment NP1112-RIBF85 was performed dedicated to the study of the isomeric and beta decays of neutron-rich Cd, In, Sn and Sb isotopes towards and beyond the N=82 neutron shell closure. In this contribution we present a first status report of the analysis of the extensive data set obtained in this experiment.

# INTRODUCTION

The region around doubly-magic $^{132}$Sn is of great importance for nuclear structure physics because it is the only region around a heavy doubly-closed shell nucleus far-off stability (8 neutrons relative to the last stable isotope $^{124}$Sn) for which detailed spectroscopic information can be obtained using modern state-of-the-art techniques. It therefore plays an essential role in testing the shell model and serves as input for any reliable future microscopic nuclear structure calculations towards the neutron drip line. In addition, this region is also relevant for nuclear astrophysics, in particular nucleosynthesis calculations, due to the close connection between the N=82 shell closure and the A$\approx$130 peak of the solar r-process abundance distribution.

The main goal of experiment NP1112-RIBF85 has been to extend the current knowledge on excited states in very neutron-rich Cd, In, Sn and Sb isotopes. In particular we were aiming i) for first experimental information on excited states in $^{136,138}$Sn via the search for $6^+$ seniority isomers in these isotopes in anology to the one known in $^{134}$Sn [1], ii) for the first observation of transitions within the $\pi g_{9/2}^{-1} \otimes \nu f_{7/2}$ multiplet in $^{132}$In populated in the $\beta$-decay of $^{132}$Cd and iii) to follow the evolution of the $\pi g_{7/2} \otimes \nu f_{7/2}$ multiplet in $^{136,138}$Sb.

The results of this experiment should serve to test the predictions of shell-model calculations in a very neutron-rich, medium-heavy region. Indeed, these nuclei, with just a few neutrons beyond $^{132}$Sn are very sensitive tests of these calculations and allow us to search for possible new physics or deficiencies in current state-of-the-art shell-model interactions. Only two regions are currently available for such studies, the one of the present experiment and the one around $^{78}$Ni.

# EXPERIMENTAL SETUP

The exotic nuclei of interest were produced by the in-flight fission of a 345 MeV/nucleon $^{238}$U beam from the RIBF facility, impinging on a 3-mm thick Be target. The ions of interest were separated from other reaction products and identified on an ion-by-ion basis by the BigRIPS in-flight separator [2]. The particle identification was performed using the $\Delta E$-TOF-$B\rho$ method in which the energy loss, ($\Delta E$), time of flight (TOF) and magnetic rigidity ($B\rho$) are measured and used to determine the atomic number, $Z$, and the mass-to-charge ratio ($A/q$) of the fragments. Details about the identification procedure can be found in Ref. [3]. The identified ions are transported through the ZeroDegree spectrometer (ZDS) and finally implanted into the WAS3ABI (Wide-range Active Silicon Strip Stopper Array for $\beta$ and Ion detection) Si array positioned at the focal plane of the ZDS (F11). The WAS3ABi detector [4] consists of eight DSSSD with an area of $60\times40$ mm$^2$, a thickness of 1 mm and a segmentation of 40 horizontal and 60 vertical strips each. A sketch of the experimental facility together with a identification plot of the isotopes implanted into WAS3ABI during experiment NP1112-RIBF85 is shown in Fig. 1. To detect $\gamma$ radiation emitted in the decay of the implanted radioactive nuclei 12 large-volume Ge Cluster detectors [6] from the former EUROBALL spectrometer [7] were arranged in a close geometry around the WAS3ABI detector.

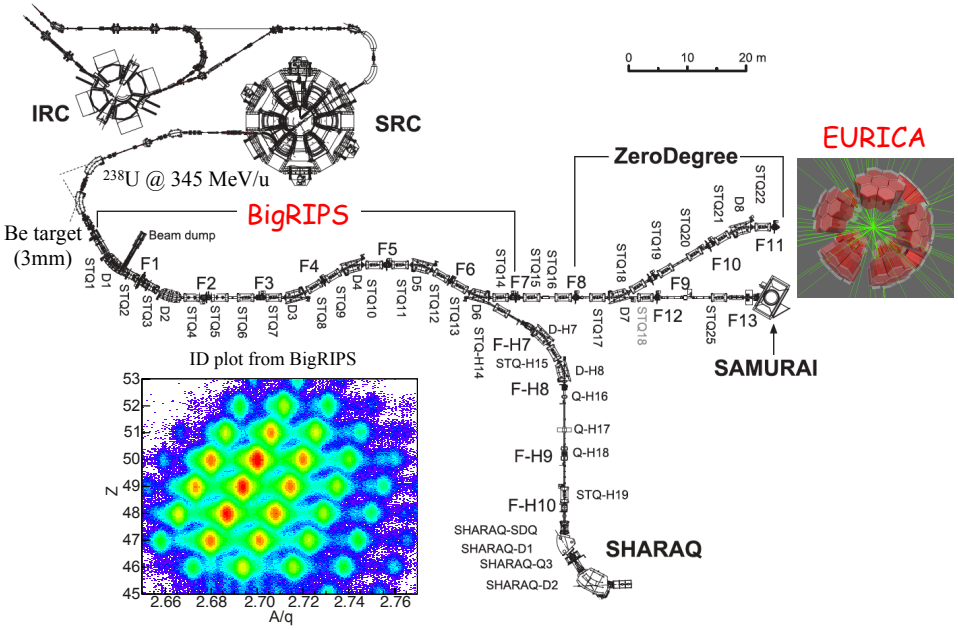


**FIGURE 1.** Sketch of the experimental facility (adopted from Ref. [5]) including the identification plot of the isotopes implanted into WAS3ABI during experiment NP1112-RIBF85.

The combination of the unprecedented high intensity of the primary U beam (on average 8-10 pnA) and the high efficiency of the setup for both the detection of $\gamma$ rays (8% at 1 MeV) and particles allowed to perform detailed decay spectroscopy in a region of the chart of nuclides which has not been accessible for this type of studies before.

## FIRST RESULTS

Delayed $\gamma$ rays were observed in coincidence with $^{136,138}$Sn and these constitute the first observation of the decay of excited states in these very neutron-rich, semi-magic nuclei. Indeed they are the nuclei with the highest N/Z ratio in this region for which excited states are known and their semi-magic nature allows just the neutron-neutron part of the shell- model interactions to be probed. Three delayed transitions have been observed for each nucleus and these have been assigned as E2 transitions from the $6^+$, $4^+$ and $2^+$ states, by analogy with $\gamma$ rays of similar energies observed from the decay of a $6^+$ isomer in $^{134}$Sn [1]. The small spacing between the $6^+$ and $4^+$ states, and their relatively pure $\nu(f_{7/2})^2$ configuration, are responsible for the isomerism.

We found that the energies of the $2^+$, $4^+$ and $6^+$ levels remain fairly constant as the number of neutrons increases from N=84 to N=88. This agrees with the predictions

of shell-model calculations performed using state-of-the-art interactions, e.g. the CD-Bonn bare nucleon-nucleon potential, renormalized using G-matrix [8] and $V_{low-k}$ [9] prescriptions. In contrast calculations performed using empirical interactions (SMPN) deviate from the experimental data [10], despite the simple nature of these nuclei. These data serve as useful input in to astrophysical r-process calculations as the path of this reaction includes these nuclei. A low excitation energy of the $2_1^+$ state can change the effective half-lives of nuclei participating in this reaction at high temperatures.

## OUTLOOK

In addition to the delayed transitions emitted from $^{136,138}$Sn, several other new isomeric decays have also be observed in this experiment, for example in $^{129}$Cd. Similarly, $\beta$-decay data on the nuclei shown in Fig. 1 are currently being analyzed and will give first half-lives and identification of excited states in many very neutron-rich nuclei. The data on the Sb and In nuclei will allow very sensitive tests of the shell-model predictions to be performed. Information on the excited states of these simple odd-Z nuclei is particularly important as the neutron-proton part of shell-model interactions is the most difficult part to reproduce. The experimentally extracted $\beta$-decay half-lives will be important ingredients for r-process calculations. To conclude, a very rich data set has been obtained from experiment NP1112-RIBF85 which took place in December 2012 during the first EURICA campaign with high intensity Uranium beams at RIKEN. Exciting results with respect to the structure of neutron-rich Cd, In, Sn and Sb isotopes will be presented in the near future.

## ACKNOWLEDGMENTS

This work has been supported by the Spanish Ministerio de Ciencia e Innovación under contracts FPA2009-13377-C02 and FPA2011-29854-C04. This work was carried out at the RIBF operated by RIKEN Nishina Center, RIKEN and CNS, University of Tokyo. We acknowledge the EUROBALL Owners Committee for the loan of germanium detectors and the PreSpec Collaboration for the readout electronics of the cluster detectors.

## REFERENCES

1. A. Korgul et al., Eur. Phys. J. A **7**, 167 (2000).
2. T. Kubo, Nucl. Instr. Meth. B204 (2003) 97.
3. T. Ohnishi et al., J. Phys. Soc. Jpn. **79**, 073201 (2010).
4. P.-A. Söderström et al., Nucl. Instr. Meth. B, in press
5. T. Kubo et al., Prog. Theor. Exp. Phys. 2012, 03C003.
6. J. Eberth et al., Nucl. Instrum. Methods Phys. Res., Sect. A **369**, 135 (1996).
7. J. Simpson, Z. Phys. A **358**, 139 (1997).
8. M. P. Kartamyshev, T. Engeland, M. Hjorth-Jensen, and E. Osnes, Phys. Rev. C 76, 024313 (2007).
9. A. Covello, L. Coraggio, A. Gargano, and N. Itaco, J. Phys.: Conf. Ser. 267, 012019 (2011).
10. S. Sarkar and M. Saha Sarkar, Eur. Phys. J. A 21, 61 (2004); Phys. Rev. C 78, 024308 (2008); Phys. Rev. C 81, 064328 (2010).

# Shapes And Collectivity In Heavy Nuclei Probed With Radioactive Beams At REX-ISOLDE

Janne Pakarinen[a] on behalf of the MINIBALL collaboration

[a]*Department of Physics, University of Jyväskylä, P.O.Box 35, FI-40014 University of Jyväskylä, Finland.*

**Abstract.** The MINIBALL Ge-detector array at the REX-ISOLDE post-accelerator has been a workhorse in diverse nuclear structure studies over the past decade. In conjunction with particle detector arrays it has provided excellent in-beam gamma-ray data. Especially, the REX-ISOLDE accelerator is unique when it comes to intense radioactive heavy-ion beams. This has been recently exploited in studies of shape coexistence and collectivity in nuclei ranging from Hg-182 to Ra-224 in Coulomb excitation experiments. The talk will focus on Coulomb excitation of Pb isotopes and how our physics program can be extended in the next generation ISOL facility such as EURISOL.

Keywords: **Nuclear structure, gamma-ray spectroscopy, Coulomb excitation, radioactive ion beams.**
**PACS: 29.30.Kv, 25.70.De, 29.38.-c**

## SHAPE COEXISTENCE IN LEAD ISOTOPES

The interplay between single-particle motion, collectivity, and pairing in light Pb nuclei is manifested as a rich gamut of coexisting nuclear shapes and exotic excitations [1-2]. One of the goals of modern nuclear physics research is to understand the origin of these structures and their relation to the fundamental interactions between the nuclear constituents. These subjects can be investigated particularly well in the Pb isotopes close to neutron mid-shell, where a relatively small proton shell gap, together with a large valence neutron space, provides fertile ground for studies of shape transitions within a small energy range. In α-decay studies, the first two excited states of the mid-shell nucleus $^{186}$Pb were observed to be $0^+$ states [3]. On the basis of α-decay hindrance factors, the $0^+_2$ state was associated with mainly π(2p−2h) configuration, whereas the $0^+_3$ state was associated with a π(4p−4h) configuration. Consequently, together with the spherical ground state [4], the three $0^+$ states with largely different structures establish a unique shape-triplet in $^{186}$Pb.

## EXPERIMENTAL DETAILS

The experiment was carried out employing the MINIBALL spectrometer [5] at the REX-ISOLDE facility, CERN [6]. The radioactive beam of neutron deficient even-mass $^{188\text{-}198}$Pb isotopes was post-accelerated up to 2.83MeV/u and was impinging on a

2mg/cm$^2$ thick $^{112}$Cd target. The beam intensity on MINIBALL target varied between $2\times10^5$-$1.4\times10^6$ Hz. The scattered particles were measured using the annular CD detector at 30mm distance downstream from the target. In figure 1, the energy of scattered particles as a function of strip number (angle) is shown. Two different kinematic branches, corresponding to the scattered target-like and projectile-like particles, labeled in white and black, respectively, can be distinguished.

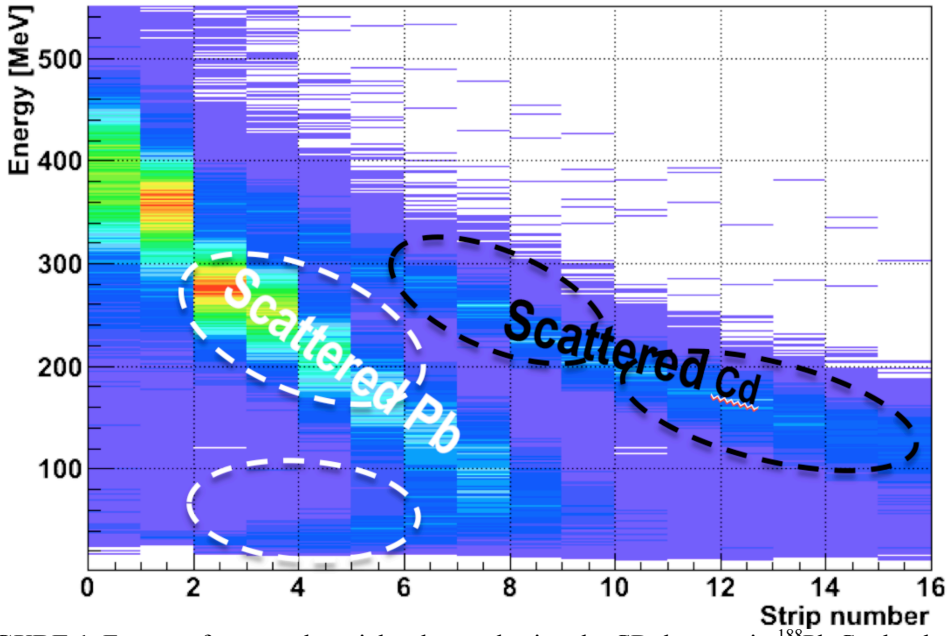


**FIGURE 1.** Energy of scattered particles detected using the CD detector in $^{188}$Pb Coulomb excitation experiment. Kinematic branch for scattered target-like (projectile-like) particles is shown in black (white). Four different angular ranges used in analysis haven been illustrated with dashed lines.

As an example, a gamma-ray energy spectrum measured in low centre-of-mass angles, Doppler corrected for projectile-like particles, is shown in figure 2. Two gamma-ray lines can be associated with $^{188}$Pb, whereas other gamma-ray lines originate from the excitation of $^{188}$Tl impurities in-beam. In this case, the purity of beam was about 50%. By using the laser on/off technique, one can extract the amount of target excitations arising from reactions with $^{188}$Tl. Similar data have been obtained for $^{190}$Pb and $^{192}$Pb, with beam contamination levels below 10%. Preliminary analysis suggests that the spectroscopic quadrupole moments and transition strengths for the first $2^+$ states in corresponding Pb isotopes can be extracted from these data. For the even-mass $^{194\text{-}198}$Pb isotopes the statistics is sufficient to obtain transitions strengths. The analysis is still in progress and final results will be published later.

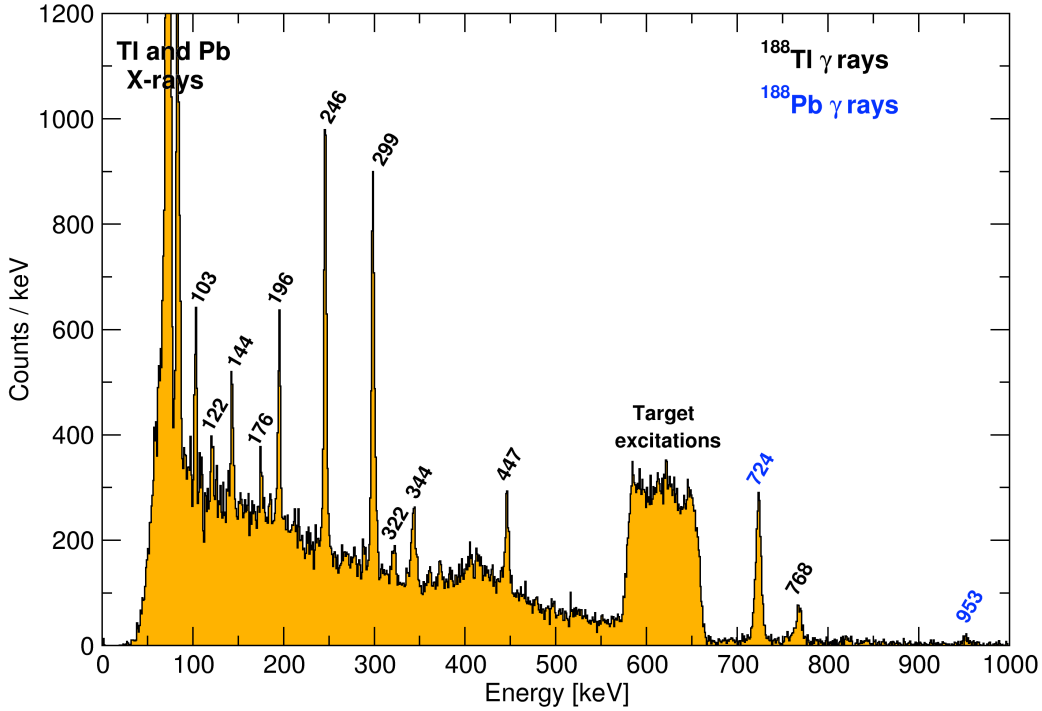


**FIGURE 2.** Gamma-rays in coincidence with scattered projectile-like particles observed in low centre-of-mass angles (Doppler corrected for projectile-like particles). Gamma-rays associated with $^{188}$Pb nuclei are labeled in blue, whereas gamma-rays from $^{188}$Tl are labeled in black.

## VIEW ON POSSIBILITIES WITH THE EURISOL FACILITY

Our experimental program continues at HIE-ISOLDE. The HIE-ISOLDE will provide improved beam intensity together with beam energies at first up to 5.5MeV/u and finally up to 10MeV/u. This will allow us to conduct multistep Coulomb excitation experiments of heavy nuclei. Multistep Coulomb excitation is essential especially when probing the shapes and collectivity of the non-yrast bands in this region. Another important step in understanding the competing structures in these nuclei will be taken when the MINIBALL array is combined with the SPEDE electron spectrometer [7]. SPEDE in conjunction with MINIBALL will allow a direct measurement of the conversion electron strengths in nuclei of interest.

The amount of effort to understand the shape evolution in neutron-deficient Pb nuclei, and very heavy nuclei in general, has been substantial. However, there are still many open questions such as:

- Confirmation of three different shapes in one nucleus
- What is the intrinsic configuration of the intruding structures
- Systematic behaviour of mixing between different shape coexisting structures
- Why is the collectivity of prolate yrast bands in Pb higher than that of the identical bands in Hg and Pt isotopes

In order to address these questions, more experimental and theoretical work is required. For example, the multiparticle-multihole structures could be directly probed via multinucleon transfer reactions, currently not feasible with existing facilities. In order to investigate the odd-mass heavy nuclei in Coulomb excitation experiments,

higher particle fluxes are needed to obtain sufficient statistics since the level density at the Fermi surface is higher. The EURISOL facility with further improved beam intensity, energy and purity will provide better opportunity to conduct these experiments.

## ACKNOWLEDGMENTS

The staff members of the REX-ISOLDE facility are gratefully acknowledged for providing smooth running conditions. This research project has been supported by a Marie Curie Intra-European Fellowship of the European Community's 7th Framework Programme under contract number (PIEF-GA-2008-219175).

## REFERENCES

1. K. Heyde and J. L. Wood, *Rev. Mod. Phys.* **83,** 1467-1521 (2011).
2. R. Julin *et al., J. Phys. G* **27**, R109 (2001).
3. A.N. Andreyev *et al.*, *Nature (London)* **405**, 430 (2000).
4. H. De Witte *et al.*, *Phys. Rev. Lett.* **98**, 112502 (2007).
5. N. Warr *et al.*, *Eur. Phys. J.* A **49**, 40 (2013).
6. O. Kester *et al., Nucl. Instrum. Methods Phys. Res. B* **204**, 20 (2003).
7. J. Pakarinen *et al., HIE-ISOLDE Letter of Intent I-107: In-beam electron spectroscopy at HIE-ISOLDE* (2010).

# Isospin mixing within the multi-reference nuclear density functional theory and beyond - selected aspects *

W. Satuła[1], J. Dobaczewski[1,2], M. Konieczka[1], and W. Nazarewicz[1,3,4]
[1] *Faculty of Physics, University of Warsaw, PL-00-681 Warsaw, Poland*
[2] *Department of Physics, University of Jyväskylä, FI-40014 Jyväskylä, Finland*
[3] *Department of Physics and Astronomy, University of Tennessee, Knoxville, Tennessee 37996, USA and*
[4] *Physics Division, Oak Ridge National Laboratory, Oak Ridge, Tennessee 37831, USA*

The results of systematic calculations of isospin-symmetry-breaking corrections to superallowed $\beta$-decays based on the self-consistent isospin- and angular-momentum-projected nuclear density functional theory (DFT) are reviewed with an emphasis on theoretical uncertainties of the model. Extensions of the formalism towards *no core* shell model approach with basis cutoff scheme dictated by the self-consistent particle-hole DFT solutions will be also discussed.

## I. INTRODUCTION

Isospin symmetry in atomic nuclei is weakly broken mostly by the Coulomb interaction that exerts a long-range polarization effect. Capturing an equilibrium between long and short range effects is a challenging task possible only within *no core* approaches, which, in heavier nuclei, reduces possible choices to formalisms rooted in the density functional theory (DFT). However, as it was recognized already in the 70's [1], the self-consistent mean-field (MF) approaches cannot be directly applied to compute isospin impurities because of spurious mixing caused by the spontaneous symmetry breaking (SSB) effects. This observation hindered theory from progress in the field for decades.

The aim of this work is to present a brief overview of recent theoretical results obtained within the isospin- and angular-momentum projected DFT on isospin-mixing effects. Our multi-reference *no core* DFT was specifically designed to treat rigorously the conserved rotational symmetry and, at the same time, tackle the explicit breaking of the isospin symmetry due to the Coulomb field. The major physics motivation behind developing the model and studying the isospin symmetry breaking (ISB) comes from nuclear beta decay. Theoretical corrections to the superallowed Fermi beta decay matrix elements $I = 0^+, T = 1 \to I = 0^+, T = 1$ between the isobaric analogue states, caused by the ISB, are critical for precise determination of the leading element $V_{ud}$ of the Cabibbo-Kobayashi-Maskawa (CKM) flavour-mixing matrix and, in turn, for further stringent tests of its unitarity, violation of which may signalize *new physics* beyond the Standard Model of particle physics, see [2] and refs. quoted therein.

## II. MULTI-REFERENCE DENSITY FUNCTIONAL THEORY

The formalism employed here starts with the self-consistent Slater determinant $|\varphi\rangle$ obtained by solving Skyrme-Hartree-Fock equations without pairing. The state violates both the rotational and isospin symmetries. The strategy is to restore the rotational invariance, remove the spurious isospin mixing caused by the isospin SSB effect, and retain only the physical isospin mixing due to the electrostatic interaction [3]. This is achieved by a rediagonalization of the entire Hamiltonian, consisting the isospin-invariant kinetic energy and Skyrme force and the isospin-non-invariant

*This work was supported in part by the Polish National Science Center and by the Academy of Finland and University of Jyväskylä within the FIDIPRO programme. We acknowledge the CSC - IT Center for Science Ltd, Finland, for the allocation of computational resources.

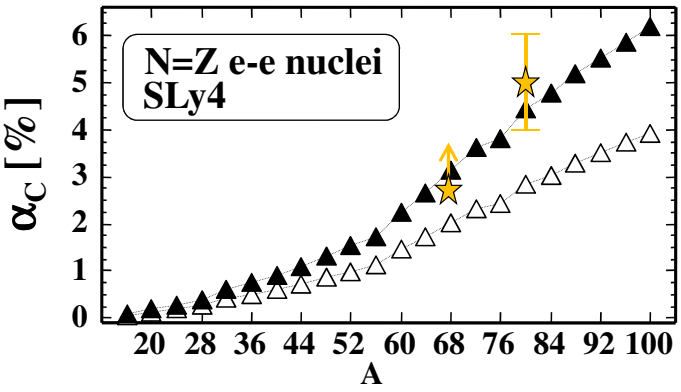


FIG. 1: Isospin impurities in even-even $N = Z$ nuclei calculated by using the SLy4 Skyrme EDF [6]. Full triangles mark the values calculated by using the isospin-projected DFT. Open triangles show mean-field values that are artificially quenched by the spurious isospin mixing. Stars mark empirical results in $^{64}$Ge [7] and $^{80}$Zr [8].

Coulomb force, in a basis that conserves both angular momentum and isospin $|\varphi; IMK; TT_z\rangle$, projected from the state $|\varphi\rangle$:

$$|\varphi; IMK; TT_z\rangle = \frac{1}{\sqrt{N_{\varphi;IMK;TT_z}}} \hat{P}^T_{T_z,T_z} \hat{P}^I_{M,K} |\varphi\rangle, \tag{1}$$

where $\hat{P}^T_{T_z,T_z}$ and $\hat{P}^I_{M,K}$ stand for the standard isospin and angular-momentum projection operators [4], respectively. One must also treat the fact that the quantum number $K$ is not conserved and set (1) is overcomplete. This requires selecting the subset of linearly independent states, known as *collective space* [4], which is spanned, for each $I$ and $T$, by the so-called *natural states* $|\varphi; IM; TT_z\rangle^{(i)}$ [5] and subsequently rediagonalizing the entire Hamiltonian in the collective space. The resulting eigenfunctions are:

$$|n; \varphi; IM; T_z\rangle = \sum_{i,T\geq|T_z|} a^{(n;\varphi)}_{iIT} |\varphi; IM; TT_z\rangle^{(i)}, \tag{2}$$

where index $n$ labels the eigenstates in ascending order of energies.

## III. ISOSPIN MIXING

The isospin or Coulomb impurities are defined as:

$$\alpha^n_{\rm C} = 1 - \sum_i |a^{(n;\varphi)}_{iIT}|^2, \tag{3}$$

where the sum extends over the norms corresponding to isospin $T$ that dominates in wave function (2).

It is well known that for modern density-dependent Skyrme and Gogny energy density functionals (EDFs), the angular momentum projection is ill-defined [9, 10]. Hence, at present, the double-projected DFT method can be safely used only with the functionals originating from the true Hamiltonian. Nevertheless, for all modern Skyrme forces, the isospin-only-projected variant of the approach is free from singularities [3]. Fig. 1 shows the isospin impurities in the ground-states of even-even $N = Z$ nuclei, calculated by using the state-of-the-art SLy4 Skyrme [6] EDF in the isospin-only-projected variant of the model [3, 11]. It is gratifying to see that the calculated impurities are consistent with the recent data extracted from the giant-dipole-resonance decay studies in $^{80}$Zr [8] and isospin-forbidden E1 decay in $^{64}$Ge [7], see Fig. 1. Both data points disagree with the pure MF results, which, due to the spurious mixing caused by the spontaneous ISB effects, are lower by almost ∼30%. The agreement with available data indicates that the model is capable of quantitatively capturing the intensity of the isospin mixing. This is important in the context of performing reliable calculations of the ISB corrections to the Fermi beta decay.

## IV. ISOSPIN-SYMMETRY-BREAKING CORRECTIONS TO THE SUPERALLOWED FERMI BETA DECAY

The $0^+ \to 0^+$ Fermi $\beta$-decay proceeds between the ground state (g.s.) of the even-even nucleus $|I = 0, T \approx 1, T_z = \pm 1\rangle$ and its isospin-analogue partner in the $N = Z$ odd-odd nucleus, $|I = 0, T \approx 1, T_z = 0\rangle$. Since the isospin projection alone leads to unphysically large isospin mixing in odd-odd $N = Z$ nuclei [11], to calculate Fermi matrix elements the double-projected method must be applied. As already mentioned, the angular momentum projection brings back the singularities in the energy kernels [11], preventing one from using the modern parametrizations of the Skyrme EDFs and forcing us to use the Hamiltonian-driven Skyrme SV EDF [12].

The g.s. of the even-even parent nucleus is approximated by the state $|\psi;\, I = 0, T \approx 1, T_z = \pm 1\rangle$, projected from the Slater determinant $|\psi\rangle$ representing the self-consistent g.s. MF solution, which is unambiguously defined by filling in the pairwise doubly degenerate levels of protons and neutrons up to the Fermi level.

The odd-odd daughter state is approximated by the state $|\varphi;\, I = 0, T \approx 1, T_z = 0\rangle$, projected from the self-consistent Slater determinant $|\varphi\rangle \equiv |\bar{\nu} \otimes \pi\rangle$ (or $|\nu \otimes \bar{\pi}\rangle$) representing the so-called anti-aligned MF configuration, obtained by placing the odd neutron and odd proton in the lowest available time-reversed (or signature-reversed) single-particle orbits. The isospin projection from Slater determinants manifestly breaking the isospin symmetry is essentially the only way to reach the $T \approx 1$ states in odd-odd $N = Z$ nuclei that are beyond the MF model space.

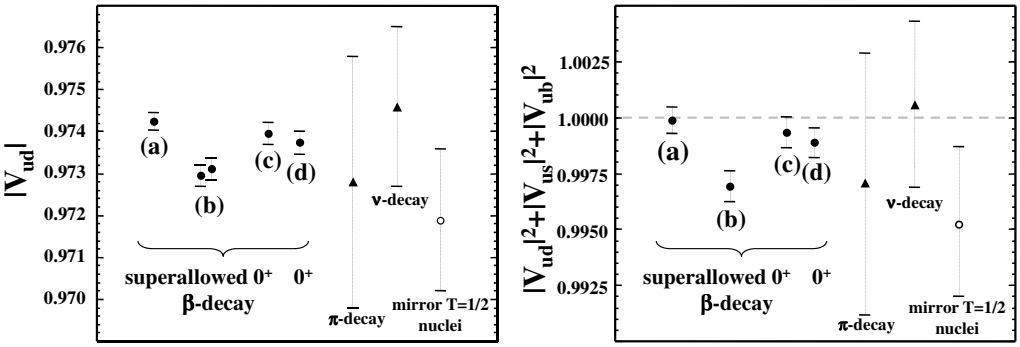


FIG. 2: Matrix elements $|V_{\rm ud}|$ (left panel) deduced from the superallowed $0^+ \to 0^+$ $\beta$-decay (dots) by using values of $\delta_{\rm C}$ calculated in: (a) Ref. [13]; (b) Ref. [14] with NL3 and DD-ME2 Lagrangians; and in our work Ref. [15] with (c) SV and (d) SHZ2 EDFs. Triangles mark values obtained from the pion-decay [16] and neutron-decay [17] studies. The open circle shows the value of $|V_{\rm ud}|$ deduced from the $\beta$-decays in the $T = 1/2$ mirror nuclei [18]. Right panel shows the unitarity condition for different values of $|V_{\rm ud}|$ [17].

.

This allows for rigorous fully quantal evaluation of the beta-decay transition matrix element and the corresponding ISB correction $\delta_{\rm C}$:

$$|M_{\rm F}^{(\pm)}|^2 = |\langle\psi;\, I = 0, T \approx 1, T_z = \pm 1|\hat{T}_{\pm}|\varphi;\, I = 0, T \approx 1, T_z = 0\rangle|^2 \equiv 2(1 - \delta_{\rm C}). \tag{4}$$

The calculated ISB corrections $\delta_{\rm C}$ lead to $|V_{ud}| = 0.97397(27)$ and $|V_{ud}| = 0.97374(27)$, for the SV and SHZ2 EDFs, respectively [15]. Both values result in the unitarity of the CKM matrix up to 0.1%. The new parametrization SHZ2 has been specifically developed to asses the robustness of our results with respect to the choice of interaction. This shows that although individual ISB corrections are sensitive to the interplay between the bulk symmetry energy and time-odd mean-fields, the value of $|V_{ud}|$ rather weakly depends on the parametrization. It is gratifying to see that our results are fully consistent with the results obtained by Towner and Hardy [13], which were obtained within a different methodology, based on the nuclear shell-model combined with mean-field wave functions. Both approaches disagree with the RPA-based study of Ref. [14]. The theoretical results are summarized in Fig. 2.

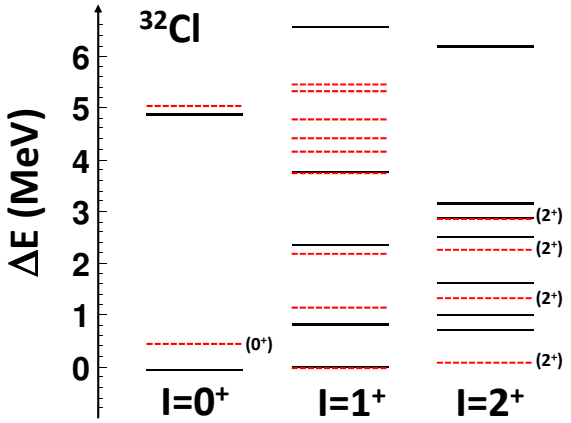


FIG. 3: Low-lying low-spin $I = 0, 1, 2$ states in $^{32}$Cl. Solid lines show theoretical levels obtained by mixing states projected from nine low-lying self-consistent particle-hole configurations. Dashed lines mark experimental data [19]. Note that spin assignments of, in particular, $2^+$ states are uncertain. The spectra have been normalized to the lowest $1^+$ state.

## V. OUTLOOK: BEYOND THE MULTI-REFERENCE DFT

Implementation of the theory that we presented above was based on a projection from a single Slater determinant, which, in odd-odd daughter nucleus, was not uniquely defined. At present, we are implementing an extended version of the model, which allows for mixing of states projected from different self-consistent Slater determinants representing low-lying (multi)particle-(multi)hole excitations in a given nucleus. Such an extension can be viewed as a variant of *no core* shell-model with two-body effective interaction (including the Coulomb force) and a basis truncation scheme dictated by the self-consistent deformed Hartree-Fock solutions. Preliminary spectrum of low-spin $I = 0, 1, 2$ states in $^{32}$Cl obtained by mixing states projected from nine low-lying particle-hole configurations is shown in Fig. 3. In spite of certain technical problems related to divergencies, which will be discussed elsewhere, the results are very encouraging. This is particularly the case in view of the fact that the self-consistent states and their mixing were determined by using the SV Skyrme EDF, which has rather poor spectroscopic properties.


[1] C.A. Engelbrecht and R.H. Lemmer, Phys. Rev. Lett. **24**, 607 (1970).
[2] I.S. Towner and J.C. Hardy, Rep. Prog. Phys. **73**, 046301 (2010).
[3] W. Satuła *et al.*, Phys. Rev. Lett. **103**, 012502 (2009); Phys. Rev. C **81**, 054310 (2010).
[4] P. Ring and P. Schuck, *The Nuclear Many-Body Problem* (Springer-Verlag, Berlin, 1980).
[5] J. Dobaczewski *et al.*, Comput. Phys. Commun. **180**, 2361 (2009).
[6] E. Chabanat, *et al.*, Nucl. Phys. **A627** (1997) 710; **A635** (1998) 231.
[7] E. Farnea *et al.*, Phys. Lett. **B551**, 56 (2003).
[8] A. Corsi *et al.*, Acta Phys. Pol. **B42**, 619 (2011); Phys. Rev. C **84**, 041304 (2011).
[9] M. Anguiano, J.L. Egido, and L.M. Robledo, Nucl. Phys. **A696**, 467 (2001).
[10] H. Zduńczuk, J. Dobaczewski, and W. Satuła, Int. J. Mod. Phys. E **16**, 377 (2007).
[11] W. Satuła *et al.*, Acta Phys. Pol. **B42**, 415 (2011); Int. J. Mod. Phys. **E20**, 244 (2011).
[12] M. Beiner *et al.*, Nucl. Phys. **A238**, 29 (1975).
[13] I.S. Towner and J.C. Hardy, Phys. Rev. C **77**, 025501 (2008).
[14] H. Liang, N. Van Giai, and J. Meng, Phys. Rev. C **79**, 064316 (2009).
[15] W. Satuła *et al.*, Phys. Rev. C **86**, 054314 (2012).
[16] D. Pocanic *et al.*, Phys. Rev. Lett. **93**, 181803 (2004).
[17] K. Nakamura *et al.* (Particle Data Group), J. Phys. G **37**, 075021 (2010).
[18] O. Naviliat-Cuncic and N. Severijns, Phys. Rev. Lett. **102**, 142302 (2009).
[19] C. Ouellet and B. Singh, Nuclear Data Sheets **112**, 2199 (2011).

# Isospin Mixing from the GDR studies

F. Camera[a,b], Simone Ceruti[a,b], A.Giaz[a,b], R.Avigo[a,b], M.Bellato[d,e], Bazzacco[d], G.Benzoni[b], N.Blasi[b], D.Bortolato[c], A.Bracco[a,b], S.Brambilla[b], M.Ciemala[f], S.Coelli[b], A.Corsi[a,b,g], F.Crespi[a,b], C.Fanin[c], E.Farnea[e], Gottardo[c], M.Kmiecik[f], S.Leoni[a,b], A.Maj[f], D.Mengoni[d,e], C.Michelagnoli[d,e], D.Montanari[d,e], A.I.Morales-Lopez[a,b], B.Million[b], S.Myalski[f], L.Pellegri[a,b], R.Nicolini[a,b], F.Recchia[d,e], S.Riboldi[a,b], J.Styczen[f], C.Ur[e], V.Vandone[a,b], J.J. Valiente-Dobon[c], O.Wieland[b], M.Zieblinski[f], and the AGATA Collaboration

[a] *Dipartimento di Fisica, Universitá degli Studi di Milano, Italia.*
[b] *INFN sezione di Milano, Milano, Italia.*
[c] *Laboratori Nazionali di Legnaro, Legnaro, Italia.*
[d] *Dipartimento di Fisica e Astronomia dell'Universitá di Padova, Italia.*
[e] *INFN sezione di Padova, Padova, Italia.*
[f] *The Henryk Niewodniczanski Institute of Nuclear Physics,PAN, Krakow, Poland.*
[g] *CEA, Centre de Saclay, IRFU/Service de Physique Nucleaire, F-91191 Gif-sur-Yvette, France.*

**Abstract.** The Isospin mixing $\alpha^2$ induced by the Coulomb interaction can be studied using a fusion-evaporation reaction (using N=Z nuclei as projectile and target) and the first-step gamma-decay of the Giant Dipole Resonance. The mixing $\alpha^2(T_{CN})$ value is directly measured at the temperature of the compound nucleus while the correspondent value at zero temperature $\alpha^2(T=0)$ could be extracted provided that at least two measurements of $\alpha^2(T)$ at different temperatures are available for the same system.

The isospin mixing was studied in $^{80}$Zr, the heaviest nucleus which can be produced using stable N=Z projectile and target, in two recent HECTOR-GARFIELD and HECTOR$^+$-AGATA experiments. The used fusion-evaporation reaction was $^{40}$Ca+$^{40}$Ca=$^{80}$Zr at $E_{beam}$ = 200 and 136 MeV and the preliminary results show that the measured Coulomb Spreading width has a value which is constant with temperature and compatible with the width of the IAS measured in $^{80}$Se.

As isospin mixing is a Coulomb driven effect, its strength increases with the mass of the N=Z compound nucleus. Therefore, intense exotic beams from an EURISOL facility will permit to produce heavy N=Z compound nuclei (i.e. $^{60}$Zn + $^{40}$Ca = $^{100}$Sn or $^{56}$Ni + $^{40}$Ca = $^{96}$Cd) and will provide a stronger mixing signal if compared to that obtained in $^{80}$Zr or lighter nuclei using stable beams. This is important in nuclear structure and beyond as the evaluation of isospin mixing provides an important correction to the superallowed Fermi transitions rates and contributes to the extraction, in a nucleus independent way, of the first element of the Cabibbo-Kobayashi-Maskawa Matrix.

**Keywords:** $^{80}$Zr, GDR, Compound Nucleus, Isospin Mixing
**PACS:** 24.30.Cz, 25.70.Gh, 24.80.+y, 24.60.Dr

# INTRODUCTION

Isospin symmetry is largely preserved by nuclear interactions and the main violations are due to Coulomb interaction [1-3]. This induce that isospin symmetry is violated and that isospin is not a completely good quantum number for the nucleus. In many cases, however, this effect can be neglected or it is small enough to be treated in a perturbative way. The breaking of isospin symmetry can be observed through decays, which would be forbidden by the selection rules if isospin mixing was not to occur as for example the neutron decay from the IAS or of the E1 decay from self-conjugate nuclei. As it is a Coulomb driven effect the degree of mixing, quantified in the mixing coefficient $\alpha^2$, is expected to increase with the atomic number (see figure 1) almost linearly for A > 50.

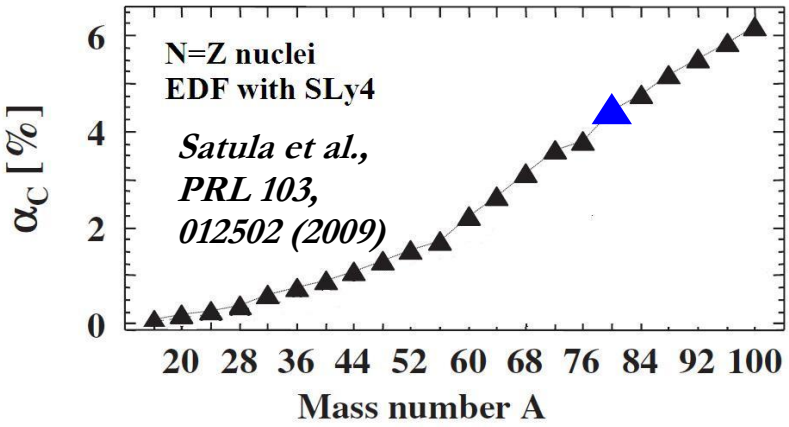


**FIGURE 1.** The isospin mixing parameter calculated for N=Z<50 nuclei [4]

The Giant Dipole Resonance (GDR) is an excitation mode where the selection rule of E1 decay can be fully exploited. Fusion-evaporation reactions allow the production of self-conjugate compound nuclei (CN) at high excitation energy which, in many cases, are far from the $\beta$-stability valley. The use of a self-conjugate projectile and target ensures that the CN produced in fusion reactions has isospin $I = 0$. Therefore, E1 emission associated with the decay of the GDR is hindered. The most direct consequence is that the first-step GDR $\gamma$ decay depends on the degree of isospin mixing of the CN. At a finite temperature one expects a partial restoration of the isospin symmetry because the degree of mixing in a CN is limited by its finite lifetime for particle decay. The competition between the timescale of the Coulomb-induced mixing and the CN lifetime (which decreases for increasing temperature) drives toward a restoration of isospin symmetry [3-8].

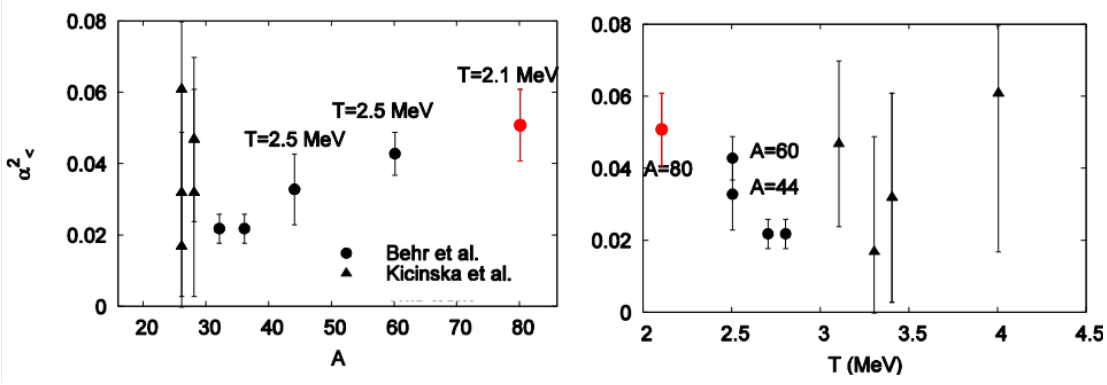


**FIGURE 2.** The isospin mixing parameter measured in N=Z nuclei using the first step gamma decay of the GDR [5-8]. The same data are plotted vs the compound nucleus mass number A=2Z (left panel) and vs the nuclear temperature of the compound nucleus (right panel). The angular momentum of the

compound nuclei is included in the calculation of the nuclear temperature. The red point indicates $^{80}$Zr (the heaviest N=Z compound nucleus which can be produced using a stable beam and target) [8].

In the past, several experiments have measured the isospin mixing coefficient through the gamma-decay of the GDR [5-8] in N=Z compound nuclei and the data shows a trend where $\alpha^2$ seems to increase with atomic mass number Z and to decrease with nuclear temperature T (see figure 2). However, the data are very inhomogeneous as each point has a different value of A, T and angular momentum.
Recent theoretical works [9-10] have calculated the temperature dependence of the isospin mixing coefficient $\alpha^2$ (see formula below) which, in the case of spin = 0, depends on the width of the IAS ($\Gamma^{\downarrow}_{IAS}$), the compound spreading width ($\Gamma^{\uparrow}_{CN}(T)$) and the width of the IVGMR ($\Gamma_{IVM}$) calculated at the excitation energy of the IAS:

$$\alpha^2_{I_0+1} \sim \frac{\Gamma^{\downarrow}_{IAS}}{\Gamma^{\uparrow}_{CN}(T) + \Gamma_{IVM}},$$

Therefore, in the case $\alpha^2$ is measured in the same system at different temperatures it could be possible to extract the zero temperature isospin mixing value substituting the value of $\Gamma^{\downarrow}_{IAS}$ with that of the Coulomb Spreading width extracted from the data as already suggested in ref [3].
This make extremely interesting the future availability of intense N=Z radioactive beams. In fact, these beams will make possible to produce heavy self conjugated compound nuclei which are expected to have a large and easier to measure isospin mixing coefficient.

## THE MEASUREMENTS

Isospin mixing in the hot compound nucleus $^{80}$Zr was studied at two different excitation energies by measuring and comparing the gamma-ray emission from the fusion reactions $^{40}$Ca+$^{40}$Ca at $E_{beam}$= 136 and 200 and MeV. A reaction where isospin mixing should do not play a role was additional performed to tune statistical model calculations. Namely, the compound $^{91}$Rb (using the reaction $^{37}$Cl+$^{44}$Ca at $E_{beam}$=95 and 153 MeV) was populated. The yield associated with the Giant Dipole Resonance is found to be different in the two reactions because in self-conjugate nuclei the E1 selection rules forbid the decay between states with isospin I=0. The two experiments were performed at the INFN Laboratori Nazionali di Legnaro. The first uses the GARFIELD-HECTOR array (to measure high-energy gamma rays, charged particles and evaporation residues) while the second employed the AGATA-HECTOR$^+$ array system for the measurement of high and low energy gamma-rays. The reaction at the highest excitation energy have been already analyzed [8] while for the reaction at lower excitation energy the analysis is in progress.

## EXPERIMENTAL RESULTS

The degree of mixing at high temperature is deduced from the statistical model analysis of the gamma-ray spectrum emitted by the compound nucleus $^{80}$Zr. From the data at high excitation energies the Coulomb Spreading width was found to be $\Gamma^{\downarrow}_{>}$ = 10 ± 3 KeV for $E_{beam}$ = 200 MeV reaction while the preliminary values for $E_{beam}$ = 136 MeV is $\Gamma^{\downarrow}_{>}$ = 12 ± 3 KeV. The two values are consistent between them and equal to the width of the IAS measured in $^{80}$Se [11] equal to $\Gamma^{\downarrow}_{IAS}$ = 9.9 keV. This aspect is extremely interesting as it experimentally confirms that the two width are very similar and independent of nuclear temperature as the mechanism producing the width is substantially the same. In addition it tells us that the Coulomb mixing can be considered as a basic intrinsic feature of the nucleus, similarly to the GDR intrinsic width, which is also found to be independent of temperature [12-14]. The plots in

figure 3 shows the measured high energy gamma rays spectra calculated for three different values of $\Gamma^{\downarrow}_{>}$ with, superimposed, the statistical model calculations.

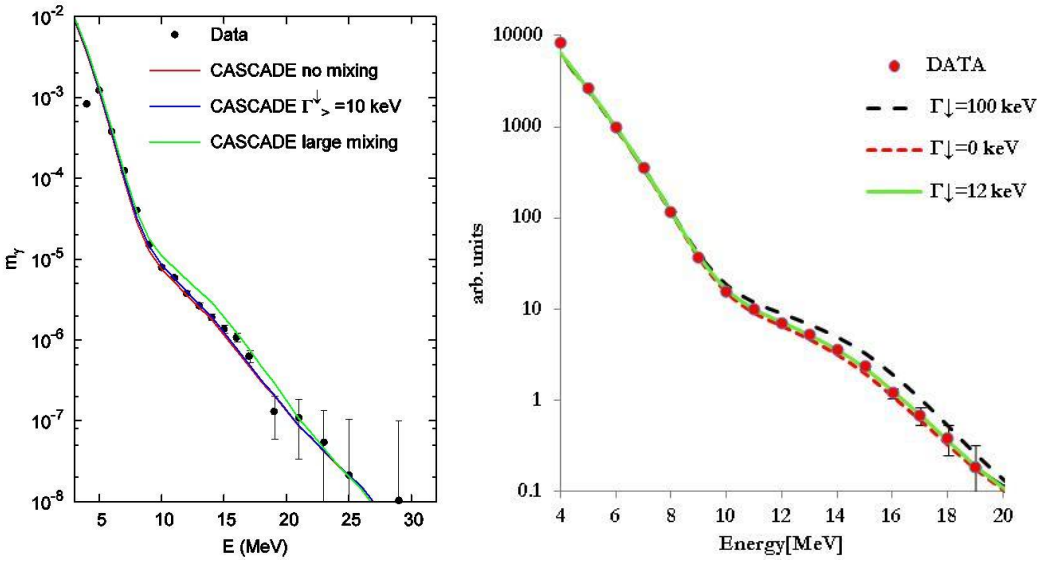


**FIGURE 3.** The measured high energy gamma rays spectra measured in the reaction $^{40}$Ca + $^{40}$Ca at $E_{beam}$ = 200 MeV (left panel) [8] and $E_{beam}$ = 136 MeV (right panel). Superimposed there are the calculations with the best fitting Coulomb Spreading width, the fully mixed isospin scenario and the case where isospin symmetry is fully restored.

The used statistical model and GDR parameters used have been extracted using the 'reference' reaction $^{37}$Cl + $^{44}$Ca = $^{81}$Rb. For both beam energies we used 100% of EWSR and a GDR centroid of 16.2 MeV while for the GDR width, as expected, we've seen a decrease from 10.6 MeV to 7 MeV due to the lower nuclear Temperature and angular momentum of the $E_{beam}$ = 136 MeV case.

The measured isospin mixing $\alpha^2$ value in $^{80}$Zr at $E_{beam}$ = 200 MeV is consistent with the theoretical prediction of reference [4] (see figure 4). The new data point which will be located in the shaded region is not yet available as the analysis work is still in progress. Once extracted it will permit an estimation of the zero temperature isospin mixing value to be compared with the theoretical one of ref [4].

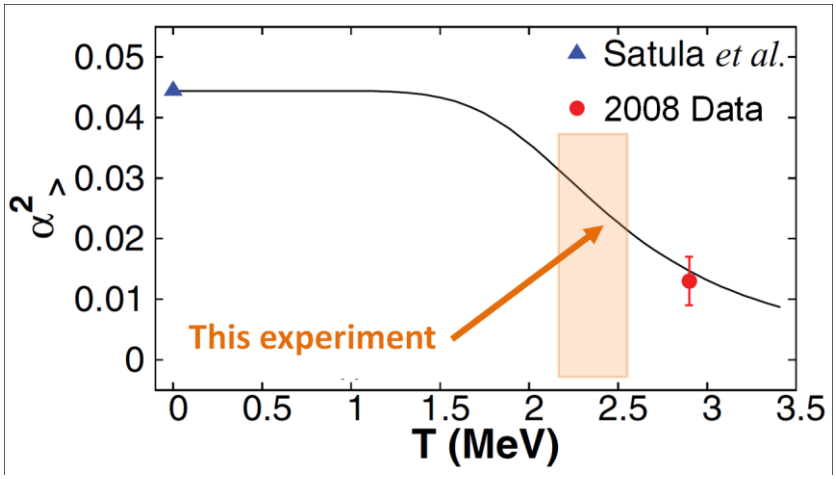

**FIGURE 4.** The temperature dependence of the mixing probability of the $^{80}$Zr using the theoretical model of ref [9-10]. The theoretical curve uses the Coulomb spreading width of [8], it has been normalized to the T=0 value of [4] and uses a width of the monopole resonance at the temperature of the Isobaric Analogue State fixed with temperature. The blue triangle is the experimental value of the isospin mixing obtained in [8], the red dot is the theoretical value calculated in [4]. The light red rectangle is the temperature region for the $E_{beam}$=136 MeV experiment.

## CONCLUSION

The $^{80}$Zr dataset here discussed is the first set of experiments where isospin mixing is measured in the same system at two different excitation energies. The preliminary results have shown that i) the Coulomb Spreading width is the same at T=2.2 and T=3 MeV and has the same values as the width of the IAS measured in $^{80}$Se, ii) the calculated zero temperature $\alpha^2$ value and the one measured in the reaction at $E_{beam}$ = 200 MeV follows the expected theoretical behavior of ref [9-10]. The technique here discussed, if fully validated, will permit the extraction of the zero temperature isospin mixing in self-conjugated nuclei starting from the measurement of the gamma decay of the hot GDR. The use of intense stable beams will permit the isospin mixing systematic study below Z=40 A=80 while the use of radioactive beams, like those allowed by the EURISOL facility, will permit the measurements of isospin mixing in nuclei heavier than A=80. In fact $^{80}$Zr is the heaviest isotope, which is possible to produce using stable beams and targets. In particular it will be possible to populate self conjugate nuclei in the mass region around $^{100}$Sn in the isospin zero channel. For example the $^{40}$Ca + $^{56}$Ni will produce the N=Z compound $^{106}$Cd.

## REFERENCES


1. N. Auerbach *et al*., Phys. Rev. Lett. **23**, 2163 (1996).
2. D. H. Wilkinson Phil. Mag. **1**, 379 (1956).
3. H. L. Harney *et al*., Rev. Mod. Phys. **58**, 607 (1986).
4. W. Satula *et al*., Phys. Rev. Lett. **103**, 012502 (2009).
5. M. N. Harakeh *et al*., Phys. Lett. B **176**, 297 (1986).
6. J.A. Behr *et al*., Physical Review Letters **70**, 3201 (1993).
7. M. Kicinska-Habior *et al*., Nuclear Physics A **731**, 138 (2004).
8. A. Corsi *et a*l., Phys. Rev. C84(2011)041304R
9. H. Sagawa *et al*., Phys. Lett. B **444**, 1 (1998).
10. G. Colo et al., Phys. Rev. C **52**, R1175 (1995).
11. S. Kailas *et al.*, Nucl. Phys. A **315**, 157 (1979).
12. P. F. Bortignon *et al*., Phys. Rev. Lett. **67**, 3360 (1991).
13. A. Bracco *et al.*, Phys. Rev. Lett. **74**, 3748 (1995).
14. O. Wieland *et al.*, Phys. Rev. Lett. **97**, 012501 (2006).

# High lying nuclear states via ineslatic scattering of $^{17}$O

L.Pellegri[*,†] and F.C.L.Crespi[*,†]

[*] *Universitá degli Studi di Milano, Via Celoria 16, 20133, Milano, Italy.*
[†] *INFN sezione di Milano, Via Celoria 16, 20133, Milano, Italy.*

**Abstract.** Inelastic scattering of $^{17}$O heavy ions at 20 MeV/u has been used to study the $\gamma$-decay from high-lying bound and unbound states in $^{124}$Sn. The description of the experimental set up is given and some preliminary results of the data analysis are shown.

**Keywords:** $\gamma$-ray spectroscopy, nuclear structure
**PACS:** 24.30.Cz, 25.70.-z

## INTRODUCTION

Giant Resonances are fundamental modes of excitation, at high frequency, corresponding to scape oscillation around the equilibrium of the nuclear system. Their study over the years has provided useful information on the nuclear structure and on the effective nucleon-nucleon interaction, as well as on the bulk properties of nuclear matter [1]. In recent years, particular attention has been given to the study of the dipole response at energies around particle threshold. Indeed, an accumulation of dipole strength, larger than that due to the tail of the Giant Dipole Resonance (GDR), is found in several neutron rich nuclei: this is commonly denoted as the Pygmy Dipole Resonance (PDR) [12]. The hydrodynamical model describes the PDR as originating from the collective oscillation of the neutron skin against a symmetric proton-neutron core [2][4][12]. From the experimental point of view, the PDR has been investigated systematically in a large number of stable nuclei with the photon scattering technique (e.g. [2][3]). Experiments using Coulomb excitation in inverse kinematics to study the PDR in unstable neutron rich heavy nuclei have been also performed [10][13][14]. In stable nuclei, by comparing results of photon scattering (or also proton scattering [15]) with those of alpha scattering experiments, a selectivity in the population of these PDR states has been observed [4][9]. In the case of $^{124}$Sn [4], the pygmy dipole structure reveals a splitting into two components: one group of states which is excited in both type of reactions, and another group of states at higher energies which is only excited in the ($\gamma$,$\gamma$') case. These findings call for additional investigation, making use of different probes to excite the resonance states (as for example heavy ions). Indeed, experiments performed with different probes are complementary, altering the relative population of the different states. Motivated by this interest, we used the inelastic scattering of $^{17}$O heavy ions at 20 MeV/u as a tool to study the $\gamma$-decay from this resonance [6][8][11].

# EXPERIMENTAL SET-UP AND DATA ANALYSIS

## Experimental set-up

In this experiment an $^{17}$O beam at the energy of 20 MeV/u in the laboratory frame, provided by PIAVE-ALPI accelerator system of the Legnaro National Laboratories, was used. The gamma ray detection system was composed by the AGATA Demonstrator [7] coupled to an array of large volume $LaBr_3$:Ce scintillators named HECTOR$^+$ [16]. The scattered $^{17}$O ions were detected by two ΔE-E Silicon Telescopes of the TRACE project [5], mounted inside the scattering chamber and covering the angular range between 12° and 22° with respect to the beam axis.

## Data analysis

### *Gamma decay from the Pygmy Dipole Resonance*

The identification of the ions detected in the silicon telescopes was performed with the standard ΔE-E technique. Fig. 1 shows the total kinetic energy (TKE) measured in one pad of the telescopes versus the energy deposit measured in the ΔE pad in the region of the oxygen isotopes. The clear mass separation in the oxygen isotopes region permits a clean gate condition on the inelastic scattering channel. Once the inelastic scattering channel has been selected, the total kinetic energy loss (TKEL), deduced from the measured energy of the scatted $^{17}$O ions, has to be correlated with the decay energy obtained from the coincidently measured $\gamma$-rays energies in order to select the decays into the ground state. This is done by applying a diagonal cut on the $\gamma$-ray energy against the TKEL matrix. Furthermore, since the typical lifetime of these states is of the order of the femtosecond, a Doppler correction for the recoil was also performed. Finally, to clearly identify the $\gamma$-decay of the PDR, a background subtraction was performed. Fig. 2 shows the $\gamma$-ray energy spectrum of the $^{124}$Sn obtained with these conditions. As can be observed the PDR states are clearly visible at energies above 5 MeV. In Fig. 2 transitions observed in previous experiments [2][3][4] are indicated.

### *Angular distribution*

It is known from previous NRF experiments [2][3] that energy spectrum measured in the PDR region is dominated by E1 transitions, however, some E2 transitions are also present. Thanks to the position sensitivity of the AGATA Demonstrator and the Silicon Telescopes, it was possible to effectively separate contributions from gamma radiation of different multipolarity, using angular distributions. In particular this is done by selecting the range of $\theta_{\gamma,rec}$ (i.e. the angle between the $^{124}$Sn recoil nucleus and the emitted $\gamma$-ray) in which the E1 and E2 component are respectively dominating in intensity. Fig. 3 displays the comparison between the $\gamma$-ray spectra of $^{124}$Sn in the pygmy region. The E1 component is enhanced in the red spectrum (angular gate: $65° < \theta_{\gamma,rec} < 115°$) instead

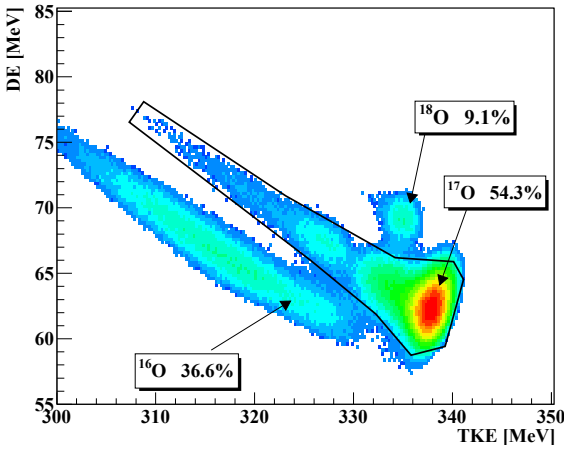


**FIGURE 1.** Total Kinetic Energy measured in one pad of the TRACE telescope versus the energy deposit measured in the ΔE pad in the region of the oxygen isotopes. The relative population of the oxygen isotopes is specified.

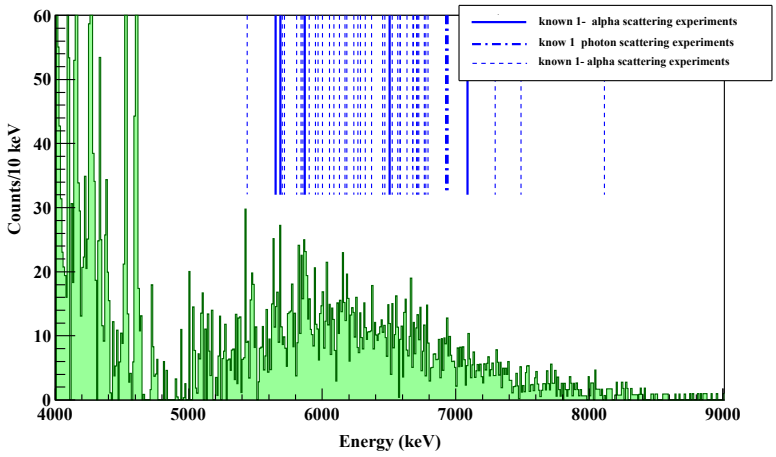


**FIGURE 2.** $\gamma$-decay in the PDR region measured with the AGATA Demonstrator array for the reaction $^{124}$Sn($^{17}$O, $^{17}$O'$\gamma$) with the gating conditions described in text.The dotted and solid black lines indicate transitions already observed in previous experiments [2][3][4].

the E2 component in the blue one (angular gate: $15°<\theta_{\gamma,rec}<65°$). As expected the PDR region is dominated by E1 transitions. The dotted and solid black lines indicate transitions observed in previous experiments [2][3][4].

## CONCLUSION

An inelastic scattering experiment, using $^{17}$O ions accelerated at 20 MeV/u, aimed at the study of the gamma-decay from PDR states in the $^{124}$Sn nucleus has been performed. Preliminary spectra show lines associated to the $\gamma$-decay from PDR states known from

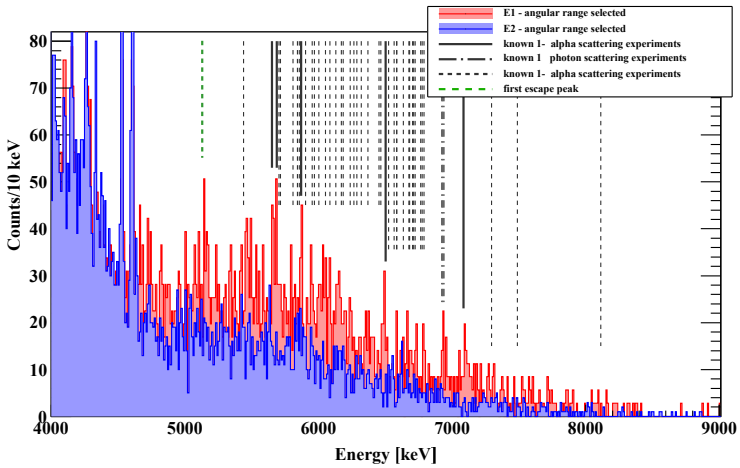


**FIGURE 3.** $\gamma$-decay in the PDR region measured with the AGATA Demonstrator array for the reaction $^{124}$Sn($^{17}$O, $^{17}$O'$\gamma$) gated on the angular distribution of the emitted $\gamma$-rays. The E1 transitions are enhanced in the red spectra (angular gate: 65°<$\theta_{\gamma,rec}$<115°) instead the E2 transitions in the blue one (angular gate: 15°<$\theta_{\gamma,rec}$<65°). The dotted and solid black lines indicate transitions observed in previous experiments [2][3][4].

previous experiments performed with different probes. The multipolarity of the observed gamma transitions is determined thanks to angular distribution measurements. The analysis performed in this work has demonstrated the unique possibility offered by heavy-ion scattering studies, in coincidence with an efficient $\gamma$-detection, to obtain important structure information on the underlying nature of the pygmy states. The experimental technique employed in this experiment could also be used at future facilities, which will be able to produce neutron-rich radioactive beams, to study, in inverse kinematics, the structure of the pygmy resonance in more neutron-rich systems.

## REFERENCES


1. P. F. Bortignon *et al.*, *Giant Resonances, Nuclear Structure at Finite Temperature, Contemporary Concepts in Physics* Harwood Academic Publishers (1998).
2. K. Govaert, *et al.*, *Phys. Rev. C* **57**, 2229 (1998).
3. S. Volz, *et al.*, *Nucl. Phys. A* **779**, 1 (2006).
4. J. Endres, *et al.*, *Phys. Rev. Lett.* **105**, 212503 (2010).
5. D. Mengoni, *PhD thesis* 2007 TRACE Project.
6. R. Nicolini, *PhD thesis* 2012 University of Milan.
7. S. Akkoyun, *et al.*, *Nucl. Instr. and Meth A*668 (2012) 26-58.
8. R. Nicolini, *Acta. Phys. Pol. B* (2011) p. 653-657.
9. D. Savran, *et al.*, *Phys. Rev. Lett.* **97**, 172502 (2006).
10. O. Wieland, *et al.*, *Phys. Rev. Lett.* **102**, 092502 (2009).
11. A. Bracco and F.C.L. Crespi, *EPJ Web of Conferences* **38**, 03001 (2012).
12. D. Savran, *et al.*, *Prog. Part. Nucl. Phys.* **70**, 210 (2013).
13. O. Wieland, A. Bracco, *Prog. Part. Nucl. Phys.* **66**, 374 (2011).
14. T. Aumann, *Eur. Phys. J. A* **26**, 441 (2005).
15. A. Tamii, *et al.*, *Phys. Rev. Lett.* **107**, 062502 (2011).
16. A. Giaz, *et al.*, *Accepted to Nucl. Instr. and Meth A.*

# Giant Dipole Resonance decay of hot rotating $^{88}$Mo

M. Ciemała*, M. Kmiecik*, A. Maj*, V.L. Kravchuk†, F. Gramegna†, S. Barlini**, G. Casini** and F. Camera‡

*Niewodniczański Institute of Nuclear Physics PAN, 31-342 Kraków, Poland
†INFN, Laboratori Nazionali di Legnaro, I-35020, Legnaro, Italy
**Dipartimento di Fisica and INFN Sez. di Firenze, Firenze, Italy
‡Dipartimento di Fisica and INFN Sez. di Milano, Milano, Italy

for the HECTOR and GARFIELD collaborations

**Abstract.** An experiment focusing on study of the properties of hot rotating compound nucleus of $^{88}$Mo was performed in LNL Legnaro using $^{48}$Ti beam at energies of 300 and 600 MeV on $^{40}$Ca target. The compound nucleus was produced at the temperatures of 3 and 4.5 MeV, with angular momentum distribution with $l_{max} > 60\ \hbar$ (i.e. exceeding the critical angular momentum for fission barrier). High-energy gamma rays, measured in coincidence with evaporation residues and alpha particles, were analyzed with the statistical model. During fitting procedure the GDR parameters were obtained, which allowed to investigate an evolution of the GDR width up to high temperatures.

Similar studies in more exotic nuclei will be possible in the context of planned radioactive beam facility of EURISOL.

**Keywords:** GDR width, high temperature
**PACS:** 21.10.Re, 24.30.Cz

## INTRODUCTION

The study of Giant Dipole Resonance properties at high temperature and angular momentum is important for investigation of nuclear structure since it provides information on behavior of nuclei under extreme conditions. In particular, the change of the GDR width with angular momentum and temperature reflects the role played by quantal and thermal fluctuations in the damping of giant vibrations [1–7].

In last years the GDR width has been measured for several nuclei at different temperatures. The highest temperature region, up to 3.7 MeV, was investigated for $^{132}$Ce showing almost linear increase of GDR width as a function of temperature [8]. The obtained GDR dependence on the temperature was found to be mainly due to the nuclear deformation increase and, at higher temperatures (above 2.5 MeV), taking into account the compound nucleus lifetime. Additionally, it was shown that very important was the evaluation of proper excitation energy of the compound nucleus considering preequilibrium processes that may occur at high energies. It was almost negligible for studied mass symmetric reaction while in mass asymmetric reactions had large impact.

Here there are presented results of new measurements of the GDR width for high temperature performed for $^{88}$Mo produced in fusion-evaporation reaction.

## EXPERIMENT

The decay of the $^{88}$Mo compound nuclei has been studied in the experiment performed at Tandem-ALPI accelerator at the laboratory of LNL Legnaro using 300 and 600 MeV $^{48}$Ti beam on $^{40}$Ca (500 μg/cm$^2$) target. The compound nucleus (CN) has been produced at 124 and 262 MeV excitation energy, corresponding to the average CN temperature of 3 and 4.5 MeV respectively. The high-energy gamma rays as well as charged particles were measured using the combined HECTOR [9] and GARFIELD [10] arrays. The GARFIELD detectors consisting of ΔE – E gaseous micro-strip and CsI(Tl) scintillation detectors were positioned at $\theta$ = 29° to $\theta$ = 82° and $2\pi$ in $\phi$ in the same gas volume. The 8 large volume $BaF_2$ HECTOR detectors were placed at backward angles. The phoswich [11] detectors were placed at forward angles to identify the evaporation residues, which provide possibility to select fusion-evaporation channel of the reaction.

To obtain GDR parameters such as centroid energy, strength and width ($\Gamma_{GDR}$), high-energy gamma-ray spectra, which were measured in coincidence with evaporation residues, were analyzed. In the analysis the GEMINI++ [12] Monte Carlo statistical model code with incorporated GDR emissio [13] was employed. The high-energy gamma-ray spectra were fitted in the GDR region to obtain the GDR parameters. Both measured and calculated spectra are presented in Fig. 1 together with the extracted strength functions.

Apart from high-energy gamma rays, also charged particle spectra have been measured allowing investigation of the preequlibrium process which after analysis occurred not to be observed in the experiment.

## THE GDR WIDTH

Since GDR can be emitted at different decay steps, namely from nucleus characterized by different excitation energy, the temperature of nucleus at which the GDR is excited is not the same as for CN. Its values are calculated at each decay step using formula:

$$T_{GDR} = [(E^* - E_{rot} - E_{GDR})/a(T)]^{\frac{1}{2}} \quad (1)$$

where $E^*$ is the excitation energy, $E_{rot}$ is the rotation energy, $E_{GDR}$ is the energy of emitted gamma and $a(T)$ is level density parameter for decaying nuclei. The temperature of nuclei after gamma emission was estimated for both experimental cases using GEMINI++ calculations taking into account all experimental conditions. As a result the calculated temperature values for beam energies 300 and 600 MeV respectively are $\langle T_{GDR} \rangle$ = 2.0(6) and 3.1(9) MeV.

The GDR widths were obtained as FWHM of the GDR strength functions for both experimental cases and found to increase from 10.3(6) MeV for 2 MeV temperature to 11.2(9) MeV at temperature equal to 3.1 MeV [14]. The measured values were compared to the theoretical predictions of the two models assuming that the damping of giant vibrations is caused by the different processes. One of the model, phonon damping model (PDM) [15, 16] (Fig. 2a), describes the GDR width due to interaction of the GDR phonons with the particle – hole, particle – particle and hole – hole excitations. It

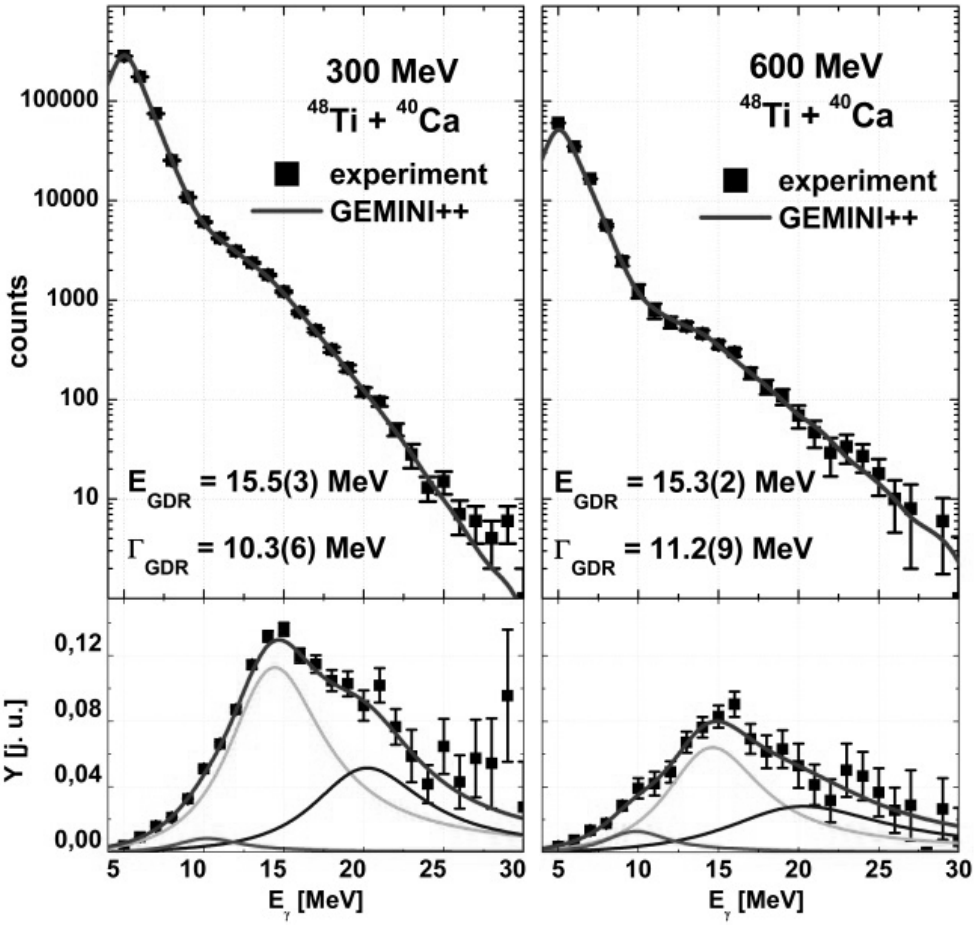


**FIGURE 1.** Upper panels: gamma rays spectra measured for 300 and 600 MeV beam energies compared to the GEMINI++ calculations. Bottom panels: GDR strength functions with their components obtained from the best fit of the GDR part of gamma-ray spectra for both energies.

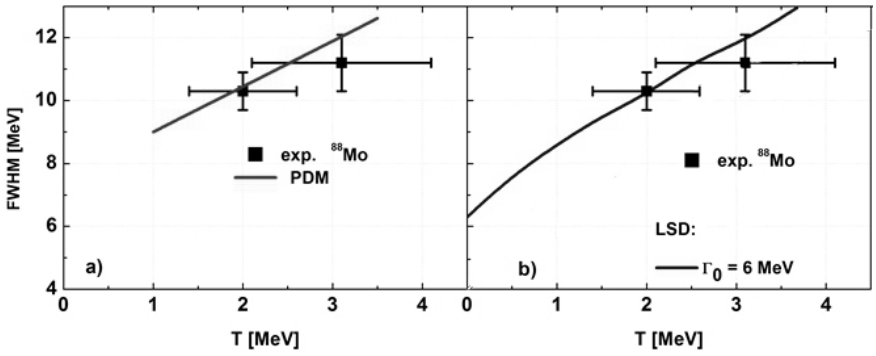


**FIGURE 2.** The temperature dependence of the GDR width obtained as FWHM of the strength function. The experimental values (points) are presented with calculations based on PDM (a) and LSD + thermal fluctuations (b) models. The horizontal error bars indicate the standard deviations of the temperature distributions.

predicts an increase of the GDR width up to certain value of temperature and then its saturation [14]. Another employed model was the recent version of the liquid drop model - LSD [17, 18] (Fig. 2b) with the thermal shape fluctuations anticipating the increase of the GDR width with temperature. The calculations were performed for $\Gamma_0$ = 6 MeV, which is GDR width at $T_{GDR} = 0$.

## CONCLUSIONS AND PERSPECTIVES

Both models predict that for $^{88}$Mo in the investigated temperature region the GDR width increase is similar to the increase observed experimentally. It is observed quite good agreement of the measured values compared to the calculations based on PDM model as well as to LSD based results shown in Fig. 2. This may indicate that both models describe well the GDR width behavior. The GDR width increase with temperature can be explained due to phonon – single particle interactions or thermal shape fluctuations increase with temperature.

Continuation of the GDR decay investigation for the neutron-rich nuclei will be possible after launch of the planned EURISOL facility. Usage of highly intensive radioactive ion beams, by example $^{68}_{28}$Ni on $^{30}_{14}$Si $\rightarrow$ $^{98}_{42}$Mo or $^{94}_{36}$Kr on $^{26}_{12}$Mg $\rightarrow$ $^{120}_{48}$Cd, will be useful for creation of nuclei at high angular momentum, which will allow in addition to study the Jacobi and Poincare shape transitions [19, 20].

## REFERENCES


1. P.F. Bortignon, A. Bracco, R.A. Broglia, *Giant Resonances: Nuclear Structure at Finite Temperature* (Harwood Academic, Amsterdam, 1998).
2. M. Gallardo et al., *Nucl. Phys. A* **443**, 415 (1985).
3. F. Camera et al., *Nucl. Phys. A* **572**, 401 (1994).
4. M. Mattiuzzi et al., *Phys. Lett. B* **364**, 13 (1995).
5. M. Kmiecik et al., *Nucl. Phys. A* **674**, 29 (2000).
6. M. Kmiecik et al., *Phys.Rev. C* **70**, 064317 (2004).
7. D. Kusnezov and E. Ormand, *Phys. Rev. Lett.* **90**, 042501 (2003).
8. O. Wieland et al., *Phys. Lett.* **97**, 012501 (2006).
9. A. Maj et al., *Nucl. Phys. A* **571**, 185 (1994).
10. F. Gramegna et al., *Nucl. Inst. Meth. A* **389**, 474 (1997).
11. M. Bini et al., *Nucl. Inst. Meth. A* **515**, 497 (2003).
12. R.J. Charity, *Phys. Rev. C* **82**, 014610 (2010).
13. M. Ciemała et al., *Acta Phys. Pol. B* **44**, 611 (2013).
14. M. Ciemała, PhD thesis, IFJ PAN Kraków 2013 (`http://www.ifj.edu.pl/publ/reports/2013/2062.pdf?lang=pl`).
15. N.D. Dang and A. Arima, *Phys. Rev. Lett.* **80**, 4145 (1998); N. Dinh Dang and A. Arima, *Nucl. Phys. A* **636**, 427 (1998).
16. N. Dinh Dang, *Phys. Rev. C* **85**, 064323 (2012).
17. K. Pomorski, J. Dudek, *Phys. Rev. C* **67**, 044316 (2003).
18. J. Dudek, K. Pomorski, N.Schunck, N. Dubray, *Eur. Phys. J. A* **20**, 15 (2004).
19. A. Maj et al., *Int. J. Mod. Phys. E* **19**, 532 (2010).
20. K. Mazurek et al., *Acta Phys. Pol. B* **42**, 471 (2011).

# Deep inelastic reactions, as tools towards high Z and A

G. Pollarolo

*Dipartimento di Fisica, Università di Torino and INFN, Sezione di Torino Via Pietro Giuria 1, I-10125 Torino, Italy*

**Abstract.** The semi-classical model GRAZING [1, 2, 3] will be used to illustrate that it is possible to use Deep Inelastic Collisions (or multi-nucleon transfer reactions) to populate nuclei heavier than the target. This may me achieved by using suitable radioactive neutron rich projectiles. Reactions for the production of neutron rich nuclei, relevant for the r-process (in particular for the waiting line N=126), will also be discussed.

**Keywords:** deep inelastic reactions, GRAZING model, radioactive beams
**PACS:** 25.70.Lm, 25.70.Pq

## INTRODUCTION

The Deep Inelastic Collisions (DIC) are characterized by large energy losses, the fragments are emerging from the reaction with an energy that is below the Coulomb repulsion of two touching spheres, and by a charge (Z) distribution of the fragments that is very large. For large energy losses these charge distributions, are centered at a Z that is smaller than the one of the projectile. These reactions played, in the past, a very important role for the understanding the reaction mechanism in particular it was possible to extract the relevant degrees of freedom of the reactants that are responsible for the evolution of the reaction. In this contribution after a short overview of DIC I will show how they may be used, with suitable choices of projectiles, to produce neutron rich nuclei in the region around N=126 and to produce nuclei that are heavier than the target thus allowing to map the nuclear chart in unknown region.

Fig. 1 shows an illustrative example of the charge distribution of the yields of a DIC plotted as a function total final kinetic energy. Here one can clearly recognize two components: a ridge that from the entrance channel extends to very low energies and to charges smaller than the one of the projectile and a broad peak centered at a very low energy and at a charge compatible with a fusion-fission process. The ridge component contains most of the reaction cross section and it is compatible with transfer reactions and evaporation processes.

# THE MODEL

For the description of the collision several models have been proposed. They can be classified in two broad classes: macroscopic and microscopic models. The macroscopic models take inspiration from the broadening of the charge distribution (the ridge component) as a function of dissipated energy and describe the exchange of mass and charge with transport equations and introduce frictional forces for the dissipation of energy and angular momentum. The microscopic models, instead, try to calculate the evolution of the reaction by using the intrinsic degrees of freedom of projectile and target. In the model I am going to use, these are identified as the isoscalar surface modes (low lying and high-lying states) and as the transfer of nucleons (neutron and protons, stripping and pick-up). This model will not be summarized here, for details refer to the refs. [1, 2, 3], here suffices to remember that the cross section are calculated by solving in an approximate way the system of coupled equations

$$i\,\hbar\dot{c}_\beta(t) = \sum_\alpha c_\alpha(t) < \beta|H_{int}|\alpha > e^{\frac{i}{\hbar}(E_\beta - E_\alpha)t + i(\delta_\beta - \delta_\alpha)} \tag{1}$$

obtained from the time dependent Schrödinger equation by expanding the total wave function of the system in terms of channel wave functions $\psi_\alpha = \psi^a(t)\psi^A(t)e^{i\delta(\vec{R})}$ corresponding to states of the asymptotic mass partitions. The coefficient $c_\beta$ gives the amplitude for the system to be in channel $\beta$. The above system of coupled equations is well known from Coulomb-excitation it is shown here since GRAZING generalizes the mentioned theory by

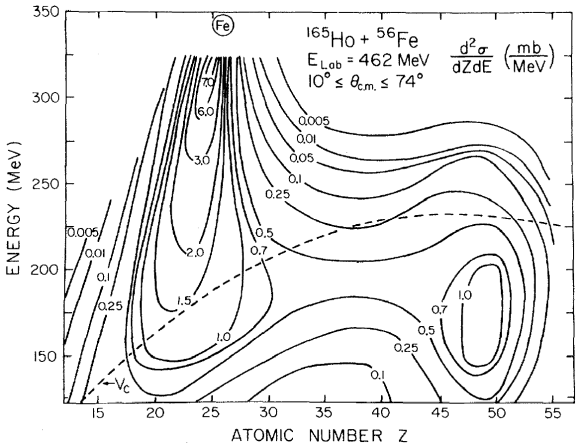


**FIGURE 1.** Double differential cross section for the $^{56}$Fe + $^{165}$Ho reaction. The dash-line corresponds to the Coulomb barrier of two touching spheres. The fact that a large fraction of the yields lies below this line indicates that the fragments separate with large deformations.

including the nuclear interaction in the excitation of the surface modes and the exchange of nucleons. The multi-nucleon transfer is considered to be only sequential.

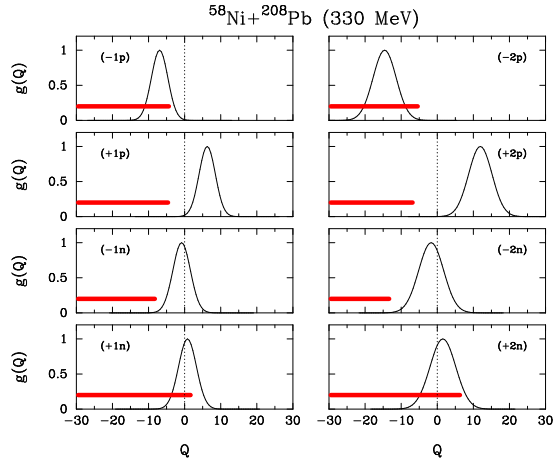


**FIGURE 2.** Adiabatic cut-off functions for one and two neutron and proton transfer channels for the reaction $^{58}$Ni+$^{208}$Pb at the indicated energy. The horizontal lines represent the location of all possible transitions.

Since we are here interested in showing how DIC may be used to produce heavy nuclei reach of neutrons I have to illustrate the main properties of a transfer process. The magnitude of a given transfer process can be estimated easily by writing down its first order Born approximation. For a given impact parameter (incoming partial wave $\ell$) the probability for the transition from the entrance channel $\alpha$ to the exit channel $\beta$ may be written in the form

$$P_{\beta\alpha}(\ell) = \left| \frac{i}{\hbar} \int_{-\infty}^{+\infty} dt\ e^{i\sigma_{\beta\alpha}t} f_{\beta\alpha}(\vec{r}) e^{i[(E_\beta - E_\alpha)+(\delta_\beta-\delta_\alpha)]t/\hbar} \right|^2 \tag{2}$$

where the time integral has to be performed along the classical trajectory for the given partial wave $\ell$. By approximating the true trajectory with a parabolic parametrization around the turning point, and taking into account that the form-factors have an exponential shape we can write the transition probability in the form

$$P_{\beta\alpha} = \sqrt{\frac{1}{16\pi\hbar^2|\ddot{r}_0|\kappa_{a'_1}}} |f_{\beta\alpha}(r_0)|^2\ g(Q_{\beta\alpha}) \qquad g(Q) = \exp\left( -\frac{(Q-Q_{opt})^2}{\hbar^2\ddot{r}_0\kappa_{a'_1}} \right) \tag{3}$$

where $\ddot{r}_0$ is the radial acceleration at the distance of closest approach $r_0$ and $\kappa_{a'_1}$ is the decay length of the form-factor (it is related to the binding energy of the single-particle states involved in the transition).

The adiabatic cut-off function $g(Q)$ defines the actual value of the transition probability, the maximum being $Q_{opt}$ at the optimum Q-value. This derives from the requirement that

the trajectory of entrance and exit channels matches smoothly close to the turning point where the contribution from the form factor peaks.

In fig. 2, for the $^{58}$Ni+$^{208}$Pb reaction is shown the adiabatic cut-off function $g(Q)$ for one and two nucleons transfer channels. In the same figure with horizontal lines are represented the location of all possible transitions. Since only channels whose Q-values lye below the bell shaped curve can actually occur, it is clear that the only allowed transfers are neutron pick-up and proton stripping. All the other channels are hindered by optimum Q-value consideration. These conclusions are valid for most projectile and target combinations obtained with stable nuclei.

## RESULTS

By looking at the chart of nuclei it is clear that one should be able to reach neutron reach heavy nuclei in the region of N=126 (i.e. below the lead) just by extracting protons from a heavy stable targets (i.e making protons pick-up reactions) or by transferring, to the target, some neutrons (i.e. making neutron stripping reactions). As seen above, proton pick-up and neutron stripping are very weak channels when stable nuclei are involved. The opening of these channels can only be obtained via the use of neutron rich projectiles as it was discussed in refs. [4, 5].

Focusing in the region of the nuclei chart close to the magic number N=126, we show on Fig. 3 how multi-nucleon transfer reactions on $^{208}$Pb evolve by using, as projectile, several isotopes of xenon. This evolution is shown by displaying, for the indicated projectile, the

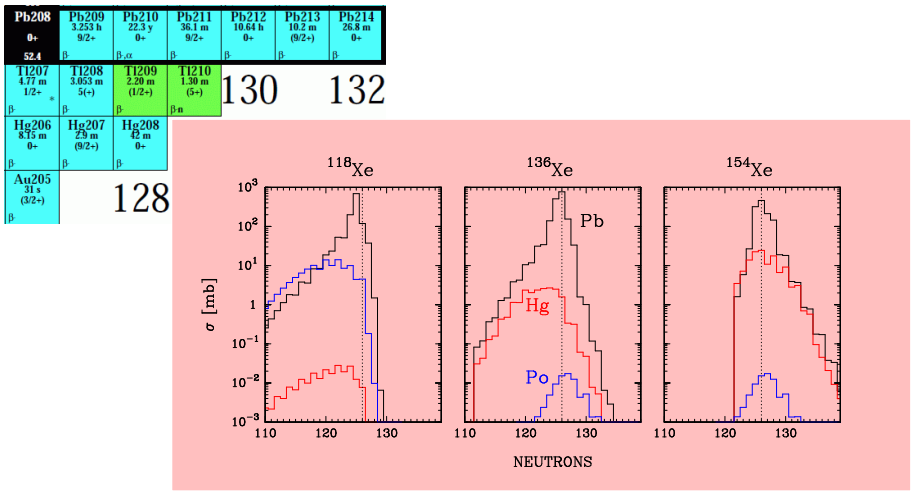


**FIGURE 3.** Isotopic distributions for the +2p (Hg) and -1p (Po) channels in the reaction of $^{118,136,154}$Xe on $^{208}$Pb reactions.

production of mercury (+2p channels) and polonium (-2p channels) isotopes. It is clear from the figure that with neutron-rich projectile the population of mercury (Hg) isotopes is strongly enhanced toward the neutron rich side.

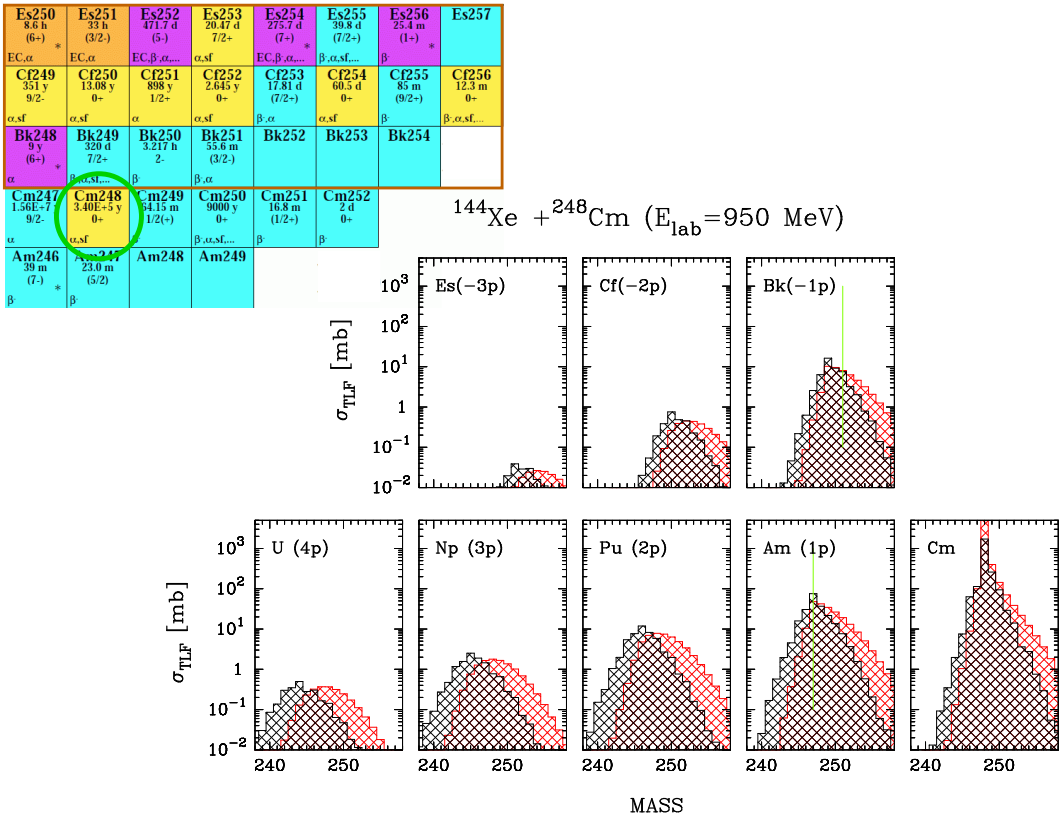


**FIGURE 4.** Isotopic distributions for the reaction of $^{144}$Xe on $^{248}$Cm reactions.

To have an idea on the population of heavier than target nuclei obtained via DIC I show the results of a collision of one of the neutron rich xenon isotopes on one of the heaviest available target, $^{238}Cm$. In Fig. 4 are shown the isotopic distributions of the different elements populated in the reactions. It is clear that the main flux goes to the population of nuclei that have a Z lower than the target but reasonable cross section are also predicted for nuclei with Z large. The red histogram represent the primordial isotopic distribution while the black one gives an idea how these distributions are altered by neutron evaporation. The vertical green lines indicated for the two ions the last known isotopes. Th

## CONCLUSTIONS

I have been showing some simple calculations, performed with a semi-classical model, that demonstrate how multi-nucleon transfer reactions, with neutron rich projectiles, provide a tool for the population of heavier than target nuclei and of neutron rich nuclei in the region around N=126. Unfortunately the calculations do not provide any hint on how these nuclei may be identified. The present spectrometers are of little use since the ions are emerging with a too low energy to be discriminated both in A and Z. The use of $\gamma$-array may only be useful trough a systematic study of the decay spectra in the neighboring nuclei (notice that the reaction mechanism populate all these nuclei at ones). Also for the $\beta$-decay one has to make similar considerations.

## REFERENCES


1. A. Winther, Nucl. Phys.**A572**, 191 (1994).
2. A. Winther, Nucl. Phys. **A594**, 203 (1995).
3. A. Winther, GRAZING, computer program. (may be downloaded from: $http://www.to.infn.it/\sim nanni/grazing$)
4. C.H. Dasso, G. Pollarolo and A. Winther *Phys. Rev. Lett.* **73**, 1907 (1995).
5. C.H. Dasso, G. Pollarolo and A. Winther *Phys. Rev.* **C52**, 2264 (1995)

# Fragment production and isospin related phenomena in heavy ion collisions

G.Casini [*], S.Barlini[†], M.Bini[*], P.R.Maurenzig[†], A.Olmi[*], G.Pasquali[*], G.Pastore[*], S.Piantelli[*], G.Poggi[*], E.Scarlini[*], A.Stefanini[*], S. Valdré[*], G. Ademard[**], A.Boiano[‡], B.Borderie[**], E. Bonnet[§], R.Bougault[¶], M.Bruno[‖], A. Chibhi[§], M.Cinausero[††], M.D'Agostino[‖], M.Degerlier[‡‡], J.D.Frankland[§], F.Gramegna[††], D. Gruyer[§], A.Kordjasz[§§], T.Kozik[¶¶], T.Kulig[¶¶], N.LeNeindre[¶], O.Lopez[¶], T.Marchi [††,***], P. Marini[§], L.Morelli[‖], A.Ordine[‡], M.Parlog[¶], M.F.Rivet[**], E.Rosato[‡], F.Salomon[**], G.Spadaccini[‡], G.Tortone[‡], E.Vient[¶] and M.Vigilante[‡]

[*]*INFN Sezione di Firenze and Università di Firenze, Italy*
[†]*Università di Firenze, Italy*
[**]*Institut de Physique Nucléaire, CNRS/IN2P3 and Université of Paris-Sud XI, Orsay, France*
[‡]*INFN Sezione di Napoli and Università Federico II di Napoli, Italy*
[§]*GANIL F-14076 Caen, France*
[¶]*Laboratoire de Physique Corpusculaire, IN2P3-CNRS/ENSICAEN/Université, Caen, France*
[‖]*INFN Sezione di Bologna and Università di Bologna, Italy*
[††]*INFN Laboratori Nazionali di Legnaro, Italy*
[‡‡]*Nevsehir University, Science and Art Faculty, Turkey*
[§§]*Warsaw University, Poland*
[¶¶]*Jagellonian University. Krakow, Poland*
[***]*Università di Padova, Italy*

**Abstract.** In view of the Eurisol project, we report on some aspects, relating the isospin degree-of-freedom to the fragment production in heavy-ion reactions. For detailed isospin investigation, a crucial point for the next experiments will be the improvement of isotopic separation (over a large solid angle) of the many reaction ejectiles produced in a broad range of sizes and velocities. The FAZIA collaboration started a program in order to build a novel detector array with unprecedented ion resolving power. Some recently obtained results are reported in view of future programmes.

**Keywords:** fragments, isospin, symmetry energy, pulse-shape-analysis
**PACS:** 25.60Pj; 25.70Jj; 25.70Mn; 25.70Pq

## INTRODUCTION

The production of nuclear fragments ($Z \geq 3$) of different sizes and energies is a common feature of many heavy-ion reactions. The properties of the fragments and their abundance depend on the reaction mechanism which varies as a function of the relative velocity and impact parameter. For example, at energies a few MeV/u above the barrier, fragments are mainly produced via asymmetric fission of nuclei formed in fusion reactions, or from the evaporation of the hot quasi-projectile (QP) or quasi-target

(QT) in dissipative collisions. In the Fermi energy domain, several experiments demonstrated that many processes contribute to fragment production. Multifragmentation of expanding systems in central collisions generates several fragments at a time. Also, the QP and/or QT can multifragment for mid-central reactions, provided that the excitation energy and the system size allow to enter the instability region. Also, fragments coming from the socalled midvelocity region are a specific feature of semiperipheral reactions at Fermi energies. These fragments are typically emitted on short time scales, overlapping with the interaction times, thus making them an essential probe to access and study the nuclear EOS very far from stability.
In the last decade the focus has been put on the link between the fragment production and the isospin degree of freedom. In fact, the isovector part of the nuclear potential is not well known at densities far from the saturation value and at high temperatures. Since the isospin observables are supposed to be related to the symmetry energy term of the nuclear EOS, a lot of work has been done in this sense, both theoretically and experimentally. The use of Radioactive Ion Beams (RIB) will help much, as the isospin will be naturally more unbalanced in such collisions, than with stable beams. However, the ISOL-RIB facilities under construction in Europe will not allow to investigate collisions at intermediate energies (maximum energies around 12 MeV/u are expected for tin beams) and this severely limits the scientific investigation on the nuclear EOS. Therefore the advent of third generation powerful facilities, like EURISOL, will strongly support the studies on the symmetry energy far from stability, especially in systems very neutron rich.
In the following, we briefly outline some physics subjects dealing with fragment production which are particularly interesting to be studied with efficient arrays, capable of extended isotopic identification. One of these detectors will be FAZIA [1], whose first results on the isospin research are shortly presented [2], in the second part of this paper, to show its potential in future experiments.

## ISOSPIN AND FERMI ENERGIES

*Disassembling of medium-mass hot nuclei formed in central collisions.* The limiting temperature is expected to decrease towards the drip-lines as a result of the broken equilibrium between several nuclear potential contributions. In particular, the level density should drop to zero at drip lines where bound levels are no more present. We cite here two experiments that try to evidence variations in the decay of excited systems formed in central collisions. Strong differences for composite systems formed in symmetric Calcium reactions at 25MeV/u have been observed by the Chimera group [3, 4], who compared two systems, mainly differing in the isospin content. The observed differences can be reproduced by a dynamical model where an asystiff isovector term is assumed. Moreover, the INDRA-Vamos collaboration started a program, using both stable and exotic Argon beams (from Spiral), to investigate evolution of the level density parameter by following the decay of Pd isotopes from near $\beta$-stability to rather n-deficient isotopes [5]. In future, this kind of studies will be extended with Eurisol beams and next-generation arrays for charged products, accessing over large solid angles the isotopic distributions of heavy species (e.g. fission fragments or even the evaporation residue) over large solid

angles.

*Exotic shapes and instabilities.* According to some dynamical models, strange shapes can appear in heavy systems formed in energetic central collisions. For instance, BUU calculations [6, 7] suggest that, with energy thresholds depending on the mass of the colliding nuclei, toroidal structures can survive for long times (300 fm/c) before the final disassembly. These structures should appear above 20-25MeV/u for systems like Au+Au and above 35MeV/u for lighter symmetric systems. Data are very scarce on this subject, no idea of the associated cross-section exists and, also, there aren't predictions about the role of the Symmetry Energy on these patterns.
Another interesting indication, somehow linked to this subject, comes from the detection of three-fold and four-fold events in the decay of semicentral Au+Au at 15 MeV/u [8]. These events have been ascribed to seemingly fast ($\tau \leq$ 100fm/c) splits of aligned QP-QT configurations. QMD calculations predict these channels but miss the lifetime: the alignement is not reproduced.
Finally, dealing with extreme nuclear shapes, we mention the possibility that very n-rich systems can survive fission at very high spins, due to the lowering of the fissility for given Z. These could permit studies on the Jacobi or Poincaré instability regimes [9], where nuclei abruptly change shape from oblate to elongated prolate or pear-like shapes, when led to extremely high spin states. These phenomena, all associated with exotic nuclear shapes, fit the range of mass-energy from Eurisol and could be studied in experiments in which most (if not all) charged fragments are well identified also in mass with sufficient angular precision. An interesting region would be the one of Ba isotopes (A from 116 to 144).

*Midvelocity emission and isospin physics.* The neutron content of the fragments which are emitted from the separation region of the QP-QT in semiperipheral reactions has been proposed to be a very powerful isospin observable [10, 11]. SMF calculations indeed predict that unbalanced neutron-proton fluxes (isospin drift) can occur between nuclear systems with different density. The net isospin flow depends on the asystiffness of the EOS; it is almost zero assuming asy-soft behaviour while it is appreciable for asy-stiff prescriptions, corresponding to a steep gradient of the symmetry potential with density. The neck region is supposed to be diluted during the QP-QT separation and the isospin drift can manifest. Several experiments, in fact, evidenced such kind of phenomenon, more in agreement with asy-stiff recipes of the nuclear EOS [12, 13]; Eurisol energetic beams of heavy nuclei will extend this investigation, in particular one could follow the evolution of the neutron enrichment of the midvelocity region with mass and energy. It could be, e.g., that fast preequilibrium emission of the abundant neutrons reduces isospin effects in the remaining system, therefore producing a rise-and-fall behavior of the excitation function of some isospin variable.

## THE FAZIA PROJECT

The FAZIA collaboration started some years ago a *R&D* towards a major step in ion identification using, as a basis module, a three-stage Si-Si-CsI(Tl) telescope. The inves-

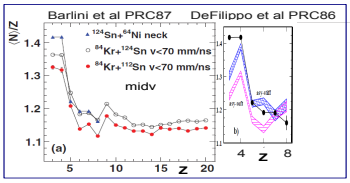


**FIGURE 1.** Average Isospin N/Z as a function of fragment charge. Data of FAZIA [2] (left) compare well with those of [12] (right). The frame dimensions of the two parts have been scaled for the sake of clarity

tigated aspects and the many results are reported in the literature (e.g. [14]). Here we note that a particular effort was made to extend ion identification for particles stopped in the first silicon layer of the telescope, thanks to digital pulse shape analysis. Various effects related to the signal production, fast sampling and processing, have been studied finally resulting in good perfomances. The excellent isotopic resolution of the detectors already permitted to perform first experiments (although in simple configurations) about isospin dynamics. An example, described in details elsewhere [2], is shown in Fig.1. It presents the average N/Z of fragments for Z up to 20 (left part) measured by FAZIA (circles) and compared with the data of [12] (triangles). The same latter data are plotted as black circles in the righ part of the Fig.1, where the experimental isospin is compared with two calculations assuming different asy-stiffness. Two observations can be done. First, the nice agreement of the two measurements, coming from different detectors and data reduction procedures, reinforces the experimental findings and can better constrain models. Then, we observe that with the FAZIA telescope one can explore the isospin on a much larger range and this is a good starting point for the next generation of high-quality experiments.

## REFERENCES


1. http://fazia2.in2p3.fr/spip/
2. S. Barlini et al., *Phys. Rev.*, **C 87** 054607 (2013),
3. F. Amorini et al., *Phys. Rev. Lett*, **102** (2009),
4. G. Cardella et al., *Phys. Rev.*, **C 85** 064609 (2012),
5. P. Marini et al., *Eur. Phys. Jour. Web of Conf.*, **2** 04003 (2010),
6. A. Sochocka et al., *Acta Phys. Pol.*, **B 39** 405 (2008),
7. B. Jouault et al., *Nucl. Phys.*, **A 591**, 497 (1995),
8. J. Wilczynski et al., *Phys. Rev.*, **C 81** 067604 (2010),
9. K. Mazurek et al., *Acta Phys. Pol.*, **B 42** 471 (2011),
10. V. Baran et al., *Phys. Rev.*, **C 85** 054611 (2012),
11. M. DiToro et al., *Eur. Phys. Jour.*, **A 30** (2006),
12. E. DeFilippo et al., *Phys. Rev.*, **C 86** 014610 (2012),
13. A. McIntosh et al., *Phys. Rev.*, **C 81** 034603 (2010),
14. S. Carboni et al., *Nucl. Instr. Meth*, **A 664** 251 (2012)

# Yrast spectroscopy of neutron-rich heavy nuclei studied with deep-inelastic collisions

Bogdan Fornal

*The Henryk Niewodniczański Institute of Nuclear Physics PAN, 31-342 Kraków, Poland*

**Abstract.** In neutron-rich nuclei, studies of excited states at high spin became possible by using deep-inelastic heavy-ion reactions and the discrete gamma-ray spectroscopy technique based on efficient Compton-suppressed germanium arrays. The measurements can be carried out by applying thick or thin target method. Thick target experiments are especially suitable for studies of heavy nuclei as they do not require product identification in magnetic spectrometers. Here, accurate assignment of gamma rays to product nuclei is provided by the gamma-gamma coincidence analysis which uses as "starting points" the known gamma rays. By applying thick targets with deep-inelastic collisions, previously inaccessible yrast structures have been located in many neutron-rich nuclei. The results include location of high-spin structures near the doubly-magic $^{208}$Pb. With the advent of high-intensity, neutron-rich radioactive beams of heavy nuclei at energies close to the Coulomb barrier, deep-inelastic processes will be a unique tool to access yrast excitations in nuclides located close to the radioactive projectile.

**Keywords:** deep-inelastic reactions, nuclear structure of $^{208}$Hg and $^{209}$Tl, shell-model calculations
**PACS:** 27.80.+w, 23.20.Lv, 23.20.En, 21.60.Cs

## INTRODUCTION

In 1959, Kaufmann and Wolfgang [1] showed that in heavy-ion reactions fragments associated with transfer of many nucleons, and, as a result, quite remote from the projectile or target, are produced with sizeable cross-sections, contrary to the expectations. It became clear that in the reaction between heavy ions a new class of processes exists – these processes acquired the name deep-inelastic or dumped collisions.

Through the 1960's and 1970's, the importance of the new deep-inelastic reaction mechanism was recognized and theoretical concepts were developed [2-5]. Characteristic features of deep-inelastic reactions include: formation of a dinuclear system which rotates almost rigidly, exchange of nucleons governed by equilibration of the neutron to proton number ratio, damping of the relative kinetic energy between the reaction partners, transfer of the angular momentum into intrinsic spin of the reaction products, and, eventually, separation into two fragments which retain the identities of the projectile and target nuclei. What regards the spin of deep-inelastic collision products, already in the early studies the angular momenta of the primary fragments produced in the damped reactions were determined [6,7]. It was demonstrated that average spin of the heavy products in such cases can be as high as

30 hbar. It became obvious that deep inelastic reactions might be very valuable as a tool of preparing excited nuclei with well-defined high angular momenta.

## ACCESSING HIGH-SPIN STRUCTURES IN NEUTRON-RICH NUCLEI

To be able to identify high-spin structures in deep-inelastic reaction products, the discrete gamma-ray spectroscopy technique had to be involved, however, the issue was not straightforward. Characteristic gamma rays from nuclei produced in deep-inelastic collisions in principle could be measured, but, since the total reaction yield is spread over many nuclei, the spectra are extremely complicated and the detection systems made of a few germanium detectors were not sufficient. The solution came with the advent of very efficient, Compton suppressed germanium arrays which were developed in the 80's and 90's - examples of those gamma-ray spectrometers included: GASP (Legnaro-Padova), EUROBALL (Legnaro, Strasbourg, GSI), GAMMASPHERE (Argonne, Berkeley). Once a highly efficient germanium gamma-ray array is available, one can use its high resolving power for the precise identification of gamma rays from the DI reaction partners. The method is rather simple. Since in such measurements the reaction products are stopped within 1-2 ps inside the target, the gamma rays emitted from the states with the cumulative lifetime longer than the stopping time are detected as sharp lines. Here, the gamma-gamma coincidences with known gamma rays provide unique assignment of the newly displayed transitions to the emitting nuclei. An especially important feature is that the coincidences between gamma rays emitted from the reaction partners may be directly observed - this can be used for identification in the cases in which spectroscopic information about the product of interest is not available.

One of the features of DI collisions, which is of main interest here, is the ability to produce nuclei with the neutron to proton number ratio (N/Z) larger than N/Z of the already neutron-rich projectile. This characteristics is related to the N/Z equilibration phenomenon that occurs in deep-inelastic reactions. For example, if one scatters a neutron-rich projectile $^{64}$Ni (for which N/Z=1.286) on a heavy target like $^{238}$U (for which N/Z=1.587), the N/Z equilibration driving force favours transfers of neutrons into the projectile while protons flow in the opposite direction. In this way states in the Ni, Co, Fe, Mn, Cr isotopes which have N/Z ratio higher than that of $^{64}$Ni are populated.

Over the last 20 years, we have performed a large number of experimental studies using thick targets with deep-inelastic collisions. We have located yrast and near-yrast structures in many nuclei which were previously inaccessible. The results include: the discovery of the doubly-magic character of $^{68}$Ni [8], the identification of a sub-shell closure at N=32 in neutron-rich nuclei [9], the location of high-spin yrast isomers in neutron-rich nuclei in the neighborhood of the doubly- magic $^{208}$Pb (e.g., [10-13]), etc.

# YRAST SPECTROSCOPY "SOUTH-EAST" OF $^{208}$PB

Now, I will concentrate on the region of $^{208}$Pb which can be considered an excellent laboratory for the effective nucleon-nucleon interaction studies. The attractiveness of the investigations in this part of the nuclidic chart relies on the fact that, since the $^{208}$Pb nucleus is the best doubly magic core, one deals here with the relatively simply structures arising from couplings of a small number of valence particles/holes. Since detailed shell model calculations of those excitations are available, extensive comparisons between experiment and theory is possible. In this way, new shell model interactions based on various nucleon-nucleon potentials can be precisely examined.

An opportunity to access yrast excitations in the neutron-rich species around $^{208}$Pb is offered by deep-inelastic processes that occur in collisions of a $^{208}$Pb beam with a $^{238}$U target. As mentioned above, this is made possible by a tendency towards N/Z equilibration of the di-nuclear system formed during the collisions. In the reactions under investigation, the lighter colliding partner, $^{208}$Pb, had lower N/Z ratio than the target nucleus $^{238}$U and, as a result, the production of nuclei with larger neutron excess than the projectile was favored.

The experiment was performed at Argonne National Laboratory using the $^{208}$Pb beam from the ATLAS accelerator and the GAMMASPHERE detection system consisting of 101 Compton-suppressed large germanium detectors.

In the case of products belonging to the "south-east" quarter in which isomeric states were known from earlier studies, the analysis of the off-beam coincidence events showed that the $^{206}$Hg, $^{208}$Hg, $^{209}$Tl, $^{210}$Pb, $^{211}$Pb nuclei were present in the data with yields sufficient to explore their structure above the isomer. Indeed, by setting gates on gamma rays which deexcite those isomers, we were able to display transitions occurring above the metastable states and to establish significant level schemes. The high detection sensitivity of the Gammasphere spectrometer was crucial for this work. Figure 1 shows the structures located in $^{206}$Hg, $^{208}$Hg, $^{209}$Tl, $^{210}$Pb and $^{211}$Pb [10-13].

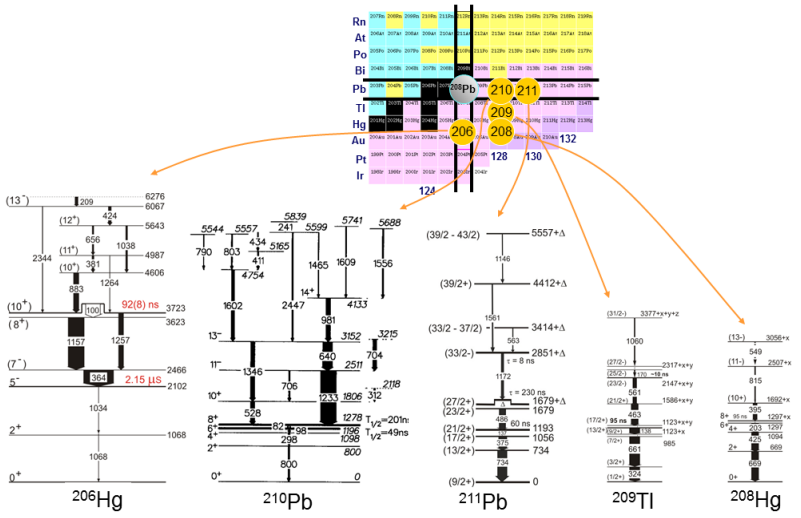


**FIGURE 1.** Level schemes for yrast states in $^{206}$Hg, $^{208}$Hg, $^{209}$Tl, $^{210}$Pb and $^{211}$Pb established by using deep-inelastic thick-target gamma-ray coincidence technique.

The new findings in nuclei belonging to the yet unexplored region of the nuclidic chart with Z<82 and N>126 could now be used to perform a stringent test of the so called $V_{low-k}$ realistic shell model interactions that became recently available. These interactions are derived from realistic nucleon-nucleon (NN) potentials without adjustable parameters. We have obtained $V_{low-k}$ effective interaction for the 50<Z<82 and 126<N<184 model space by using the Computational Environment for Nuclear Structure (CENS) by T. Engeland, M. Hjorth-Jensen and G.R. Jansen [14], based on [15].

The shell model calculations have been performed using the OXBASH code [10]. We allowed the valence protons occupy the five single particle levels $0g_{7/2}$, $1d_{5/2}$, $1d_{3/2}$, $2s_{1/2}$, and $0h_{11/2}$ of the Z=50-82 shell, while for valence neutrons the model space included the $2g_{9/2}$, $1i_{11/2}$, $1j_{15/2}$, $3d_{5/2}$, $4s_{1/2}$, $2g_{7/2}$, and $3d_{3/2}$ orbitals of the N=126-184 shell. We used the experimental single particle energies defined with respect to the $^{208}$Pb core. The results for $^{210}$Pb and $^{208}$Hg N=128 isotones are displayed in Fig. 2. Considering that no adjustable parameters have been involved in the procedure of deriving the shell model two-body matrix elements from the NN potential, the agreement between experimental and calculated level energies is satisfactory.

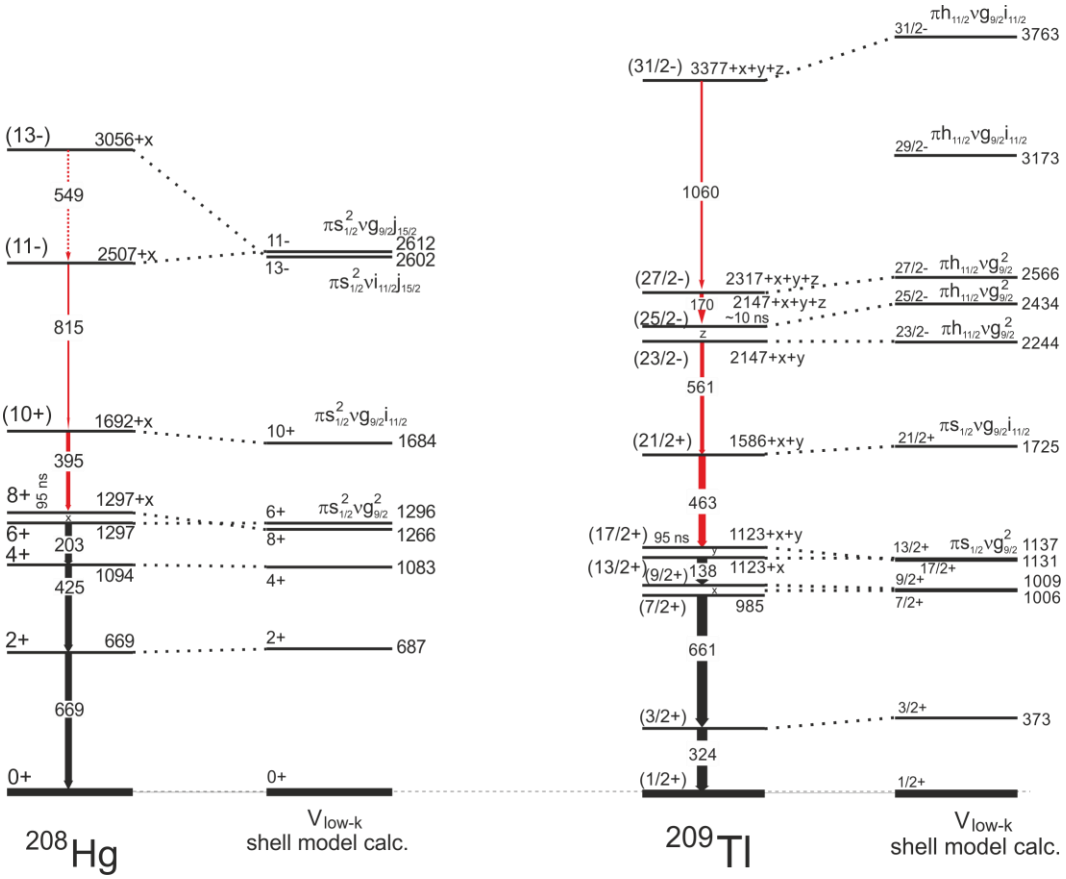


**FIGURE 2.** The level schemes for $^{208}$Hg and $^{209}$Tl with the results of shell model calculations performed with the $V_{low-k}$ realistic effective interaction.

## CONCLUSION

Concluding, discrete in-beam gamma-ray spectroscopy with deep-inelastic reactions turned out to be efficient in elucidating high-spin structures in neutron-rich nuclei. In particular, identification of high-spin structures in neutron-rich nuclei around doubly-magic $^{208}$Pb was possible with this method. These structures can serve as a testing ground for the shell-model calculations with the realistic nucleon-nucleon interaction derived from the free nucleon-nucleon potentials. The agreement between the results of such calculation with the realistic $V_{low\text{-}k}$ shell model interaction seem to be very successful in describing yrast states in nuclei located "south-east" of $^{208}$Pb. It is almost certain that discrete in-beam gamma-ray spectroscopy of deep-inelastic reactions products will greatly benefit from radioactive beams. Experiments using the radioactive beams and modern tracking germanium arrays should extend the investigations of high-spin structures toward the „terra incognita".

## ACKNOWLEDGMENTS

A number of research groups contributed to the results presented in this contribution. The names of the participants of this endeavor are listed in cited publications and they include: B. Szpak, R.V.F. Janssens, R. Broda, M.P. Carpenter, G. Dracoulis, W. Królas, G. Lane, K.H. Maier, T. Pawłat, D. Seweryniak, J. Wrzesinski, S. Zhu.

## REFERENCES

1. R. Kaufmann and R. Wolfgang, *Phys. Rev*. **121**, 192 (1961).
2. V.V. Volkov, *Physics Reports* **44**, 93 (1978).
3. L.G. Moretto and R.P. Schmitt, *Rep. Prog. Phys.* **44** (1981).
4. A. Gobbi, *Lecture Notes in Physics* **168**, pp. 159-174 (1982).
5. W.U. Schroeder and J.R. Huizenga, Dumped Nuclear Reactions in *Treatise on Heavy-Ion Science*, Ed. D.A. Bromley. N.Y.; London, pp 113-726 (1985).
6. P. Glässel et al., *Phys. Rev. Lett.* **38** (1977).
7. M.N. Namboodiri et al., *Phys. Rev. C* **20** (1979).
8. R. Broda et al., *Phys. Rev. Lett.* **74**, 868 (1995).
9. R.V.F. Janssens et al., *Phys. Lett. B* **546**, 55 (2002).
10. B. Fornal et al., *Phys. Rev. Lett*. **87**, 212501 (2001).
11. G. Lane et al., *Nucl. Phys. A* **682** (2001).
12. G. Lane et al., *Phys. Lett. B* **606** (2005).
13. B. Fornal et al., *Journal of Physics: Conf. Ser*. **267**, 012035 (2011).
14. T. Engeland, M. Hjörth-Jensen and G.R. Jansen, CENS, a Computational Environment for Nuclear Structure (in preparation).
15. M. Hjörth-Jensen, T.T.S. Kuo, E. Osnes, *Physics Reports* **261**, 125 (1995).